

# **Microfluidic Synthesis and Assembly of Multi-Scale Polymer Composite Particles Towards Sensoric and Labeling Applications**

---

## **Dissertation**

Submitted to

**Faculty of Mathematics and Natural Science  
Technical University of Ilmenau, Germany**

To obtain the academic degree

**doctor rerum naturalium**

**(Dr. rer. nat.)**

By

**M. Sc. Nikunj Kumar Visaveliya**

(born on April 12, 1986 in Devkigalol, India)

Research Supervisor

**Prof. Dr. J. Michael Köhler**





## **Doctoral Committee**

**Chairman: Prof. Dr. rer. nat. habil. Andreas Schober**

(Institute of Chemistry and Biotechnology,  
Technical University of Ilmenau, Germany)

**Referees: Prof. Dr. rer. nat. habil. J. Michael Köhler**

(Department of Physical Chemistry and Microreaction Technology,  
Technical University of Ilmenau, Germany)

**Prof. Dr. rer. nat. habil. Uwe Ritter**

(Department of Chemistry,  
Technical University of Ilmenau, Germany)

**Prof. Dr. Christophe A. Serra**

(School of Chemistry, Polymers and Materials (ECPM)  
University of Strasbourg, France)

**Members: Dr. rer. nat. G. Alexander Groß**

(Department of Physical Chemistry and Microreaction Technology,  
Technical University of Ilmenau, Germany)

**Prof. Dr. Klaus Heinemann**

(Head of functional polymer systems and Physical Research  
Thuringian Institute of Textile and Plastics Research, Germany)

**Date of the viva voce: 11.11.2015**

**Date of the defense: 18.11.2015**



**My deepest salutation and gratitude to the**

Universal truth, Yogeshwar Shree Krishna

and

Active philosopher, Revered Pandurang Shastri Athavale

***To my parents***

*for their love and consistent encouragement*

## I. Abstract

Polymer nanoparticles and microparticles of various sizes, shapes and compositions have attracted ubiquitous attentions in various fields such as biomedical science, biotechnology and nanotechnology. A key challenge in the synthesis of multicomponent nano and microparticles for various applications is obtaining the particles with reproducibility and monodispersity in a minimum number of preparation steps, and also with well-defined surface and physicochemical properties. To progress in such criteria with successful achievements, the presented work demonstrates the microfluidic synthesis of size, shape, morphology and composition tuned multi-scale polymer particles for sensoric and labeling applications. The work in this thesis is divided in two main parts: (i) polymer nanoparticles and their assembly and (ii) polymer microparticles and their compositions.

For the nanoparticles regime, a Si holeplate-based cross-flow microfluidic arrangement has been used for producing the spherical poly(methyl methacrylate) (PMMA) nanoparticles of defined size. The emulsion was formed by pressing the dispersed phase through an array of micro-pores into a fast streaming aqueous phase. By precisely fluctuating two immiscible liquid phases at various flow rate ratios and by varying the concentration of different surfactants in the aqueous phase, the size tuned spherical PMMA nanoparticles can be obtained with high homogeneity. The size and surface morphology of the polymer nanoparticles together with their functional properties such as fluorescence play a crucial role in determining their biological fate in various biomedical applications. Therefore, here, four different strategies for the spherical shape as a model system have been developed and successfully implemented to tune the nanoparticles size, surface charge and fluorescence intensities simultaneously by embedding the fluorophores in the nanoparticles interior via random dispersion as well as entrapping via covalent-linking, adsorption on the surface via hydrophobic interaction, and immobilization through covalent, electrostatic and secondary (biotin-streptavidin) interactions. Moreover, by controlling the appropriate surface charges of the antagonistically charged particles, size as well as distance-controlled PMMA-Ag heterogeneous nanoassemblies were prepared.

A spherical shape of the nanoparticles is a standard case for amorphous materials which can be determined by the minimization of interfacial area. Beyond the standard case, to generate the anisotropic shape of polymeric materials in a single-step synthesis is a real challenge. Here, precisely controlled ellipsoidal, dumbbell and further linear shaped complex polymer

nanoparticles in a microfluidic platform through single-step process were synthesized, and the formation mechanism is hypothetically described on the basis of limited polarization, partial repulsion and moderate electrostatic interaction. To extend such unusual phenomena, the flower-shaped and branched nanoparticles were also synthesized via in-situ nano-assembling under the controlled reaction environment. Formation of the flower-shaped nanoparticles is driven by the solvation and mobility factors which are explained here with detail. The synthesis of the polymer nanoparticles with shell-like surface layer have also been performed via copolymerization approach of hydrophobic as well as hydrophilic domains in one-step process at precise microfluidic condition and at polymerizing temperature. A shell-like layer, in this case, swells in the aqueous medium which allows the electrostatic entrapping of smaller polymer nanoparticles to form the homogeneous and heterogeneous nanoassembly particles for fluorescence and SERS applications. And at last, the flow parameters such as concentration effect, temperature effect, and residence time among the others have been systematically studied to form the controlled nanoassembly of size and shape controlled polymer and metallic nanoparticles for fluorescence and SERS sensing activities by flow-assembling microflow technique.

Microparticles regime: The homogeneity and quality of the polymer microparticles which are produced in the liquid phase are mainly dependent on the initial local conditions of nucleation and on the homogeneity and reproducibility of the conditions of particles growth. Microfluidic techniques can provide very homogeneous reaction environment for particles nucleation and growth because of their advantages such as, fast phase transfer, efficient reaction mixing and narrow residence time distribution. Therefore, highly homogeneous size-controlled polymer microparticles were produced here in the cross-flow microfluidic platform for fluorescence labeling as well as for surface-enhanced Raman scattering (SERS) sensing applications. In first part, a simultaneous size and color tuned poly-tripropylene glycol diacrylate (polyTPGDA) microparticles of diameter between 40  $\mu\text{m}$  and 500  $\mu\text{m}$  were prepared via photopolymerization process in a single-step microflow-through technique. Moreover, a wide range of mixed colored microparticles for particle-based fluorescence labeling were obtained by controlled *in-situ* mixing of the different fluorophores during the continuous flow. In second part, a micro-continuous flow process is applied for the preparation of swellable polyacrylamide/silver composite microparticles for sensoric application. The combined approach of photopolymerization and photoreduction were performed in the flow synthesis of such microgel composite particles where smaller silver

nanoparticles are *in-situ* embedded in the microparticles interior. In addition, metal-catalyzed metal nanoparticles enforcement was also applied for the realization of sensor particles for enhanced SERS sensing application. Finally, to extend the SERS sensing phenomena in the flow condition, a compact arrangement for microflow SERS measurements using the sensor particles have been developed. An arrangement and the applied particles can be regenerated in case of the applied analytes by application of a rinsing process by acid solution. Therefore, they are suited for repeated measurements in microflow conditions.

Overall, the size, shape, assembly and composition controlled multi-scale polymer particles between nanometer and micrometer size regimes have been synthesized for labeling and sensoric applications. The surface and physicochemical properties of the generated particles were studied for the formation of heterogeneous and homogeneous nano-assemblies. The obtained polymer particles were characterized by SEM, DLS, zeta potential, fluorescence microscopy, fluorescence spectroscopy, surface-enhanced Raman spectroscopy and UV/VIS spectroscopy.





## II. Research publications based on the thesis

1. **N. Visaveliya**, C. Hoffmann, A. Groß, E. Täuscher, U. Ritter, and J. M. Köhler, “Micro-flow assisted synthesis of fluorescent polymer nanoparticles with tuned size and surface properties”, *Nanotechnology Reviews*, **2015**, (Accepted).
2. **N. Visaveliya** and J. M. Köhler, “Microfluidic Assisted Synthesis of Multipurpose Polymer Nanoassembly Particles for Fluorescence, LSPR, and SERS Activities”, *Small*, **2015**, DOI: 10.1002/sml.201502364 (In Press).
3. **N. Visaveliya**, S. Lenke and J. M. Köhler, “Composite Sensor Particles for Tuned SERS Sensing: Microfluidic Synthesis, Properties and Applications”, *ACS Appl. Mater. Interfaces*, **2015**, 7 (20), 10742–10754.
4. **N. Visaveliya**, S. Lenke, and J. M. Köhler, “Microflow SERS Measurements Using Sensing Particles of Polyacrylamide/Silver Composite Materials”, *Chem. Eng. Technol.*, **2015**, 38 (7), 1144-1149.
5. **N. Visaveliya** and J. M. Köhler, “Role of Self-Polarization in a Single-Step Controlled Synthesis of Linear and Branched Polymer Nanoparticles”, *Macromol. Chem. Phys.*, **2015**, 216 (11), 1212-1219.
6. **N. Visaveliya** and J. M. Köhler, “Simultaneous Size and Color Tuning of Polymer Microparticles in a Single-Step Microfluidic Synthesis: Particles for Fluorescence Labeling”, *J. Mater. Chem. C*, **2015**, 3, 844–853.
7. **N. Visaveliya** and J. M. Köhler, “Control of Shape and Size of Polymer Nanoparticles Aggregates in a Single-Step Micro Continuous Flow Process: A Case of Flower and Spherical Shapes”, *Langmuir*, **2014**, 30, 12180–12189.
8. **N. Visaveliya** and J. M. Köhler, “Single-Step Microfluidic Synthesis of Various Non-Spherical Polymer Nanoparticles via in-Situ Assembling: Dominating Role of Polyelectrolytes Molecules”, *ACS Appl. Mater. Interfaces*, **2014**, 6 (14), 11254–11264.
9. **N. Visaveliya**, S. Li and J. M. Köhler, “Heterogeneous Nanoassembling: Microfluidically Prepared Poly(methyl methacrylate) Nanoparticles on Ag Microrods and ZnO Microflowers”, *Part. Part. Syst. Charact.* **2013**, 30, 614–623.
10. **N. Visaveliya** and J. M. Köhler, “A Self-Seeding Synthesis of Ag Microrods of Tuned Aspect Ratio: Ascorbic Acid Plays a Key Role”, *Nanotechnology*, **2013**, 24(34), 345604.



### III. Declaration for reproduction of published work

Parts of this work have been published already by the author is mentioned here section-wise with the references. Moreover, the mentioned images in the “Chapter 1 (Introduction)” were published by other authors whose reference is also given here by correlating the numbers of Figures (in Chapter 1) and References (in Chapter 6).

<b>Chapter 1</b>	Figure 1.1	Copyright from	Ref. <b>7</b>
	Figure 1.2	Copyright from	Ref. <b>20</b>
	Figure 1.3 A	Copyright from	Ref. <b>54</b>
	Figure 1.3 B	Copyright from	Ref. <b>37</b>
	Figure 1.3 C	Copyright from	Ref. <b>37</b>
	Figure 1.3 D	Copyright from	Ref. <b>55</b>
	Figure 1.3 E	Copyright from	Ref. <b>30</b>
	Figure 1.3 F	Copyright from	Ref. <b>56</b>
	Figure 1.3 G	Copyright from	Ref. <b>57</b>
	Figure 1.3 H	Copyright from	Ref. <b>58</b>
	Figure 1.4	Copyright from	Ref. <b>9</b>
	Figure 1.5 A-C	Copyright from	Ref. <b>117</b>
	Figure 1.5 D-F	Copyright from	Ref. <b>121</b>
	Figure 1.6 A	Copyright from	Ref. <b>128</b>
	Figure 1.6 B	Copyright from	Ref. <b>129</b>
Figure 1.6 C	Copyright from	Ref. <b>130</b>	
<b>Chapter 2</b>	Section 2.1.1	Part is modified from	[ <b>a</b> ]
	Figure 2.1	Part is modified from	[ <b>a</b> ]
	Figure 2.2	Part is modified from	[ <b>E</b> ]
	Figure 2.3	Part is modified from	[ <b>D</b> ]
	Figure 2.4	Part is modified from	[ <b>A</b> ]
	Figure 2.5	Part is modified from	[ <b>B</b> ]
<b>Chapter 3</b>	Section 3.1	Part is modified from	[ <b>G</b> ]
	Section 3.2.1	Part is modified from	[ <b>F</b> ]
	Section 3.2.2	Part is modified from	[ <b>F</b> ]
	Section 3.2.3	Part is modified from	[ <b>C</b> ]
	Section 3.2.4	Part is modified from	[ <b>E</b> ]
	Section 3.5.1	Part is modified from	[ <b>H</b> ]
	Section 3.5.2	Part is modified from	[ <b>G</b> ]
Section 3.5.3	Part is modified from	[ <b>G</b> ]	
<b>Chapter 4</b>	Section 4.1	Part is modified from	[ <b>D</b> ]
	Section 4.2	Part is modified from	[ <b>A</b> ]
	Section 4.3	Part is modified from	[ <b>B</b> ]

### Author publications

- A. N. Visaveliya, S. Lenke and J. M. Köhler, “Composite Sensor Particles for Tuned SERS Sensing: Microfluidic Synthesis, Properties and Applications”, *ACS Appl. Mater. Interfaces*, **2015**, 7 (20), 10742–10754. Reproduced by permission of The American Chemical Society (ACS).
- B. N. Visaveliya, S. Lenke, and J. M. Köhler, “Microflow SERS Measurements Using Sensing Particles of Polyacrylamide/Silver Composite Materials”, *Chem. Eng. Technol.*, **2015**, 38 (7), 1144–1149. Reproduced by permission of WILEY-VCH Verlag GmbH & co. KGaA, Weinheim.
- C. N. Visaveliya and J. M. Köhler, “Role of Self-Polarization in a Single-Step Controlled Synthesis of Linear and Branched Polymer Nanoparticles”, *Macromol. Chem. Phys.*, **2015**, 216 (11), 1212–1219. Reproduced by permission of WILEY-VCH Verlag GmbH & co. KGaA, Weinheim.
- D. N. Visaveliya and J. M. Köhler, “Simultaneous Size and Color Tuning of Polymer Microparticles in a Single-Step Microfluidic Synthesis: Particles for Fluorescence Labeling”, *J. Mater. Chem. C*, **2015**, 3, 844–853. Reproduced by permission of The Royal Society of Chemistry (RSC).
- E. N. Visaveliya and J. M. Köhler, “Control of Shape and Size of Polymer Nanoparticles Aggregates in a Single-Step Micro Continuous Flow Process: A Case of Flower and Spherical Shapes”, *Langmuir*, **2014**, 30, 12180–12189. Reproduced by permission of The American Chemical Society (ACS).
- F. N. Visaveliya and J. M. Köhler, “Single-Step Microfluidic Synthesis of Various Non-Spherical Polymer Nanoparticles via in-Situ Assembling: Dominating Role of Polyelectrolytes Molecules”, *ACS Appl. Mater. Interfaces*, **2014**, 6 (14), 11254–11264. Reproduced by permission of The American Chemical Society (ACS).
- G. N. Visaveliya, S. Li and J. M. Köhler, “Heterogeneous Nanoassembling: Microfluidically Prepared Poly(methyl methacrylate) Nanoparticles on Ag Microrods and ZnO Microflowers”, *Part. Part. Syst. Charact.* **2013**, 30, 614–623. Reproduced by permission of WILEY-VCH Verlag GmbH & co. KGaA, Weinheim.
- H. N. Visaveliya and J. M. Köhler, “A Self-Seeding Synthesis of Ag Microrods of Tuned Aspect Ratio: Ascorbic Acid Plays a Key Role”, *Nanotechnology*, **2013**, 24(34), 345604. Reproduced by permission of IOP publishing Limited.

**Publication of co-authors in Technical University of Ilmenau (Department of Physical Chemistry and Microreaction Technology)**

- a. J. M. Köhler, F. Möller, S. Schneider, P. M. Günther, A. Albrecht, G. A. Groß; Size-Tuning of Monodisperse PMMA Nanoparticles by Micro-Continuous-Flow Polymerization using a Silicon Micro-Nozzle Array. *Chemical Engineering Journal*, **2011**, 167, 688-693.

Copyright © 2013 Reproduced by permission of WILEY-VCH Verlag GmbH & co. KGaA, Weinheim

Copyright © 2013 Reproduced by permission of IOP Publishing limited.

Copyright © 2014 Reproduced by permission of The Royal Society of Chemistry (RSC)

Copyright © 2014 Reproduced by permission of The American Chemical Society (ACS)

Copyright © 2015 Reproduced by permission of The American Chemical Society (ACS)

Copyright © 2015 Reproduced by permission of WILEY-VCH Verlag GmbH & co. KGaA, Weinheim



---

**[Front Matter]**

<b>I</b>	<b>Abstract.....</b>	<b>VII</b>
<b>II</b>	<b>Research publications based on the thesis .....</b>	<b>XI</b>
<b>III</b>	<b>Declaration for reproduction of published work .....</b>	<b>XIII</b>

**Contents**

<b>1</b>	<b>Introduction.....</b>	<b>1</b>
1.1	Polymer particles .....	1
1.2	Various properties and applications of polymer particles .....	3
1.3	Shape control of polymer nanoparticles .....	5
1.4	Composition and assembly of polymer particles.....	6
1.5	Particle-based fluorescence labeling.....	7
1.6	Particle-based SERS sensing .....	8
1.7	Why microfluidics is particularly promising for polymer particles?.....	9
1.8	Unique parameters of the microfluidic techniques.....	10
1.9	Challenges and central questions.....	16
1.10	Aim and objective.....	18
<b>2</b>	<b>Materials and methods .....</b>	<b>21</b>
2.1	Microfluidic systems for the synthesis of polymer particles .....	21
2.1.1	Fabrication of the microreactor device.....	21
2.1.2	Silicon holeplate-based cross-flow microfluidic arrangement .....	23
2.1.3	Silanization of Si microchip .....	25
2.2	Particles synthesis.....	28
2.2.1	Spherical polymer nanoparticles .....	28
2.2.2	Non-spherical polymer nanoparticles synthesis .....	28
2.2.3	Synthesis of layered polymer nanoparticles and their nanoassembly .....	29
2.2.4	Fluorescent polymer nanoparticles.....	29
2.2.5	Synthesis of heterogeneous nanoassembly.....	31
2.2.5.1	Synthesis of Ag microrods of tuned aspect ratio.....	31
2.2.5.2	Synthesis of PMMA/Ag assembly particles.....	31

2.2.6	Flow assembling of size and shape controlled polymer nanoparticles.....	32
2.2.7	Size and color tuned polyTPGDA microparticles synthesis .....	32
2.2.7.1	Synthesis of monochromatic microparticles (size-tuned) .....	32
2.2.7.2	Synthesis of mixed and multi-colored microparticles.....	33
2.2.8	Polyacrylamide/silver composite sensor microparticles .....	33
2.2.8.1	Microfluidic synthesis of Ag-embedded polyacrylamide particles.....	33
2.2.8.2	Procedure for Ag enforcement in sensoric hydrogel particles .....	34
2.3	Characterization.....	36
2.3.1	Scanning electron microscopy (SEM).....	36
2.3.2	Sputter coater.....	37
2.3.3	Dynamic light scattering (DLS) .....	37
2.3.4	Zeta potential measurements .....	38
2.3.5	Fluorescence spectroscopy .....	39
2.3.6	Optical microscopy.....	40
2.3.7	UV-visible spectroscopy .....	41
2.3.8	Surface-enhanced Raman scattering (SERS) measurements .....	42
<b>3</b>	<b>Results and discussions-1: Polymer nanoparticles and their assembly .....</b>	<b>45</b>
3.1	Spherical polymer nanoparticles.....	45
3.2	Shape controlled polymer nanoparticles.....	48
3.2.1	Formation of ellipsoidal and dumbbell-like polymer nanoparticles.....	49
3.2.2	Formation of controlled rodlike polymer nanoparticles .....	54
3.2.3	Formation of linear and branched polymer nanoparticles.....	57
3.2.4	Formation of flower-shaped polymer nanoparticles.....	62
3.3	Shell-like layered polymer nanoparticles and their nanoassembly synthesis.....	72
3.3.1	Formation of surface layered polymer structure .....	72
3.3.2	Tuning in particles size.....	74
3.3.3	<i>In-situ</i> electrostatic polymer-polymer nanoassembly.....	75
3.3.4	Electrostatic polymer-metal nanoassembly.....	77
3.4	Fluorescent polymer nanoparticles .....	79
3.4.1	Dye-embedded fluorescent polymer nanoparticles .....	80
3.4.2	Dye-anchored fluorescent polymer nanoparticles .....	83
3.4.3	Dye-functionalized fluorescent polymer nanoparticles.....	83
3.5	Heterogeneous nanoassembly of the particles.....	86



---

3.5.1	Synthesis of Ag microrods .....	86
3.5.2	Electrostatic concept for nanoassembly .....	87
3.5.3	Formation of PMMA/Ag nanoassemblies.....	88
3.6	Flow assembling of polymer nanoparticles .....	90
3.6.1	Flower-sphere flow assembly.....	91
3.6.2	Sphere-sphere flow assembly .....	92
<b>4</b>	<b>Results and discussion-2: Polymer microparticles and their composition .....</b>	<b>97</b>
4.1	Microfluidic synthesis of polyTPGDA microparticles.....	97
4.1.1	Size tuned microparticles by surfactant and flow rate control .....	97
4.1.2	Droplets generation mechanism in microreactor.....	98
4.1.3	Monochromatic fluorescent microparticles .....	99
4.1.4	Mix-colored microparticles: color tuning in flow condition .....	100
4.1.5	Fluorescent hydrogel particles.....	105
4.2	Microfluidic synthesis of sensor particles for SERS sensing .....	106
4.2.1	Size-tuned composite hydrogel microparticles .....	106
4.2.2	Surface porosity of the sensor particles.....	108
4.2.3	Silver tuning in sensor particles for SERS sensing .....	108
4.2.4	SERS sensing application.....	112
4.3	Flow and sequential SERS measurement .....	116
4.3.1	Flow measurement concept and device arrangement.....	116
4.3.2	Sequential SERS measurements under flow conditions.....	117
<b>5</b>	<b>Conclusion .....</b>	<b>121</b>
<b>6</b>	<b>References.....</b>	<b>125</b>
<b>7</b>	<b>Appendix.....</b>	<b>141</b>
7.1	Chemicals .....	141
7.2	Abbreviations.....	143
7.3	Scientific publications .....	144
7.4	Curriculum vitae .....	147
7.5	Acknowledgement .....	148
7.6	Selbstständigkeitserklärung .....	151



# 1 Introduction

From photonic crystals to drug delivery vehicles, the particulate polymers have captured enormous attentions due to their multi-featured properties [1-3]. Homogeneity and reproducibility of the polymer particles are fundamental requirements for their uniform performances in various applications, for instance, the size-specific delivery vehicles for biomedical application [2]. In past two decades, many methods have been proposed and implemented successfully for producing the homogeneous polymer nano and microparticles. The synthesis methods of polymer particles, their responses against various stimuli, their surface and physicochemical properties, and various applications in the biomedical and optical fields are active topics for the current academic and industrial research. It is also of great interest to control the shape, assembly and composition together with diverse functionality of polymer nano and microparticles. By conventional methods, the architecture of the shape and assembly is difficult in minimum number of synthesis steps. To address the issue of homogeneity as well as hybrid assemblies with diverse functionalization, the microfluidic techniques are highly promising due to their unusual advantages such as fast heat transfer, short diffusion paths and efficient reactants mixing in the confined volumes [4-6]. Therefore, with progressive outlook in the direction of qualitative generation and to study the surface properties at nanoscale level for controlled composition, an optimized droplets-based microfluidic platform has been used here for producing the size, shape, morphology and composition tuned functional polymer nano and microparticles.

## 1.1 Polymer particles

Polymer particles (**Figure 1.1**), as referred to in this thesis, are solid, polymolecular objects that vary in size from about 10 nm to 1 mM. Such particles are dispersed in the aqueous or organic solvents and have a large number of important uses. The common polymer particles can mainly be prepared either by thermally or by photochemically induced polymerization techniques. Polymer is a soft material and therefore it is interesting for many bio-related applications. It also exhibits many noteworthy fundamental properties such as elasticity, high tensile strength, swellability, among the others that differentiate the polymeric network from substances composed of simpler molecules. In polymeric network, the stable covalent chemical bonds are formed between combining monomer units apart from the other processes, such as crystallization, in which the large number of atoms and molecules aggregates under the influence of weak intermolecular forces in selected facets. Particulate

polymer is generally a cross-linked network and adopts the appropriate shapes at minimized surface energy in the surrounding medium. At one hand, the shape organization of the polymer particles is promising phenomena for providing the wide range of complexity, diversity, unusual functionality and surface properties. And on other hand, the assembling and composition of polymer particles with heterogeneous and homogeneous materials building the nano and microstructures which combine the properties of two and more different domains.

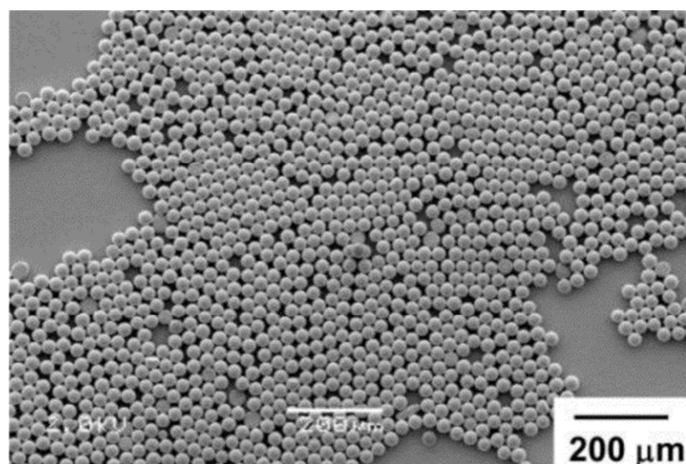


**Figure 1.1** Scanning electron microscope (SEM) image of the poly(lactic-co-glycolic acid) microparticles [7].

Generation of the polymer particles of different sizes can be realized by the emulsion, dispersion or suspension polymerization processes. Emulsion polymerization, in which monomers are dispersed in the aqueous phase, produces the monodispersed particles with a size range of 50-1000 nm. Emulsion can be obtained via water/oil, oil/water, water/oil/water or oil/water/oil systems by utilization of the charged surfactant in dispersion medium [8]. Oppositely, in dispersion polymerization, monomers are dissolved in the organic solvent and produces the particles (after evaporation of volatile solvent) with a size range of about 1-10 μm [9]. Beside these both fundamental processes, the suspension polymerization is a heterogeneous radical polymerization process produces the larger particles which usually derived directly from the droplet templates. Polymer particles of different length scale (multi-scale) can allow embedding and adsorbing many active molecular and particulate ingredients and displaying the wide range of physical, chemical and physicochemical properties [10, 11]. Some of the basic properties of the polymer particles are described below briefly.

## 1.2 Various properties and applications of polymer particles

Micro-droplets, capsules, microgels as well as micro and nanoparticles of polymeric materials are exhibiting wide range of physicochemical and surface properties. For example, thermoresponsive polymer colloids can be used for drug delivery and cancer therapy [12]. One of the great challenges is to develop the technique to deliver the efficacious drug at the site of action with high dose by minimizing off-target effects. Several effective drugs which are typically low molecular weighed and hydrophobic and are resultantly difficult, therefore, to administer intravenously due to poor solubility and clearance of the renal system [12]. To address such problems, if free drugs are encapsulated within the stimuli responsive polymer particles, the delivery can be effective at high rate of target uptakes. Usually, stimuli-responsive polymer particles as a drug-delivery vehicles display a sharp change in their properties when exposed to the external stimuli; for instances, a change in the solubility with temperature or pH parameters [13-15]. Thermoresponsive polymer particles display a non-linear relationship with temperature and the common property is that of solubility contrast to the properties of other materials [12]. Thermoresponsive materials become either soluble or non-soluble at a sharp transition temperature. The temperature is known as lower critical solution temperature (LCST) when transition is realized from a more soluble to a less soluble state. LCST decide the target effect because when temperature is raised above the LCST, phase separation is favorable over the dissolution due to the domination of entropic contribution (according to the Gibbs free energy equation). A brilliant example of thermoresponsive polymer particles is prepared of poly[(lactic acid)-co-(glycolic acid)] (PLGA) microparticles [7] coated with thermo-responsive poly-[(ethylene glycol methyl ether methacryl-ate)-co-(propylene glycol methacrylate)] [Poly(EGMEMA-co-PGMA)] random copolymers and were tested for the cell delivery and tissue engineering applications [16].

Beside the thermoresponsive effect, various types of physical, chemical, bio-related and multi-stimuli responsive polymeric particles and capsules are utilizing for the triggered and sustained release of active ingredients at targeted sites [2, 17, 18]. In general, deliverable cargos (drugs and therapeutic agents) can be loaded in the microparticles by emulsification, LBL assembly, coacervation and inertial phase separation methods among the others [19]. The functional and loaded microparticle image is shown in **Figure 1.2**.

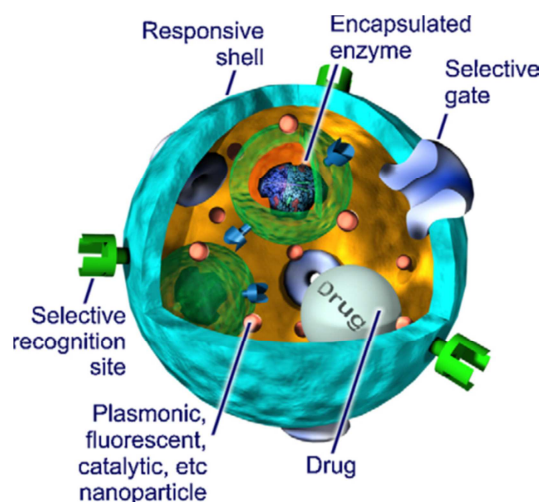


**Figure 1.2** A schematic illustration of the intelligent multifunctional ingredient-loaded particle [20].

On other hand, polymer particles exhibiting the surface wrinkling properties to provide the high surface area and surface textures to interact with various nano-objects [21-23]. It is of particular interest if polymer particles hollow framework can be prepared so that they can be utilized in photonic crystals [1]. Polymer microgel particles are used as absorbent and therefore can be applicable in many cosmetics products. Moreover, the swelling-shrinking profile of the microgel particles make them ideal candidates for many of the on-demand loading and release (like shutter) of various heterogeneous molecular and colloidal materials [24]. When fluorescence materials encapsulate or embed to the polymer particles, they can be excellent alternative of the semiconducting quantum dots and interestingly also applicable for biological systems due to their non-toxic nature [25]. The colloidal particle-based microscopic application is widely explored area. For example, fluorescent hard-sphere polymer colloids can be used in the confocal microscopy [26]. Various architectures such as, core/shell structure [27, 28], Janus like structure [29, 30] and assembly of polymer particles exhibits multi-domain properties and can be applied to the biomedical and nanotechnological applications [30, 31]. Probes, tags and sensors are ubiquitously demanding for detecting the trace amount of various compounds [32-36]. Therefore, wide range of polymer nano and microparticles can be generated for demanded sensoric applications. Moreover, due to the high surface to volume ratio of polymer colloidal particles provides broad coverage of sensing area and realizing strong outcome. Polymer particles can also be utilized as surface-enhanced Raman scattering substrates.

Besides all of these properties and applications listed here, there is persistent demand of the various types of polymer particles in other areas too.

### 1.3 Shape control of polymer nanoparticles

Shape and morphology controlled polymer nanoparticles are particularly increasing in many of the biological applications such as, in phagocytosis and targeted drug delivery [37-39]. Shape of the simple polymer nanoparticles can either be determined by minimization of interfacial area or by minimization of energy. Usually in such situation, the polymer particles adopt a standard spherical shape [40]. The shapes of the crystalline materials, on other hand, is directed by different crystal types, different crystal symmetries and the ratio of axis which leads to a considerable variability, for example, in case of the metal nanoparticles [41-44]. Thus, the shape controlled metallic nanoparticles can easily be obtained. In direct contrast, therefore, to tailor the shapes of polymer particles with homogeneous characters is complex process because of their amorphous or semi-crystalline nature with molecular flexibility. Many methods have been developed, however, to produce the non-spherical polymer particles [45-49]. Some of the model non-spherical polymer particles are shown in **Figure 1.3**. For instances, seeded emulsion polymerization forms the dumbbell-shaped particles and shape anisotropy can also be achieved by pH-triggered swelling and solvent evaporation procedures [46, 48], by template assisted self-assembly methods as well as via heterogeneous nucleation method [50, 51]. In addition, directed bonding between the closely approaching colloids also forms the stable assembled composed structures *via* oppositely charged interactions or by external electric field [52, 53]. But, all of these reported methods demand for the multi-step synthetic procedures to achieve the desired shapes. It is possible to achieve the desired shape, such as elliptical disks, rods, and plugs by shaping the device framework in one step process [54]. But, in those cases the polymer particles with non-spherical shapes are produced of micrometer length scale [49, 54]. There is a strong motivation and search for the production of shape controlled polymer nanoparticles in a minimum synthesis step (single-step process) with high reproducibility and homogeneity.

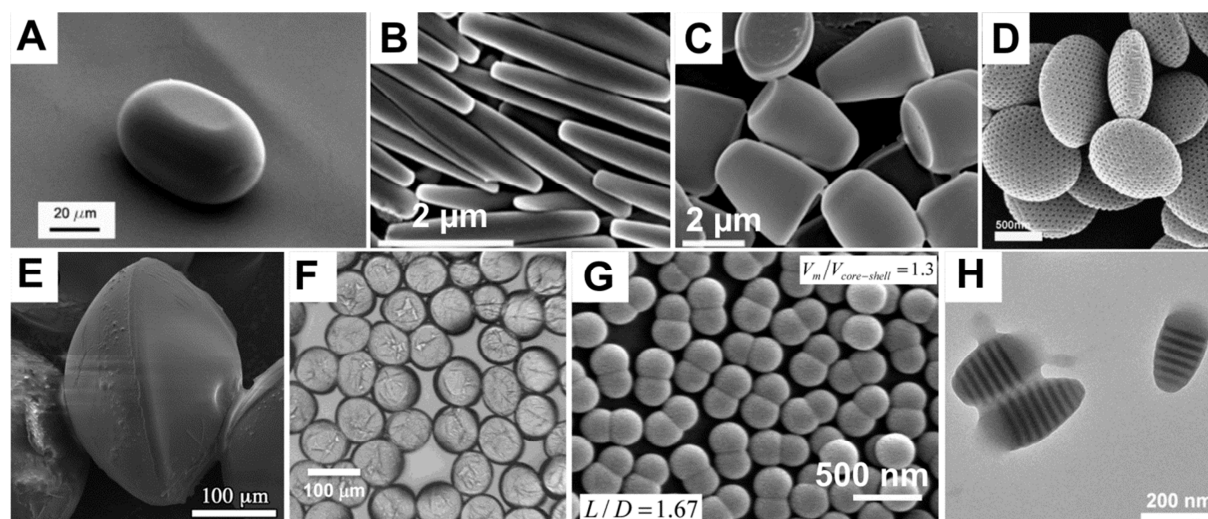


**Figure 1.3** SEM images of the various complex polymer particles; (A) plug-shaped polymer microparticles [54], (B) rectangular disks [37], (C) polymeric micro bullets [37], (D) polymer particles made up of block copolymer in which one domain has been removed by ozonation process [55], (E) rugby-like Janus particles [30], (F) polyuria microcapsules [56], (G) asymmetric dumbbell-shaped particles [57], (H) PS-b-PVP/PMMA Janus particles [58].

#### 1.4 Composition and assembly of polymer particles

Insulator polymer particles become conductive if they assembled with metallic materials such as silver nanoparticles [59]. Both components can be varied to a large extent: metal by formation of the alloys and different solid morphologies [60] and polymer by the monomers types and composition in case of copolymers [61]. Similarly, magnetic and fluorescence effect of the polymer particles can be realized after individual association of magnetic and fluorescence materials, respectively. Several other nanomaterials composition can be used for the electrochemical sensing and biomedical applications [62-65]. In general, the composite particles display combined properties of two or more different domains simultaneously [66, 67]. There are different methods for the formation of composite particles; by incorporating or encapsulating the metallic particles into polymer particles, by direct electrostatic interaction at the surface, by layer-by-layer (LBL) assembly process, by specific molecular coupling (for instance, DNA hybridization) or by secondary interaction (antigen-antibody binding). Hence the composite particles act as smart platform for multi-featured properties.

On other side, at nanometer length scale, the assembly of the small objects forms the building blocks for studying the effect similar to the colloidal molecules [68, 69]. The assembly of the identical entities provides shape variability and multi-functional characteristics. Moreover, the block-like domains can be obtained in a single object by the assembly of multi-



component systems. The broad variety of assembling process under the electrostatic environment able to produces multi-domain homogeneous and heterogeneous nanoassemblies if controlled surface interactions at nano level objects can be managed. There is a search for such phenomena to be observed and also for the generation of nanoassembly particles in a single-step process.

## **1.5 Particle-based fluorescence labeling**

Particle-based fluorescence labeling and molecular barcoding are the attractive technologies for detection processes in clinical diagnostics, micro toxicological screening, gene expression studies and micro droplet-based drug screening [39, 70-75]. Different types of fluorophores such as fluorescent dyes [76], quantum dots [77, 78] and plasmonic metal nanoparticles [79] are widely utilizing for detection techniques. Inorganic semiconducting quantum dots (Qdots) are generally used for the multiplexed targeted analysis, because it shows narrow tunable emission peaks and broad excitation bands during the light exposition [80]. However, due to the blinking nature and non-radiant dark fraction, Qdots are not appropriate candidates for many of the photonic applications [81]. Various methods and processes were developed to overcome these limitations [82-84], but several other issues such as toxicity (due to leaching of heavy metal ions) does not allow them for cell-sensitive biological applications.

On other side, polymer particles are non-toxic and suitable for biological systems too. Therefore, the fluorophore modified polymer particles, defined as the fluorescent polymer particles (Pdots), can be an ideal alternative of Qdots. Moreover, they can be easily prepared and exhibiting exceptionally bright and stable fluorescence together with availability of biocompatible and functionally active host polymer materials [85, 86]. Encapsulation of different types of hydrophobic and hydrophilic fluorescence dyes of different emission wavelengths to the polymer particles can produce the broad library of colored particles for multiplexed biological assays and probes. The probes made up of the free molecular dyes are not suitable because of the easy photo-bleaching for high-sensitive imaging techniques and also for the high-throughput assays [25, 87, 88]. Hence, the various types of dye-embedded and dye-anchored polymer nanoparticles are the ideal platforms for biological as well as microfluidic applications such as labeling and imaging [89, 90]. Besides the fluorescence labeling and probes, fluorescent polymer nanoparticles have many other applications, for instance, used as photonic crystal [91], used for confocal microscopy [26], for multiphoton fluorescence imaging [85], and so forth. Therefore, the homogeneity of the polymer

nanoparticles is key issue for the uniform performance. For the preparation, particles first swells in the dispersion solvent and embed the fluorophores (for instance, dye) [92] or the fluorophores can attach to the outer surface through electrostatic interaction [93]. In both cases, however, two or more steps are required to obtain the final product. It is highly demanding that the fluorescent polymer nanoparticles should be stable, homogeneous and monodispersed, and should obtain by minimum number of synthesis steps (one-step). And the motivation for such requirements is active research area for producing the size, shape and composition tuned fluorescent polymer particles of high quality.

### **1.6 Particle-based SERS sensing**

Normal blood lactate level is necessary for good health because elevated lactate levels can cause several diseases such as congestive heart failure and hypoxia [94]. It is therefore be useful to real-time detection of lactate for monitoring these medical conditions. The measurement can be performed by enzyme-mediated electrochemical methods and by using handheld lactate sensors. However, these methods are indirect and only reports on lactate concentration at discrete intervals. Surface-enhanced Raman spectroscopy (SERS) presents novel approach for real-time monitoring of lactate by direct measuring the vibrational spectrum of molecules [94]. Moreover, the trace amount (down to the sub- $\mu\text{M}$  range) of toxic substances in foods and biological systems can be detected by SERS platform. The local electromagnetic field around the roughened surface of metallic nanostructure enhance the Raman scattering outcome upon the irradiation of light [95]. The development, preparation and characterization of SERS-active substrates are one of the most important research areas in SERS [96]. Roughened silver electrodes with nanostructured features were used as SERS substrates in former time. There is an increasing interest for the fabrication of stable, reliable and reproducible particles-based SERS substrate for high enhancement factor of the SERS intensity. Here, in the presented work, the procedure for the preparation of particle-based SERS substrate is shown with their versatility for better performance to detect the lower range of concentrations of different analytes.

It is also a growing interest for sequential SERS measurements of the different analytes by using single SERS substrate. In this work, the microflow sequential measurement of different analytes by the flow condition with regeneration procedure is performed.

In general, all different types of size, shape, assembly and composition-tuned polymer nano- and microparticles (which are shown in Chapter 3 and Chapter 4) are produced in the microfluidic platform due to their fascinating advantages.

### **1.7 Why microfluidics is particularly promising for polymer particles?**

The production of polymer particles can be determined by two most convenient and reliable techniques within microfluidic devices: (a) the emulsification of liquid monomers by another immiscible fluid followed by the thermally initiated polymerization and (b) the direct polymerization of the generated droplets via photochemical solidification. Microfluidics deals with the manipulation of small fluids volumes (from  $10^{-9}$  to  $10^{-18}$  liter) using channels dimensions from tens to hundreds of micrometers [4, 97, 98]. The droplet generation in the microchannel is crucial parameter [99, 100] where the droplets diameters ranging from the hundreds of nanometer to tens of micrometer possess many active ingredients. An individual droplet acts as a nanoreactor in a continuous mode for the synthesis of functional nano and micro particulate materials. Moreover, microfluidics is an intrinsically interdisciplinary field of science that provides a potential platform to influence the subject area in physics, biology, chemistry, engineering, materials science, and nanotechnology [3, 4, 10, 101-104]. A considerable reduction of chemical consumption, predictable and fast heat/mass transfer rates, rapid mixing, short residence time distribution, decoupling between the reaction volumes and channel walls, and ability of performing complex chemical reaction in highly controlled manner makes a microfluidic platform very suitable for qualitative production of particulate polymers [6, 97, 105]. Droplets of aqueous solution or of the organic liquids with many ingredients are generated in the shear force of continuous flow in microchannel. Moreover, the wide range of size, shape and composition controlled polymer particles can be produced in the droplet-based microfluidic techniques as schematized in **Figure 1.4**.

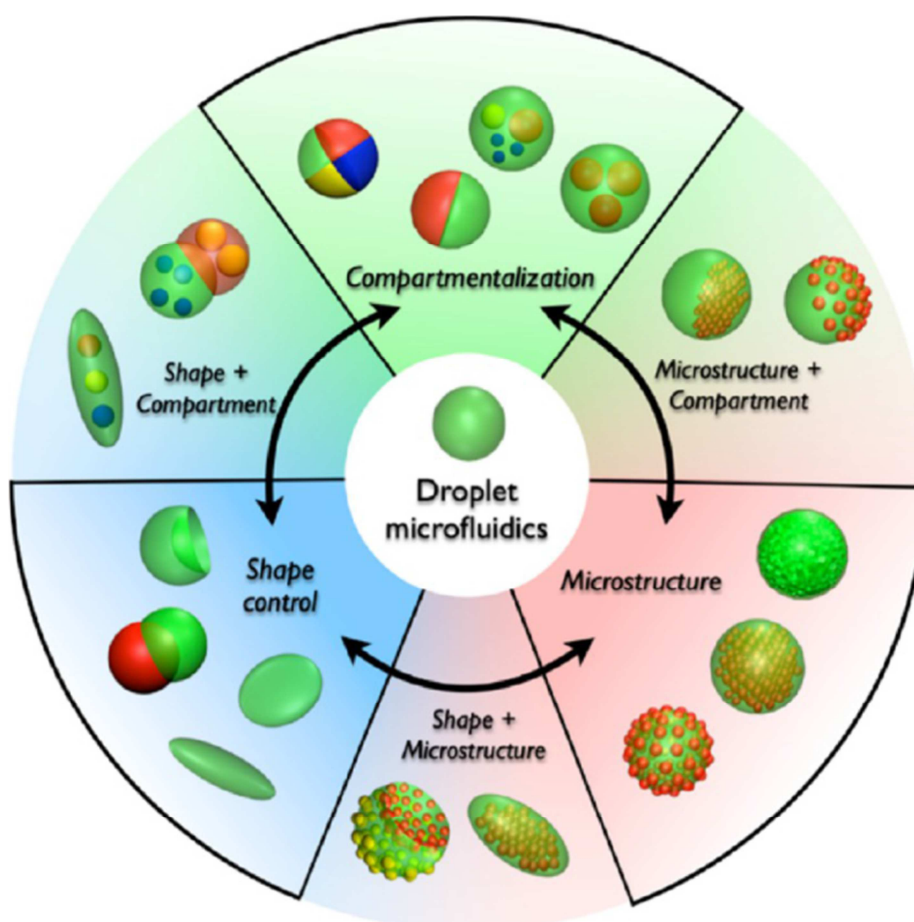


**Figure 1.4** Schematic of the shape and composition tuned functional microparticles classification can be prepared by the droplet microfluidic techniques [9].

A droplet is a heart in the microfluidic techniques. A single droplet contains all reactants in the small volume [106] and therefore their manipulation and stability is a crucial task [107]. The droplet compartmentalization, homogeneity, material synthesis and composition of heterogeneous materials are influenced by the device design [108-110].

## 1.8 Unique parameters of the microfluidic techniques

Some of the factors affecting the droplet generation mechanism and their stability are listed below which helps to produce highly homogeneous polymeric particulate products.

### Microfluidic device geometry

The formation, transport and stability of the droplets are important for the production of monodispersed polymeric and other particulates materials [111-113]. And on other hand, the appropriate devices for the formation of uniform droplets of different phases are required [8, 114, 115]. The semiconductor-related technologies (based on silicon materials) generally

fabricate the microfluidic devices of different types. Therefore, the lithographic procedure (for instance, mask lithography) are commonly used to etch silicon, glass or polydimethylsiloxane (PDMS) micro-channels [116]. The dispersed phase is driven in to the microchannel where it encounters the immiscible carrier liquid which is driven independently [117]. Geometry of the junction, where two immiscible fluids meet, together with physical properties (interfacial tension and viscosities) and different flow rates decide the local flow field which in turn deform the interface and eventually leads to drops pinch-off [117].

The prescribed droplets are generated by using three different device geometry types:

- (a) co-axial injection
- (b) cross-flowing stream
- (c) elongated strained flow

A device for the co-flow stream can be designed to a cylindrical glass tube where two streams flowing in a parallel direction near the nozzle and is aligned with a rectangular outer channel (as shown in **Figure 1.5 A**). Here, the drops or elongated jets can be formed at different flow rates of either of the fluid phase. Usually the drop formation is occurs at low carrier flow. A transition from the drops to jet can be realized when carrier flow velocity increases above the critical value [117]. Secondly, the cross-flow device (T-junction) can be arranged where two phases flowing through two orthogonal channels and forms the droplets when they meet at junction (**Figure 5.1 B**). Here, the droplets are pinched-off when the viscous shear stress overcomes the interfacial tension [117]. Droplets size can be controlled precisely by variation of individual flow rates as well as flow rate ratios in cross-flow device design. Third dominating microfluidic device is flow-focusing arrangement [118, 119] as shown in **Figure 5.1 C**. In the arrangement, a dispersed phase is slugged by two counter-flowing streams of the continuous fluid.

### **Different modes of the droplets**

Droplets are generally of  $\mu\text{m}$  length scale and the interfacial and viscous effects become dominate over the bulk forces here. Liquid drop formation is takes place when fluid instabilities can realized [120]. In the flow of two immiscible liquids, the inner or dispersed liquid become unstable due to the surface tension forces strive to minimize the surface area. And oppositely, a viscous force which suppress the growth of deformation and form the long fluid thread [120].

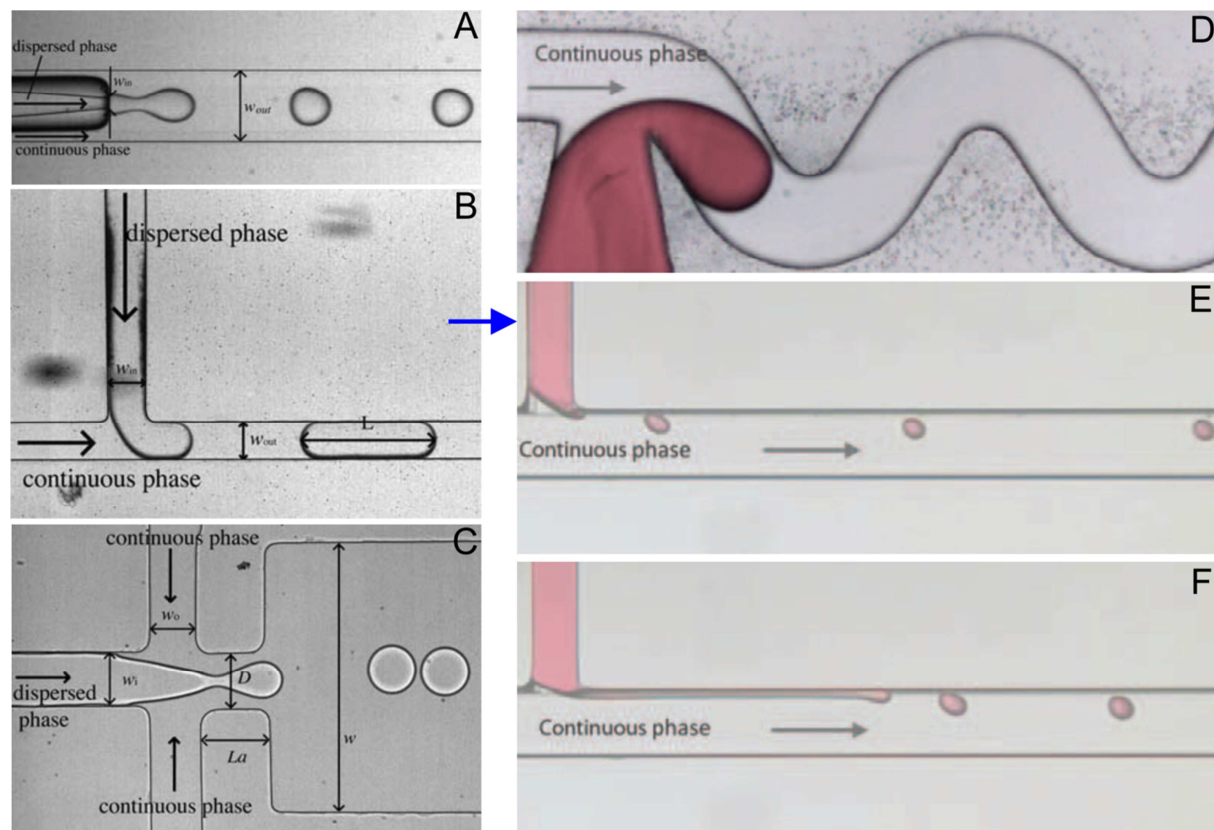


**Figure 1.5** Three different examples of the droplets production: (a) in a co-axial injection device, (b) in a T-junction device and (c) in a flow-focusing device [117]. Particularly in a T-junction device, three different modes of droplet formation: (d) squeezing regime, (e) dripping regime and (f) jetting regime [121].

For the production of size tuned droplets, three main regimes (dripping, jetting and squeezing modes) of the thread of dispersed phase is important. The simplest device geometry for droplet formation is a T-junction where dispersed phase is dosed perpendicular to the main carrier flow. An emerging droplet grows until it occupies nearly the whole cross-section of the channel and then breaks up due to the squeezing by the continuous phase at low flow rates and is usually known as a squeezing or slugging regime [111, 121]. On other hand, the droplets is formed earlier at higher flow rates due to the higher shear force and generally termed as dripping regimes. In this regime, the droplets are significantly smaller than the channel diameter. This mode of the droplets is therefore fascinating for easy further processing in the flow where no contact is taking places to the channel wall. Third important mode of the droplet formation is jetting regime where elongated thread of the dispersed phase is formed and the droplets are break up somewhere downstream [121]. The droplet formation regimes are shown in **Figure 1.5 (D-F)**.

**Fast phase and heat transfer**

In microfluidic technique, particularly in the segmented-flow process, a rapid mixing of various reactants is realized due to the small dimensions and substantial internal convection within a short time [122, 123]. The flow is laminar in a microchannel because of the high viscous force and interfacial effects, and the transition of laminar flow to the segmented flow is accompanied by the circulation of the fluid segments [6]. Moreover, the constant fluid motion causes a rapid mixing effect with fast phase transfer. Resultantly, the permanent convective mass transfer [124] is realized between the central and periphery parts of the fluid segment.

On other side, the rapid heat transfer can realize by the fluid segments in continuous flow process as the channel diameter is considerably small. Therefore, the micro-segmented flow is particularly suited for the implementation of rapid initiation of thermal activation [125]. Furthermore, the rapid cooling of the segments is also possible at critical reaction intermediate time.

**Short residence time distribution**

One of the most crucial demands in the microflow condition is the realization of narrow residence time distribution (RTD) [126, 127]. Time interval for the nucleation and therefore the growth of the particulate materials is depends on the range of RTD. Generally, the RTD is much larger during the reaction in conventional vessel. Moreover, even in miniaturized flow systems when laminar flow takes place, the larger RTD realized because of the parabolic velocity profile at low Reynolds numbers [6]. This problem of microfluidic can be overcome by application of the micro-segmented flow. The unique and narrow residence time is observed for all parts of the whole reaction volume because all fluid segments are moving with same velocity and passes through certain part of the microreactor at distinct time interval.

### **Controlled nucleation**

Two main phases, nucleation and growth, is obtained in the nanoparticles formation. The uniform growth is realized only when nucleation phase is homogeneous. Therefore, it is important to have a fast and homogeneous initiation of the nucleation phase of whole reaction volume. In the segmented flow, an efficient reaction mixing and fast phase transfer is attained in a small volume. Moreover, the required time is strongly connected with the segment size, their transport and flow rates. Therefore, the controlled and focused nucleation can be realized by fusion of segments, by injection into preformed segment, or by mixing during the segment formation [6]. In addition, the nucleation can also be initiated by physical activation in flow condition, such as by fast heat exchange (and also by rapid cooling), by focused photochemical activation, or by confocal excitation within extremely short residence time.

### **Synchronized growth**

A systematic, controlled and uniform growth is prerequisite for obtaining the high quality of particulate nanomaterials [121]. Similar to the nucleation phase (explained above), high homogeneous growth can be realized in segmented flow process. As segments are moving to the fluid, it is possible to apply changes at the intermediate stage between nucleation and growth phase for realizing the optimal synchronized growth conditions. This is particularly important when mixing steps is required after the nucleation phase for addition of other reactants, to change the pH and ionic strength, or addition of interfacial molecules [6].

### **Controlled particles assembling**

Particles of the crystalline or amorphous materials are formed by controlled aggregation of atomic species through weak intermolecular forces or by connection of small molecules through covalent bonding. Besides these both types, advantageously, the in-situ assembling of two or more particulate species can assembled in microfluidic flow conditions by geometric constraints to form the compact particles. These types of assembling are generally obtained due to the electrical surface properties (for instance, controlled polarization and electrostatic interactions). Segmented-flow technique provides the highly homogeneous reaction environment due to the efficient mixing and small channel dimensions.



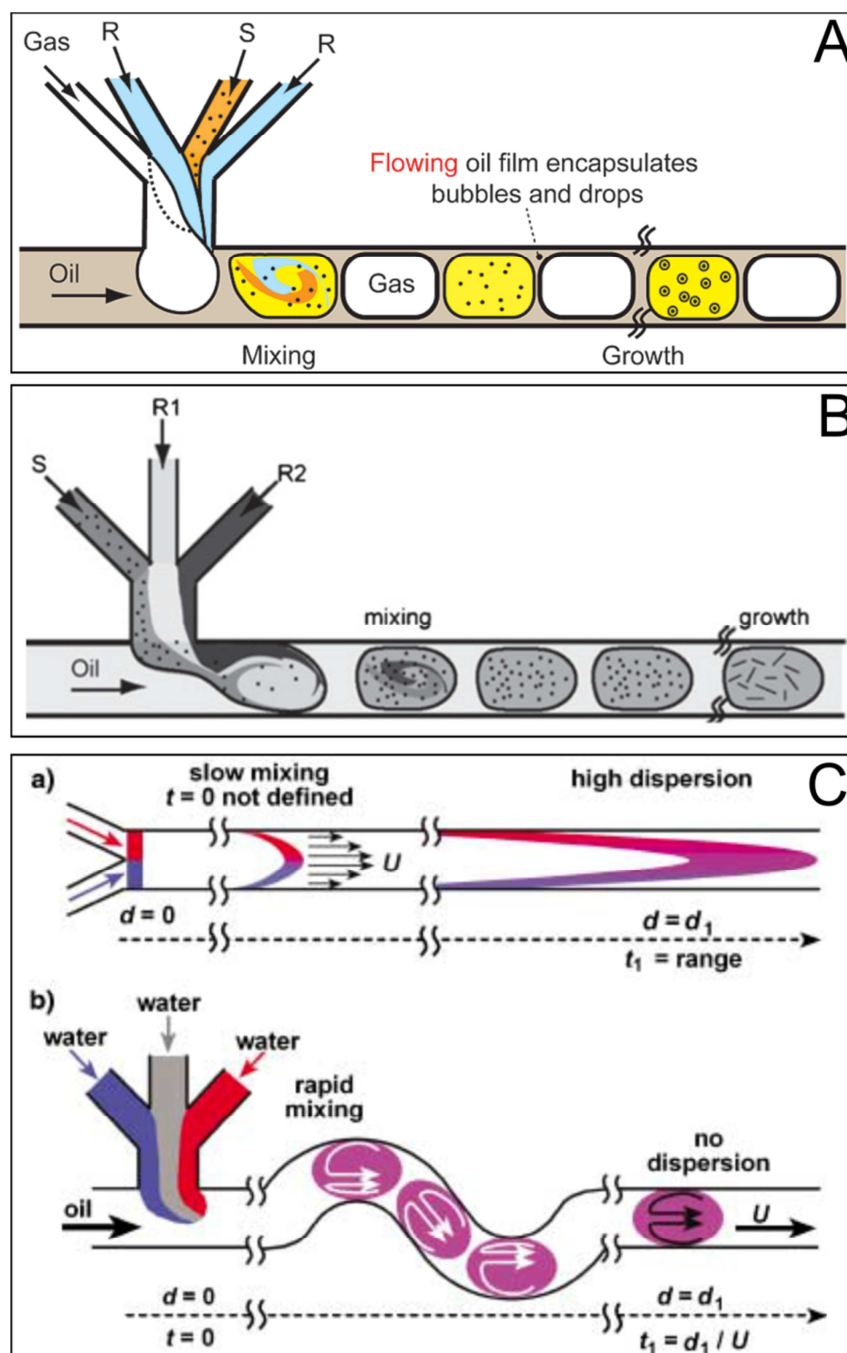


**Figure 1.6** (A) Two-dimensional schematic of the composite foam formation microfluidic arrangement [128]. (B) Schematic for the droplet-based synthesis of nanomaterials [129]. (C) Schematic comparison of a reaction conducted (a) in a standard pressure-driven microfluidic system device and (b) in the multi-phase T-junction microfluidic device [130].

Overall, the microfluidic techniques (some examples shown in **Figure 1.6**) are particularly beneficial over the conventional batch process because of their advantages such as, fast phase and heat transfer, efficient mixing, narrow residence time distribution and very homogeneous reaction environment in small volumes. Therefore, these techniques were successfully

applied for producing the high quality metal nanoparticles [59, 131-135], dielectric nanoparticles [136], metal oxide nanoparticles [125, 137, 138], semiconducting nanoparticles [134], different types of polymer particles [30, 116, 121, 139-144] and others nano and microstructures [145].

### 1.9 Challenges and central questions

The interpretation, formation and classification of the size, shape and composition tuned polymer nano and microparticles is a strong motivating research area for the industrial as well as academic understating. Moreover, the structure of complex polymer particles demonstrates the platform for studying the surface and physicochemical properties. As particulate polymers are fascinating materials, there are many difficulties and severe challenges for their production:

- Biological, optical and chemical outcome of the polymer particles (which are being utilized) should be extremely uniform. Such uniform consequences depend on the size homogeneity and monodispersity of the polymer particles. The production of highly homogeneous and systematic size-tuning of polymer particles is a real challenge. There should be some developed technology available to address such concern by providing extremely homogeneous reaction environment.
- In current time, there is growing interest for the shape-controlled polymer nanoparticles synthesis. Polymer is an amorphous or semi-crystalline material. In order to minimize the interfacial energy, nanoparticles generally adopt the spherical shapes. Hence, to control the shape at nanometer length scale in a single-step process is a real challenge. There is strong need for such suitable reaction strategy for *in-situ* core assembling to form the compact (non-spherical) polymer nanoparticles.
- Association of polymer nanoparticles with heterogeneous or homogeneous particulate materials forms the assembly particles and combines the properties of two different domains. An absolute challenge is to control the assembly interaction at the surface of nanoparticles without uncontrolled aggregation. There is a requirement of the defined strategy for precisely regulate the surface potential of oppositely charged particles.

- Fluorescent polymer nanoparticles are non-toxic and therefore suitable for the *in-vivo* applications. To tune the size, surface charge and fluorescence properties of the polymer particles in a single-step process is an actual challenge. There should be some strategy required where fluorophores can be linked inside the matrix interior, at the surface as well as after layer-by-layer controlled functionalization of the polymer nanoparticles.
- Fluorescent polymer microparticles are useful for barcoding and labeling applications. Size parameter is controllable, but the controlled mixing of individual and mixed-colored fluorophores together with size-tuning is a challenging task. There is platform needed where single-step process can produce the size as well as color tuned polymer microparticles.
- Usually, the formation of polymer nanoparticles with shell-like surface layer is at least more than one-step process. The formation of such nanoparticles with monodispersed size tunability is a real challenge. There should be one of the excellent techniques available for production of multi-phase polymer nanoparticles in a single-step process.
- Polymer-based sensor particles can be used as excellent SERS substrate for detecting the trace amount of biochemical and organic compounds. Smaller size and highly porous surface are key parameters of the sensor particle. Size, porosity and composition of the particles should be realized in a synchronized manner. There should be suitable platform required for the production of ideal sensor particles.
- If single sensing particle can detect the multiple-analytes in a single experiment is an important perspective. To obtain the extremely consistent and harmonized SERS signals of alternative analytes with identical sensor particles is strong motivation. There should be distinct arrangement and quality of sensor particles needed for the sequential and flow SERS sensing measurement.

### 1.10 Aim and objective

As explained in all above sections, the applications of polymeric particles are ubiquitous. The production of high quality polymer particles with well-defined size, size distribution, shape-architecture, surface functionalization and their assembly becomes increasingly important for various uses ranging from drug-delivery vehicles to label particles in screening applications. The microfluidic techniques are highly promising not only for size-controlled factor but also for the shape tuning, in-situ assembling, surface architecture and synchronized approach due to their excellent parameters such as, fast phase transfer, efficient mixing and narrow residence time distribution. Resultantly, it allows the production of high quality (simple to complex) polymer particles.

The aim of this work is to investigate how microfluidics can be used for the production of multi-scale (from several tens of nanometer up to higher micrometer) polymer particles of different shapes, assembly, morphology and composition together with additional functionality (such as fluorescence) and surface architectures. Consequently, this research should follow the tasks listed below:

- Selection of an appropriate example of the microfluidic technique
- Optimization of the cross-flow microfluidic platform
- Surface functionalization process of the microreactor chip for production of the precise sized droplets
- Investigation of the effect of flow rates, flow rate ratios, temperature and reactants composition for the production of size-tuned polymer (PMMA) nanoparticles via emulsion polymerization reaction in microfluidic platform
- Production of various shape-controlled polymer nanoparticles (ellipsoidal, dumbbell, linear, branched and flower-shaped) in cross-flow microfluidic platform
- Production of size-tuned layered polymer nanoparticles and their nanoassembly with smaller polymer and metal nanoparticles
- Development of different strategies for the formation of various types of fluorescent polymer nanoparticles
- Production of size and color tuned polyTPGDA microparticles in a single-step microfluidic reaction for fluorescence labeling application

- Synthesis of noble metal/polymer nanoparticles assemblies
- Batch (ex-situ), in-situ and flow assembly of the size and shape controlled polymer nanoparticles
- Synthesis of sensor particles (polyacrylamide/silver microgel) in microfluidic arrangement for SERS sensing applications
- Investigation of microflow and sequential SERS sensing measurements of various analytes in the compact SERS arrangement by use of composite sensor particles
- Characterization of all types of polymer particles (multi-scale) by SEM, zeta potential measurement, DLS, fluorescence spectroscopy and microscopy, UV/vis spectroscopy and surface-enhanced Raman scattering (SERS)



## 2 Materials and methods

### 2.1 Microfluidic systems for the synthesis of polymer particles

All different kinds of size, shape, and composition tuned polymer nano and microparticles were prepared in the cross-flow microfluidic arrangement. The microreactor should be precisely designed and modified, because it is playing pivotal role for the uniform generation of polymer particles. For this aim, different experimental set-ups with certain modification of microreactor were developed which will be described in detail below.

#### **Microfluidic system A: for emulsification of two immiscible fluids to obtain polymer nanoparticles**

The formation of homogeneous polymer nanoparticles of different sizes and shapes is obtained when accurate emulsification of liquid monomer droplets was realized by another immiscible liquid fluid. For the same, an emulsifying micro-device is fabricated by lithographic means.

##### **2.1.1 Fabrication of the microreactor device**

The silicon (Si) nozzle array was lithographically fabricated previously [61] as shown in **Figure 2.1**. For the preparation, a photolithographic procedure using an optical mask aligner (Suess) and a dry etching process (RIE) for the micro-patterning of the mask layer was applied. A  $\text{Si}_3\text{N}_4$  films has been applied on the two-sided polished silicon (100) wafer by a physical enhanced chemical vapor deposition (PE-CVD) process [61]. In a double-side photolithographic procedure, these films act as etch mask layers. Later, at the front side, a small etch windows were generated with specific diameter and distance of the prospective pores of an array. Similarly, a large window with a size of the fluid interconnection was generated at the back side. A central part of this window was aligned to the center of the pore array on a front side. The pyramidal shape of pores on the back side was generated by a time-controlled execution of anisotropic crystallographic wet etching process which forms a silicon membrane at the bottom. Multi cycles of the anisotropic reactive ion etching process were applied by which the pores of the array with smaller diameter were realized. The lithographic process was uniformly performed and hence, the pores of the array were obtained with high homogeneity (**Figure 2.1 c1**). After cleaning, the Si-chip was placed inside the two walls of chamber (micro-channel assembly) in the position where continuous aqueous phase is flowing over the front side of the chip. The width of the capillary slit of

about 0.2 mm was adjusted between the both surfaces of channel walls. Monomer droplets were generated through a dripping mode at T-junction by a flowing high sheared continuous aqueous phase. The Si membrane ( $1 \times 2.6 \text{ mm}^2$ , thickness) carrying the array was placed on a rectangular shaped chamber with sloped side walls inside the Si chip with an outer size of  $1.6 \times 3.3 \text{ mm}^2$ . For generation of the spherical, ellipsoidal, dumbbell-like, branched, flower-shaped, and shell-like surface layered polymer nanoparticles; a same microfluidic setup has been used with variation in different reactants during the synthesis of different types of polymer nanoparticles.

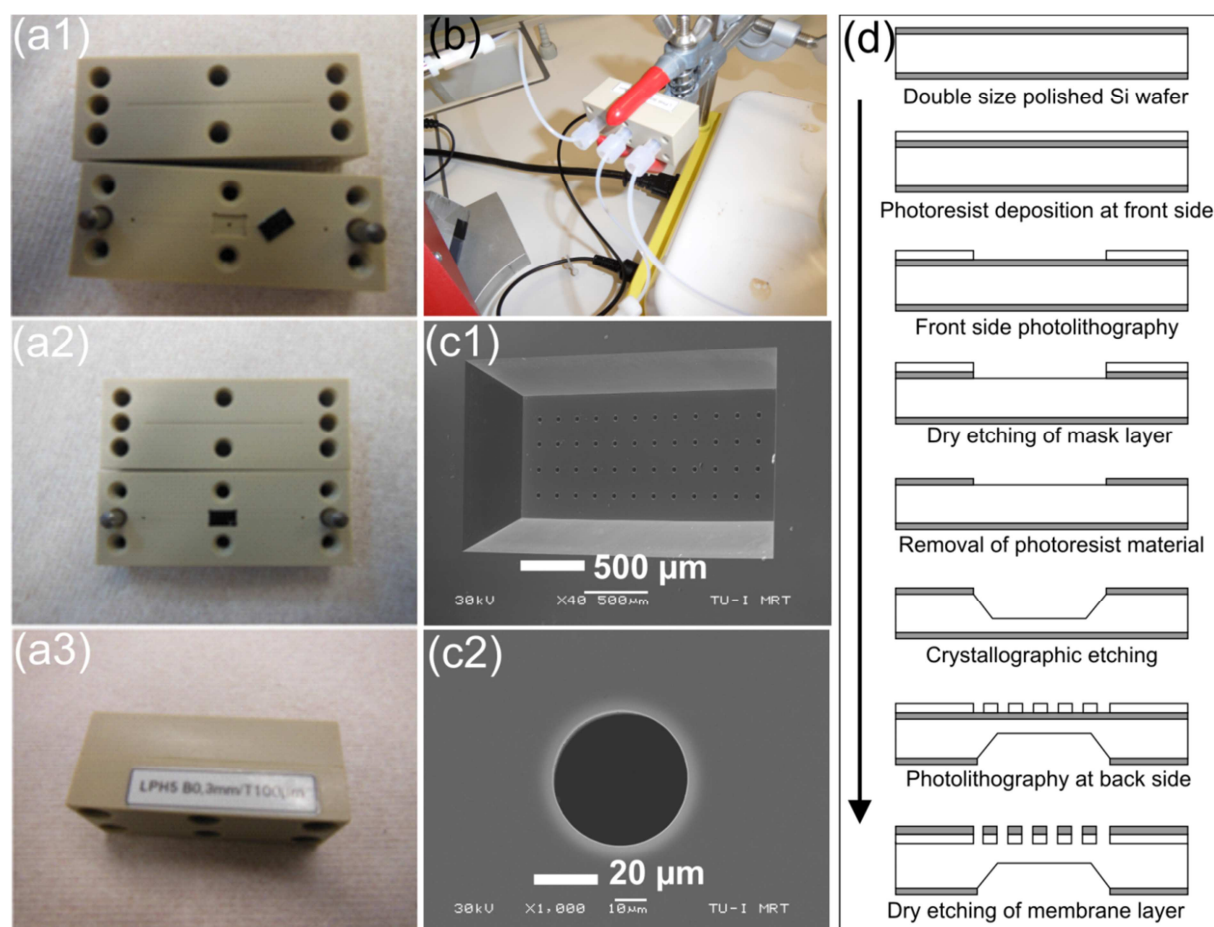


**Figure 2.1** Microreactor constructions: (a1-a3) Camera pictures of the microreactor with integrated micro holeplate chip, (b) camera picture of an integrated microreactor with three fluid ports (cross-section), SEM pictures of the micro-holeplate chips with silicon membrane with (c1)  $16 \times 48$  lithographically etched micro-holes (hole diameter:  $20 \mu\text{m}$ ) and (c2) a single micro-hole (hole diameter:  $40 \mu\text{m}$ ), and (d) schematic for the microlithography process for preparation of the nozzle array (micro holeplate) [61].



### 2.1.2 Silicon holeplate-based cross-flow microfluidic arrangement

A complete microfluidic arrangement (shown in **Figure 2.2**) made up of two online-monitored syringe pumps for actuation of two immiscible liquids, a microreactor, heating block, liquid carrying nozzles, and a collection tube. The emulsifying micro-device contained a main channel with a symmetrically arranged inlet and outlet for aqueous liquid and the formed emulsion. The central part of this main channel is covered by a silicon nozzle array which supplying monomer phase to form the emulsion of two immiscible liquid phases in presence of interfacial stabilizing agent in aqueous solution. The droplets of monomer liquid are generated by a shear force of streaming continuous aqueous phase at T-junction.

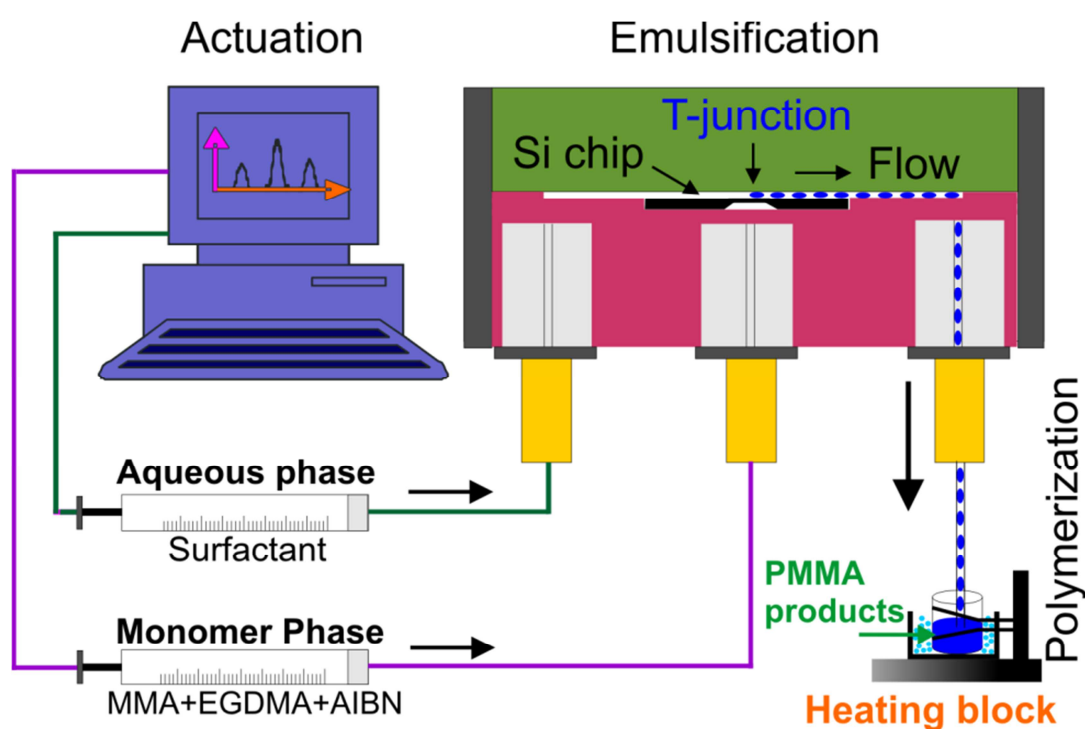


**Figure 2.2** Schematic of microfluidic setup for synthesis of size and shape controlled polymer nanoparticles. Precise sized droplets generate at T-junction where continuous phase meets monomer phase between the two walls of the Si chip-embedded microreactor.

#### Microfluidic system B: for obtaining mix-colored fluorescent polymer microparticles for labeling applications

A Si microchip with single hole of different size (between 40  $\mu\text{m}$  and 160  $\mu\text{m}$ ) was used in the cross-flow microreactor for production of precise sized micro droplets to form the polyTPGDA microparticles via continuous flow photochemical polymerization process. The carrier phase was made up of the aqueous solution with different types of the surfactants and

the monomer phase is a mixer of polymerizing functional material (monomer, photoinitiator, cross-linker and fluorescence dye). An irradiation source (mercury lamp) is provided at the output end of the micro nozzle. Moreover, for tuned mixing of two as well as four different kinds of fluorescence dyes prior to the generation of monomer droplets at T-junction, the Y-shaped connector (**Figure 2.3 b**) and multi-fold (**Figure 2.3 c**) has been attached to the main microreactor, respectively.

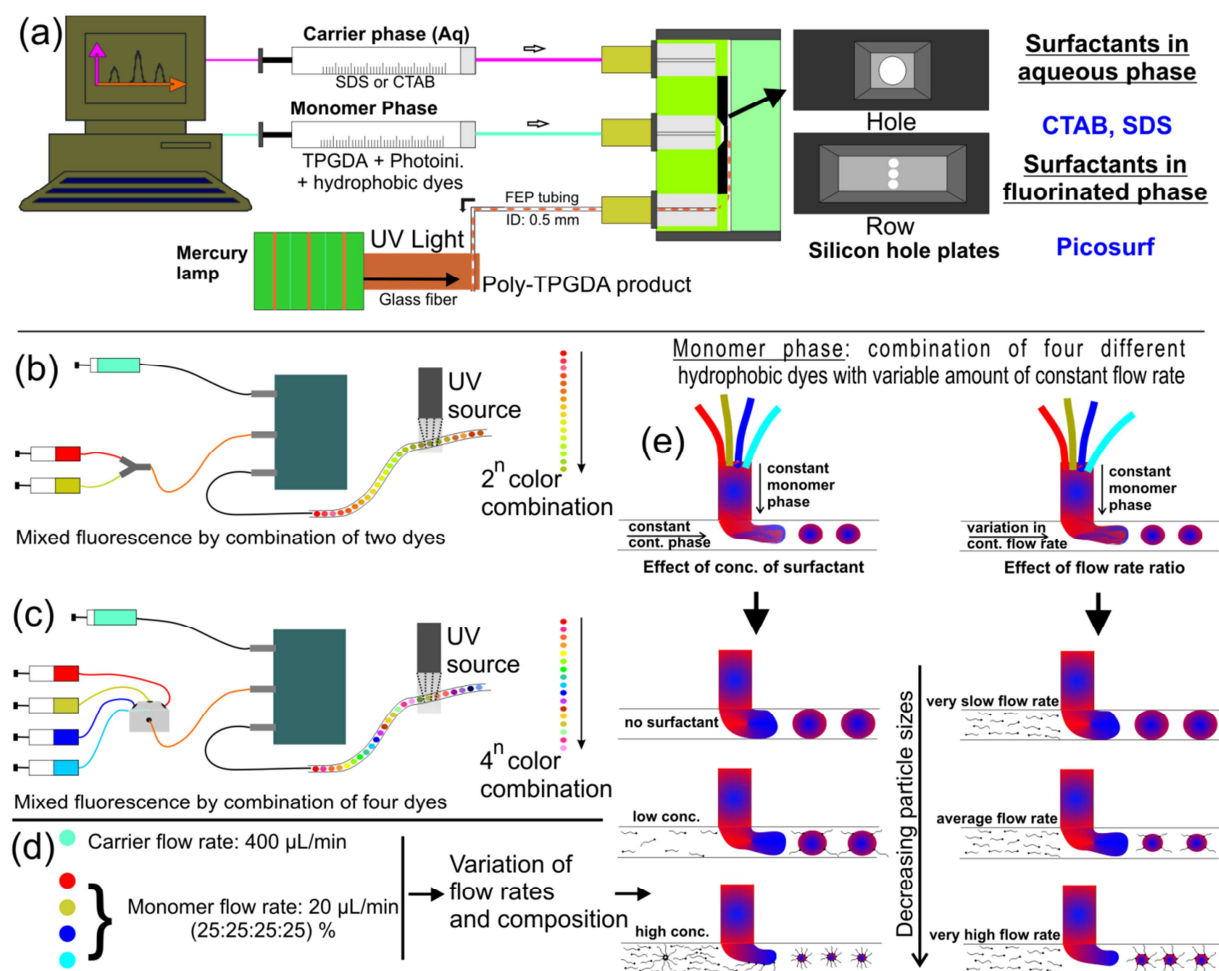


**Figure 2.3** (a) Schematic of the microfluidic set-up for the synthesis of polyTPGDA microparticles, (b) and (c) are the schematic of the microreactor arrangement where tuned and programmed combination of two and four dyes in the monomer phase takes place respectively to obtain the microparticles with a tuned composition of fluorophore, (d) flow rate variation program, and (e) a scheme for the droplet tuning mechanism which depends on the surfactant and flow rate variation parameters.

### Microfluidic system C: for obtaining composite microgel sensor particles for SERS sensing

For production of sensoric hydrogel particles, a similar kind of cross-flow microfluidic arrangement has been used after surface modification of Si microchip. Here, the monomer phase is aqueous solution, and therefore, the surface of the microchip should be non-aqueous for generating the homogeneous droplets. The aqueous phase is a fluorinated solution (Novec 7500). Hence, silanization process (described below) is performed to make the surface of the Si microchip fluoro-compatible. A complete arrangement of microfluidic set is shown in **Figure 2.4**.

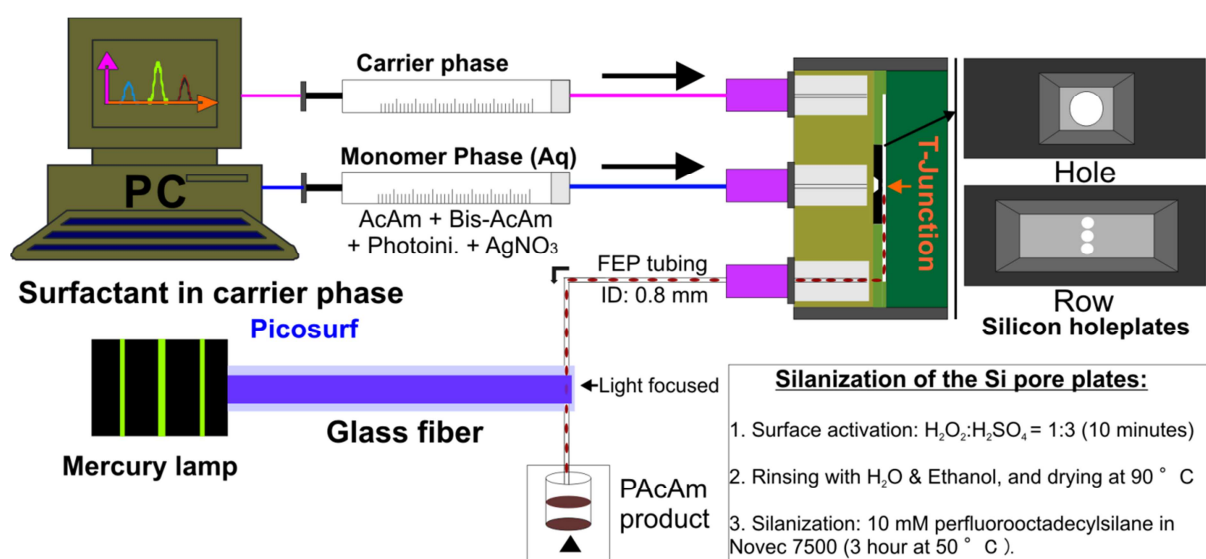


**Figure 2.4** Schematic of microfluidic arrangement for the synthesis of silver/polyacrylamide composite microparticles.

#### 2.1.3 Silanization of Si microchip

A Si micro holeplate chip of 40  $\mu\text{m}$  hole diameter has been poured inside the  $\text{H}_2\text{O}_2:\text{H}_2\text{SO}_4$  (1:3) solution for about 10 min for the purpose of surface activation. With this step, the surface of a chip becomes more hydrophilic with excessive hydroxyl functional groups. The Si chip then rinsed with double distilled water and successively with ethanol several times. The Si chip has been placed, afterwards, inside a heating oven at 90  $^\circ\text{C}$  for drying. In next step, one droplet (10  $\mu\text{L}$ ) of Novec 7500 and then 20  $\mu\text{L}$  of perfluorooctadecylsilane were applied on the chip surface. The silanization reaction kept running for about 5 hours at 50  $^\circ\text{C}$ . Finally, the chip was rinsed with Novec 7500 and placed inside the microreactor chamber for

droplet generation of monomer solution at T-junction in a cross-flow microfluidic arrangement as shown in **Figure 2.4**.

### Microfluidic system D: Flow SERS measurement system

A compact SERS arrangement (**Figure 2.5 a**) has been designed for investigating the SERS sensing effect of the sensor particles in batch as well as in flow condition.

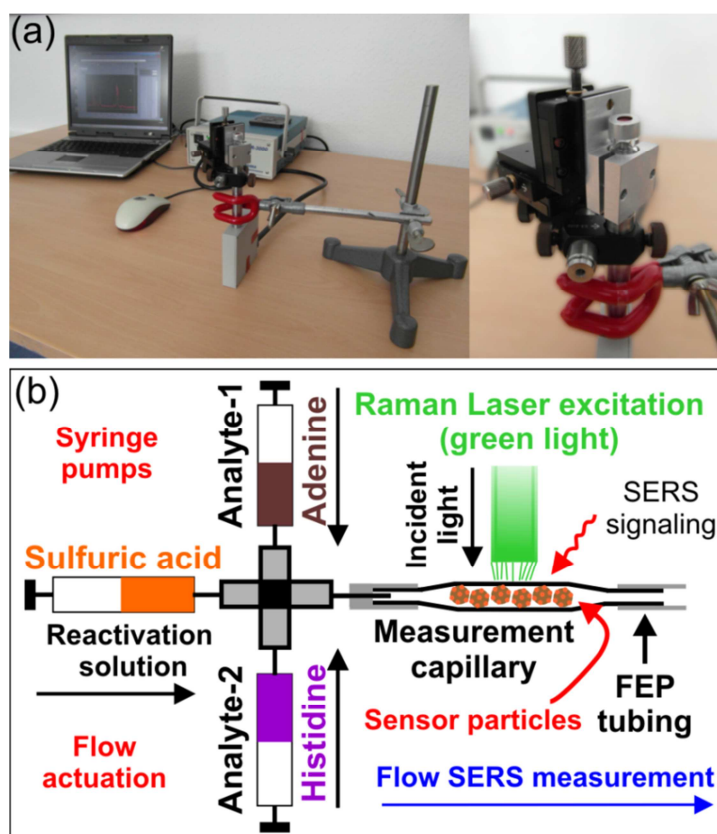


**Figure 2.5** (a) is a compact arrangement for SERS measurement and (b) is the schematic of microflow arrangement for in-situ SERS measurement using composite microgel sensor particles by interaction with different analytes in continuous flow.

For the flow SERS measurement, a set of sensor particles (about 10 particles) was filled in the glass capillary. The glass capillary was then connected to the silicon tube for actuation of analyte solution. Three syringe pumps carrying two different analyte solutions (for instances, adenine and histidine) and a regeneration solution (diluted sulfuric acid) are arranged to the cross-connection shown in **Figure 2.5 b**. The light focus is arranged at the center of glass capillary where sensor particles are placed. The online-monitored constant flow of different solution has been applied to the sensor particles for recording the flow SERS spectra in the series at an interval of 0.5 second integration time. Here, the Raman system (R-3000) with

green laser (532 nm excitation laser source) and 50 mW laser power has been used for SERS measurement.

### Microfluidic system E: Flow assembling of the polymer nanoparticles

At precise surface interactions to form the nanoassembly of antagonistically charged shape and size tuned polymer nanoparticles were performed in the flow condition by varying different parameters such as, temperature, flow rate, residence time, length of knot mixer, and particles concentrations. Mixing of the two different types of particles suspension were obtained by the continuous (**Figure 2.6 a**) and segmented flow (**Figure 2.6 b**) arrangement. The purpose for the flow assembly is to provide highly homogeneous reaction environment for regular interactions of the oppositely charged nanoparticles at reduced volume. Syringe pumps (TSE systems, [www.tse-systems.com](http://www.tse-systems.com)) were used for the fluid actuation of immiscible liquids separately. FEP (fluorinated ethylene propylene) tubes with an internal diameter (ID) of 0.5 mM and 1 mM were used for the fluid transport and for realizing the residence loop.

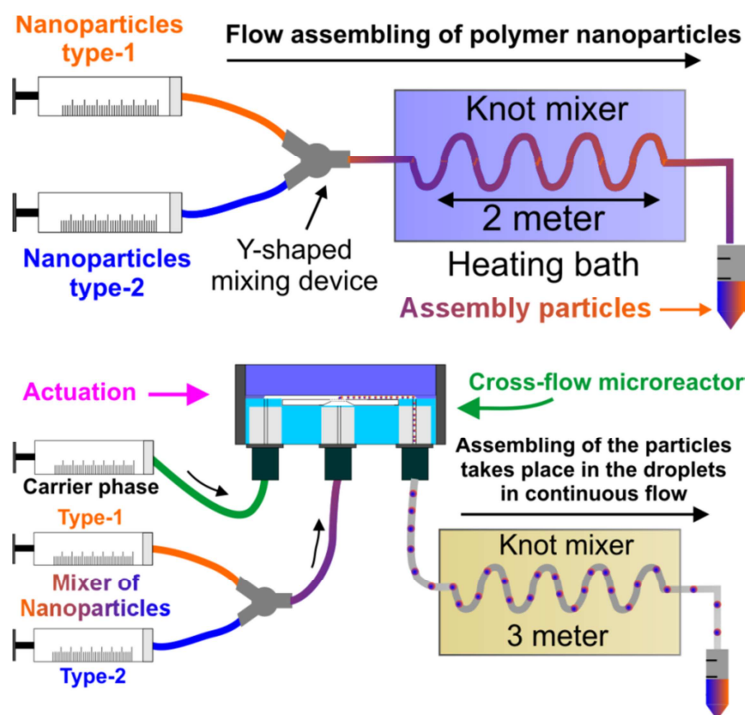


**Figure 2.6** Flow arrangement used for the assembling of size and shape controlled polymer nanoparticles.

## 2.2 Particles synthesis

### 2.2.1 Spherical polymer nanoparticles

A silicon (Si) holeplate-based cross-flow microfluidic reactor was used for the synthesis of size-controlled poly(methyl methacrylate) (PMMA) spherical nanoparticles. An aqueous phase is guided through a capillary slit in perpendicular direction to the monomer flow. To prepare the solution of aqueous phase, 18 mg of anionic surfactant sodium dodecyl sulfonate (SDS) dissolved in 50 mL of deionized water. For different experiments, the concentration of SDS has been varied from 1 mM down to 0.1  $\mu$ M. The aqueous solution of SDS has been filled up in a glass syringe and fixed to the syringe pump for actuation. Meanwhile for the preparation of monomer (dispersed) phase, 10  $\mu$ L (1 %) of ethylene glycol dimethacrylate (EGDMA) cross-linker and 3.5 mg thermal initiator azobisisobutyronitrile (AIBN) has been dissolved in 990  $\mu$ L of methyl methacrylate (MMA) monomer liquid. Formation of the emulsion from two immiscible liquid phases started at cross-point of microreactor (shown in **Figure 2.2**) where monomer mixture meets a streaming aqueous phase of surfactant. The emulsion solution was collected in a heated tube for completion of the polymerization reaction. Temperature of the heating block for polymerization reaction has been set out 97 °C. Size-controlled PMMA nanoparticles of sizes between 110 nm and 500 nm (negatively charged) were obtained at the end of polymerization reaction, and were washed and dried for further use. Similarly, the positively charged polymer nanoparticles of size range between 70 nm and 350 nm were obtained when different concentration of cetyl trimethylammonium bromide (CTAB) has been used in the aqueous phase.

### 2.2.2 Non-spherical polymer nanoparticles synthesis

Similar microfluidic setup (as shown in **Figure 2.2**) has been used for the synthesis of shape-controlled polymer nanoparticles. The role of interfacial agents (surfactants or polyelectrolytes) is dominating for deciding the shape of nanoparticles. Especially for obtaining the size-tuned ellipsoidal and dumbbell shaped polymer nanoparticles, poly(4-styrenesulfonic acid-co-maleic acid) sodium salt (PSS-co-PM) with different concentrations between 0.01 mM and 0.5 mM (repeating unit concentration) were used in the aqueous phase. On other hand, for obtaining linear (with high aspect ratio) and branched polymer nanoparticles, the role of poly(sodium-p-styrenesulfonate) (PSSS) is crucial. Therefore, different concentrations (between 0.05 mM and 20 mM, repeating unit concentration) of PSSS of three different molecular weight (70 kDa, 500 kDa and 1000 kDa) were used in the

continuous aqueous phase. To obtain the flower-shaped polymer nanoparticles, various concentrations between 0.5 mM and 10 mM (repeating unit concentration) of four different molecular weighed non-ionic polymer polyvinylpyrrolidone (PVP) (10 kDa, 25 kDa, 40 kDa and 55 kDa) were used in continuous aqueous phase. Monomer phase (1 mL) is a mixture of 990  $\mu$ L MMA, 10  $\mu$ L (1 %) EGDMA and 3.5 mg AIBN. Polymerization temperature of the heating block (collection tube) has been set to the 97 °C. Different flow rate ratios of the two immiscible phases were applied to obtain the size (length and width) controlled polymer nanoparticles of different shapes.

### **2.2.3 Synthesis of layered polymer nanoparticles and their nanoassembly**

A distinct in-situ copolymerization approach has been applied here for producing the shell-like surface layered PMMA nanoparticles (PMMA-polyDADMAC). Two antagonize liquid phases interact at the T-junction of microreactor (as shown in **Figure 2.2**) where aqueous phase is made up of different concentrations of hydrophilic monomer diallyldimethyl ammonium chloride (DADMAC) and dispersed phase is the mixture of 990  $\mu$ L MMA, 10  $\mu$ L EGDMA and 3.5 mg AIBN (hydrophobic monomer solution). Polymerization reaction has been performed at 95 °C.

In a second step, controlled amount of additional emulsified solution (aqueous phase: different concentration of SDS and monomer phase: mixture of MMA, EGDMA and AIBN) inserted to the particles suspension for in-situ formation of size tuned spherical nanoparticles in the polyDADMAC shell interior of preformed nanoparticles during the swelling phase via electrostatic interaction. Moreover, in another experiment, citrate-stabilized gold (Au) nanoparticles were electrostatically binds on the surface of polymer particles with increasing concentration ratio. And in the last step, for realizing the obtained particles for SERS sensing, the additional silver (Ag) enhancement was applied via metal-catalyzed metal nanoparticles synthesis on the surface by different concentrations of silver salt and ascorbic acid.

### **2.2.4 Fluorescent polymer nanoparticles**

The emulsion polymerization process in the proposed microfluidic setup is performed for obtaining the fluorescent polymer nanoparticles of different types.

At first, for non-covalent distribution of dye doped polymer nanoparticles, 0.1 mg Nile red (fluorescence dye) or 12-(7-Nitrobenzofuran-4-ylamino)dodecanoic acid (Nbfd) dye was dissolved in 1 mL of monomer mixture (MMA, EGDMA and AIBN). Similar to the above

procedure of particles synthesis, red (Nile red embedded) and yellow (NBFD embedded) colored nanoparticles were obtained after completion of polymerization reaction at 97 °C.

At second, for obtaining the covalent linking of fluorescence dye doped polymer nanoparticles, the MMA molecules have been pre-functionalized with suitable fluorophore (5-Methyl-2-(pyridin-2-yl)thiazol-4-yl methacrylate) prior to the polymerization process and then the polymerization reaction has been performed at 97 °C.

At third, a selective fluorophore (Titan yellow) is playing triple role at same time to control the particles size, their surface charge and fluorescence intensity at different concentration in aqueous phase. 34.5 mg of Titan yellow dissolved in 50 mL of deionized water (1 mM) and has been filled up this solution in a glass syringe which served as the continuous phase. Different concentrations of Titan yellow between 1 µm to 1 mM were used for tuning the nanoparticles diameter between 80 nm and 200 nm.

And in last type, the surface functionalization approach via covalent, electrostatic and secondary interactions has been performed for making the entire polymer network a fluorescently active. Firstly, 1 mg of poly-L-glutamic acid (PGA) was dissolved in 1 mL of PBS buffer solution (pH 7.4). Then, 1 hour incubation reaction at moderate stirring condition keep running after centrifuged PMMA nanoparticles were dispersed in PGA solution (electrostatic interaction). In next step, 1 mg of poly-L-lysine (PLL) was dissolved in 1 mL of PBS buffer solution (pH 7.4) in a separate vial. PGA covered PMMA nanoparticles were re-dispersed (after repeatedly washing process) in PLL solution and again a moderate stirring have been applied during the incubation for 1 hour (electrostatic interaction). Later, the nanoparticles were re-dispersed in 1 mL of NHS-biotin solution which is also prepared in PBS buffer solution (covalent interaction). And in a last step, PBS buffer solution of fluorescence dye-labelled streptavidin was added to the collection tube which contained PLL covered PMMA nanoparticles (secondary interaction, streptavidin-biotin). Blue colored nanoparticles were obtained which have been characterized by fluorescence measurements.



**Table 2.1** Reactants in carrier and dispersed phase for obtaining different types of polymer nanoparticles.

Polymer nanoparticles type	Carrier (aqueous) phase	Dispersed phase
Spherical	CTAB, CTAC and SDS	MMA, EGDMA and AIBN
Ellipsoidal, dumbbell, rodlike, necklacelike	PSSS, PSS-co-PM and PAES	
Linear and branched shaped	PSSS	
Flower-shaped	PVP	
Hydrophilic shell layered hydrophobic nanoparticles	DADMAC and poly-DADMAC	
Fluorescent polymer nanoparticles	CTAB, SDS and Titan yellow	MMA, EGDMA, AIBN and various hydrophobic dyes

### 2.2.5 Synthesis of heterogeneous nanoassembly

The synthesis of PMMA/Ag nanoassembly has been performed in a batch reaction. Components, Ag microrods and PMMA nanoparticles, were separately synthesized in a batch and a microflow process (section 2.2.1), respectively.

#### 2.2.5.1 Synthesis of Ag microrods of tuned aspect ratio

In a first step, the solution (60  $\mu$ L) of AgNO<sub>3</sub> (0.25 M, in ethylene glycol) was added quickly into 5 mL preheated ethylene glycol (EG) under vigorous stirring at 160 °C. Afterward, 60  $\mu$ L of PVP solution in EG (0.35 M related to the repeating unit, molar weight: 25 kDa) was added. In last step, EG solution of 20  $\mu$ L of ascorbic acid (experiments with different concentrations between 10 mM and 1 M) were inserted quickly after PVP addition. All three reactants (3 mL AgNO<sub>3</sub>, 3 mL PVP, and 1 mL ascorbic acid) were added drop-wise within 7 minutes. The formation of Ag microrods of tuned aspect ratio was obtained at different reaction conditions.

#### 2.2.5.2 Synthesis of PMMA/Ag assembly particles

A batch synthesis of composite particles was performed at room temperature as well as at elevated temperature. In a typical experiment for synthesis of PMMA/Ag composite particles, 20  $\mu$ g PMMA dried particles were dispersed in 500  $\mu$ L deionized water. Afterward, the PMMA suspension was added to the 1 mL suspension of Ag microrods solution, which

contains 80  $\mu\text{g}$  of dried Ag microrods. After the reaction mixture was heated at 90  $^{\circ}\text{C}$  under continuously stirring condition for 30 min, it was cooled down to room temperature. For investigating the binding interaction in assembly of two oppositely charged particles, the reaction time was changed from 5 min up to 2 hours. A reaction has been performed under very dilute condition to avoid the undesired and random inter-particles aggregations.

### 2.2.6 Flow assembling of size and shape controlled polymer nanoparticles

Two different types of oppositely charged polymer nanoparticles were filled in two different glass syringes. Later, by actuating the syringe pumps with defined flow rates, the electrostatic assembling of the two antagonistically charged particles were takes place in a microreactor (as shown in **Figure 2.6**). The continuous flow of mixed particles is travel through a knot mixer of 2 m long FEP tube which is poured in the heating water bath where temperature of bath has been varied for different batch of reactions between 50  $^{\circ}\text{C}$  and 95  $^{\circ}\text{C}$ . For flower-sphere controlled assembly, 1 mL of diluted suspension of negatively charged flower nanoparticles has been filled in a syringe and another syringe was filled with equally diluted 1 mL of positively charged spherical particles suspension. At 40  $\mu\text{L}/\text{min}$  flow rate, the product is then collected in a collection tube which is arranged at output end of flow tubing (**Figure 2.6**). Similarly for sphere-sphere assembly, two different sized and different surface-charged polymer nanoparticles were actuated in flow arrangement.

### 2.2.7 Size and color tuned polyTPGDA microparticles synthesis

#### 2.2.7.1 Synthesis of monochromatic microparticles (size-tuned)

In the cross-flow microfluidic arrangement as shown in **Figure 2.3**, the carrier aqueous phase is made up of the different concentrations of SDS and CTAB (1 mM, 3 mM and 5 mM), and a dispersed phase contains the mixture of hydrophobic fluorescence dye (different dyes in different experiments), monomer, cross-linker and photo-initiator. For the dispersed phase, 40  $\mu\text{L}$  of 2-hydroxy-2-methylpropiophenone (photoinitiator) and 1 mg of hydrophobic dye (Nile red) were dissolved in 2 mL of tripropylene glycol diacrylate (TPGDA). Both liquid phases loaded glass syringes were connected to the microreactor where the Si chip was placed inside the chamber (diameter of the hole is 40  $\mu\text{m}$ ). The UV irradiation zone was settled at an output end of the micro nozzle. The online-monitored syringe pumps program were started to actuate the individual carrier and disperse phase for generating the droplets of precise sizes at appropriate flow rate ratio. Monomer droplets were generated at the T-

junction of a microreactor which subsequently polymerized and the monochromatic particles were formed under the exposition of UV light.

### 2.2.7.2 Synthesis of mixed and multi-colored microparticles

Two different dyes (Nile red and 12-(7-Nitrobenzofuran-4-ylamino)dodecanoic acid (Nbfd)) were dissolved separately in the monomer solution (1 mg each in 2 mL monomer solution). For obtaining the particles with identical size and different color-composition, total actuation of monomer flow rate was 50  $\mu\text{L}/\text{min}$ . Similarly, four different dyes (Nile red, Nbfd, Sudan Black B, and Reichardt's dye) were used for the tuning of the particles colors with individually different concentration and also for tuning of the composition with four different colors. In this case also, the total monomer flow rate was 50  $\mu\text{L}/\text{min}$ . For variation of the color composition such as, 25:10:10:5 ( $\mu\text{L}$ ) and 15:10:10:15 ( $\mu\text{L}$ ) and so on, the flow rate programs for the monomer phase were changed in order to get mixed color composition in the obtained microparticles. On other hand, an aqueous carrier phase was replaced by the fluorinated phase for the extension of the addressed size range of particles from 40  $\mu\text{m}$  up to 500  $\mu\text{m}$ . With gradually varying the picosurf (surfactant) concentration in carrier phase, the particles size can be tuned in a wide range.

### 2.2.8 Polyacrylamide/silver composite sensor microparticles

#### 2.2.8.1 Microfluidic synthesis of Ag-embedded polyacrylamide particles

**Figure 2.4** represents the microfluidic setup for obtaining the hydrogel microparticles where carrier phase is a fluorinated liquid (Novec 7500) and dispersed phase is an aqueous monomer solution. Carrier phase made up of the fluorinated surfactant 'picoSurf' dissolved in the Novec 7500 (300  $\mu\text{L}$  of 5 % picosurf in 10 mL Novec 7500). Aqueous monomer phase contains the mixture of silver salt, monomer, cross-linker and photo-initiator. 0.6 g of Acrylamide: Bis-acrylamide (19:1) was dissolved in 2 mL of de-ionized water. 23.8 g silver nitrate ( $\text{AgNO}_3$ ) was added to the monomer phase. 16  $\mu\text{L}$  of 2-Hydroxy-2-methylpropiophenone (HMPP) (photoinitiator) in 24  $\mu\text{L}$  ethylene glycol was added sequentially to the monomer solution for initiation of photopolymerization as well as photoreduction simultaneously. Both syringes were connected with lithographically prepared microreactor with two successive orifices for entries. A silanized Si chip placed inside the microreactor chamber (diameter of the hole is 40  $\mu\text{m}$ ). The mercury lamp applied for UV source at the output end of micronozzle which carrying the droplet-embedded continuous

flow. Residence time of the droplets under UV ray in photochemical reaction station is about 0.5 s. After formation of particles, the carrier solution was decanted from the collection tube. Then, particles were repeatedly washed by ethanol and by deionized water several times to remove the impurities. The color of particles was yellow due to the in-situ formation of Ag nanoparticles inside the microgel particles during photopolymerization. Further Ag enforcement was applied on the surface of Ag embedded polyacrylamide microgel particles in a following step.

In another experiment, for obtaining Au-embedded hydrogel microparticles, separately synthesized citrate-capped Au nanoparticles were dispersed in the monomer phase and photopolymerization reaction was performed in same microfluidic setup (**Figure 2.4**). Moreover for the synthesis of monochromatic and mixed-colored fluorescent hydrogel particles, different hydrophilic fluorophores (fluorescence dyes) were dissolved in the monomer phase, and controlled flow rate variation program has been applied.

### **2.2.8.2 Procedure for Ag enforcement in sensoric hydrogel particles**

The embedded Ag nanoparticles in the polyacrylamide microparticles initiates the further enforcement of Ag nanoparticles at the surface (through pores) via Ag catalyzed Ag nanoparticles synthesis. Therefore to process this reaction, 50  $\mu\text{L}$  of 5 mM ascorbic acid solution was added to the microgel suspension (also further experiments with different concentrations of ascorbic acid). In the following step, 50  $\mu\text{L}$  of 10 mM  $\text{AgNO}_3$  solution was inserted. Immediately, the color of the matrix turns to brown or black which indicates the formation of additional Ag nanoparticles on the surface of microgel particles. Different concentrations of  $\text{AgNO}_3$  were applied for tuning the density of Ag nanoparticles on the surface uniformly. Ag enforcement was characterized by SEM and optical microscope imaging. In further experiments, different analytes were applied to the composite particles for SERS measurements.

**Table 2.2** Reactants in carrier and dispersed phase for obtaining different types of polymer microparticles.

<b>Polymer microparticles type</b>	<b>Carrier phase</b>	<b>Dispersed phase</b>
Polyacrylamide/silver composite microparticles	Picosurf in Novec 7500 and PP9	Acrylamide, photoinitiator, and AgNO <sub>3</sub>
Polyacrylamide/gold composite microparticles	Picosurf in Novec 7500	Acrylamide, photoinitiator, and 20 nm sized gold nanoparticles suspension
Colour-tuned polyTPGDA microparticles	Picosurf in Novec 7500 and CTAB or SDS in water	TPGDA, photoinitiator and various hydrophobic dyes
Polymer nanoparticles embedded polyacrylamide microparticles	Picosurf in Novec 7500	Acrylamide, photoinitiator, and CTAB covered polymer nanoparticles
Fluorescent hydrogel particles	Picosurf in Novec 7500 and PP9	Acrylamide, photoinitiator, different fluorescence dyes

## 2.3 Characterization

In this section, a brief description of different characterization techniques is given to illustrate the obtained particulate products. Optical microscopy and electron microscopy were used for the size and shape controlled polymer nano and microparticles images. UV-vis and fluorescence spectroscopy are used for the absorption and emission spectra of the metallic and fluorescent nanoparticles, respectively. Dynamic light scattering and zeta potential measurements were utilized for the investigation of particles size and surface charge, respectively. The scattering enhancement factor of the sensor particles after interaction with different analytes was investigated by surface-enhanced Raman spectroscopy. The brief theoretical description of all such techniques used in this thesis is given below.

### 2.3.1 Scanning electron microscopy (SEM)

Scanning electron microscope is a type of electron microscope that produces the image of sample surface by scanning it with a high-energy electron beam in a vacuum chamber. When electron beam strikes the material (sample) which is to be identified, the electrons interact with atoms in the sample and emit various signals that contain information about the surface topography and composition [146]. Usually, the electron beam propagating from a tungsten filament which possess energy in the range from 0.5 keV to 40 keV. In the SEM, the resolution of sample can be achieved up to or better than 1 nm. The most commonly used signals are secondary electron (SE), the back scattered electron (BSE) and X-rays. The imaging mode collects low-energy SE (<50 eV) that are ejected by an inelastic scattering interaction with beam electrons [146]. These electrons originate within a few nanometers from the sample surface due to their low energy. The SE signal contains essential information on the morphology and topography of the samples. The BSE consist of high-energy electrons originating in the electron beam that are reflected by elastic scattering interactions with specimen atoms. Moreover, the BSE signal is most valuable for illustrating the contrasts in composition in multiphase samples. For elemental analysis, the characteristic X-rays are generally used. It is necessary to have a solid phase of the material which is being analyzed by SEM. The SEM also can produce images with high spatial resolution and therefore, the closely spaced features can be examined at high magnification.

For the particles characterization (size, shape and morphology) in this thesis, FE-SEM (Hitachi S-4800) and SEM (JEOL JSM-6380) instruments were used. All different kinds of size, shape and composition-tuned polymer nano and microparticles were washed several

times with deionized water with repeated centrifugation and re-dispersion process for the preparation of samples for SEM investigation. One drop of particles suspension was deposited on silicon chip (5 x 5 mM) and dried at room temperature until evaporation of water naturally. To cover the surface of polymer particles, a gold-palladium sputtering has been applied for 1 minute and then the SEM chip brought into the vacuum chamber of electron microscope.

### **2.3.2 Sputter coater**

For covering the polymer particles surface with conductive layer, the Balzers SCD 004 (sputter coater) instrument was used. The sample (polymer particles which are fixed to the Si chip) is first placed in the chamber of the instrument. The vacuum switch is then pressed for creating the vacuum up to  $5 \times 10^{-2}$  mbar in the chamber where sample is located. Afterward, for applying the conduction beam to cover the soft surface of the polymer particles, a time has been set out to about 80 s. Finally, the current (22 mA) applied for a given time, and later the pressure released slowly to remove the sample which is being characterized in the SEM.

### **2.3.3 Dynamic light scattering (DLS)**

The process of dynamic light scattering (DLS) perform the size measurement of the particles by measuring the Brownian motion in the solution. The process is working by illuminating the particles with laser light and analyzing the intensity fluctuation in the scattered light [147]. In general, when a particle is illuminated by a laser, the scattering of the light from a particle will observe in all directions as particles are smaller than the light wavelength. If more than one particle (tens of thousands) is dispersed in the solution, the screen which is kept close to the particles showing a speckle pattern of the scattered light in the form of bright and dark areas. The diffracted light from all of the particles can either interfere constructively (bright areas) or destructively (dark areas). The scattered light by the particles at bright areas are observed at the screen with a same propagation phase and interferes constructively, whereas the phase addition are mutually destructive at the dark areas and cancelling each other at the end [147]. This process is repeated at short time intervals and the resulting set of speckle patterns (which consist of bright and dark areas) are analyzed by an auto correlator that compares the intensity of scattered light at each spot over time.

In a solution, the suspended particles cannot be stationary because they moving constantly due to the Brownian motion. The Brownian motion is the movement of particles due to the

random collision with molecules of the liquid at the surrounding of particles. For DLS, a Brownian motion has unique characteristic where larger particles move slowly and smaller particles move quickly. It is now clear that the DLS instrument (here it is Zetasizer Malvern) measures the fluctuation in scattering intensity and uses this to measure the mean size of the particles in solution. If larger particles are being measured (which are moving slowly), the fluctuation in the intensity of speckle pattern is slower. Likewise, if smaller particles are being measured then, the fluctuation of intensity is quick because the particles motion is rapid. In a DLS process, the particles size can be measured by intensity, volume and number distribution.

To measure the particles size in the solution, DLS spectra were obtained from the Zetasizer nano zs (Malvern) instrument at about 1/50 dilution of original particles suspension. Diluted suspension of the polymer particles were filled in a transparent cuvette and the average size of the particles were measured.

### **2.3.4 Zeta potential measurements**

By determining the electrophoretic mobility (which is obtained by measuring the particles velocity) and applying Henry equation, the zeta potential (electrochemical potential) of the particles can be calculated. In the solution, two regions exist; an inner region also called as Stern layer where ions are strongly attached and an outer layer where the diffusion of ions takes place and is weakly attached [148]. Hence, electrical charged double layer exists around each particle in the solution. Due to gravity, particles are moving together with the charges surrounded to them. However, in the outer layer, only ions which are close to the particles surface are moving with particles, and there is a certain boundary beyond which the ions are not moving, called slipping plane. The zeta potential is triggered by the net electrical charge surrounded within the region bounded by the slipping plane (boundary of electrical double layer), and also depends on the location of that plane. The particles in suspension with higher zeta potential are stable. Usually, the particles with zeta potential higher than  $\pm 30$  mV in respective direction are considered as stable. A value of pH is also playing major role in zeta potential measurement, because the particles with negative surface ions showing more negative zeta potential upon addition of alkaline solution to the particles suspension. Upon the applied electric field, the electrical charges on particles surface showing certain effects which are collectively defined as electrokinetic effects, and they covers mainly electrophoresis and electroosmosis. The ions on the particles surface suspended in electrolyte



can move towards the opposite charged electrode when electric field is applied. At the equilibrium point between electrical force and viscous force (which oppose the movement of charged particles in solution), the particles move with constant velocity, and such velocity of a particle in an electric field is defined as its electrophoretic mobility. Moreover, the zeta potential can be calculated by application of Henry equation (given below) [148].

$$U_E = \frac{2 \cdot \epsilon \cdot z \cdot f(ka)}{3 \cdot \eta} \quad (2.1)$$

Where  $z$  is the zeta potential,  $U_E$  is an electrophoretic mobility,  $\epsilon$  is the dielectric constant,  $\eta$  is viscosity, and  $f(ka)$  is the function of Henry's equation.

In this thesis, zeta potential of all kinds of size, shape and morphology tuned polymeric and metallic particles were measured in Zetasizer nano zs (Malvern) instrument. All samples were prepared for zeta potential measurements with about 1/30 dilution in 1 mM sodium chloride (NaCl) solution. Particles were washed with deionized water six times for removing impurities prior to the measurements. Suspension of the particles was filled in a transparent Zetasizer cell for the measurements.

### 2.3.5 Fluorescence spectroscopy

The fluorescence spectrometer contains three basic items: a source of light, a sample holder and a detector. Tungsten-halogen lamp or a mercury lamp is generally used as a light source, and photomultiplier tubes are used as detectors.

In principle, a hot body emit the radiations due to heat. All other forms of the light emission are called luminescence where system loses energy (it is a form of cold body radiation). For continuous emission, some form of external energy must be supplied from elsewhere (IR, visible or UV light). Under the light illumination, electrons of the detecting materials absorbs the energy in form of photons (packets of energy) and get excited from ground state to singlet and further unstable state. Immediately, the unstable electrons return (relaxation) to the stable state and emit the excess energy or photons. This process of relaxation is called fluorescence which is takes place very rapidly in  $10^{-5}$  sec. or less [149]. Fluorescence is a type of luminescence, and is taking place in atoms or molecules. The fluorescence quantum yield ( $\Phi$ ) is depends upon the absorption and emission amounts of the light. Therefore,  $\Phi$  is defined as:

$$\text{Fluorescence quantum yield, } \Phi = \frac{\text{No. of photons emitted}}{\text{No. of photons absorbed}} \quad (2.2)$$

It is necessary to assume that the radiant energy can only be absorbed in definite units or quanta. The energy  $E$  carried by any one quantum is proportional to its frequency of oscillation. Therefore,

$$E = h\nu = \frac{hc}{\lambda} \quad (2.3)$$

Where,  $\nu$  is frequency,  $\lambda$  is related wavelength and  $h$  is the plank's constant ( $6.624 \times 10^{-27}$  erg/sec).

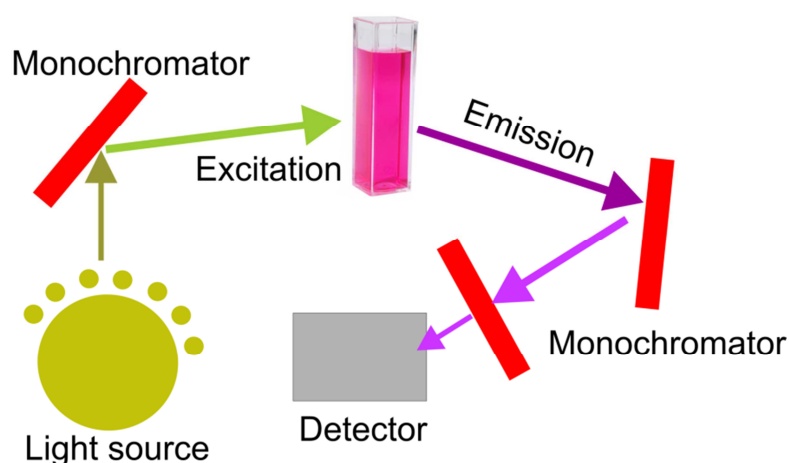


**Figure 2.7** Schematic principle of the fluorescence spectroscopy (according to [149]).

Here, for the measurement of wavelength-resolved fluorescence spectra of all kinds of fluorescent polymer nanoparticles and microparticles, a PerkinElmer spectrofluorometer has been used. The water suspension of different sized dye-doped polymer particles have been filled in a transparent cuvette of 1 cm path length and the spectra were recorded at different concentrations of particles suspension. The fluorescence spectra were obtained at 100 nm per 4 second speed.

### 2.3.6 Optical microscopy

An optical microscope, particularly fluorescence microscope is based on the phenomenon where certain fluorescent material emits energy (photons) detectable as visible light when irradiated with the light of a specific wavelength supplied by the external source. The fluorescence microscope is generally used to capture the images of materials such as fluorescent particles. The sample being analyzed can either be fluorescing in its natural form like chlorophyll, or treated with fluorescence materials such as dyes. The fluorescence microscope is capable of revealing the presence of a single molecule. By using the multiple

fluorescence labeling, several of targeted molecules can simultaneously be identified. A bright light source, generally a mercury lamp, producing the correct wavelengths for excitation of system is also required for fluorescence microscopy. **Figure 2.8** represents the basic arrangement of a fluorescence microscope.

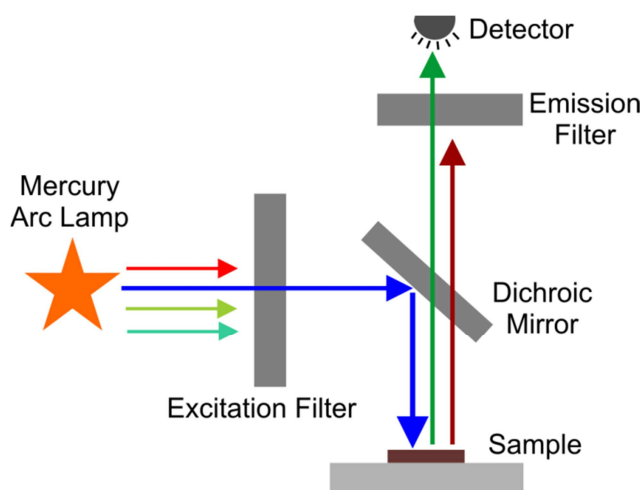


**Figure 2.8** Schematic arrangement of fluorescence microscope (according to [150]).

In this work, a fluorescence microscope (Axioplan 2 imaging, Zeiss) with photo camera (SONY, model number: SLT-A37) was used for recording optical images of all kinds of monochromatic as well as mixed colored polymer microparticles and composite particles. The particles were deposited on the cover glass slide and brought them under the light focus of the microscope.

### 2.3.7 UV-visible spectroscopy

UV-vis spectroscopy (also called absorption spectroscopy) is a technique for chemical structure analysis in the ultraviolet-visible region of light, and it directly affects the perceived color of the chemicals involved [151]. The UV-vis technique is matching to the fluorescence spectroscopy. The fluorescence technique is dealing with the transitions from excited state to the ground state whereas in the UV-vis technique a transition from the ground state to the excited state is being measured. These measurements are compared at each wavelength to quantify the wavelength dependent extinction spectrum (sum of the absorbed and scattered light) of the sample. The spectrometer measures the intensity of light passing through the sample ( $I$ ), and compares it to the intensity of incident light ( $I_0$ ). The ratio of both intensities ( $\frac{I_0}{I}$ ) is called the transmittance (% T). This technique is generally used to

quantitatively determine the concentration of sample which is calculated on the basis of Beer-lambert's law (given below) [152].

$$A = \log_{10} \left( \frac{I_0}{I} \right) = \varepsilon \cdot c \cdot l \quad (2.4)$$

Where  $A$  is the absorbance,  $\varepsilon$  is the molar absorptivity,  $c$  concentration of absorbing molecules and  $l$  is the path length of sample cuvette.

Theoretically, the free electrons in metal nanoparticles, especially of gold and silver materials, are collectively oscillating at a resonant frequency upon the irradiation of light [151]. These collective oscillations are known as surface plasmon resonance. Moreover, the frequency and amplitude of the resonance are sensitive to particles shapes which determine how the free electrons are polarized and distributed on the surface.

In this work, the UV-vis spectra of the size and shape controlled metallic nanoparticles were obtained from the Specord 200 (Analytic Jena) UV-vis spectrophotometer. The particles suspension was filled in the transparent UV cuvette of 1 cm path length and recorded the spectra at scanning speed between 10 nm/s and 25 nm/s.

### **2.3.8 Surface-enhanced Raman scattering (SERS) measurements**

SERS is an analytical tool for sensitive and selective detection of the trace amount of molecules adsorbed on noble metal nanostructures (mainly silver and gold). The SERS phenomena explaining that the intensity of normal Raman scattering cross-section can be enhanced up to  $10^{10}$  to  $10^{11}$  fold, which means the technique may detect single molecule [153]. Moreover, the enhancement factor,  $EF_{\text{SERS}} = 10^6$  can be understood by two contributions: an electromagnetic enhancement mechanism which proposes the excitation of localized surface plasmon and a chemical enhancement mechanism which proposes the formation of charge transfer complexes [154]. The technique can also be used to investigate the vibrational properties of adsorbed molecules yielding structural information on the molecule and its local interactions.

In this work, the SERS spectra were recorded by using Raman instrument (Raman System, R-3000). For the SERS measurement, a single particle or a couple of particles were filled in the small glass vial. Different intensity with optimal enhancement of the Raman light was observed after scattering due to the SERS sensing. The laser spot size on the sample was usually 2-3 mm in diameter. Green laser with 532 nm excitation laser source and 50 mW

laser power has been applied for SERS measurement of all different kinds of the sensor particles upon the application of different analytes with concentration from 10 mM down to 1  $\mu$ m.



### 3 Results and discussions-1: Polymer nanoparticles and their assembly

In this chapter, a detailed explanation for the obtained results of microfluidically prepared size and shape controlled polymer nanoparticles with their assembly and functionality is given. The effects of flow conditions in microfluidic platform, various reaction parameters and different surface properties of the obtained polymer nanoparticles are discussed. In addition, the formation mechanism for the spherical as well as non-spherical (ellipsoidal, dumbbell, linear, branched and flower-shaped) polymer nanoparticles are proposed. The obtained results are shown systematically in the sequence by characterizing them in different characterization techniques such as SEM, DLS, zeta potential, UV/VIS spectroscopy and fluorescence spectroscopy.

#### 3.1 Spherical polymer nanoparticles

Microflow-through techniques are emerging platform for the synthesis of polymer particles at nano and micro scale level [139, 155-157]. In the droplet-based microfluidic systems, the nucleation and growth processes take place under very homogeneous conditions due to the advantages of these processes such as, fast phase transfer as well as efficient mixing of all reactants within a short time interval [5, 108]. Resultantly, the polymeric particulate product obtained with high homogeneity. Different types of size, shape and composition-tuned polymer particles are widely used in various applications ranging from fluorescence imaging to targeted drug delivery [37-39]. By differently designed microreactors, the polymer particles with various functionalities have been reported in the literature [155, 158-161]. Here in this work, the size-controlled poly(methyl methacrylate) (PMMA) nanoparticles synthesis in the cross-flow microfluidic setup (shown in **Figure 2.2**) is performed. The monomer droplets are formed at T-junction of microreactor by the shear force of flowing continuous phase. Surfactant reduces the surface tension at interface, and therefore the size of the droplets (particles) can be controlled by different concentration of surfactant in aqueous phase [135, 162]. The strong effect of concentration of cationic surfactant CTAB (between 0.1  $\mu\text{M}$  and 1 mM) on the particles sizes is well illustrated in **Figure 3.1** and **Figure 3.2 a**. Smaller PMMA nanoparticles of about 70 nm were obtained at higher CTAB concentration (1 mM) in aqueous phase, whereas larger nanoparticles of about 350 nm were formed at lower CTAB concentration (0.1  $\mu\text{M}$ ). In this way, by keeping constant flow rate ratio of both immiscible liquids (1200  $\mu\text{L}/\text{min}/70 \mu\text{L}/\text{min}$ , aqueous/monomer), the size of PMMA

nanoparticles can be systematically tuned between about 70 nm and 350 nm at different CTAB concentration (**Figure 3.1 a-e**). Along with size, the surface charge of nanoparticles depends on the concentrations of CTAB in aqueous phase too, which have been characterized by zeta potential measurements. Higher zeta potential of the particles (about +42 mV) is realized when 1 mM CTAB has been used in the aqueous phase (**Figure 3.2 b**). The surface charge of the particles is gradually decreases with decrease in CTAB concentration. Similarly, a simultaneous effect on the particles size and surface potential were obtained when cationic CTAB has been replaced by anionic SDS. Size of the obtained nanoparticles was about 105 nm when 1 mM SDS has been used in the aqueous phase (**Figure 3.2 a**). Particles size increased up to about 500 nm when SDS concentration gradually decreased down to 0.1  $\mu\text{M}$ . As SDS is an anionic surfactant, the surface charge of the PMMA nanoparticles increases in negative direction with increase in SDS concentration in aqueous phase. The zeta potential of nanoparticles can be tuned between about -5 mV and -24 mV with variation in concentration of SDS between 0.1  $\mu\text{M}$  and 1 mM in aqueous phase (**Figure 3.2 b**).

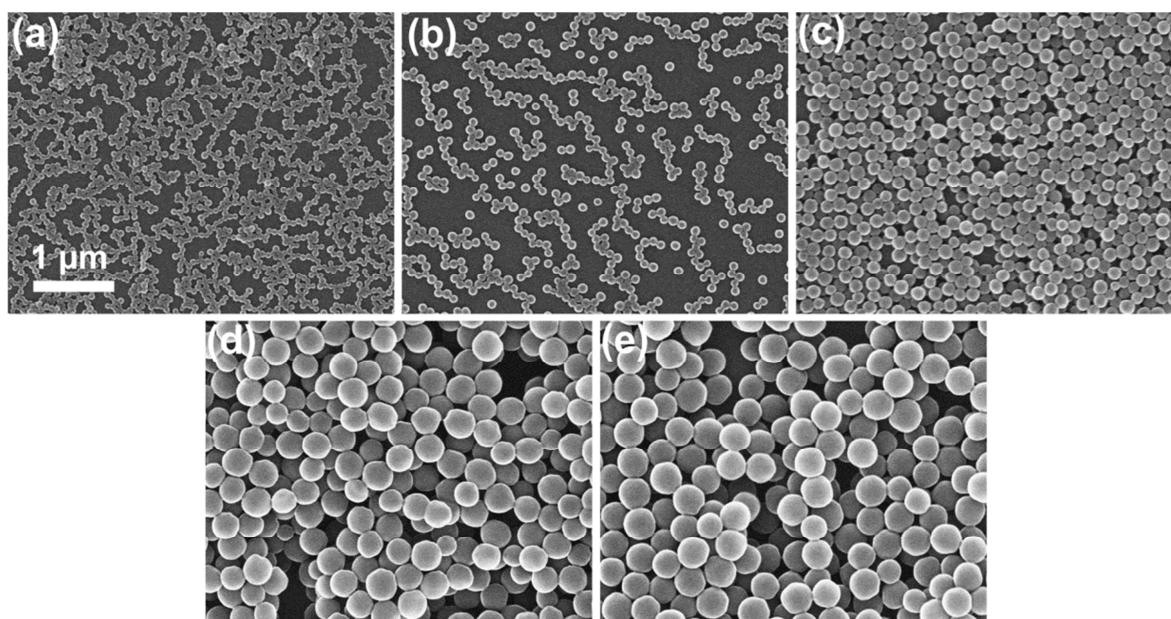


**Figure 3.1** (a-e) SEM images of the PMMA nanoparticles obtained when different concentrations of CTAB were used in the aqueous phase; (a) 1 mM, (b) 0.1 mM, (c) 0.01 mM, (d) 1  $\mu\text{m}$ , and (e) 0.1  $\mu\text{m}$ , (flow rate ratio of both immiscible liquids was 1200  $\mu\text{L}/\text{min}/70 \mu\text{L}/\text{min}$ , aqueous/monomer). Scale bar for all five images are same (1  $\mu\text{m}$ ).

Initially, when emulsified solution (made up of two immiscible phase) comes in to the contact with polymerizing temperature (97  $^{\circ}\text{C}$ ), the nucleation of the nanoparticles can



initiates. The polymer nanoparticles nucleation can possibly occurs via two different routes, a micelle nucleation or a homogeneous nucleation. In continuous phase, when concentration of surfactant is above critical micelle concentration (CMC), the obtained particles follow a micelle nucleation mechanism, and the formation of particles is assisted by the homogeneous nucleation mechanism in the case when concentration of surfactant is below CMC. For example, the CMC of SDS is about 8 mM at 25 °C [163]. Here, the nanoparticles are obtained via homogeneous nucleation mechanism, because the concentrations of both surfactants (SDS and CTAB) are below the CMC. Initiation starts when thermal radical attacks on the monomers at 97 °C and forms the nucleated particles. Simultaneously, the surfactant molecules are adsorbs on the surface. During the homogeneous nucleation, the adsorbed surfactant molecules may desorbs out and monomers addition (diffusion) takes place meanwhile to the small nucleated particles in order to obtain the primary growth [163]. The process of the monomers addition to the growing particles is continued until the end of polymerization reaction. Finally the surfactant molecules adsorbed irreversibly on the surface of obtained polymer nanoparticles at the end of polymerization reaction. The density of the surface charge, and therefore the nanoparticles size, depends on the concentration of surfactant used in the aqueous phase (**Figure 3.2**). Thus, when higher concentration of CTAB or SDS was used, the number of particles is higher and due to the suppression ability through charges, the particles are of smaller sizes. The graphical results for the tuning of size and surface charge of PMMA nanoparticles are shown in **Figure 3.2 (a, b)**.

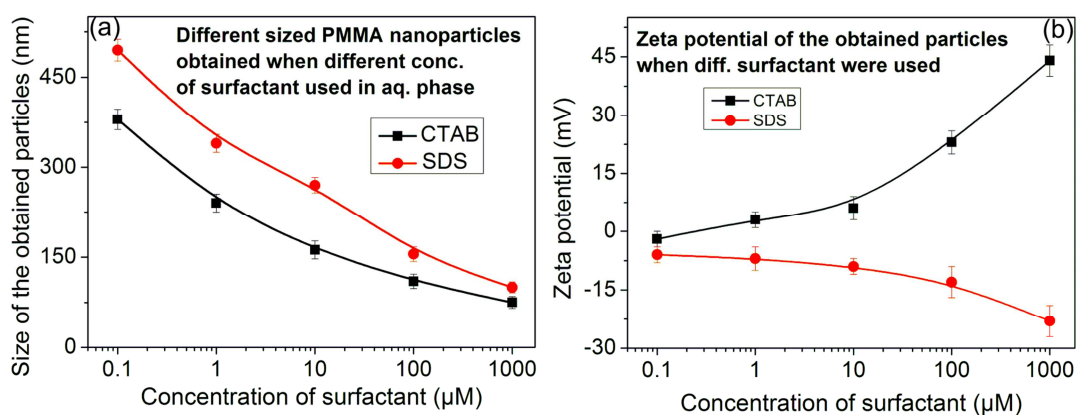


**Figure 3.2** (a) and (b) are the graphical representations of nanoparticles size and zeta potential in dependence of the concentration of cationic CTAB and anionic SDS surfactants in aqueous phase.

### 3.2 Shape controlled polymer nanoparticles

The deviation from a spherical shape means a symmetry breaking. Shape and morphology controlled polymer nanoparticles are particularly interesting for various biological applications such as, phagocytosis and targeted drug delivery [37-39]. Therefore, it is of interest for obtaining new functional properties, special aggregation behaviour or nano architectures, and realizing new materials. The shape of the simple nanoparticles is either determined by a minimization of interfacial area or by minimization of energy by arranging the atoms or molecules in regular lattices. The arrangement of the atoms and molecules in crystalline materials is uniform in the regular facets under thermodynamic control, and therefore, the shape-directed inorganic crystal structures can easily be controllable [44, 164]. In direct contrast, the polymer is an amorphous or semi-crystalline material with flexible molecular nature. Therefore, the ability to construct the shape of polymer particles in a single-step process via bottom-up synthetic approach and at nanometer scale level is highly challenging.

In the liquid solution, binding by complementary surface functionalization is a powerful strategy for connecting the nanoparticles. This strategy can be applied, for instance, for the assembling of metal nanoparticles after functionalization with complementary oligonucleotides and selective hybridization [165]. Moreover, such type of assembly particles can be achieved by use of charged ligands, by formation of suited electrochemical potential or even simply by utilization of charged surfactants or surface-attached polyelectrolyte molecules. The accessibility of surface active agent have several functions during the polymerization process, such as stabilization of the emulsion via micelles formation and the interfacial interactions with solvent as well as with other components and growing particles in solution. It can be well imagined that the strategy for irreversible interactions between two or more growing nano sized spherical particles can be used for the generation of composed non-spherical nanoparticle of different types. The generation of differently shaped nanoparticles by particle/particle interactions is a general route for the synthesis of complex nanomaterials [37, 166]. Various methods have been employed previously for the synthesis of non-spherical polymer particles [45-49]. But, these reported methods demand for the multistep synthetic procedures to achieve the desired shapes. In the following, a new microfluidic method for the single-step synthesis of different non-spherical polymer nanoparticles by emulsion polymerization is presented here in this section (3.2). Furthermore, the formation of composed non-spherical polymer nanoparticles is described by proposing

the electrically dominated mechanism for the control of in-situ interaction of particles during the continuous growth.

### 3.2.1 Formation of ellipsoidal and dumbbell-like polymer nanoparticles

In general form of the polymer nanoparticles obtained via emulsion polymerization is a spherical shape at lowest interfacial energy. The interaction between the solvent (water) and surfactant at interface between the growing nanoparticle and aqueous phase suppresses the direct contact between the separately growing particles in solution. In addition, if ionic surfactants are used, the electrostatic force repels the particles and keeps them at certain distance from each other. Such electrical force is given by the type of used surfactant. The strength of electrical repulsion is determined by the density of surfactant molecules inside the liquid/liquid interface and by the number of charges per molecule. The electrical polarization of nanoparticles in case of an approaching other charged nanoparticle is low. It is derived by the field-induced deformation of particles or by pushing the charged surfactant molecules inside the liquid/liquid interface to opposite sides. It is to assume that the both effects are low in case of surfactants with low molecular weight (**Figure 3.3 A(a, b)**). Under these conditions, the polymer nanoparticles are “hard multi-charged nano-objects”.

The situation concerning the electrical polarizability of growing nanoparticles is completely changed if interfacial agent with polyelectrolyte character is used. In this case, the mobile charged part of the molecules is well solvated by water and more or less stretched by the electrostatic repulsion between the single charged functional groups. This results into a “hedgehog” shape of the particles consisting of the polymer core and radially stretched chains of the surfactant macromolecules. If two of these particles are approaching, the charged chain of polyelectrolyte molecules moves to the opposite directions in order to minimize the electrostatic repulsion which corresponds to a polarization of particles (**Figure 3.3 A(c, d)**). In such situation, the nanoparticles with adsorbed poly-ionic molecules behave as “soft multi-charged nano-objects”. This polarization effect means also a reduction of repulsion in comparison with stiff objects with the same surface charge. This might cause a direct contact (joining) between two nanoparticles if their relative velocity overcomes the repulsive forces. Two nanoparticle cores, in such conditions, can be united irreversibly, and this joining event can take place at different phases of nanoparticle growth during the ongoing emulsion polymerization. The shape of the final nanoparticles is deviated to different degrees from a spherical one in dependence of the time of core assembling. Ellipsoidal nanoparticles will be

formed in case of the earlier binding events and dumbbell-like particle dimers are obtained in the case of late binding events (**Figure 3.3 B**).

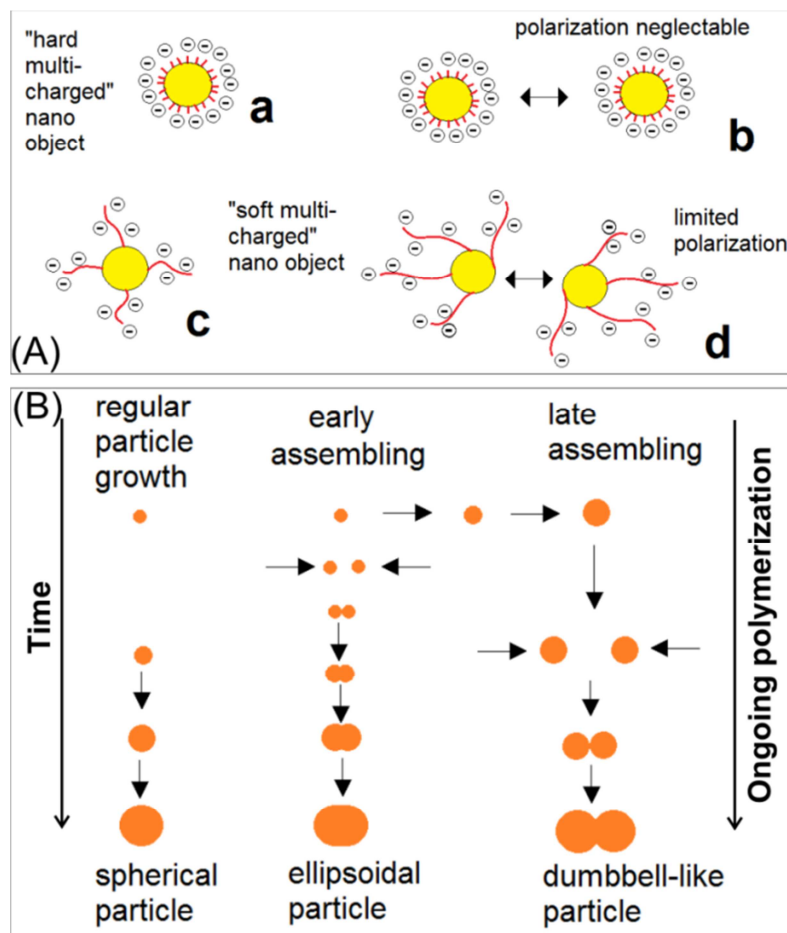


**Figure 3.3** (A) The cartoons (a-d) represent the scheme for the interaction of growing polymer nanoparticles and role of adsorbed polyelectrolyte molecules. (B) Principle of in-situ dimerization and assembling of nanoparticles at different stages of the growths.

At high flow rate ratio of aqueous phase (containing 0.09 mM poly(4-styrenesulfonic acid-co-maleic acid) sodium salt (PSS-co-PM)) and monomer phase, the formation of ellipsoidal nanoparticles was observed, in general. It is assumed that these particles are formed by joining events between two spherical nanoparticles at an early stage of the nanoparticle growth. The further growth of the particle dimers in ongoing polymerization leads to a compact but non-spherical (ellipsoidal) final particle shape (**Figure 3.4**).

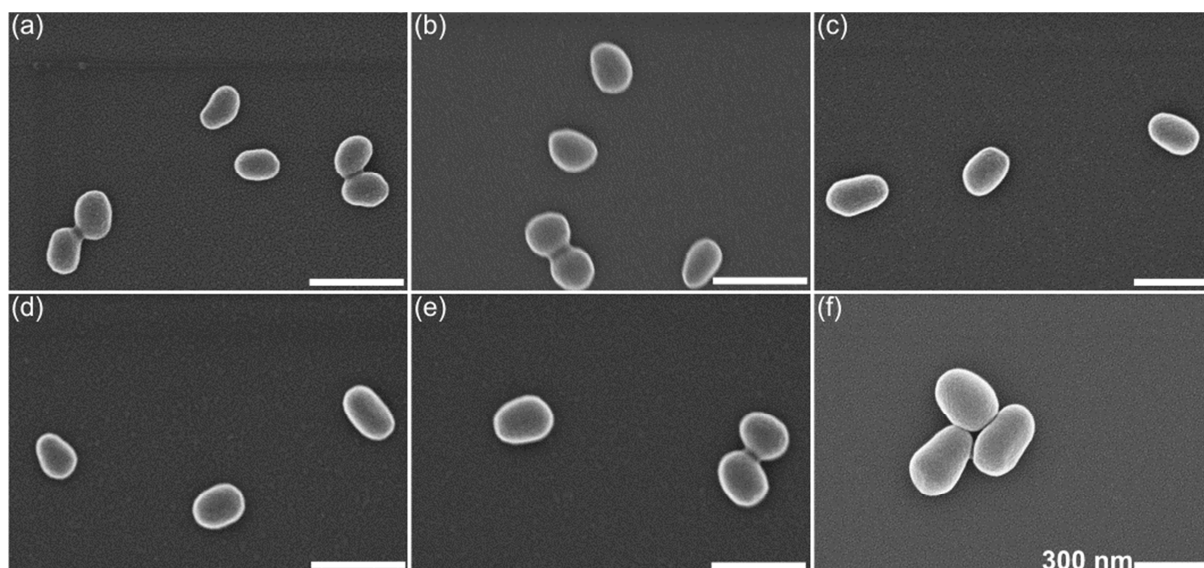


**Figure 3.4** SEM images of the ellipsoidal polymer nanoparticles formed by early dimerization of spherical nanoparticles in the presence of PSS-co-PM. Effect of flow rate ratio and concentration of PSS-co-PM on the size of particles: 0.09 mM, (a) 3430/32 (aq/mon,  $\mu\text{L}/\text{min}$ ), (b) 2230/32, and (c) 2030/32; 0.05 mM, (d) 2430/32, (e) 2230/32, and (f) 2030/32. Scale bar for all images is 300 nm.

In particular, the fast emulsification and regular streaming conditions in the microfluidic arrangement support a fast initiation of polymerization as well as a synchronized growth of the particles. It is to suppose that the electrostatic conditions in all growing particles are comparable, which leads to similar conditions for electrostatic repulsion. The postulated homogenous condition at nm-scale is probably the precondition for nearly exclusive formation of the ellipsoidal particles and the narrow distribution of particle shapes. The applied high flow rate ratio in the experimental series leads to the formation of ellipsoidal particles, which can be hypothesized by nucleating the nanoparticles at higher density of polyelectrolyte molecules. It can be supposed that the strong Brownian motion of the small nanoparticles at early stage of particles growth helps to overcome the repulsive forces and leads to the dimerization of small polymer cores. The high number of polyelectrolyte molecules at the liquid/liquid interface seems to prevent a further particle aggregation in the later phase of particle growth. The formation of the ellipsoidal nanoparticles is comparatively robust against deviations in the process conditions. The obtained aspect ratios shows only slight deviations if the flow rates and the surfactant concentrations are changed moderately (**Table 3.1**).

**Table 3.1.** Effect of various concentrations of polyelectrolyte (PSS-co-PM, aqueous phase) and flow rate ratio of both liquids on PMMA nanoparticles size and shape.

Ellipsoidal shape regime			(Aqueous phase) PSS-co-PM conc. (rep. unit conc.)	Dumbbell shape regime		
Flow rate ratio (aq/mon, $\mu\text{L}/\text{min}$ )	Length (nm)	Width (nm)		Flow rate ratio (aq/mon, $\mu\text{L}/\text{min}$ )	Length (nm)	Width (nm)
3430/32	~150	~120	<b>0.09 mM</b>  or <b>(0.0030%)</b>	800/40	~405	~210
2230/32	~160	~125		300/40	~450	~235
2030/32	~170	~130		260/40	~460	~240
2430/32	~155	~125	<b>0.07 mM</b>  or <b>(0.0023 %)</b>	360/40	~450	~240
2230/32	~180	~130		300/40	~470	~240
2030/32	~200	~140		260/40	~480	~250
2430/32	~170	~130	<b>0.05 mM</b>  or <b>(0.0017 %)</b>	360/40	~480	~240
2230/32	~200	~150		300/40	~500	~250
2030/32	~280	~200		260/40	~510	~260

Higher number of polyelectrolyte charges causes a decrease in particles size. Therefore, at constant PSS-co-PM concentration (0.09 mM), the lateral diameter of the obtained nanoparticles is about 120 nm and 130 nm at the aqueous flow rate of 3430  $\mu\text{L}/\text{min}$  and 2000  $\mu\text{L}/\text{min}$ , respectively. On other hand, the concentration of polyelectrolyte affects the particle size at constant total flow rate ratios, too. When three different PSS-co-PM concentrations (0.09 mM, 0.07 mM and 0.05 mM) were used, the diameter of the obtained nanoparticles are of 125 nm, 130 nm and 150 nm at similar flow rate ratio, respectively. These both effects, flow rate ratio and concentration of polyelectrolytes, support the exclusive effect of polyelectrolyte charges to control the size of particles.

A significant other type of particle dimers (dumbbell) was formed if the flow rate ratio (aqueous/monomer) of both liquids was drastically reduced down to the range between about 800  $\mu\text{L}/\text{min}$  and 260  $\mu\text{L}/\text{min}$  (**Figure 3.5**). During the lower aqueous flow rate (300  $\mu\text{L}/\text{min}$ ), the polyelectrolyte charge density on the surface is comparatively low and, therefore, comparatively lower suppression ability is realized for the particle growth. In such situation, there is a competition at the early stage of polymerization between assembling of two cores

and individual growth of the spheres. In the dynamic adsorption and desorption process, the MMA monomers enters very quickly into the soft polyelectrolyte micelles-like network, and this process is realized by all individual growing spheres at same time into the ongoing polymerization reaction at 97 °C. Therefore, the growth of individual particles is preferred over the assembling event at very early stage. However, the assembly obtained at critical middle stage of growth as shown in **Figure 3.3 B**. Particularly at this stage, the charges are dense enough at the particles surface after joining event of two cores to repel the additional particles in the solution for further assembling. Therefore, the controlled assembly of dumbbell particles is obtained in high yield at the end (**Figure 3.5**).

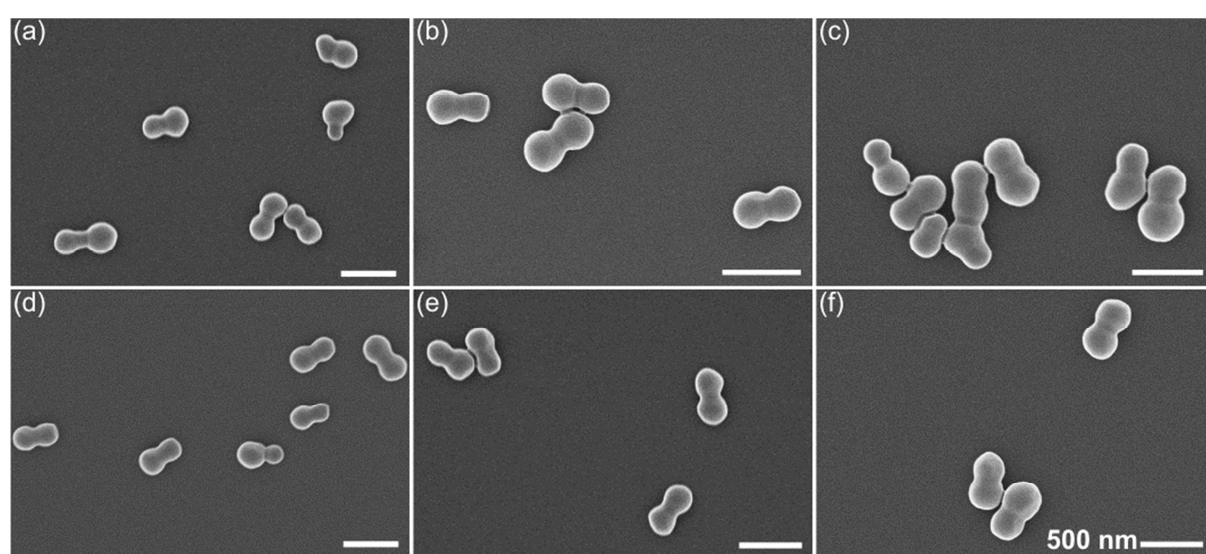


**Figure 3.5** SEM images of the dumbbell shaped nanoparticles formed by late pairing of growing PMMA nanoparticles in the presence of PSS-co-PM. Effect of flow rate ratio and concentration of PSS-co-PM on the size of particles: 0.09 mM, (a) 800/40 (aq/mon,  $\mu\text{L}/\text{min}$ ), (b) 300/40, and (c) 260/40; 0.07 mM, (d) 360/40, (e) 300/40, and (f) 260/40. Diameter of the particles increases with decreasing continuous aqueous flow rate. Scale bar for all images is 500 nm.

### 3.2.2 Formation of controlled rodlike polymer nanoparticles

The control over the number of assembling events of growing particles in the polymerizing solution depends upon the available charged molecules per particles. The ratio of charged molecules and number of particles core can be precisely managed by actuating the accurate flow rates of individual liquid phases. Longer assembly with aggregation of three and four cores were formed typically at 80-100  $\mu\text{L}/\text{min}$  flow rates of the monomer phase and 300-600  $\mu\text{L}/\text{min}$  aqueous PSS-co-PM flow rates (**Figure 3.6**). The dominance of stretched over compact aggregates can be explained by the assumption of electrostatic effects on the nanoparticle interaction. Compact particles of three or more cores can only be formed when electrostatic repulsion is much lower than the particle/particle affinity. In contrast, a significant repulsion and a polarization of one particle in case of the electrostatic field of an approaching second charged particle leads to the effect of “single-particle contact” as described above. The particles are growing rapidly, and therefore the surface energy is lowering.

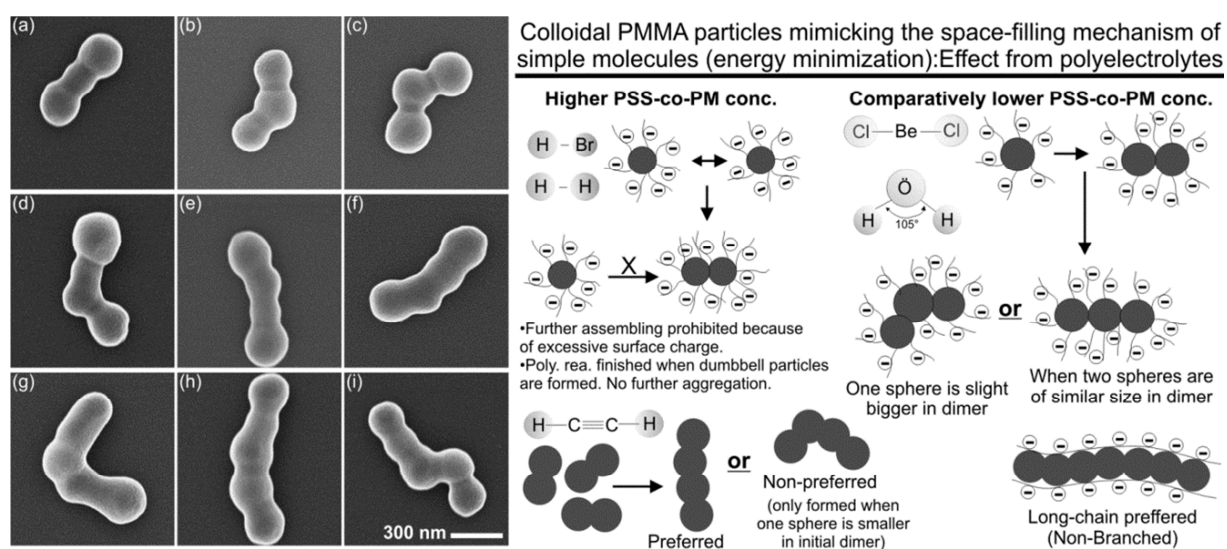


**Figure 3.6** SEM images of the polymer nanoparticle assemblies formed at lower flow rate ratios: (a-c) nanoparticle assemblies formed by three core particles in one direction at 600/80  $\mu\text{L}/\text{min}$  (aqueous/monomer), (d-f) rod-like assemblies formed by four core particles at 440/80, (g-i) necklace-like particles formed by five core nanoparticles at 300/80. The concentration of PSS-co-PM in aqueous phase is 0.09 mM. The scale bar is same for all (a-i) images (300 nm). On right side, schematic of the proposed mechanism for particles assembly and final shapes that mimic the space-filling mechanism of colloidal molecules.

An assumption from the effect of concentration ratio between the polyelectrolyte molecules and growing nanoparticles on the electrical forces between polymer nanoparticles is well



supported by the measurements of the zeta potential of obtained nanoparticles. In all cases, a negative zeta potential was observed which corresponds well with the negative charge of the polyelectrolyte components. This potential significantly increases in negative direction with increasing polyelectrolyte concentration and also slightly during the variation in flow rate ratios (**Figure 3.7**).

The way of particles clustering, here, is dominated by energy minimization, and therefore, the colloids adopt the shapes similar to mimic the space-filling mechanism of simple chemical molecules, such as H<sub>2</sub>O, CO<sub>2</sub>, acetylene, and so forth (**Figure 3.6**). In other terms, the particles are so-called colloidal molecules [47, 68]. The controlled clustering via depletion interaction is well-known [69, 167], but the phenomenon of the depletion is occurs when two different sized colloids or entities are presents in the liquids. In contrast to such phenomenon, here the controlled assembling of identical sized particles is obtained during the ongoing polymerization reaction. The adoption of the final particles shape is governed by the dominance of energy minimization, and entire assembling process in precise manner is depends on the polyelectrolyte charge density (with different chain-length and different concentration). On other side, when polyanetholesulfonic acid sodium salt (PAES) and poly(sodium-p-styrene sulfonate) (PSSS) were used in the aqueous phase, the assembly of many spherical particles in one direction are obtained (**Figure 3.8 f, g**).

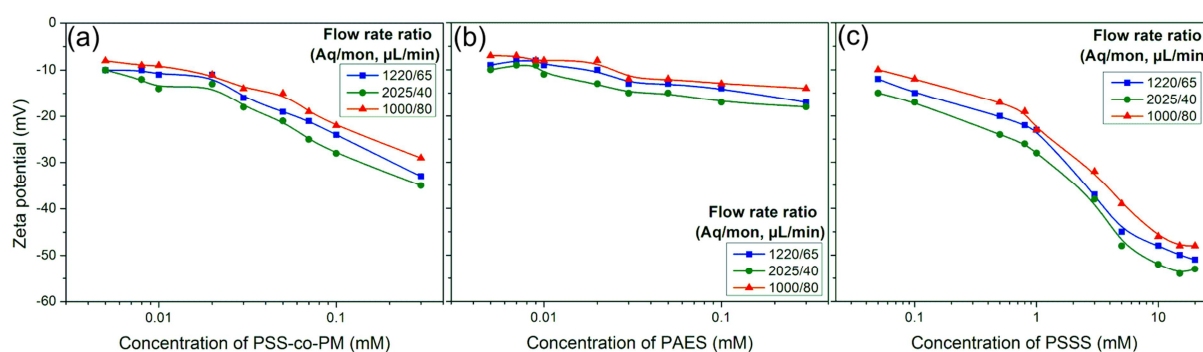


**Figure 3.7** Graphical results for the dependence of the zeta potential (final stage) of polymer nanoparticles suspensions on the concentration of (a) PSS-co-PM, (b) PAES and (c) PSSS at different flow rate ratio.

When PSS-co-PM concentration in aqueous phase were decreasing gradually, the final shape of the particles are transforming from dumbbell to deformed dumbbell to spheroidal-like (**Figure 3.8 a-c**). Spherical shape is the usual form in emulsion polymerization. Therefore, at 0.009 mM PSS-co-PM concentration, the shape is not assisted by dominance of limited polarization through polyelectrolyte. At the end, to confirm the particle assembly inside the polyelectrolyte layer at surface, the dumbbell and rod-like shaped polymer particles were kept longer time under the influence of electron beam in SEM vacuum chamber (**Figure 3.8 h-k**).

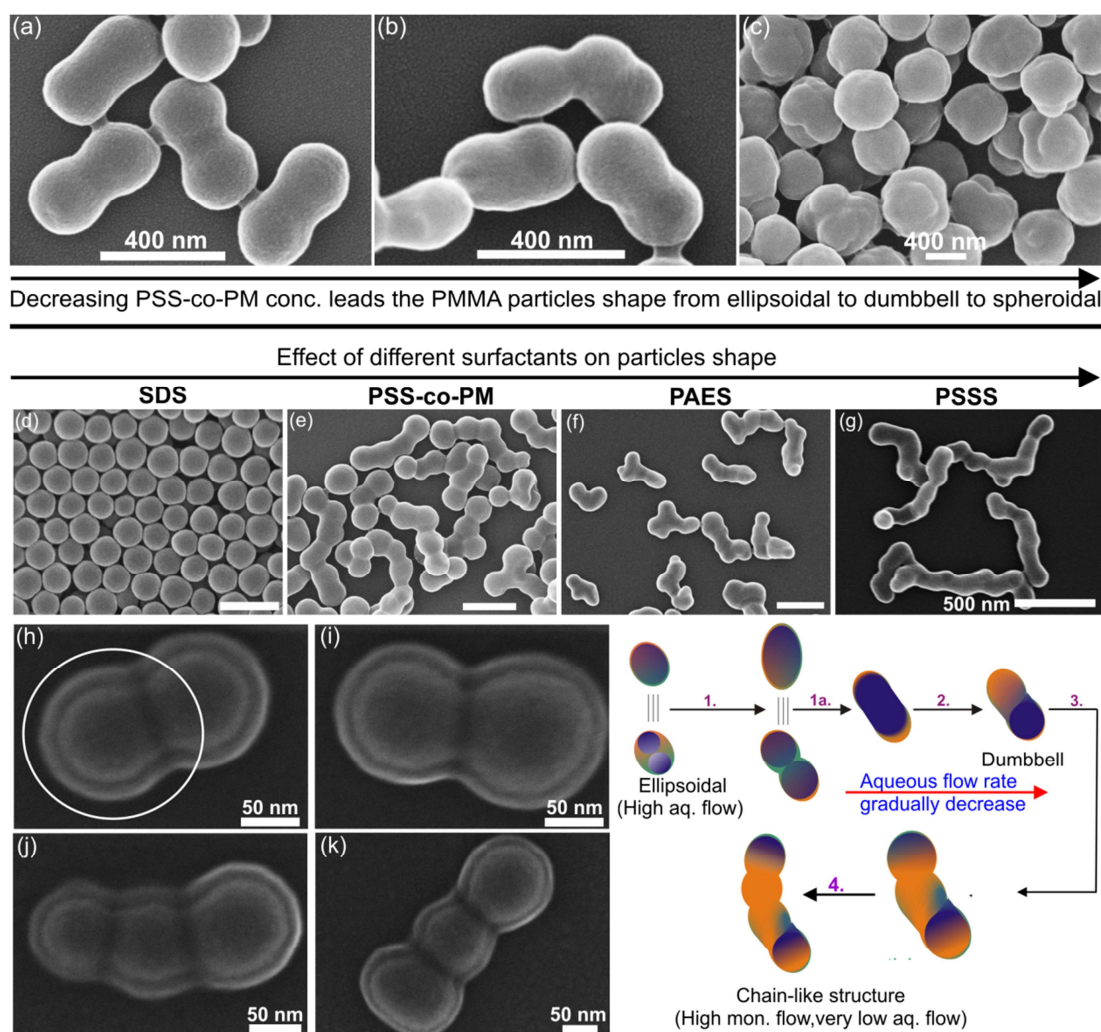


**Figure 3.8** SEM images of the particles at different concentrations of PSS-co-PM: (a) 300/40 (aqueous/monomer,  $\mu\text{L}/\text{min}$ ), 0.05 mM, (b) 1220/65, 0.02 mM, and (c) 1220/65, 0.009 mM. (d-g) SEM images represent the different shapes of particles obtained from the effect of different surfactant; SDS, PSS-co-PM, PAES, and PSSS, respectively. (h-k) dimer and trimer particles after longer focus of electron beam in the SEM chamber, and the drawing shows the adoption of particles shape at different reaction condition.

### 3.2.3 Formation of linear and branched polymer nanoparticles

The linear (with high aspect ratio) and branched polymer nanoparticles is the results of a function of long chained PSSS used in the aqueous phase. At very low ionic strength with lower charge concentration of PSSS, long-range electrostatic repulsion is important. For moderate or high ionic strength, minimum inter-droplet separation is determined by the physical space occupied by species in adsorbed layer. Different chain lengths (molecular weights) of PSSS play a major role for tuning the controlled size (length and width) of the obtained in-situ linear assembly. In particular, PSSS (70 kDa, molecular weight) provides the anionic charge density where the length of nanoparticles is obtained of about 400 nm (**Figure 3.9 A1**). PSSS having a flexible molecular nature and can be arranged on the growing nanoparticles surface. An approximate length of PSSS (70 kDa) molecule on the particles is about 135 nm. But, the linear geometry of obtained nanoparticles is a result of the controlled assembly of spheres at central range of continuous growth in ongoing polymerization reaction. Thus, the final length of obtained polymer nanoparticles is indeed longer than the total length of PSSS molecule at the surface. Three parameters, an appropriate PSSS chain-length, the density of adsorbed PSSS molecules as well as controlled repulsive force during the growth phase of polymer nanoparticles, therefore, determine the final size of linear assembly. Typically, the polymer nanoparticles of about 500 nm and 600 nm length are obtained when 500 kDa and 1000 kDa (molecular weight) PSSS were used in the aqueous phase, respectively (**Figure 3.9 A**). The final length of linear (non-branched) nanoparticles can be tuned between 300 nm and 900 nm during the utility of different PSSS concentration at varied flow rate ratios (**Figure 3.9 and 3.10**).

In general term, the nanoparticles which initiate the interaction with other entities required a certain kind of external force to direct them in to a defined structure or assembly [167]. Here, the conformation of PSSS and their appropriate concentration in aqueous phase provide the platform through a principle of limited polarization. The nanoparticles are more in total numbers when higher concentrations of PSSS (10 mM, repeating unit conc.) were used in the aqueous phase as obtained dispersion is less milky (semi-transparent). In this case, at high PSSS concentration, it is believed that the continuous diffusion rate of the monomer units through surface layer in the growing nanoparticle is slower during the dynamic adsorption and desorption events of polyelectrolyte at 97 °C polymerizing temperature. Resultantly, the obtained lateral diameter of polymer nanoparticles is slightly smaller compare to the particles obtained at lower PSSS concentration. As PSSS concentration decrease down to 7 mM and

5 mM, the width of the obtained nanoparticles increases up to about 250 nm (**Figure 3.9 B and Figure 3.10**).

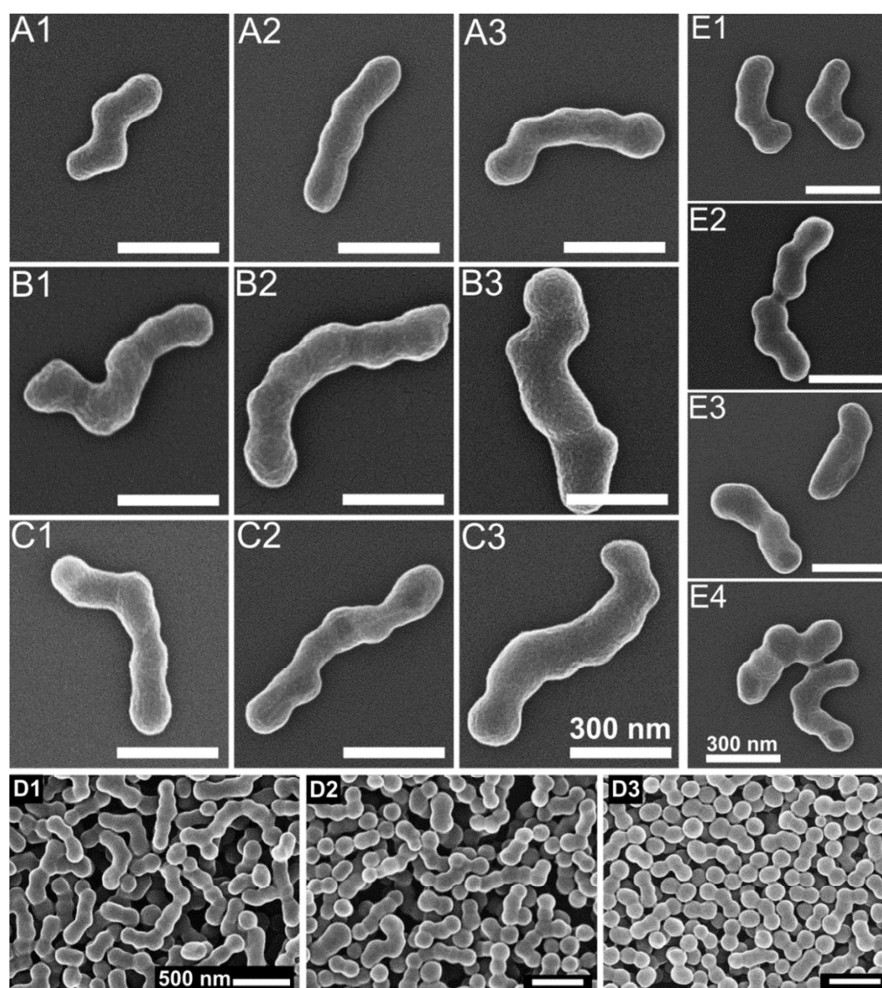


**Figure 3.9** SEM images of linear PMMA nanoparticles obtained at different reaction conditions. (A) Effect of PSSS mol. wt.: (A1) 70 kDa, (A2) 500 kDa, and (A3) 1000 kDa, at flow rate ratio (1200/70) and PSSS concentration (15 mM). (B) Effect of different PSSS concentrations (repeating unit concentration): (B1) 15 mM, (B2) 10 mM, and (B3) 7 mM, at flow rate ratio (1200/100) and 500 kDa PSSS molecular weight. (C) Effect of the flow rate ratio of both immiscible liquids: (C1) 1800/70 (aqueous/monomer,  $\mu\text{L}/\text{min}$ ), (C2) 1800/110, and (C3) 1800/150, at 8 mM PSSS concentration and 500 kDa PSSS. (D) SEM images of the polymer nanoparticles obtained at different flow rate ratio: 500 kDa PSSS, (D1) 1200/100, (D2) 700/100, and (D3) 500 /100. (E) SEM images of the polymer nanoparticles obtained at different flow rate ratio: 70 kDa PSSS, (E1) 1200/70, (E2) 1200/80, (E3) 1200/90, and (E4) 1200/100. Scale bar for images (A-C) and (E1-E4) are 300 nm and for (D1-D3) is 500 nm.

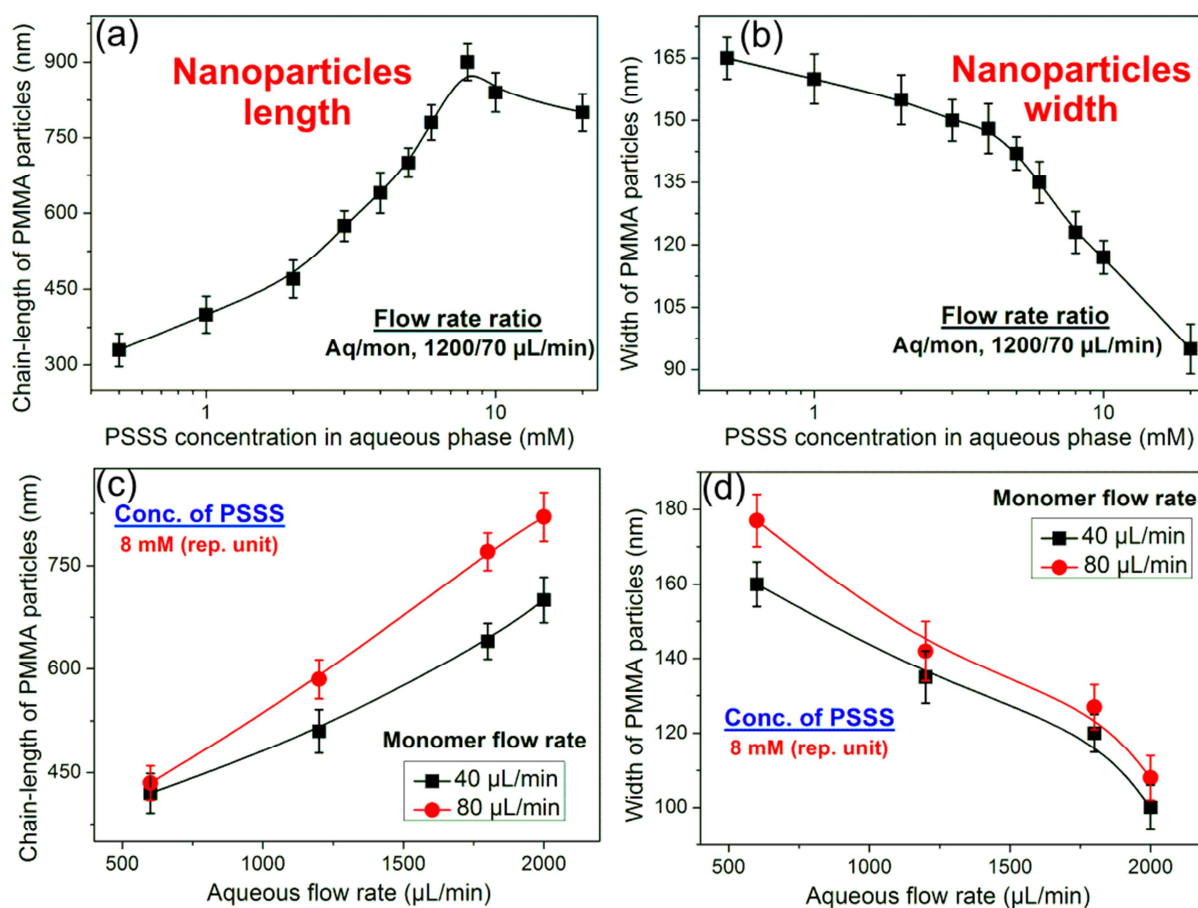


**Figure 3.10** Graphical representations for the tuning of polymer nanoparticles size (length and width) with respect to the flow rate ratios of both immiscible liquid phases and the PSSS concentrations.

In continuous flow synthesis, the number of charges per generated droplets can be precisely controlled by variation in the flow rate ratios of both immiscible liquid phases. Higher aqueous flow rate supply more anionic charges and higher space for Brownian motion for the growing particles. Therefore, at a high flow rate ratio of 1800  $\mu\text{L}/\text{min}/70 \mu\text{L}/\text{min}$  (aqueous/monomer), the obtained polymer nanoparticles are comparatively thinner in diameter (about 100 nm) because of the low monomer units are available for similar number of electrical charge particles in high volume. The width of the polymer nanoparticles can also be tuned by varying the monomer flow rates at a constant aqueous flow rate (**Figure 3.9 C** and **Figure 3.10**). When PSSS of particular molecular weights (70 kDa) was used at defined flow rate ratio, the tuning in the width and length of the obtained nanoparticles were realized as shown in **Figure 3.9 E**. Polymer nanoparticles with lower aspect ratio (length/width), in case of 70 kDa PSSS, are the results of a short chain-length of PSSS.

On other side, when repulsive effect between the joining nanoparticles is significant lower, the nanoparticles with branched character are obtained (**Figure 3.11**). It is assumed that the repulsive effect, which is the most probable reason for the formation of linear nanoparticle assemblies, is reduced in case of lower PSSS/nanoparticle ratios. In result, there are certain probabilities of joining events in the central region of preformed linear assembly. A low PSSS-loading per nanoparticle results in a weaker polarization in case of electrostatic interaction between the preformed linear nanoparticle and a joining spherical particle; the branched particles are formed at the end. The increasing branching tendency in the assembly formation with decreasing ratio of PSSS to monomer mixture supports the proposed model of electrostatic interaction, moderate repulsion and partial polarization due to the flexibility of attached polyanionic molecules.

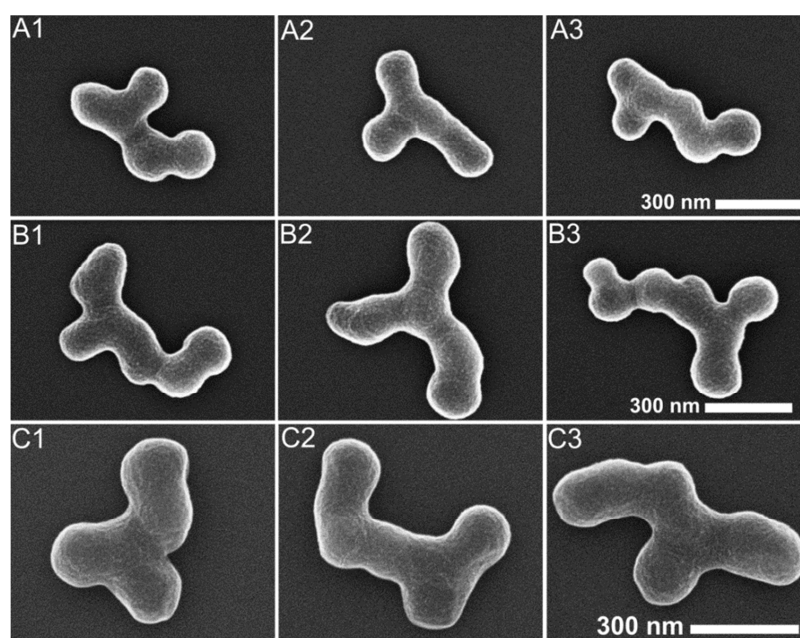


**Figure 3.11** SEM images of the branched polymer nanoparticles obtained at different flow rate ratio: (A1-A3) 800  $\mu\text{L}/\text{min}$ /150  $\mu\text{L}/\text{min}$  (aqueous/monomer), (B1-B3) 600  $\mu\text{L}/\text{min}$ /150  $\mu\text{L}/\text{min}$  and (C1-C3) 1500  $\mu\text{L}/\text{min}$ /300  $\mu\text{L}/\text{min}$ . The concentration of PSSS (500 kDa) was 6 mM (repeating unit concentration). The scale bar for images (A1-A3, B1-B3 and C1-C3) is 300 nm.

The linear and branched joining site obviously depends on the highly controlled and limited polarization which is systematically observed by zeta potential measurements (**Figure 3.12**). Therefore, for the assembling of the particles even at lateral position, the reduced charge potential is minimum prerequisite. Branched nanoparticles of comparatively smaller size were obtained when flow rate ratio of about 5.3 (800/150) has been applied (**Figure 3.11 A**). With decreasing aqueous flow rate in such range (600/150), the total size of the nanoparticles



in pole as well as lateral direction slightly increases which support the result of assembling under the reduced repulsive force at surface (**Figure 3.11 B**). During the ongoing polymerization, the particles are growing with high Brownian motion and the controlled assembling as well as continuous diffusion of the monomer units also depends on the total reaction volume of mixing solution. Therefore, even at the constant flow rate ratio of about 5 (1500/300) with higher flow rates of the individual regimes, the obtained nanoparticles are of slightly different size as shown in **Figure 3.11 C**.

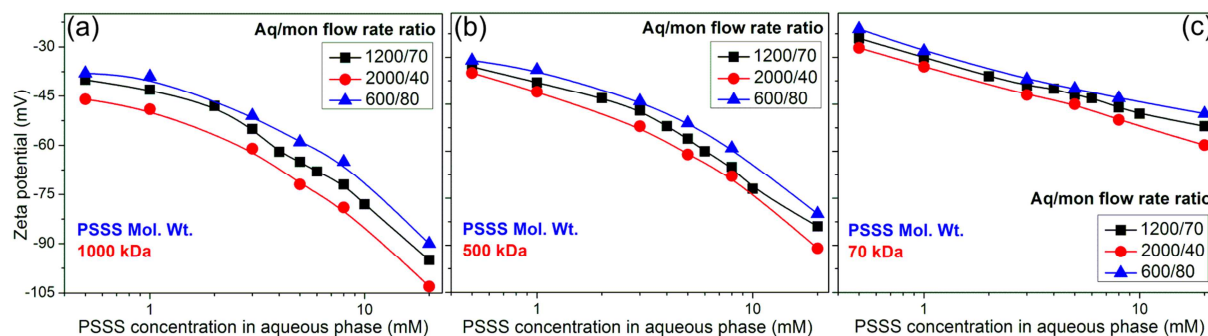


**Figure 3.12** Zeta potential measurements of the polymer nanoparticles obtained at different reaction conditions. The standard deviation for the all individual measurements is  $\pm 4-8$  mV.

Overall, it is to assume that the combination of moderate electrostatic repulsion with molecular flexibility of nanoparticle-connected macromolecules is a promising general strategy for generating non-spherical particles via in-situ nanoassembly principle.

### **3.2.4 Formation of flower-shaped polymer nanoparticles**

The composed flower-shaped polymer nanoparticles were synthesized via emulsion polymerization process in the identical microfluidic arrangement (as shown in **Figure 2.2**). The interpretation of the character of processes during the synthesis of composed nanoparticles depends on the reaction conditions and on different approaches. The formation of nanoparticle assemblies in solution can be regarded as a chemical reaction between nanoparticles on one hand or as the interaction of very small solids on the other hand. The first viewpoint corresponds well with the stochastic character of nanoparticle motion, which is in connectivity and through energy exchange. But it deteriorates from the distribution of shapes and sizes of nanoparticles, which is obtained normally in a typical nanoparticle synthesis. Moreover, it stays in strong contrast to the uniform character of molecules of a pure chemical substance. The second approach corresponds well with the condensation of atoms and molecules to the particles, and with the formation of phases and interfaces. But it is almost unable to describe the specific properties of dispersed states and specific character of the systems with enormous high internal interface areas, in particular, in case of a larger distribution of sizes and shapes of the elementary nanoparticles. Thus, the desire to control the formation of regular composed nanoparticles in liquid phase demands for two basic things: (a) the state of colloidal system should be stable and uniform during the whole process of nanoparticle assembling in order to avoid the uncontrolled coagulation, precipitation and large-scale agglomeration, and (b) the formations of nanoparticles assembly should be well defined in size, shape and composition. Fast destabilization, short interaction time and efficient reconstitution can be a promising way for a controlled assembling. Here, the microfluidic technique provides the entire platform for realizing all required preconditions of fast mixing, fast heat transfer and regular streaming patterns, which is also an efficient strategy for controlled nucleation and growth of the elementary nanoparticles [108, 168]. In this section, we have investigated how these processes can lead to the formation of flower-shaped polymer nanoparticles.

#### **Effect of different PVP concentration**

The continuous phase is made up of the precise concentration of polyvinylpyrrolidone (PVP), which attached to the particles surface and controls the size. The nucleation of the polymer particles initiates when emulsified solution of both immiscible liquid phase comes to the contact with polymerizing temperature (97 °C). In contrast to the formation of usual spherical



shape, the formation of structured and mainly flower-like polymer nanoparticles were obtained when PVP was used in the aqueous phase for emulsion polymerization process. The character of the obtained flower nanoparticles is strongly depends on the ratio of monomer and the used PVP concentrations. This ratio can be varied either by changing the concentration of PVP in aqueous phase or by the variation of flow rate ratio between dispersed and continuous phase. Many parameters such as flow rate ratio, mass ratio, concentration of PVP, different chain length of PVP are influencing the final particulate product. Particularly when different concentrations of PVP were used, slight changes in the nanoparticles mean diameters are observed. As shown in **Figure 3.13**, the nanoparticles diameter is smaller at higher PVP concentration (5 mM) compared to the particles obtained at lower PVP concentration (from 3 mM down to 1 mM).

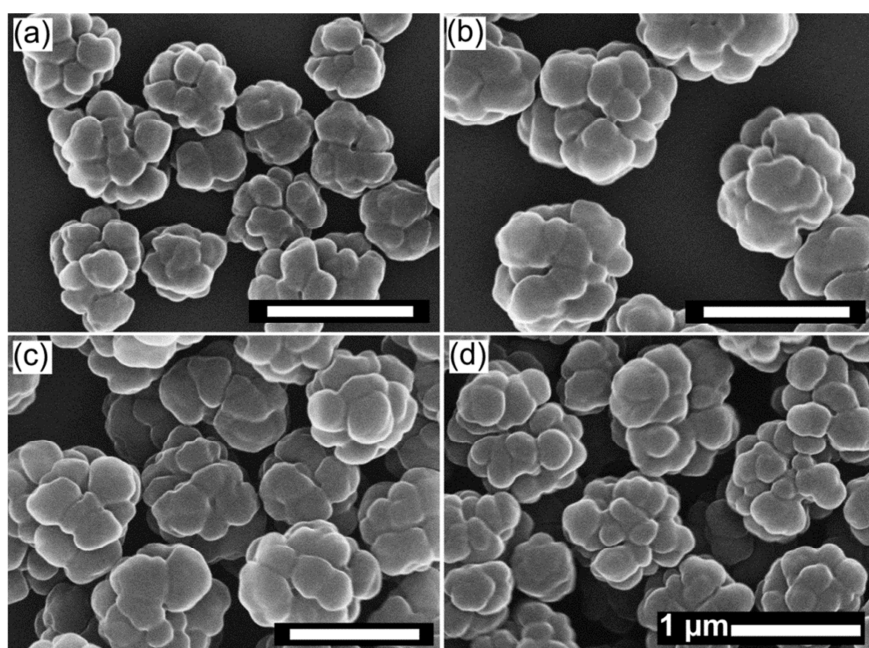


**Figure 3.13** SEM images of flower-shaped PMMA nanoparticles obtained at different concentration of PVP (25 kDa) in continuous phase: (a) 5 mM (repeating unit conc.), (b) 3 mM, (c) 2 mM, and (d) 1 mM. Carrier/monomer flow rate ratio: 1200/70 ( $\mu\text{L}/\text{min}$ ). Scale bar for all images is 1  $\mu\text{m}$ .

### Proposed mechanism

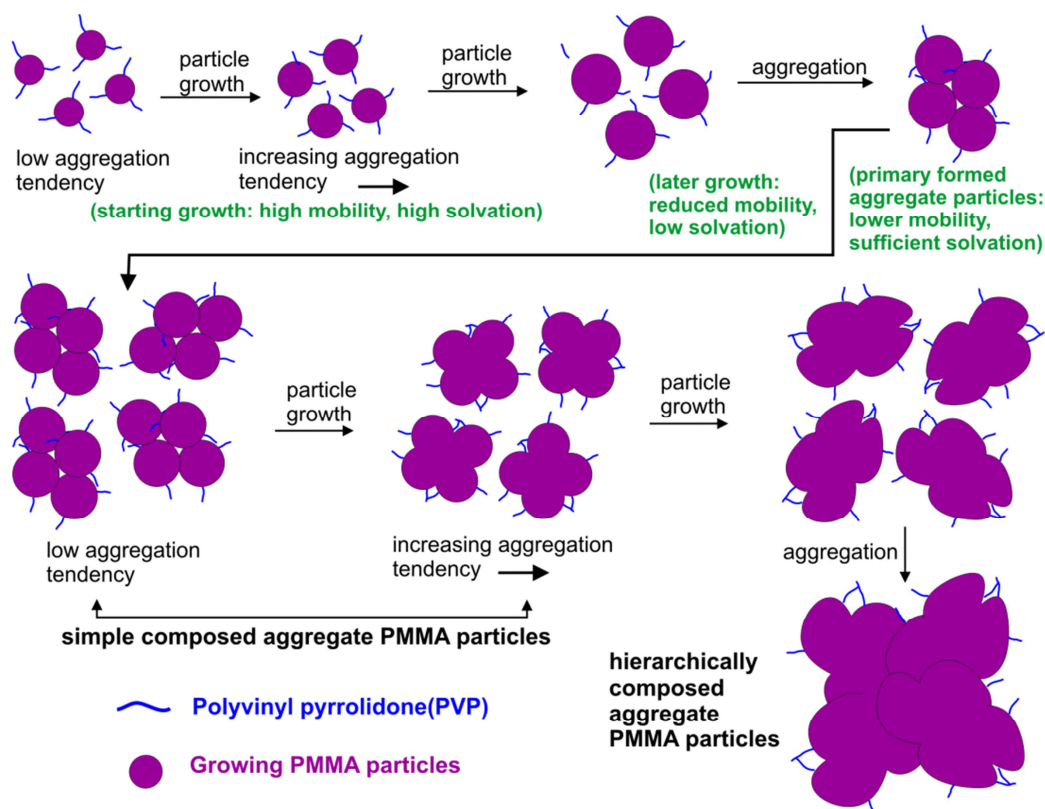
Different types of nanoparticles formation can be explained by a nucleation/assembling mechanism, for instance, in case of the star-like gold nanoparticles [169-171]. It is assumed that the electrical charges, their changes during the particle growth and variation in the electrostatically caused repulsion between the nanoparticles in colloidal solution play an essential role in these processes [172]. Electrical forces are also responsible for the formation

of elliptical, dumbbell and linear polymer nanoassemblies, which are formed in the presence of polyelectrolyte molecules. PVP is a non-ionic hydrophilic polymer, and it is well soluble in aqueous medium. Moreover, it has ability to bind at the surface of polymer particles. It has to be assumed that the stabilization of the particles in a colloidal state with non-ionic polymer is mainly due to the solvation parameter. PVP molecules adsorbed at the surface of growing polymer particles and contributing the effect for solvation of nanoparticle. At lower PVP concentrations, the nanoparticles are not enough stabilized by solvation and tend to aggregate. The strength of aggregation is dependent on the mobility of particles in relation to their solvation or repulsive forces. The mobility can be roughly characterized by the mean particle velocity  $u$ :

$$u \sim \sqrt{\frac{3kT}{4\rho\pi r^3}} \sim r^{-\frac{3}{2}} \quad (3.1)$$

Where  $k$  is the Boltzmann's constant,  $T$  is temperature, and  $r$  is the radius of the particles. The solvation  $s$  can be roughly derived as,  $s \sim 1/r$ . In addition, the solvation  $s$  should be determined by the number of surface-attached macromolecules in the form of their density and their lengths. The PVP-supported solvation could be lowered if surface-attached molecules are incorporated partially or completely into the polymer matrix during the growth process of a nanoparticle. Larger particles are moving slowly according to dynamic light scattering theory and their solvation is supported by a higher number of adsorbed PVP molecules. Therefore, an assembling of the few particles to a little larger particle can lead to the stabilization of the colloidal solution in form of dispersed assembled nanoparticles due to their higher solvation and lower thermal motion. At initial growth stage, the solvation power is very high, and mobility of small particles inside the solution is also higher. Subsequently when small particles are growing continuously, the mobility and solvation power decreased down considerably (**Scheme 3.1**). In result, the reduced mobility can be realized after certain growth; and several of such primarily grown particles are aggregates by adjusting the position of PVP macromolecules to minimize the local interfacial energy of the individual particles in the reaction system. Furthermore, the mobility can even decreased down significantly at primary aggregation stage of the particles because of the bigger size, but the solvation power is again sufficient (high) at this phase compared to the phase before primary aggregation. There are still free monomers available in the solution which adheres on the primarily aggregated particles and therefore the growth is continued. Obviously, the solvation energy is again decreased down along with continuously decreasing mobility of the particles at certain

point. To minimize the surface energy of whole system, a second aggregation can realized. The aggregation tendency is everlasting until all the free monomers are consumed and the polymerization reaction is completed. At the end, hierarchically composed aggregated particles with homogeneous character are obtained due to the homogeneous nucleation and growth condition throughout the polymerization reaction (**Scheme 3.1**).



**Scheme 3.1.** Scheme for the flower-shaped PMMA nanoparticles nucleation and growth in the ongoing polymerization process.

### Effect of PVP molecular weight

The solvation, mobility and aggregation tendency of generated particles largely depends upon the lengths and concentrations of PVP. To study the effect of PVP chain length on the formation of final particles assembly, four different molecularly weighed PVP were used (10, 25, 40 and 55 kDa) in the aqueous phase. Sphere like nanoparticles are obtained when 10 kDa PVP was used in aqueous phase. In this case, it can be assumed that the step by step aggregation is rapid and the growth process is finished at early stage before the aggregation of two or more separately growing particles takes place because of the low solvation power. If PVP with middle chain-length (25 kDa) was used, a hierarchical growth of particles was observed. Obviously the number of aggregation steps is enhanced if 40 kDa PVP or 55 kDa

PVP have been used in the aqueous phase. The mean diameter results of the final structured polymer nanoparticles are shown in **Figure 3.14**.

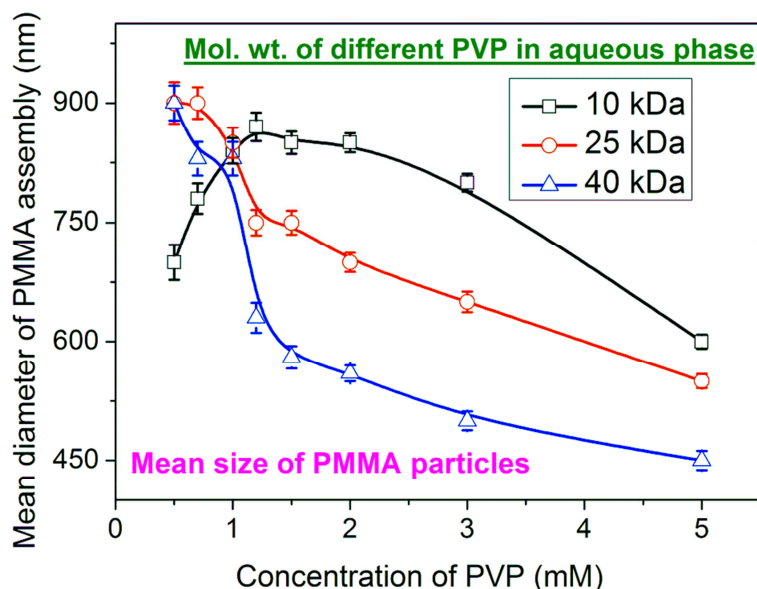


**Figure 3.14** Graphical representation for the dependence of mean diameter of PMMA nanoparticles assembly upon various concentration of different molecular weighed PVP in the continuous phase.

#### Effect of different flow rate ratio

Upon the variation in flow rates and flow rate ratio of both immiscible phases, a strong effect of PVP on the obtained particles character is appeared. The transition from a flow rate ratio of about 50 (2050  $\mu\text{L}/\text{min}/40 \mu\text{L}/\text{min}$ ) to 4.5 (450  $\mu\text{L}/\text{min}/100 \mu\text{L}/\text{min}$ ) causes the formation of more compact particles as shown in **Figure 3.15**. The aggregate character is still clear in case of 4.5 flow rate ratio, but with certain reduction in comparison with the higher flow rate ratio. Higher flow rate of the aqueous phase, of course, supply more number of the PVP molecules, and additionally also provides more space for the mobility of growing particles in the solution. When mobility of growing particles is higher in solution, the hierarchical aggregation takes place and the structured assembly can obtain at the end.

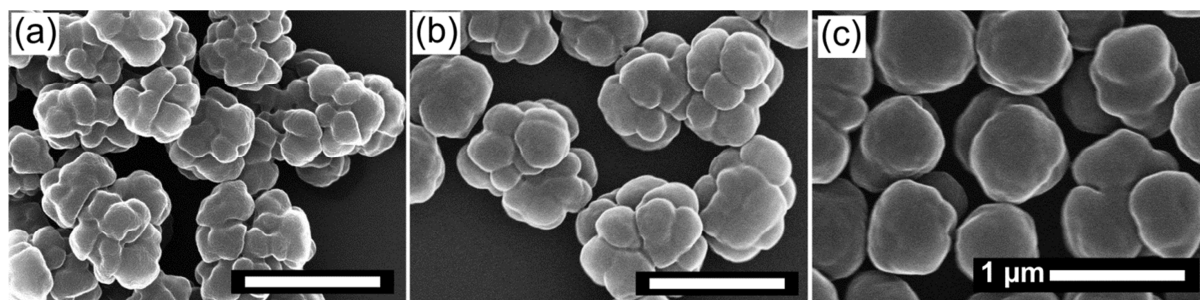


**Figure 3.15** SEM images of PMMA nanoparticles obtained when 25 kDa (molecular weight) PVP (1 mM, rep. unit conc.) was used in the continuous phase at different flow rate ratios of both liquids: (a) 2050/40 ( $\mu\text{L}/\text{min}$ , aqueous/monomer), (b) 1200/70, and (c) 450/100. Scale bar for all images are same (1  $\mu\text{m}$ ).

Nanoparticles formation is divided in two main phases, nucleation and growth. Growth of the nanoparticles proceeds with the time factor, and many events occurred in between until the end of final particles formation. As discussed above, smaller the particles at early stage, higher the solvation power and higher mobility of the particles in solution. The fusion of the particles during the continuous growth can be divided in three different processes: agglomeration, aggregation and coalescence. The ‘agglomeration’ is defined as a collection of weakly bound particles where external surface area is similar to the sum of the surface areas of the individual components [171]. The forces holding agglomerate together are weak forces, for example, van der Waals forces. On other hand, ‘aggregation’ is described as comprising strongly bonded or fused particles where resulting external surface area significantly smaller than the sum of calculated surface areas of the individual components. PVP layer on the nucleated PMMA particles becomes comparatively weak at certain critical point during early growth and initial aggregation realized. Finally, the term ‘coalescence’ is a process where two phase domains forms the large phase domain, and it reduces the total interfacial area [171]. A merging of aggregates means coalescence. In other words, coalescence is the aggregates of aggregates. A structured flower shaped PMMA nanoparticles is the integration of many aggregated phase where many domains attached with strong forces (**Figure 3.16 a**). The complex shape of most of nanoparticles reported, here, is obviously the product of a multi-step assembling mechanism. This hypothesis is suggested by the structure of nanoparticles as shown in **Figure 3.13**. The whole flower-like particle of size between about 500 nm and 1  $\mu\text{m}$  obtained at various reaction conditions is composed by compact component particles. These component particles are not spherical, but structured, and seem to be formed by an earlier assembling process. The different particle characters are given by different levels of assembling and the time between initiation of polymerization, the single assembling steps and the duration of final growth (principle shown in **Scheme 3.1**). The

advantage of the microfluidic emulsification consists in the efficient and regular convection of liquids and it caused high homogeneity of local reaction conditions. This results in to the formation of particles with similar shape and size under the constant conditions. Moreover, it supports the suppression of formation of larger aggregates and precipitations, and contributes to the stabilization of the nanoparticle suspension.

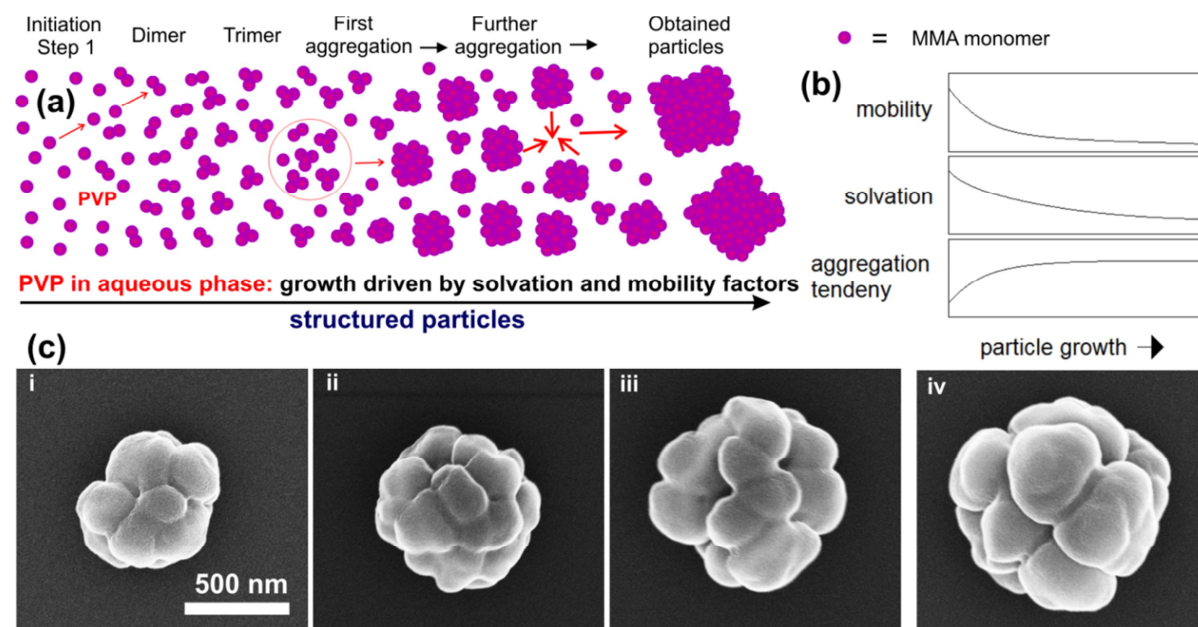


**Figure 3.16** (a) Schematic for the particles nucleation and step by step growth in dependence of time. (b) Graphical drawing for the relation of particles growth with mobility, solvation and aggregation tendency. (c) SEM images of final PMMA particles obtained at different repeating unit concentration of 25 kDa PVP: (i) 5 mM, (ii) 4 mM, (iii) 3 mM, and (iv) 2 mM, scale bar for all four SEM images are same (500 nm).

### Effect of interfacial agents

The addition of ionic surfactant, 0.1 mM sodium dodecyl sulfate (SDS), to the aqueous phase along with non-ionic PVP leads to the formation of small spherical PMMA particles of about 100 nm in diameter (**Figure 3.17**). The interaction between solvent (water) and surfactants at the interface becomes important to decide the final shape of the nanoparticles during mixed surface active agents is being used. Moreover, in such case, the final shape is dependent on the dominating concentrations of individual surfactant. The strength between inter-particles repulsive force is determined by the type and density of surfactant molecules in aqueous phase. For investigating the dominating effect on obtaining shape of particles, two systems (PVP:CTAB and PVP:SDS) were used separately. The enhancement of CTAB and SDS concentration at constant PVP concentration caused a decrease in the diameter of spheres

down to 150 nm and 100 nm, respectively (**Figure 3.17 a-h**). Nanoparticles with assembly character are obtained if the SDS concentration is lowered down to 0.1  $\mu\text{M}$  at constant PVP concentration (5 mM). At high concentration of ionic surfactant (SDS or CTAB), the formation of sphere-like particles is governed by micellar mechanism whereas the flower-like formation of particles is resulted from solvation and mobility factors during high PVP concentration.

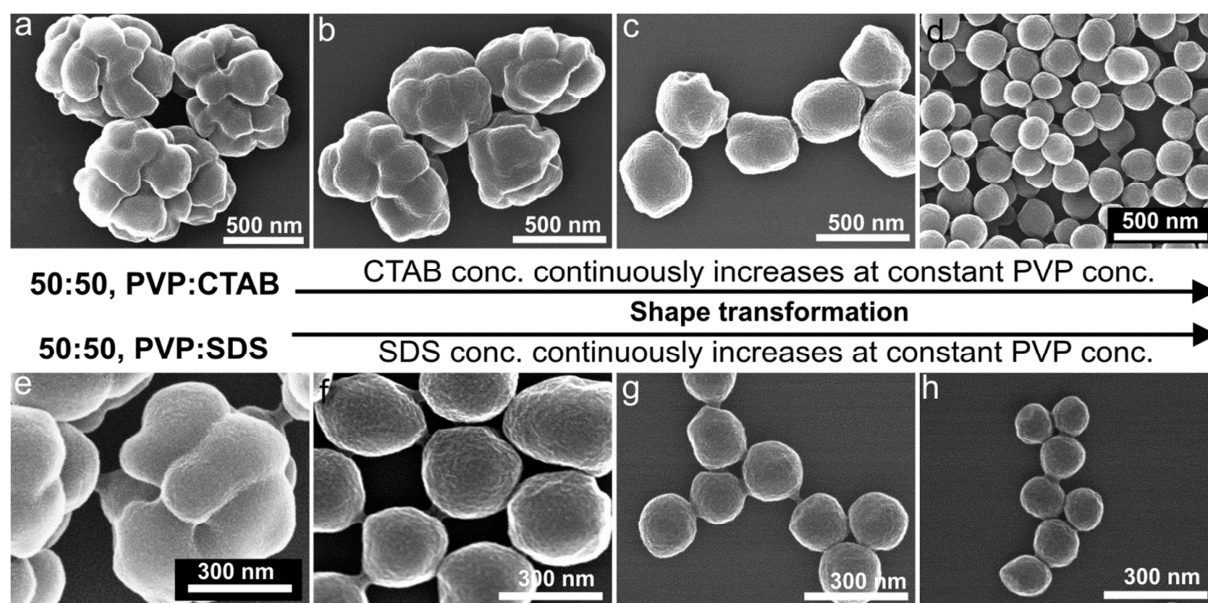


**Figure 3.17** (a-h) are SEM images of PMMA particles obtained when mixed surfactants (PVP and CTAB/SDS) were used in aqueous phase at different concentration. 50:50 (%) PVP/CTAB, (a) 5 mM/0.1  $\mu\text{M}$ , (b) 5 mM/1  $\mu\text{M}$ , (c) 5 mM/10  $\mu\text{M}$ , and (d) 5 mM/100  $\mu\text{M}$ ; 50:50 PVP/SDS, (e) 5 mM/0.1  $\mu\text{M}$ , (f) 5 mM/1  $\mu\text{M}$ , (g) 5 mM/10  $\mu\text{M}$ , and (h) 5 mM/100  $\mu\text{M}$ . Scale bar for images a-d (500 nm) and e-h (300 nm) are same.

The obtained result of dominating effect of the particular surfactant on shape-controlled polymer nanoparticles is well supported by zeta potential measurements. The particles obtained by increasing SDS concentration in aqueous phase showing increasing electrical charge in negative direction (**Figure 3.18**). Eventhough zeta potential does not describes direct potential of the particles, it can be assumed that the particles potential is correlated with zeta potential and the shift of particles charge moves in the same direction as zeta potential indicates. In case of only PVP in aqueous phase (in absence of SDS or CTAB), the particles shows always about -15 mV potential. The zeta potential of particles is lowered down to about -20 mV in case of only SDS (1 mM) surfactant in aqueous phase (**Figure 3.18 a**). Shape of the polymer nanoparticles is transforming from flower to sphere-like structure when SDS concentration is step by step increases at constant PVP concentration in aqueous phase.



Meanwhile, with increase in SDS concentration, the collective zeta potential (PVP + SDS) is move to high value in negative direction up to about -40 mV (**Figure 3.18 d**).

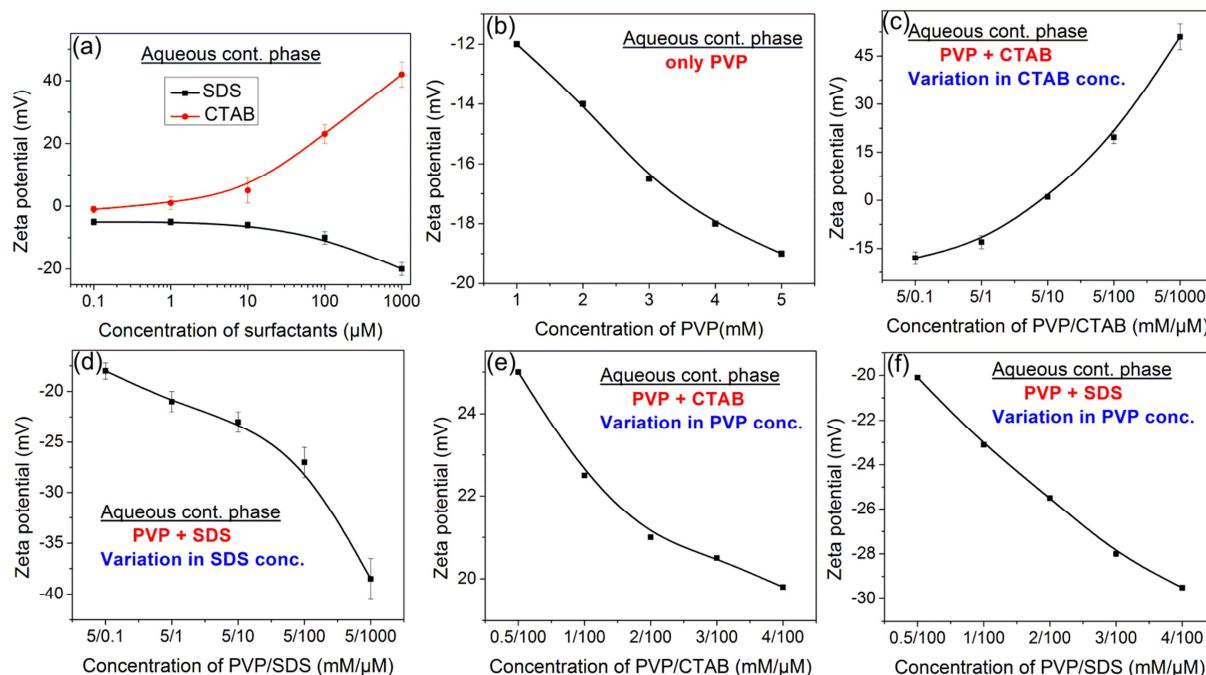


**Figure 3.18** (a-f) are the graphical representation of the zeta potential measurements of PMMA particles obtained when different concentration of individual and mixed surfactants (CTAB, SDS and PVP) were used in the continuous phase.

On other side, a shift of the zeta potential in the opposite direction is observed if CTAB is mixed with PVP in aqueous phase. The surface potential increases from about -2 mV up to about +40 mV in case of only CTAB from 0.1  $\mu\text{M}$  to 1 mM concentration, respectively. The enhancement of particle charge by SDS (in negative direction) or by CTAB (in positive direction) supports the stability of nanoparticles by the contribution of electrostatic repulsion at all levels. A decrease of ionic surfactant concentration at constant PVP concentration causes the formation of flower-like nanoparticles of a complex structure, which is formed after a primary and a second assembling process during ongoing polymerization reaction. The mutual interaction of mixed-surfactants with each other during the ongoing polymerization makes strong suppression on particles growth. Therefore, the particles of comparatively smaller size with planar surface are obtained at the end of thermal polymerization reaction. **Figure 3.19** represents the size tuning effect of obtained particles when individual and mixed-surfactants were used in the aqueous phase at different concentrations. In all cases, it is clear that the size of the final particles is decreased down significantly with increase in the concentration of individual or mixed surfactant in aqueous phase.



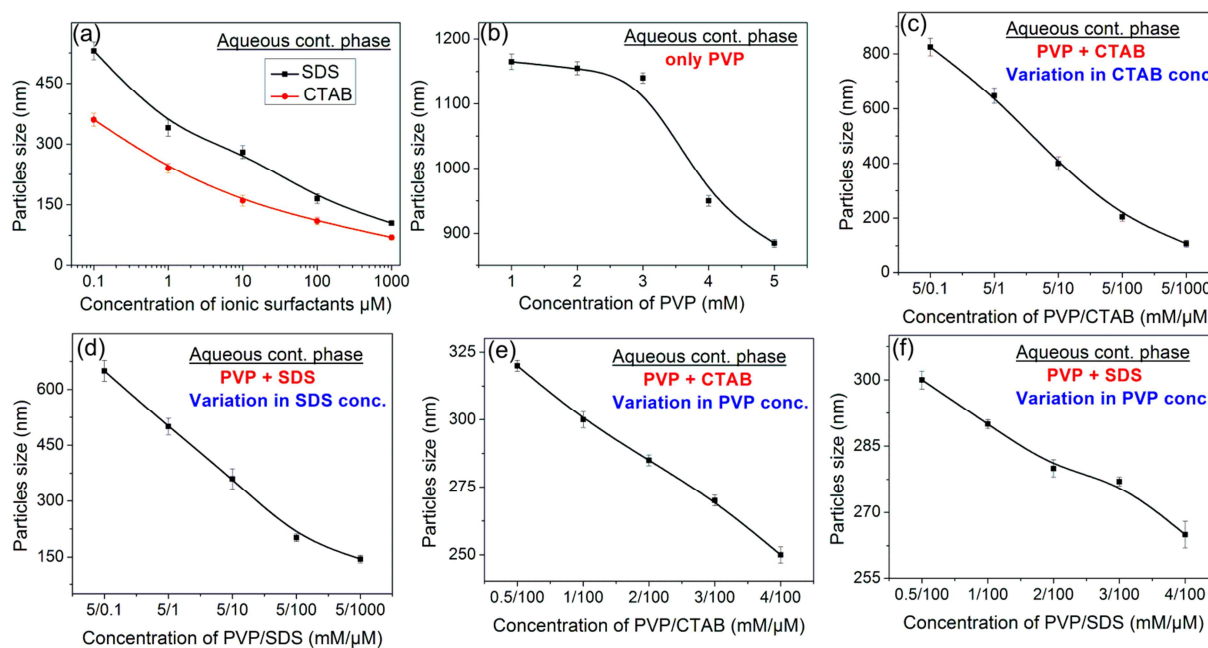


**Figure 3.19** (a-f) Size measurements (by dynamic light scattering) of the PMMA particles obtained when different types (CTAB, SDS and PVP) and at different concentration of individual and mixed surfactants were used in continuous phase. Particles sizes strongly depend on the concentration of surfactants.

Overall, the complex flower shaped polymer nanoparticles is prepared in the controlled semi-microfluidic platform by the application of non-ionic polymer (PVP) in aqueous phase. The mechanism of the formed particles is explained by mobility, solvation and multiple aggregation phases during ongoing polymerization process.

### 3.3 Shell-like layered polymer nanoparticles and their nanoassembly synthesis

Here, an *in-situ* copolymerization approach for obtaining hydrophobic core with hydrophilic shell layered polymer nanoparticles is presented in a similar semi-microfluidic arrangement as shown in **Figure 2.2**. It is particularly interesting for various biomedical applications that a single system (delivery vehicle) occupies hydrophilic as well as hydrophobic regimes to deliver the triggered release two or more types of non-miscible active components at targeted sites. A major challenge in the synthesis is obtaining the reproducible and homogeneous nanoparticles with minimum number of preparation steps. Here, due to the advantages of microfluidic platform for providing fast phase transfer and efficient mixing condition, the polymeric nanoparticles with surface layer are prepared in a single-step. Moreover, their electrostatic assembly with oppositely charged polymer and metal nanoparticles is shown for the optical application such as SERS.

#### 3.3.1 Formation of surface layered polymer structure

The requirement of drug delivery system for high encapsulation yield and potential for specific targeting is the development of smart multifunctional targeted nanoparticles [173, 174]. To control the shell thickness of metallic or semiconducting materials is a reliable process due to their crystalline nature [175, 176]. In direct contrast, due to the amorphous nature of polymeric materials, the core size with shell-like structure in a single-step together with tunability in the shell thickness is a complex process. Here, a systematic *in-situ* copolymerization approach of the surface layered polymer nanoparticles synthesis in single-step is performed.

Early stage of initiation should occur under the extremely homogeneous environment for obtaining regular nucleation and therefore the growth in uniform manner. For obtaining the polymeric shell-like layered nanoparticles, hydrophilic monomer diallyldimethyl ammonium chloride (DADMAC) in aqueous phase and hydrophobic monomer MMA in dispersed phase were used. DADMAC can also act as interface active agent to control the particles size and surface charge simultaneously. Droplets of MMA monomers generates by the shear force of DADMAC solution in micro continuous flow. Thermal initiator dissolved in the dispersed phase which forms radical at heating temperature (95 °C) and initiates the nucleation of PMMA core particles. Together with growing PMMA core, the simultaneous attack of core radicals can realize by the hydrophilic monomers DADMAC at the interface and forms the

soft poly polyDADMAC layer as a shell in the aqueous environment. MMA is a hydrophobic monomer and also showing partial solubility in the aqueous phase. Therefore, the inner core of growing PMMA nanoparticles is completely hydrophobic and surface remains slightly hydrophilic which can cross-link with polyDADMAC at the outer surface through weak force (such as van der Waals force). Here, no any additional intermediate agents required for connecting the hydrophobic and hydrophilic regimes at the interface. The polymerization of shell layer is obtaining in the aqueous environment and therefore, this layer is not dissolved but swells in the solution phase. Meanwhile, during the swelling phase of shell layer, it can be assumed that the continuous addition of DADMAC free monomers takes place together with diffusion of MMA units through the pores of a shell layer. Thus, the simultaneous growth of the core and surface shell layer is obtained with high homogeneity as schematically shown in **Figure 3.20 A**.

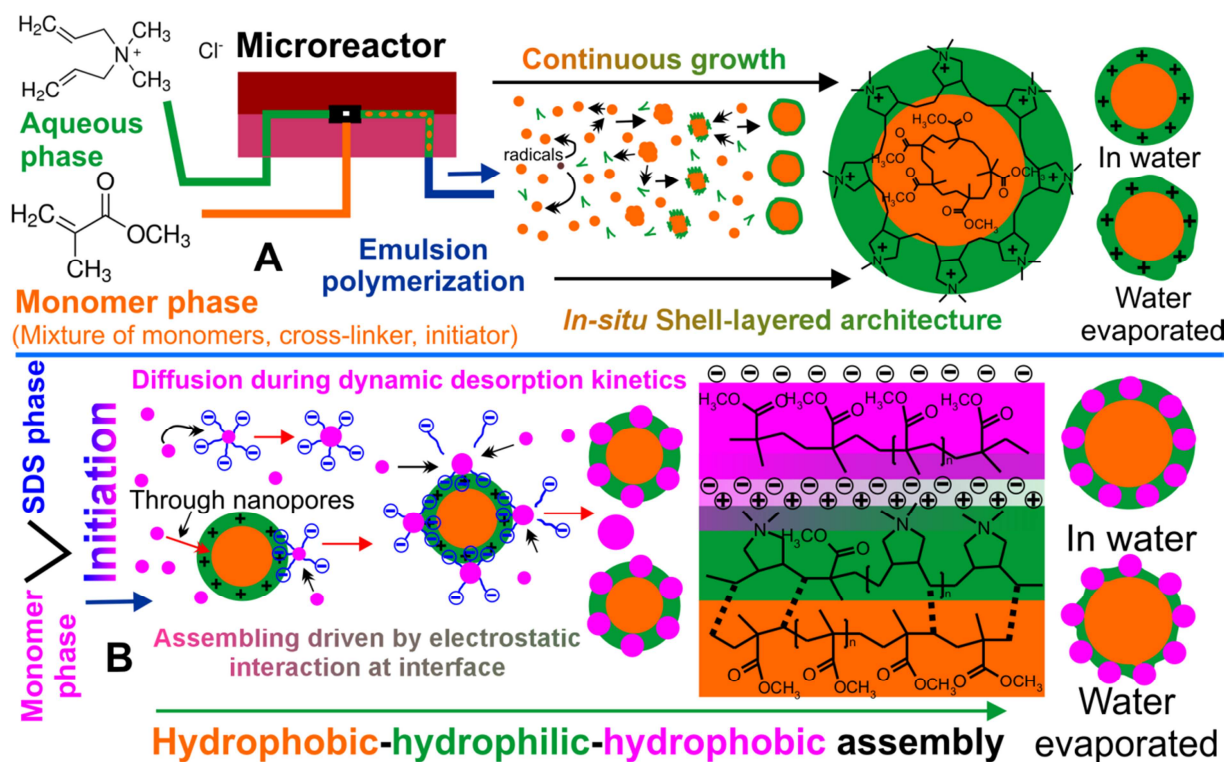


**Figure 3.20** Schematic representations for: (A) *in-situ* formation of the shell-like surface layered polymer nanoparticles in semi-microfluidic platform and (B) controlled electrostatic nanoassembly of smaller polymer nanospheres with charged polymer particles.

### 3.3.2 Tuning in particles size

Mean size of the nanoparticles can be uniformly tuned by changing the reaction parameters such as concentrations and flow rate ratios of both immiscible liquid phases in microreactor. Hydrophobic PMMA core is comparatively harder than the growing hydrophilic polyDADMAC shell layer in aqueous environment. Moreover, as aqueous monomer playing role of interfacial stabilizing agent too, the weight amount is certainly lower compared to the core monomers amount. Polymer particles of about 550 nm mean size were obtained at 6 mM DADMAC concentration in aqueous phase and 1200/70 (aqueous/monomer,  $\mu\text{L}/\text{min}$ ) flow rate ratio of both immiscible phases. Average particles size increases consistently with step by step increase in MMA flow rate at constant aqueous flow rate. Polymer particles of about 700 nm are obtained at flow rate ratio of 1000/100. On the other hand, at enhanced aqueous flow rate, the particles size is decreased considerably because of strong charged surface layer which are responsible for nucleating the more numbers of particles. Hence, the obtained particles are of only 400 nm at 1800/40 flow rate ratio. Besides the total flow rate ratios, the concentrations of aqueous monomer contributing the governing impact to tune the particles size. It is well known that the particles size decreases with increase in surfactant concentration [61]. Therefore, the particles are obtained of about 650 nm and 500 nm respectively at 1.5 mM and 3 mM DADMAC concentration in the aqueous phase with constant flow rate ratio of 1200/70. The interesting effect observed here is; the particles size constantly increases (instead of decreasing) with further increase in the DADMAC concentration in aqueous phase. The particles of 550 nm and 600 nm sized are obtained at 6 mM and 12 mM DADMAC concentration, respectively. Here, it is assumed that the shell thickness increases with constant core size at a higher DADMAC concentration. The size tuning effect of the obtained particles is shown in **Figure 3.21**.

Surface charge of the obtained particles is measured by zeta potential measurements. It is always positive because of the positively charged surface layer of polyDADMAC on the PMMA cores as shown in **Figure 3.21 e**. Moreover, the particles potential is changing upon variation in concentration of hydrophilic monomers in aqueous phase. Graphical results of size tuning of obtained particles is shown in **Figure 3.21 f**.

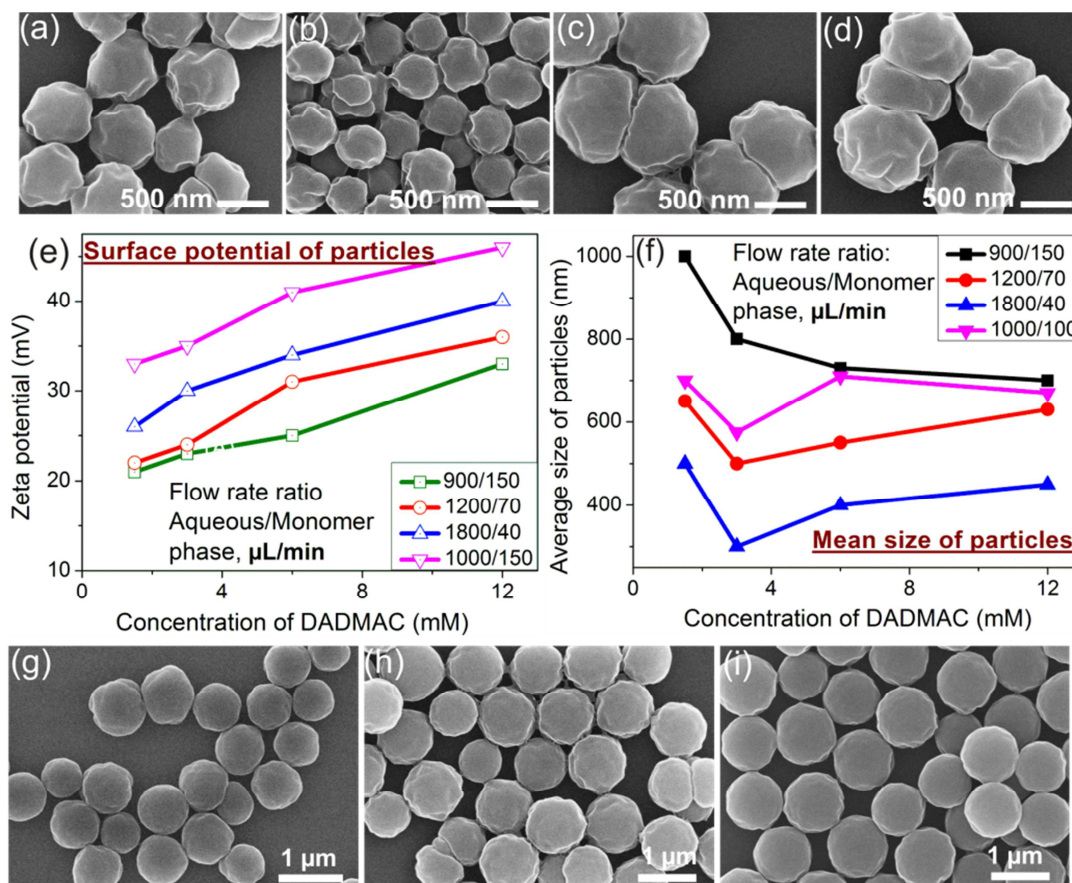


**Figure 3.21** (a-d) SEM images of the particles obtained at different flow rate ratios (aqueous phase: 6 mM DADMAC): (a) 1200/70 (aqueous/monomer,  $\mu\text{L}/\text{min}$ ), (b) 1800/40, (c) 1000/100, and (d) 900/150. Graphical representation of the (e) zeta potential and (f) size with respect to DADMAC concentration in aqueous phase. Standard deviation for zeta potential measurements is  $\pm 4$  mV and for size measurement is  $\pm 50$  nm. SEM images of the obtained particles at different concentrations of DADMAC in aqueous phase (flow rate ratio: 900  $\mu\text{L}/\text{min}/150 \mu\text{L}/\text{min}$ ): (g) 12 mM, (h) 6 mM, and (i) 1.5 mM.

### 3.3.3 *In-situ* electrostatic polymer-polymer nanoassembly

Hydrophilic shell is a highly dense cationic charged layer of polymer particles and allows further entrapping of oppositely charged colloidal polymer nanoparticles in porous interior. An *in-situ* approach of the hydrophobic-hydrophilic-hydrophobic assembly is performed here for preparing the assembly polymer particles. For growing the smaller nanoparticles at the surface of pre-formed charged polymer nanoparticles, controlled emulsion solution is inserted to the particles suspension through microreactor as shown in **Figure 3.20 B**. The polymerization reaction starts at 95  $^{\circ}\text{C}$ . The used SDS concentration in aqueous phase is between 10  $\mu\text{M}$  and 1 mM, and is responsible for controlling the size of growing nanoparticles accordingly. Once the polymerization reaction is completed, the negatively charged smaller nanoparticles are *in-situ* assembled with positively charged particles through



electrostatic interaction. Size and density of the growing nanoparticles is depends on the SDS concentration in aqueous phase and total emulsion amount to the surface layered charged particles suspension (**Figure 3.22**). When very high emulsion volume is supplied to the diluted particles suspension, the smaller particles are formed in the shell interior as well as separately in aqueous medium. The particles size in the shell interior is always smaller than the separately growing nanoparticles in water (**Figure 3.22 d**). The negatively charged SDS molecules binds to the positively charged shell surface and therefore the rate of monomer diffusion is comparatively slower than the freely growing nanoparticles.

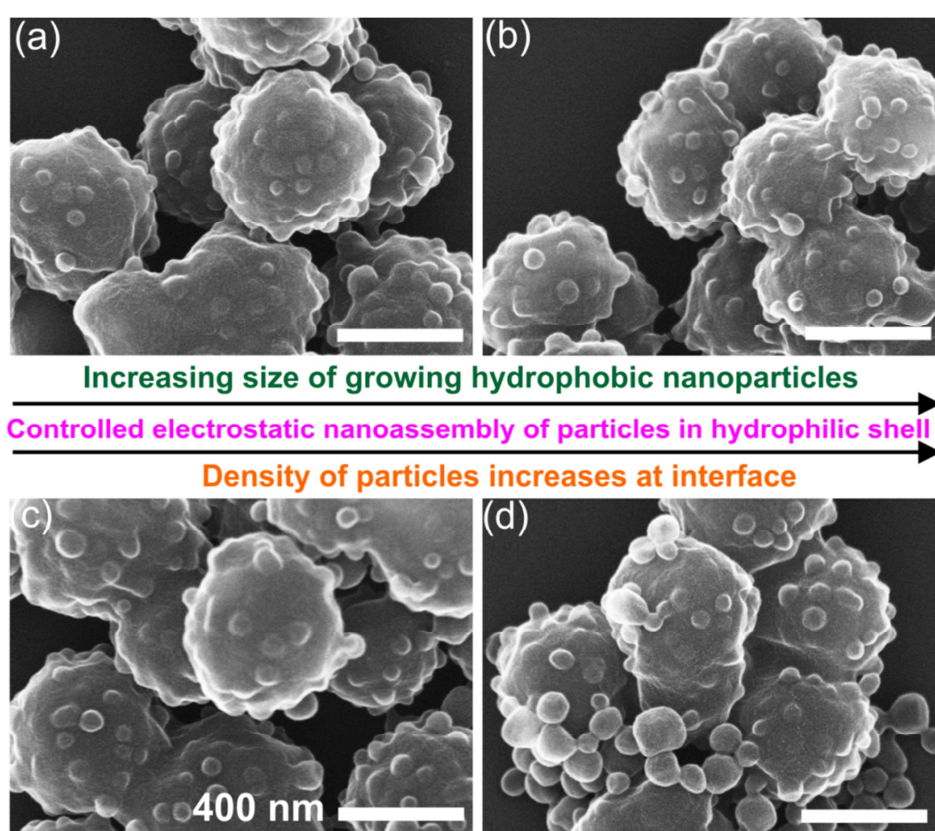


**Figure 3.22** SEM images of the controlled electrostatic polymer-polymer assembly at different reaction condition: emulsion solution contained (a) 0.1 mM and (b) 0.01 mM SDS in the aqueous phase. Assembly obtained at different volume of emulsion solution, (c) 60  $\mu$ L and (d) 100  $\mu$ L. Scale bar for all SEM images (a-d) are same (400 nm).

### 3.3.4 Electrostatic polymer-metal nanoassembly

Metal nanoparticles, particularly gold (Au) nanoparticles, exhibit intense optical phenomena which are useful for many photonics as well as biomedical applications. The association of Au nanoparticles with polymeric nanoparticles combines the properties of two different regimes. Therefore, in this work, the controlled Au-polymer assembly particles of different concentration ratios are prepared in the flow condition through electrostatic interaction. It is shown in **Figure 3.21 e** that the surface charge of the surface layered polymer particles is between +20 mV and +45 mV. On other side, the negatively charged Au nanoparticles (zeta potential about -22 mV) have strong affinity, therefore, to bind the surface of positively charged polymer particles. For the preparation of the heterogeneous nanoassembly particles, both suspensions have been filled in the glass syringes and 25  $\mu\text{L}/\text{min}$  flow rate of both syringes were actuated simultaneously for 10 min through knot mixture at room temperature. PMMA-polyDADMAC particles of about 600 nm size is used for the preparation of PMMA-Au assembly particles (**Figure 3.23 a**).

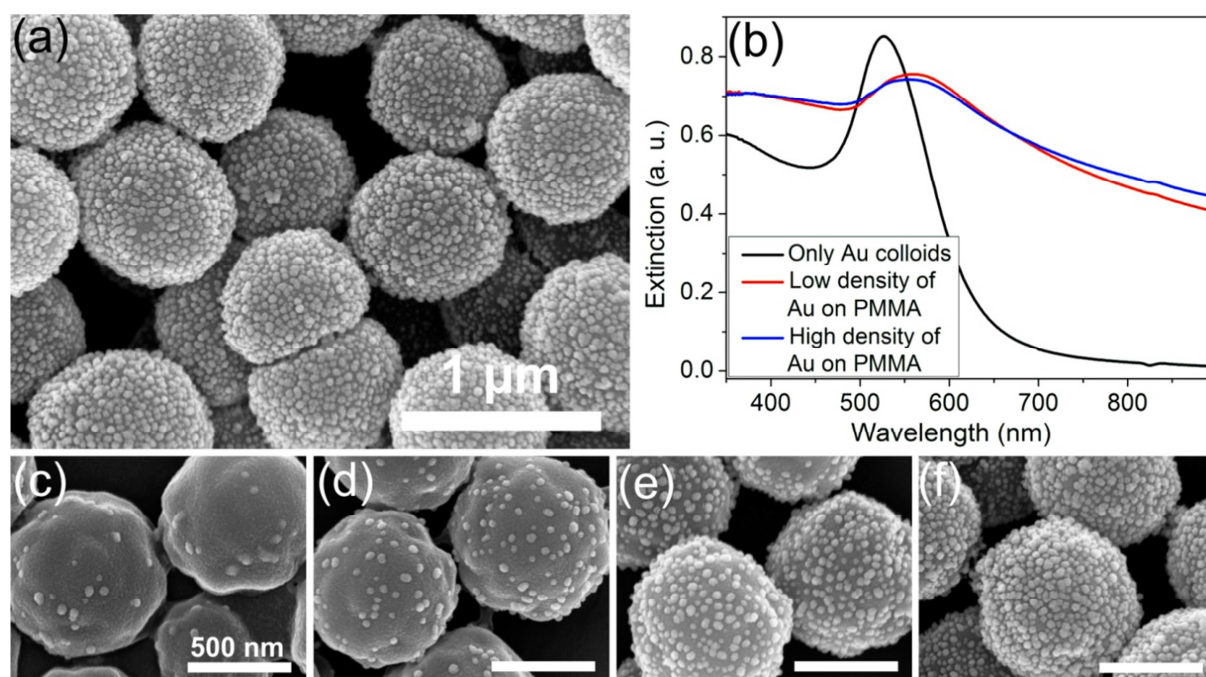


**Figure 3.23** (a) SEM image of the polymer-Au assembly particles and (b) UV/vis spectra of the pure Au nanoparticles and PMMA-Au assembly particles. (c-f) SEM images for the increasing Au density on polymer particles (50  $\mu\text{L}$  particles suspension in 1 mL water): (c) 5  $\mu\text{L}$ , (d) 10  $\mu\text{L}$ , (e) 25  $\mu\text{L}$  and (f) 50  $\mu\text{L}$  Au nanoparticles suspension in 1 mL water. Scale bar for the images (c-f) are same (500 nm)

High density and strong binding of the Au nanoparticles is observed as the positively charged polymer shell layer is swellable in the aqueous medium. Colloidal Au nanoparticles exhibit the plasmon resonance at about 515 nm (**Figure 3.23 b**). However, the bathochromic shift and broadening of the plasmonic peak is realized when colloidal Au nanoparticles (of about 30 nm) assembled with polymer particles. Polymer-Au assembly particles show the plasmon peak at 560 nm. Various weight ratios of both components were used for tuning the Au density on the surface of polymer particles. The assembly particles with high Au density is observed when 50:50 ( $\mu\text{L}$ ) ratio of Au:polymer has been used (**Figure 3.23 f**).

On other hand, silver (Ag) nanoparticles is more attractive for optoelectronic and sensing because of its higher plasmonic efficiency and superior electromagnetic enhancement in the visible range [177]. Surfactant is usually required for the stability against undesired aggregation in a solution based Ag nanoparticles synthesis. Such adsorbed surface layers of molecules restrict the application of silver material in biosensing because they prevent the adsorption of the reporter molecules on the nanoparticles surface [177]. Here, metal catalyzed metal nanoparticles synthesis approach is applied for the polymer/Au/Ag controlled assembly where Au acts as nuclei for additional Ag enhancement. Different concentrations of Ag amount are realized as shown in **Figure 3.24**. Ag surface is more suitable for the interaction of different analytes for the surface-enhanced Raman scattering sensing applications. A detailed SERS study of the different analytes is described in chapter 4 (section 4.2.4).

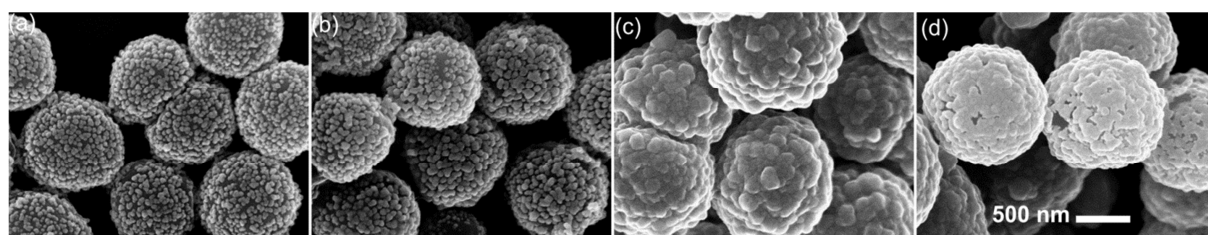


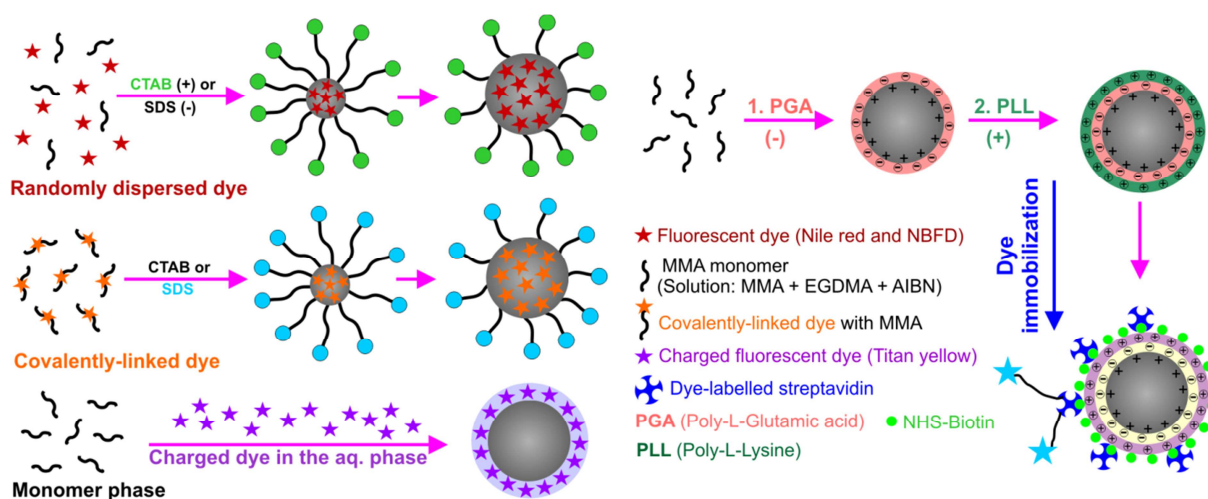
**Figure 3.24** SEM images of the Ag enforced Au-polymer assembly particles with increasing density of Ag on the surface: (a) 3 mM, (b) 5 mM, (c) 10 mM and (d) 20 mM  $\text{AgNO}_3$  (50  $\mu\text{L}$ ) to the 20  $\mu\text{L}$  particles suspension in presence of 50  $\mu\text{L}$  25 mM ascorbic acid. Scale bar for all SEM images are same (500 nm).

Overall, in this section, the controlled polymer nanoparticles with tunable core size and shell-like surface layer thickness together with PMMA/PMMA, PMMA/Au and PMMA/Au/Ag nanoassembly is prepared in a semi-microfluidic platform.



### 3.4 Fluorescent polymer nanoparticles

Fluorescent nanoparticles play a vital role in large number of labeling, barcoding and other biomedical related applications [178]. In most of the cases, inorganic semiconducting quantum dots (Qdots) are used as appropriate probes for the multiplexed targeted analysis owing to their narrow tunable emission peaks and broad excitation bands [80]. But, because of their toxicity for some sensitive uses, they cannot be applicable for *in vivo* and other cellular activities. Moreover, free molecular dyes are also not perfect candidates for the development of high-sensitive imaging techniques and high-throughput assays because of their low absorptivity and poor photostability [25, 87, 88]. As a direct replacement (alternative), dye-doped fluorescent polymer nanoparticles (Pdots) can be used as promising probes for multiple biological applications because of their simple preparation and exceptionally bright and stable fluorescence nature [85, 86]. Moreover, polymer particles are non-toxic and, therefore, can be frequently used in the *in vivo* applications too along with some other uses for instances, as photonic crystals [91], used for confocal microscopy [26], for multiphoton fluorescence imaging [85], and so forth. In addition, for the uniform performances in various applications, the homogeneity of the polymer nanoparticles is key requirement.



**Scheme 3.2** Schematic overview of the different strategies for preparing four different classes of fluorescent PMMA nanoparticles.

In this work, the size and surface charge controlled homogeneous fluorescent polymer nanoparticles of four different types are prepared in semi-microfluidic platform (as shown in **Figure 2.2**). Different strategy for preparing the fluorescent polymer nanoparticles are demonstrated where dyes can be embedded, adsorbed, anchored and functionalized to the

nanoparticles. The schematic overview of different strategies is shown in **Scheme 3.2** and obtained results are described below.

### 3.4.1 Dye-embedded fluorescent polymer nanoparticles

Two different routes are shown here for the dye-embedded polymer nanoparticles: (a) non-covalent linking and (b) covalent linking of fluorescence dye in the nanoparticles interior. There are various methods available to incorporate the fluorescence dyes inside the polymer matrix such as, by swelling methods and others [92, 179]. But, these methods are multi-steps processes and also the homogeneous distribution of dyes inside the polymer matrix cannot be achieved. Therefore, in first part, two different fluorescence dyes are randomly dispersed (non-covalent linking) separately in the monomer phase and subsequently polymerized in microfluidic platform (single-step process) to generate the nano fluorescent beads of high homogeneity and of different emission wavelengths. Here, Nile red dye is used as a model hydrophobic fluorescence dye, and the obtained nanoparticles showing fluorescence emission at 593 nm (**Figure 3.25 c**).

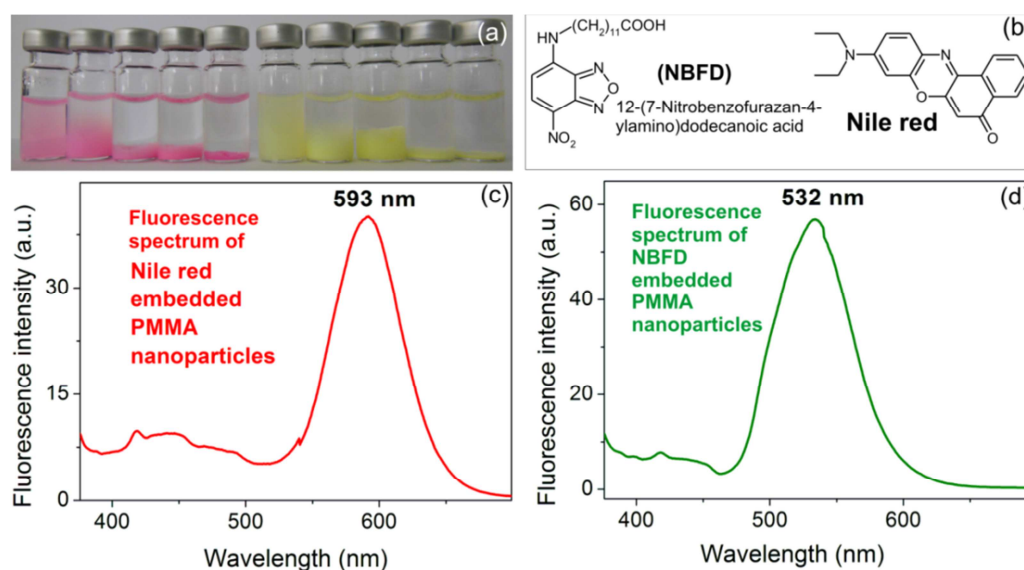
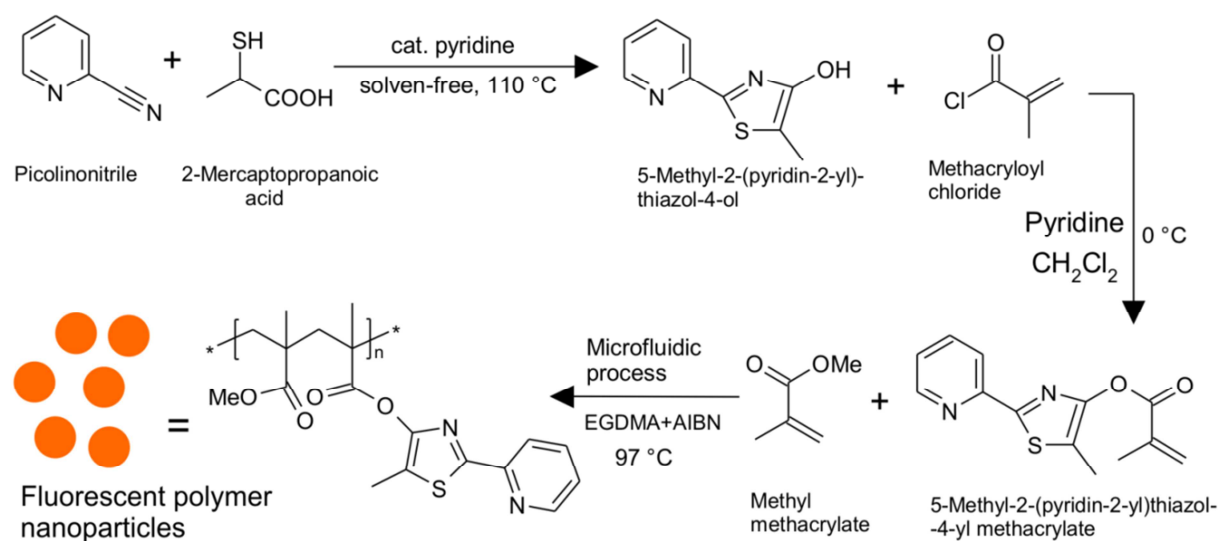


**Figure 3.25** (a) Camera picture of the Nile red and NBFD-embedded PMMA nanoparticles suspension (smaller nanoparticles suspension (left) is stable and bigger nanoparticles (right) are settled down at bottom after 2 hours), (b) the chemical structures of used dyes, and (c) and (d) are the fluorescence spectra of the Nile red and NBFD embedded PMMA nanoparticles, respectively.

Moreover, the nanoparticles surface is covered with charged surfactant layer of CTAB and therefore, the particles are well-dispersed in aqueous medium which is particularly interesting for several of fluorescence application such as, labeling, sensing and materials for photonic crystals. The particles size can be tune by variation in applied CTAB concentrations in

aqueous phase and also by varying flow rate ratios of both immiscible phases in microfluidic setup. Smaller particles have higher surface charge and therefore, the particles suspension is stable for longer time period due to the high Brownian motion (**Figure 3.25 a**). On other hand, the fluorescence strength of the obtained size-tuned nanoparticles can be managed by varying the dye concentration during synthesis. Nbfd (dye of another emission wavelength) embedded polymer nanoparticles shows fluorescence peak at about 532 nm (**Figure 3.25 a, d**).

Usually, an aqueous suspension of fluorescent nanoparticles is preferred for the labeling application. But, sometimes due to the contact of organic medium (solvent), free dye molecules released to the surrounding medium from the particles interior during a swelling phase and then the brightness of label particles is decreased down. To avoid such leaking concern, the fluorophore (dye) should be covalently linked in a polymer network. For the covalent linking, the monomer units were functionalized with fluorescent organic compound prior to the polymerization reaction as shown in **Scheme 3.3**.



**Scheme 3.3** Scheme shows the chemical synthesis of fluorophore-functionalized monomer (5-Methyl-2-(pyridin-2-yl)thiazol-4-yl methacrylate) molecule and polymerization reaction for the covalent linking of fluorophore in the nanoparticles interiors (part of the Scheme is modified from [180]).

An organic molecule 4-hydroxythiazol sub-structure was prepared as described earlier [180] by a Hantzsch like reaction; employing 2-cyanopyridine and 2-mercaptoacetic acid under solvent-free conditions at elevated temperatures using pyridine as a catalyst. The functionalization of MMA with 5-Methyl-2-(pyridin-2-yl)thiazol-4-yl methacrylate forms 5-Methyl-2-(pyridin-2-yl)thiazol-4-yl methacrylate (**Scheme 3.3**). Functionalized MMA is a solid

compound and dissolved to the pure MMA solution at different ratio for performing the liquid phase polymerization reaction. Here, a microflow process is performed to obtain the covalently linked fluorophore-PMMA nanoparticles of different sizes between 70 nm and 400 nm (**Figure 3.26 a-d**) where different mixing ratio of fluorophore-functionalized MMA and pure MMA were used in the monomer phase.

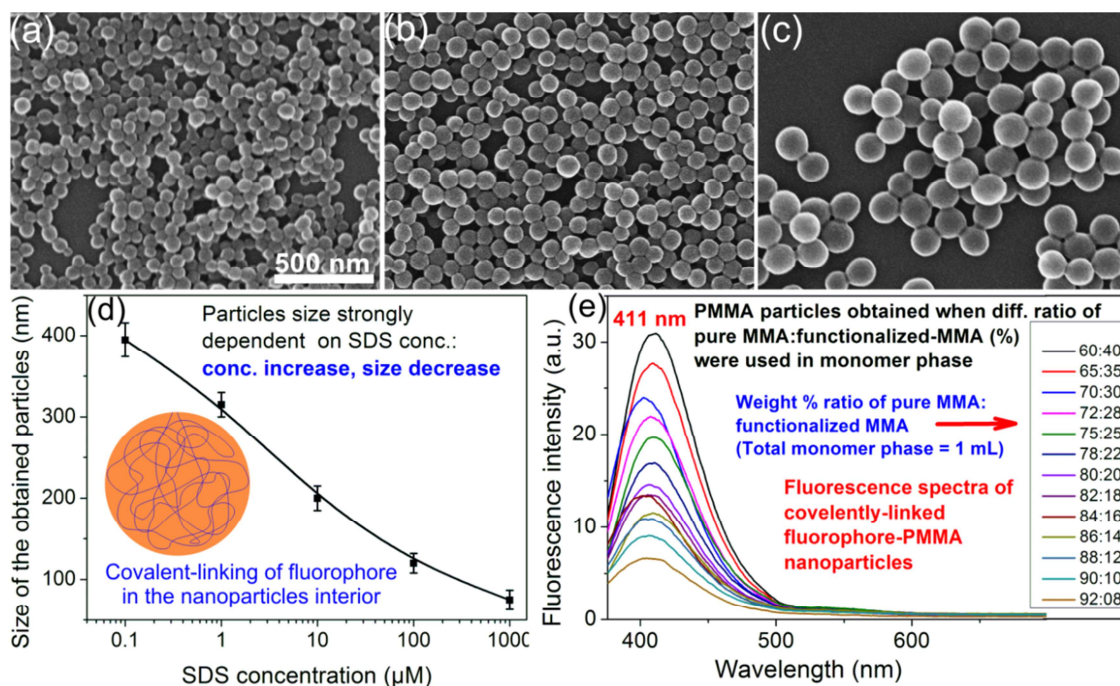


**Figure 3.26** (a-c) SEM images of the covalently linked fluorophore-embedded PMMA nanoparticles obtained when different concentrations of SDS, (a) 1 mM, (b) 0.1 mM and (c) 0.01 mM were used in the aqueous phase (flow rate ratio 1200/70  $\mu\text{L}/\text{min}$ , aqueous/monomer). Scale bar for all three SEM images are same (500 nm). (d) Graphical result of particles size dependent on SDS concentrations in aqueous phase. (e) Fluorescence spectra of the obtained nanoparticles at different % ratio of pure MMA and fluorophore-functionalized MMA in the monomer phase.

By varying the concentrations (weight ratio) of fluorophore functionalized-MMA in the pure MMA solution and also by varying the SDS concentration in aqueous phase at different flow rate ratios, the size and surface potential controlled fluorescent polymer nanoparticles is obtained (**Figure 3.26**). Fluorescence intensity of the obtained nanoparticles is consistently increases with increasing amount of functionalized MMA.

### 3.4.2 Dye-anchored fluorescent polymer nanoparticles

Surfactant plays a dominating role for controlling the size and surface charge of the nanoparticles during polymerization reaction. In case of high surfactant concentration, the nanoparticles are obtained of smaller size and also in large numbers. The challenging task for preparing the functional nanoparticles is; it should be obtained in a minimum number of preparation steps and should consume minimum types of reactants. Interestingly here, the aqueous phase is made up of the charged amphiphilic fluorophore (chemical structure shown in **Figure 3.27 a**, Titan yellow) which play a role similar to the charged surfactant for controlling the size and surface charge simultaneously. As shown in **Figure 3.27 c**, the size of the PMMA nanoparticles decreased from about 200 nm down to 80 nm when concentration of Titan yellow in aqueous phase increases from 0.01 mM up to 1 mM. A complete mechanism is not clear about the role of Titan yellow for tuning the particles size. But, it can be assumed that the diffusion rate of monomers during the ongoing polymerization is higher when surface layer of the Titan yellow is weak (lower concentration), and therefore, the bigger sized nanoparticles are obtained. Moreover, the surface charges of the obtained particles can be tuned between about -10 mV and -45 mV by using Titan yellow concentration between 0.01 mM and 1 mM in aqueous phase (**Figure 3.27 d**). Besides the size and surface charge, Titan yellow concentration at the particles surface also contributing the key effect for tuning the fluorescence intensities (emission at 425 nm) of polymer nanoparticles simultaneously as shown **Figure 3.27 b**.

### 3.4.3 Dye-functionalized fluorescent polymer nanoparticles

A detection of targeted site by particle-based labeling and sensoric materials relies on the fast, sensitive and reproducible interaction [181]. Particles homogeneity and surface functional groups are, therefore, important for uniform interactions [182]. Different sized PMMA nanoparticles between 60 nm and 300 nm are functionalized with layer-by-layer modification approach (**Figure 3.28 a**). At initial point, CTAB covered 160 nm sized PMMA nanoparticles (surface potential of about +20 mV) interact with poly-L-glutamic acid (PGA) in aqueous suspension (interaction between  $-\text{NH}_3^+$  and  $-\text{COO}^-$ ). After first modification, the particles surface charge (zeta potential) becomes negative (about -10 mV) as shown in **Figure 3.28 d**. Surface potential of the PMMA nanoparticles again becomes positive (about +40 mV) after second modification step with cationic polypeptide, poly-L-lysine (PLL).



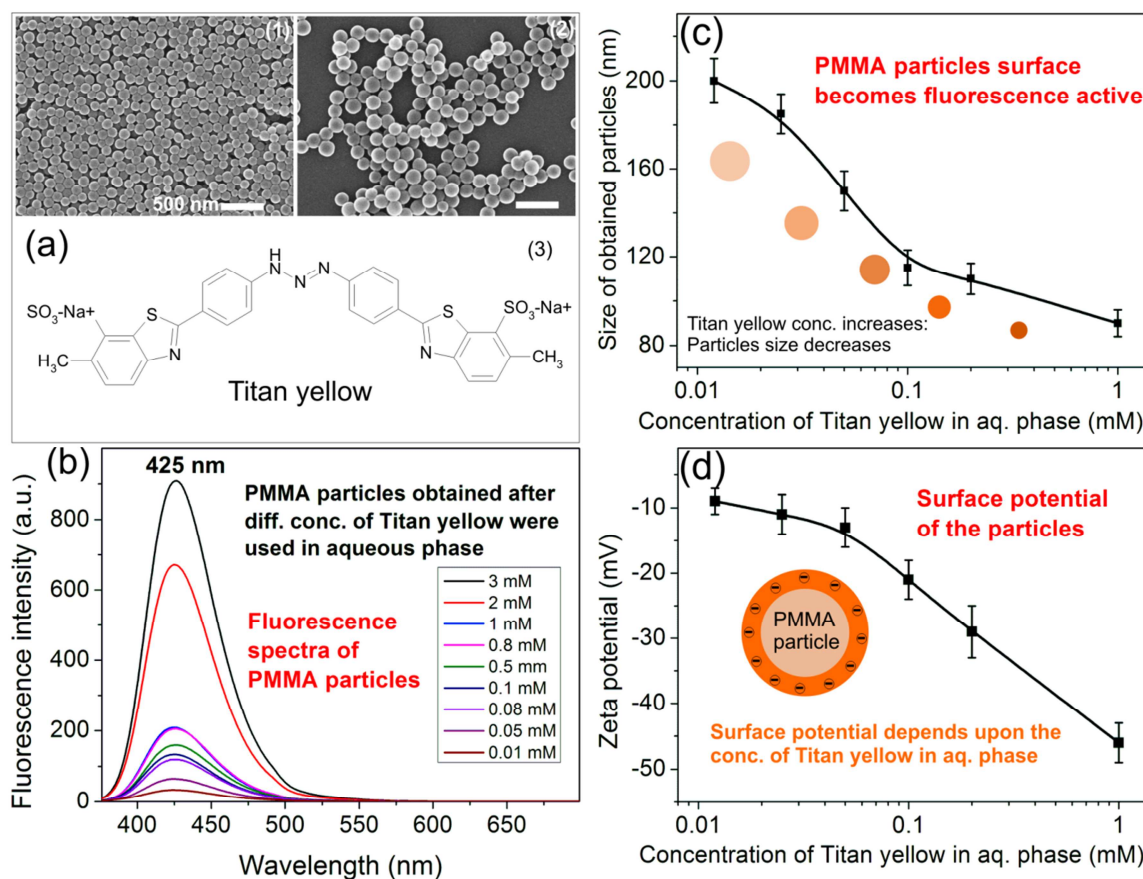


**Figure 3.27** (a) SEM images of the obtained PMMA nanoparticles when different concentrations of Titan yellow were used in the aqueous phase, (1) 0.1 mM and (2) 0.025 mM, and (3) a chemical structure of Titan yellow. (b) The fluorescence spectra of the PMMA nanoparticles obtained when different concentration of Titan yellow was used in the aqueous phase. Graphical results of the obtained nanoparticles (c) size and (d) zeta potential when different concentrations of Titan yellow were used in the aqueous phase.

Various types of polyelectrolytes can be used for building functional layers [183-190], and due to the biocompatibility as well as strong binding affinity through electrostatic interaction, PGA-PLL assembly is most promising [191]. To study the biological processes such as cell reporters and labeling of targeted site, biotinylation is widely used in which biotin interacts with various functional targeted sites [192, 193]. The process of biotinylation is rapid and specific due to the small size of biotin molecules (244 Da), and therefore, can be conjugated to many proteins without altering their biological activities. Therefore, in this work, biotin molecular layer is applied on the surface of PLL covered PMMA nanoparticles (zeta potential: becomes about -40 mV). On other hand, biotin has a strong affinity to linked with streptavidin through secondary interaction [193, 194]. This interaction takes place at a dissociation constant of about  $1.3 \times 10^{-15}$  M, besides the electrostatic and covalent interaction

[195]. To make the entire PMMA nanoparticles network a fluorescence-active, therefore, the dye-labelled streptavidin (AlexaFluor 594 conjugate) have been applied to the biotin-covered particles. The streptavidin covered nanoparticles are excited at 590 nm and emit the fluorescence light at about 619 nm as shown **Figure 3.28 e**.

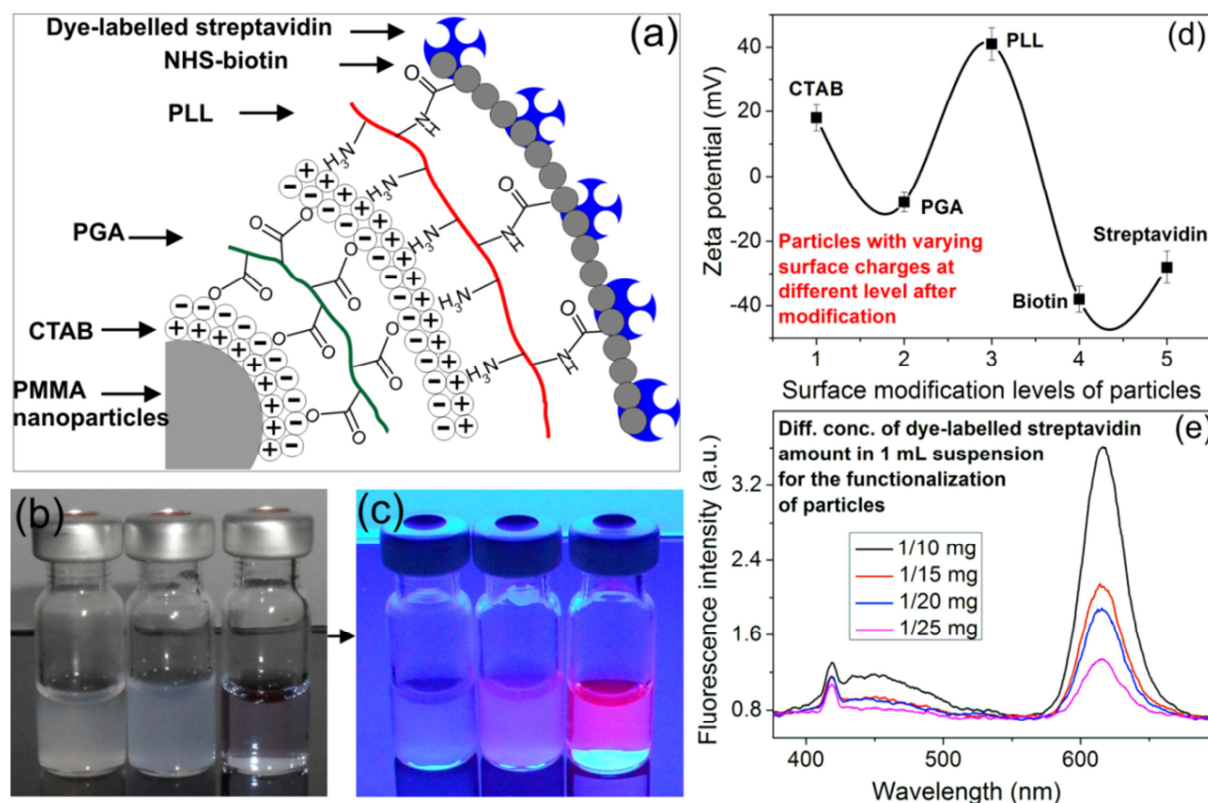


**Figure 3.28** (a) Schematic of the layer-by-layer surface modification via electrostatic, covalent and secondary binding. Camera pictures of the three glass vials which possess biotin covered particles, dye-labelled streptavidin covered particles and only dye-labelled streptavidin solution, respectively, (b) without UV lamp and (c) with irradiation of UV light. (d) Graphical results of the nanoparticles zeta potential after layer-by-layer surface modification. (e) Fluorescence spectra of PMMA nanoparticles after functionalization with different concentration of dye-labelled streptavidin.

In general, in section 3.4, four different strategies for preparing the fluorescent polymer nanoparticles is shown with obtained results. These kinds of fluorescent nanoparticles can be used as labels and probes in various biological and microfluidic applications.

### 3.5 Heterogeneous nanoassembly of the particles

In this work, electrostatically assisted nanoassemblies of metal/polymer particulate materials are performed. Ag microrods are prepared in a batch synthesis and PMMA nanoparticles of different sizes are prepared in the semi-microfluidic platform. In below section, the synthesis of individual components and nanoassembly particles is described with obtained results.

#### 3.5.1 Synthesis of Ag microrods

A facet directed growth forms the Ag microrods of tuned aspect ratio in polyol synthesis at elevated temperature.  $\text{Ag}^+$  ions are reduced by reducing agent and form the nuclei with fluctuating structure by combining several of Ag atoms together and most nuclei incorporate twin boundary defects to minimize their surface energy [196, 197]. Ethylene glycol (EG) acts as milder reducing agent as well as solvent at elevated temperature. A reaction solution is made up of 5 mL EG, 3 mL 0.25 M  $\text{AgNO}_3$  (in EG) and 3 mL 0.35 M PVP (in EG). Moreover, the aspect ratio of Ag microrods (length/diameter) strongly depends upon the concentration of ascorbic acid (external reducing agent) in reaction mixture. At 160 °C, a simultaneous addition of 1 mL 0.1 M ascorbic acid initially forms the penta twinned nanostructures and finally they grown as long Ag microrods via subsequent growth mechanism [198, 199]. **Figure 3.29** (top drawing) shows the synthetic strategy of Ag microrods in batch arrangement.

Noble metals, which adopt a face-centered cubic (fcc) lattice, possess different surface energies for different crystal planes. For the fcc crystal structure, the surface energies of low index crystallographic facets is given in the order of  $(111) < (100) < (110)$  [200]. Therefore, the growth of Ag microrods obtained in one particular direction of high energy surface (110) by passivation of the side surface (100) with PVP molecules. It is claimed that the PVP molecules are adsorbing on the microrods surface through Ag-O co-ordination bond [201]. In this work, it is found that the PVP: $\text{AgNO}_3$  concentration ratio of 1.4 (that is the concentration of PVP is 0.35 M and of  $\text{AgNO}_3$  is 0.25 M) is critical to obtain the highest yield of Ag microrods and also of high aspect ratio. Ag microrods of wider diameter are obtained because of early nucleation in the case when high concentration of ascorbic acid is used during the synthesis. The size tuned Ag microrods at different reaction condition is shown in **Figure 3.29 a-d**.



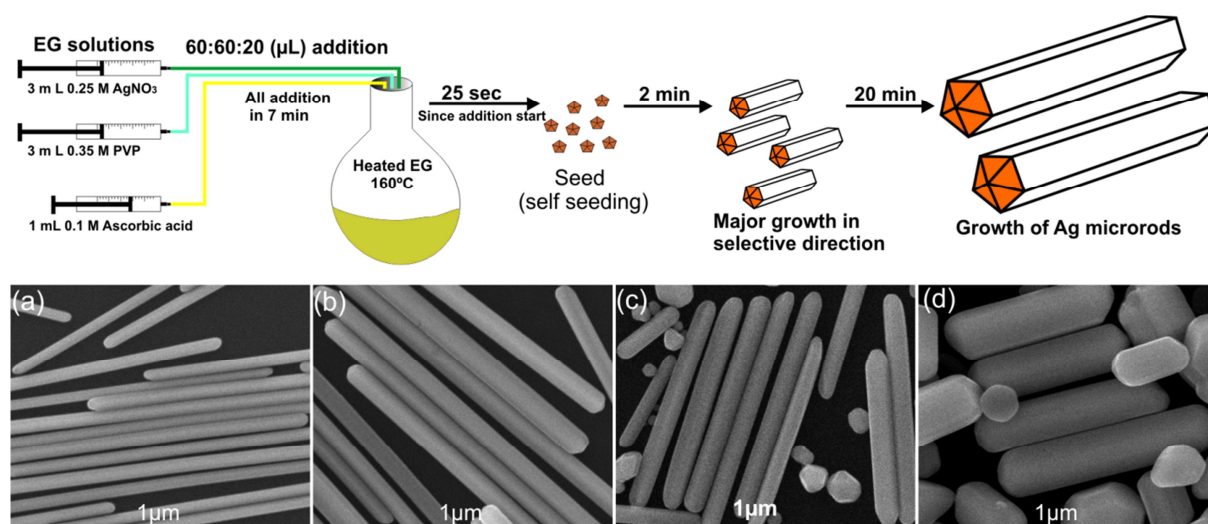


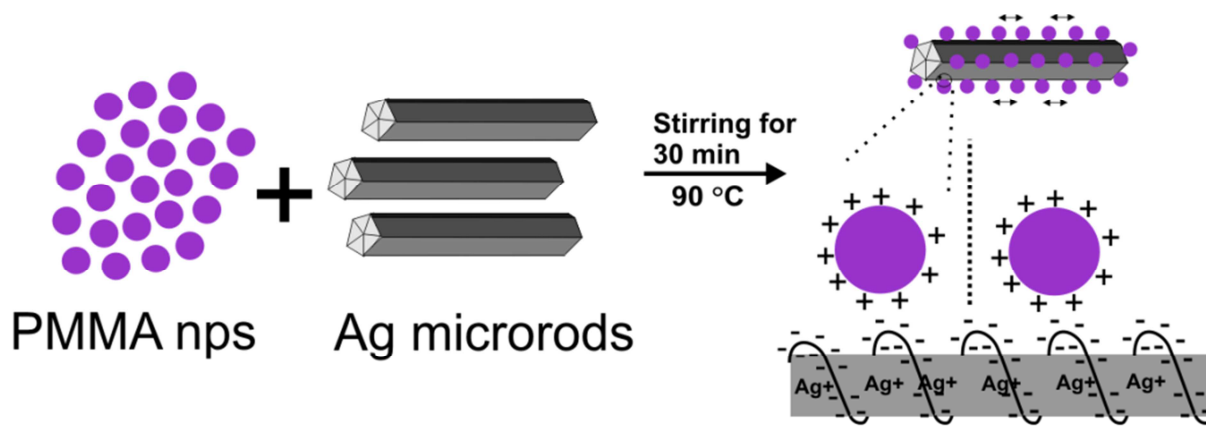
**Figure 3.29** Top drawing is a schematic of Ag microrods synthesis. Bottom: SEM images of the size controlled Ag microrods synthesized by adding different concentration of 1 mL ascorbic acid (AA) at different time interval along with 3 mL of each, 0.25M  $\text{AgNO}_3$  and 0.35M PVP (repeating unit conc.) in ethylene glycol at 160 °C: (a) 0.1 M AA, simultaneous drop-wise addition of  $\text{AgNO}_3$ , PVP and AA together within 7 minutes by keeping ratio of addition 3:3:1 (60:60:20  $\mu\text{L}$ ) of  $\text{AgNO}_3$ :PVP:AA in sequences, (b) 0.1M AA, first successively addition of 600  $\mu\text{L}$  of each  $\text{AgNO}_3$  and PVP, then 200 $\mu\text{L}$  of AA, all addition within 7 minutes simultaneously, and (c) and (d) 0.3 M AA, simultaneously drop-wise addition with addition ratio 3:3:1 (60:60:20  $\mu\text{L}$ ) of  $\text{AgNO}_3$ :PVP:AA within 7 minutes and 4 minutes, respectively. Scale bar for all SEM images are same (1  $\mu\text{m}$ ).

An assembling concept and the obtained results of nanoassembly particles are described below in detail with obtained results.

### 3.5.2 Electrostatic concept for nanoassembly

Coupling of nanoparticles by use of the attractive forces between antagonistically charged objects can be a powerful approach for the formation of complex composed nano objects. The real challenge is to avoid an uncontrolled aggregation of mixed composed three-dimensional particle networks which resulting in undesired precipitates. This issue can be solved by applying reaction in diluted mixtures and choosing suitable concentration ratios of the reactants. The concept is based on the general approach of electrostatically supported assembling similar to the deposition of polyelectrolyte multilayer [202]. An interaction between a multi-ionic object and a surface of nanoparticle is frequently accompanied by an overcompensation of electrical surface charge. A similar way has been chosen here for the interaction of two antagonistically charged nanoparticles. A precipitation by the formation of larger aggregates was suppressed by the reduction of the concentration of larger components

(Ag microrods) together with spherical PMMA nanoparticles. Furthermore, a higher weight ratio of polymer particles to larger components was applied in order to push all larger particles quickly into the oppositely charging state of PMMA particles by fast compensating and overcompensating of the original particles charges. A schematic overview is given in **Scheme 3.4**.



**Scheme 3.4** Schematic overview of the heterogeneous nanoassemblies of PMMA nanoparticles/Ag microrods.

### 3.5.3 Formation of PMMA/Ag nanoassemblies

PVP is strongly adsorbs to the Ag microrods surface during synthesis. The free oxygen atoms of the PVP molecules create negative charges at outer surface through enolization process because of the slight basic pH of aqueous dispersion of Ag microrods. This assumption is well supported by zeta potential measurement as the obtained microrods shows negative potential (about -35 mV). On other hand, PMMA nanoparticles of positive charges were prepared by emulsion polymerization (as explained in section 3.1) with positively charged CTAB as surface layer. The PMMA nanoparticles possess high affinity to bind with negatively charged surface of Ag microrods. **Figure 3.30 a, b** shows the regular order of the spherical PMMA nanoparticles attached on the Ag microrods surface.

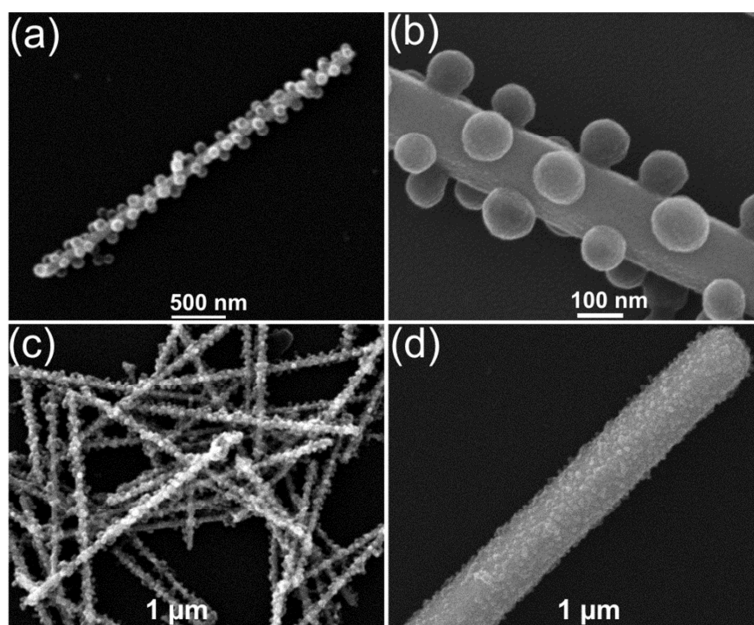


**Figure 3.30** SEM images: (a) low and (b) high magnified SEM images of regularly arranged 110 nm sized PMMA nanoparticles on 5  $\mu\text{m}$  longer Ag microrods. (c) and (d) are the assembly of 70 nm sized PMMA nanoparticles on shorter and longer Ag microrods, respectively.

PMMA nanoparticles adsorb on the Ag microrods surface by maintaining certain distance from adjacent PMMA particles. There must be a mechanism for controlling the arrangement of polymer particles on the Ag microrods. It is obvious that the distance between polymer particles is almost uniform. It is supposed that the inter-particles repulsion between PMMA nanoparticles is responsible for this effect. This repulsion as well as the binding to the Ag microrods can be interpreted by an electrostatically dominated assembling mechanism.

The maximal loading of the Ag microrods surface might be controlled by the complementary charges of its surface and the binding polymer particles. **Figure 3.30 a-d** compares the binding density between PMMA nanoparticles of 70 nm and 110 nm sized, and Ag microrods with small diameter of 150 nm and large diameter of 900 nm. Smaller PMMA nanoparticles have high surface charge (zeta potential about +42 mV) and initiate the strong interaction at room temperature with Ag microrods (zeta potential about -35 mV). Therefore, a dense particulate assembly is obtained as shown in **Figure 3.30 c, d**. A similar type of assembly behavior was also found in case of PMMA nanoparticles of larger diameter of about 110 nm. The zeta potential of 110 nm sized PMMA nanoparticles is about +22 mV. The reaction has been performed for about 25 minutes at 90 °C temperature in heating bath for obtaining the controlled nanoassembly. In this case, a high regularity of the assembled polymer nanoparticles is obtained. Moreover, the surface charge of 110 nm sized PMMA is critical to

obtain the heterogeneous nanoassembly by maintaining certain distance between adsorbing spherical nanoparticles (**Figure 3.30 a, b**). The assembling behavior becoming weakens with further decrease in surface charge of the PMMA nanoparticles (size of nanoparticles increases). Therefore, for the 240 nm sized PMMA nanoparticles (zeta potential about +8 mV), only a weak and irregular assembly is obtained, and at certain point the assembly is not obtained at all for larger PMMA nanoparticles.

Overall, the heterogeneous nanoassembly of two antagonistically charged heterogeneous particulate materials is performed in batch reaction. The assembly behaviours have been explained on the basis of controlled surface charge of particles through electrostatic dominated interactions.

### **3.6 Flow assembling of polymer nanoparticles**

In many of the particles system, a basic problem in the process of assembling the particles in batch platform is the formation of undesired, random and irregular aggregations due to the lack of homogeneous environment at nanoscale level. In direct alternative, a microflow platform, particularly continuous flow and segmented flow, provides very homogeneous reaction environment due to low volume and reduced interface area. Moreover, micro segmented flow is particularly important due to its parameter such as, decoupling between reaction solution and wall, droplet (slug) flow transport behaviour, compartmentalization of a liquid in distinct volume, and fast phase and heat transfer by flow-induced segment internal convection among the others [6]. The controlled interaction is realized between two antagonistically charged heterogeneous or homogeneous particles in a flow platform for obtaining the size-tuned nanoassemblies with different concentration ratio. In this work, the flow assembling process of two different size and shape controlled polymer nanoparticles is performed: (a) flower-sphere flow assembly and (b) sphere-sphere flow assembly. The flower shaped polymer nanoparticles is covered with PVP layer (detail description is given in section 3.2.4) and spherical polymer nanoparticles is covered with SDS and CTAB layer (section 3.1). Moreover, for the layer-by-layer approach, different levels of specific surface functionalization are applied for adjusting the type and density of the available charges at outer surface of nanoparticles.

### 3.6.1 Flower-sphere flow assembly

At first, the negatively charged flower-shaped PMMA nanoparticles (zeta potential about -15 mV) is modified to positively charged (zeta potential about +40 mV) by applying cationic polyelectrolyte polyDADMAC layer on the surface. Afterwards, the interface interaction between the flower nanoparticles and smaller spherical nanoparticles (zeta potential about -24 mV) is performed in flow arrangement as shown in **Figure 2.6** for obtaining the controlled assembly particles at different parameters. In the arrangement, T-shaped junction allows the mixing of two aqueous dispersions in continuous flow. The flow is travel through knot mixture for realizing the strong interaction between oppositely charged polymer nanoparticles. It is found that the assembly reaction of about 110 nm sized spherical nanoparticles on the surface of flower particles is faster at 90 °C reaction temperature. The interaction at room temperature is realized at comparatively longer time interval and also with irregular assembly. The effect of temperature on the obtained assembly particles is summarized in **Table 3.2**. On other side, the spherical nanoparticles with different concentration ratios can be systematically tuned by applying appropriate concentration of individual particles as shown in **Figure 3.31**.

Besides the temperature effect, assembling interaction is depends on the applied residence time in flow condition as well as on the spherical nanoparticles size and therefore the surface charges. Higher the surface charges, stronger the affinity to bind on the flower surface. Therefore, smaller sized nanoparticles arranged quickly and as sphere size increases (with decrease in surface charge) the assembling behaviour becomes weaken. Moreover, the critical residence time is important for the flow assembling reaction. Different sized positively charged PMMA nanoparticles have high affinity to bind the flower surface without modification with cationic polyelectrolytes too. In flower-sphere assembly, it is possible to fluctuating and adjusting the surface charge of the both types of nanoparticles by surface modification. All different parameters for obtaining the nanoassembly particles in flow condition are summarized in **Table 3.2**.

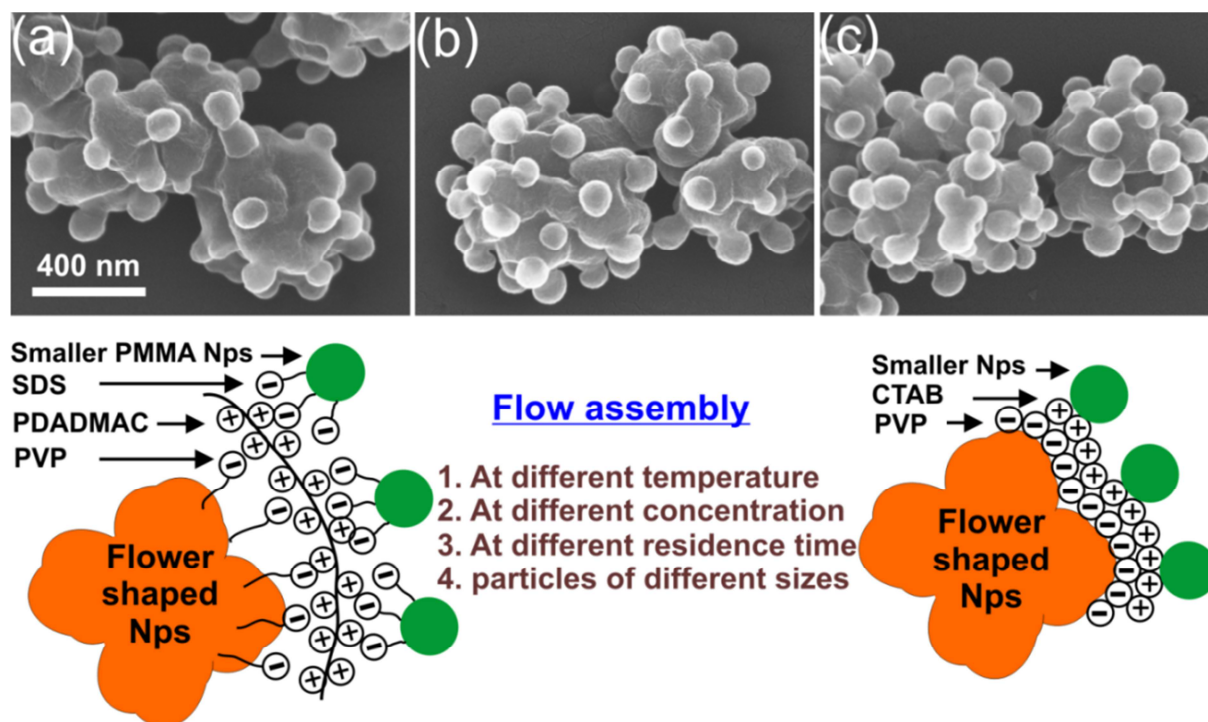


**Figure 3.31** Flower-sphere flow assembly: (a-c) are SEM images for the different concentration of 110 nm sized positively charged spherical polymer nanoparticles assembling on the surface of negatively charged flower-shaped nanoparticles (50  $\mu\text{L}$ ); (a) 10  $\mu\text{L}$ , (b) 20  $\mu\text{L}$  and (c) 30  $\mu\text{L}$ . Scale bar for all SEM images is same (400 nm). Drawing represents the Scheme for assembling of oppositely charged flower and spherical polymer nanoparticle.

### 3.6.2 Sphere-sphere flow assembly

Initially two different sized spherical polymer nanoparticles were prepared by using different concentration of SDS in aqueous phase. The smaller particles of about 110 nm size and -24 mV surface charge is obtained at 1 mM SDS concentration whereas larger spherical particles of about 280 nm size and -8 mV surface charge is obtained at 0.01 mM SDS concentration in aqueous phase. Surface of the larger nanoparticles is then modified with cationic polyelectrolyte as shown in **Figure 3.32** (drawing) for the interaction with oppositely charged smaller particles. Larger particles (zeta potential about +28 mV) make strong assembling interaction with smaller sized polymer nanoparticles at 95  $^{\circ}\text{C}$  within a 10 min in continuous flow condition. Assembly particles were obtained at different temperature and also at different residence time for assembling behaviour. The complete result of sphere-sphere nanoassembly is summarized in **Table 3.2** (bottom rows). By applying the suitable concentration ratio of both particles in aqueous stream, the ratio of smaller spherical nanoparticles can be systematically tuned on the surface of larger spheres. Therefore, when 10  $\mu\text{L}$  aqueous suspension of about 110 nm sized polymer nanoparticles in 1 mL water mixed

with 50  $\mu\text{L}$  suspension of larger spheres, the density behaviour in assembly particles is minimal. The density behaviour increases with increase in suspension amount of smaller sphere at constant larger sphere volume (**Figure 3.32 a-c**). Further increase in the amount of smaller sphere forms the assembly particles with random coagulation.

**Table 3.2** Obtained flow assembling result at various reaction parameters.

	Assembly type	Type of particles	Diff. reaction parameters for obtaining assembly	Change	Assembling behavior (product)
<b>Flow- assembly of polymer nanoparticles</b>	<b>Flower-sphere</b>	Flower: zeta potential: -18 mV.	At different temp. (res. time : 10 min, sphere size: 110 nm)	RT	Average
				50 °C	High
				95 °C	Strong
		Sphere: zeta potential: between +2 mV and +42 mV.	At diff. sphere size (temp: 95 °C, res. time: 10 min)	70 nm	Strong
				110 nm	High
				160 nm	Average
			At diff. resi. time (temp: 95 °C, size: 110 nm)	250 nm	Not at all
				1 min	Low
				5 min	Controlled
		Flower with modified surface: zeta potential: +43 mV.	At diff. temp. (sphere size: 110 nm, res. time: 10 min)	10 min	High/Strong
				20 min	Strong
				RT	Low
		Sphere: zeta potential: between -3 mV and -22 mV.	At diff. sphere size (temp: 95 °, res. time: 10 min)	50 °C	Low/average
				95 °C	High
				110 nm	High
	At diff. res. time (temp: 95 °C, sphere size: 110 nm)		165 nm	Negligible	
			240 nm	Not at all	
			1 min	Not at all	
	<b>Sphere-sphere</b>	Surface modified sphere: zeta potential: +33 mV.	At diff. res. time (temp.: 95 °C, sphere size: 110 nm)	5 min	Negligible/low
				10 min	High
20 min				High	
1 min				Negligible	
Small sphere: zeta potential: -22 mV.		At diff. temp. (res. time: 10 min, sphere size: 110 nm)	5 min	Average	
	10 min		Strong		
	20 min		Strong		
				RT	Low
				50 °C	High/strong
				95 °C	Strong



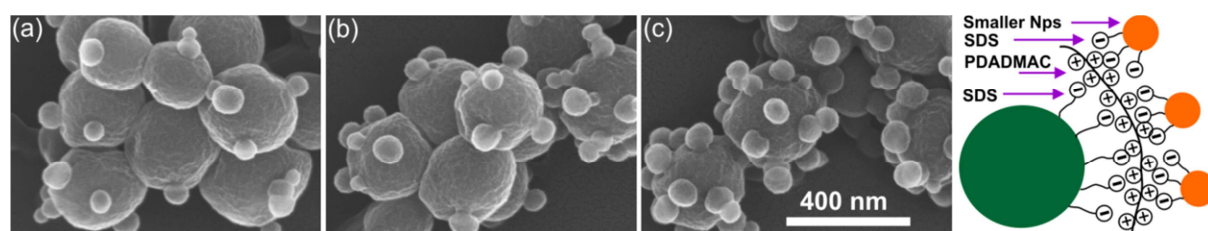


**Figure 3.32** Sphere-sphere flow assembly: (a-c) are SEM images of the controlled assembly of different concentration ratio of smaller PMMA nanoparticles (110 nm sized) on the surface of 280 nm sized larger nanoparticles (50  $\mu\text{L}$  suspension); (a) 10  $\mu\text{L}$ , (b) 20  $\mu\text{L}$  and (c) 30  $\mu\text{L}$ . Scale bar for all SEM images are same (400 nm). Right side drawing is a Scheme for electrostatic assembly of two different sized spherical PMMA nanoparticles.

The layer-by-layer surface modification technique with polyelectrolyte macromolecules is particularly interesting because of the availability of the intense charges with flexible or fuzzy surface [202]. Such active surfaces allow the assembling of different types of charged nano-objects. Here, four levels of the alternative charged polyelectrolytes layers are applied and the particles were characterized by zeta potential measurements (**Figure 3.33**).

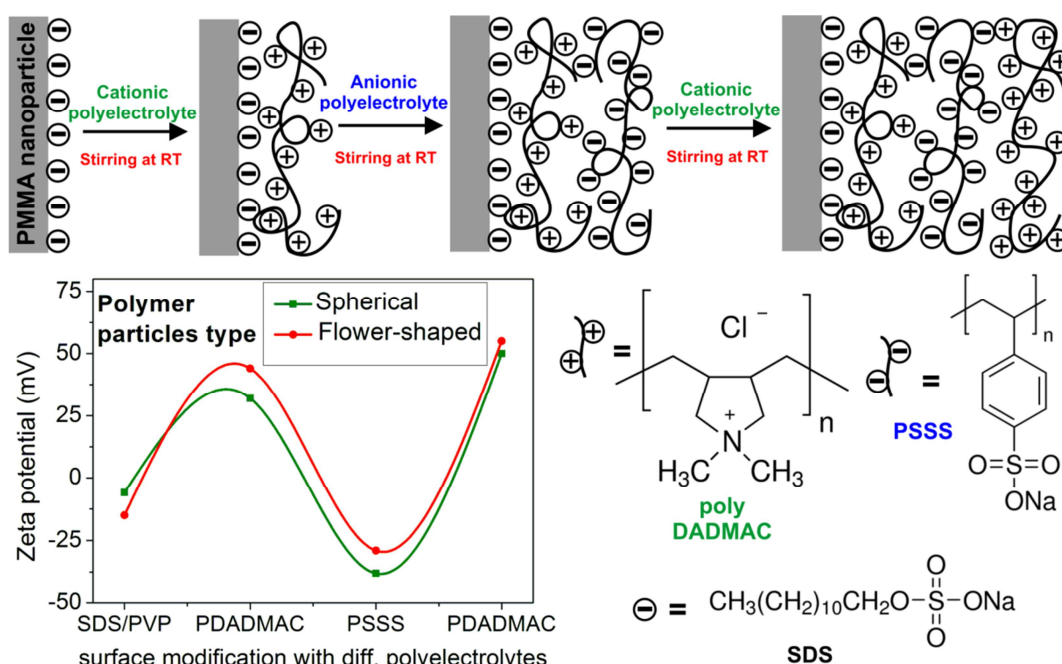


**Figure 3.33** Top drawing is a schematic for the surface modification of spherical and flower shaped polymer nanoparticles with different polyelectrolyte (layer-by-layer). Bottom left is a graphical result of the spherical and flower-shaped polymer nanoparticles zeta potential at various modification levels. The standard deviation for all measurement is about  $\pm 4$  mV.

Overall, the flow platform provides very homogeneous and efficient environment for assembling the oppositely charged polymer nanoparticles of different size/shape and with



different concentration ratios. Resultantly, the nanoassemblies are obtained with high homogeneity which is interesting for combining the functional properties of two different regimes such as mixed fluorescence.



## 4 Results and discussion-2: Polymer microparticles and their composition

This chapter mainly presents the results of size, color and composition tuned polymer microparticles for the fluorescence labeling and SERS sensing applications. Different kinds of hydrophobic and hydrophilic microparticles (microgel) have been prepared in the cross-flow microfluidic arrangement through photopolymerization process. The effects of different microfluidic parameters such as flow rate variation, functionalization of microreactor, continuous flow composition of various reactants, and effect of surfactant concentration on particles size, among the others are systematically studied here. In first section, the effect of various fluorophores for the fluorescence outcome of labelled particles is described. In second part, the size and composition tuned sensor particles were prepared in the microfluidic platform and their SERS sensing effect with different analytes are studied. In last section, the flow and sequential SERS measurement of different analytes and rinsing solution is shown with obtained results.

### 4.1 Microfluidic synthesis of polyTPGDA microparticles

Here, the monochromatic and mixed-colored fluorescent microparticles of different size are prepared in normal and modified microfluidic arrangement, respectively. The different features of the obtained microparticles are described in below subsections.

#### 4.1.1 Size tuned microparticles by surfactant and flow rate control

A cross-flow microfluidic platform as shown in **Figure 2.3** was used for the synthesis of poly(tripropylene glycol diacrylate) (polyTPGDA) microparticles. The monomer phase is a mixture of hydrophobic monomer liquid, cross-linker and photoinitiator, and the carrier phase is made up of the aqueous surfactant (SDS or CTAB). The generated droplets in continuous flow are solidified by UV light source and the particles with different loading of active compounds are obtained similar to droplets size. Size of the microparticles is strongly depends upon the surfactant concentration and flow rate ratios of both immiscible liquid phases. Therefore, when a flow rate ratio of 7.5 (300  $\mu\text{L}/\text{min}/40 \mu\text{L}/\text{min}$ , carrier/monomer) was applied, the polyTPGDA particles of about 150  $\mu\text{m}$  size were obtained. Particles size gradually decreased down with consistently increasing SDS concentration in continuous aqueous phase (**Figure 4.1**). At constant flow rate ratio of 20 (400  $\mu\text{L}/\text{min}/20 \mu\text{L}/\text{min}$ ), the obtained particles size were about 120  $\mu\text{m}$  and 70  $\mu\text{m}$  when 3 mM SDS and 5 mM SDS have

been used in the aqueous carrier phase, respectively. Analogous to anionic SDS, cationic CTAB also tunes the particles size in a similar way. The SEM images of the obtained microparticles are presented in **Figure 4.1 a-c**. Moreover, at a similar concentration of SDS (3 mM) in aqueous phase, the diameter of the obtained particles can be tuned between 50  $\mu\text{m}$  and 155  $\mu\text{m}$  at varied flow rate ratio between 5 and 40 (**Figure 4.1 d**). The obtained particles are of smaller size because of the early release of droplets during the high aqueous flow rate. Furthermore, the particles size consistently increases with increasing monomer flow rates. The particles size can be tuned between 50  $\mu\text{m}$  and 350  $\mu\text{m}$  (broad size spectrum), if the aqueous phase was replaced by a perfluorinated phase (Novec 7500 with picosurf) as shown in **Figure 4.1 e**.

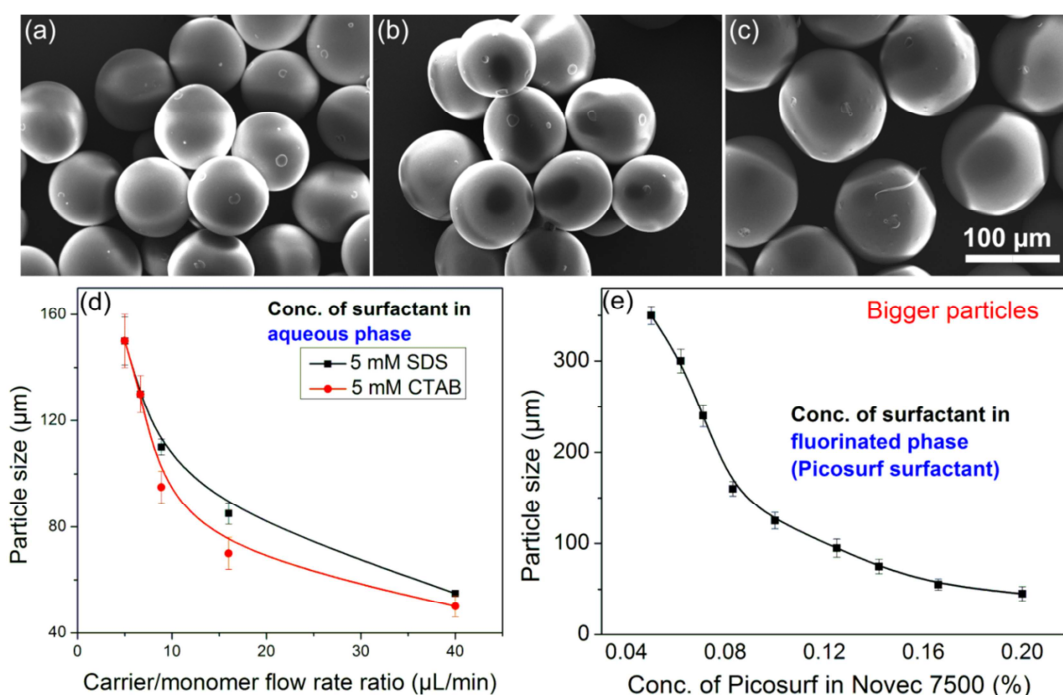


**Figure 4.1** SEM images of polyTPGDA microparticles obtained at different flow rate ratio: (a) 400/10 (carrier/monomer,  $\mu\text{L}/\text{min}$ ), (b) 400/15 and (c) 300/20. The graphical representation for tuning of the particles size at different concentration of (d) SDS and CTAB in aqueous phase, and (e) Picosurf in Novec 7500.

#### 4.1.2 Droplets generation mechanism in microreactor

Droplets, enclosed with different fluorescence additives, generated in the microreactor when monomer thread breaks down by a strong shear force of the continuous phase (**Figure 2.3 e**). For generation of the precise sized droplets, different parameters playing crucial roles: (a) The surface tension [162] due to strong shear force of continuous phase have tendency to breaks-off the liquid monomer thread to release the droplets. (b) Viscosity of the continuous

phase influences considerably to release the droplets of different size. (c) Channel diameter is also contributing the dominating effect for controlling the droplets diameter. As the droplets are of micrometer size, the parameters such as viscosity, inertial stress, surface tension, diffusion becomes significant to understand the formation mechanism of droplets [203]. Moreover, in the microfluidic techniques, the parameter such as Reynolds number, Peclet number and Capillary number are playing crucial role for the droplet generation mechanism [203]. The Reynolds number is defined as the ratio of counter laminar flow force to viscous force, and can be calculated as  $Re = l * v/\nu$ , where  $l$  is the channel diameter, and  $v$  and  $\nu$  are the velocity and viscosity of the applied liquid, respectively. The generated droplets are of smaller size because of high Reynolds number when shear force of the continuous phase is very high. On other hand, the Capillary number is strongly related to the surface tension, carrier liquid flow and viscosity of the carrier phase [54]. Droplets of different size are generates at T-junction of microreactor when changes takes place in the Capillary number. The Capillary number can be defined as,  $Ca = v_c\mu/\gamma$ , where  $v_c$  is the velocity of the flow,  $\mu$  is the viscosity of the fluid, and  $\gamma$  is an interfacial tension [49]. Surfactant reduces the surface tension at the interface of particles [162, 204]. Moreover, the reduced surface tension enhancing the Ca value, because Ca is the ratio of viscous force to surface tension forces. With same diameter of the micro channel, the shear force increases with increased velocity of the continuous phase. Resultantly, with increase in the Ca value, the shear force increases in comparison to the surface tension forces which leads the generation of smaller sized droplets [162, 205].

#### 4.1.3 Monochromatic fluorescent microparticles

The functional polymer particles can be efficiently used in the bead-based labeling and sensing applications for read-out of chemical information from micro fluid segments. To progress with this criterion, here, the fluorescence microparticles are prepared by incorporating specific fluorophores during the in-situ synthesis in droplet-based microfluidic platform. Four different hydrophobic fluorescence dyes were used separately for producing the polyTPGDA microparticles of different colors. **Figure 4.2** represents the fluorescence microscope images of colored microparticles. On one hand, the red colored microparticles were generated when a long ranged emission wavelength fluorophore (Nile red) mixed to the monomer solution prior to the particles synthesis. Nile red embedded microparticles are excited at the 510-560 nm light wavelength (**Figure 4.2 a**). Similarly on other hand, when 12-(7-Nitrobenzofuran-4-ylamino)dodecanoic acid (Nbfd), Sudan Black B, and Reichardt's dye

were used; yellow, bluish violet and violet colored microparticles are obtained, respectively. Strong emission of fluorescence light at about 515 nm wavelength is observed in the Nbfd embedded microparticles (**Figure 4.2 b**).

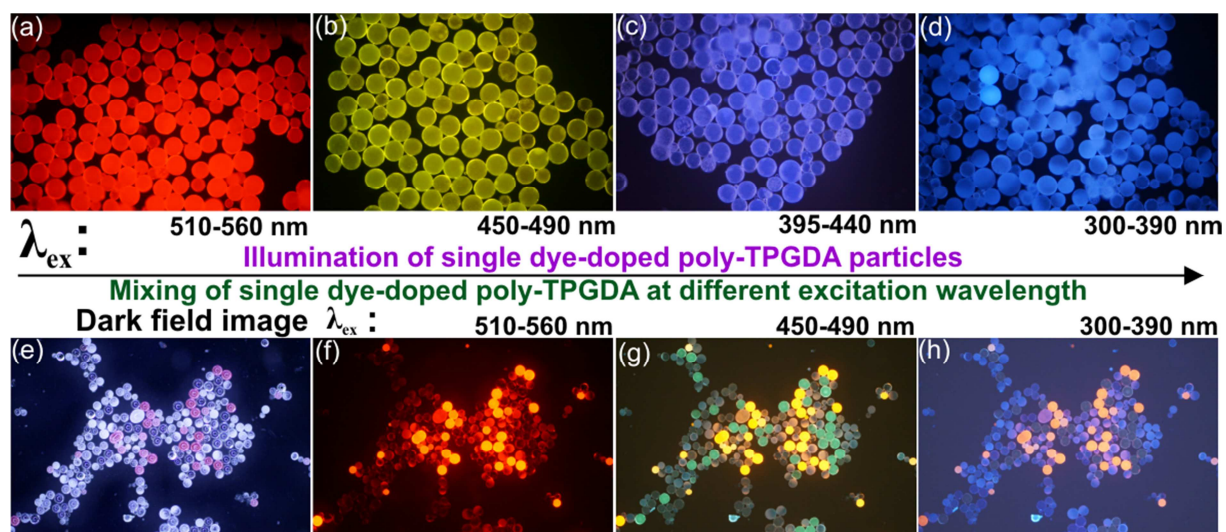


**Figure 4.2.** Fluorescence microscope images of different dye-doped polyTPGDA microparticles at different excitation wavelength: microparticles contained (a) Nile red dye, (b) Nbfd dye, (c) Sudan Black B dye, and (d) Reichardt's dye. Mixer of three individually colored particles at different excitation wavelength: (e) dark field image, (f-h) excitation at different wavelength (same spot of the particles excited at different fluorescence light filter).

In a next step, three identical sized different monochromatic microparticles were mixed together and differentiated them by the colors. In the particles mixture, Nile red contained microparticles (red colored) are excited at the wavelength range of 510-560 nm. Likewise, Nbfd (yellow colored) and Reichardt's dye (blue colored) embedded microparticles are emitted the fluorescence light at 515 nm and 420 nm, respectively (**Figure 4.2 e-h**). Similarly, when four different colored particles mixed with the particles of four different size,  $(4 \times 4)^n$  fluorescence patterns can be obtained. This mixing process of microparticles with many different colors and size can creates even more number of distribution and sequence for the controlled fluorescence labeling and screening applications.

#### 4.1.4 Mix-colored microparticles: color tuning in flow condition

By modifying the droplet generating microfluidic arrangement, mix-colored polyTPGDA microparticles of two, three, and four different fluorescence emissions were prepared. For such purpose, a Y-shaped flow device is arranged in the monomer nozzle prior to the central orifice of the main microreactor. The controlled mixing of two different fluorophores with

specific concentration was inserted through Y-junction to microreactor for generating the droplets of precise size by the shear force of continuous flow. Total monomer flow rate is 50  $\mu\text{L}/\text{min}$  at different carrier flow rates. Here, the continuously tuned concentration ratio of binary composition of two different fluorophores (Nile red and NBFD) at 30 s of time interval can produce the microparticles with systematic color transformation (**Figure 4.3**). Only red colored particles (excited at 510-560 nm) were obtained when total monomer flow rate was supplied from Nile red contained monomer solution. On other side, when total monomer flow was supplied from NBFD-dissolved monomer solution, the obtained particles were yellow colored (excitation at 450-490 nm). Mix-colored microparticles of two different fluorophores can be obtained as shown in **Figure 4.3** by continuous varying composition of total monomer flow rate such as, 40:10 ( $\mu\text{L}/\text{min}$ ), 30:20, 20:30, and so on. The color of the particles is transforming from red and yellow to greenish yellow as NBFD amount is increasing step by step.

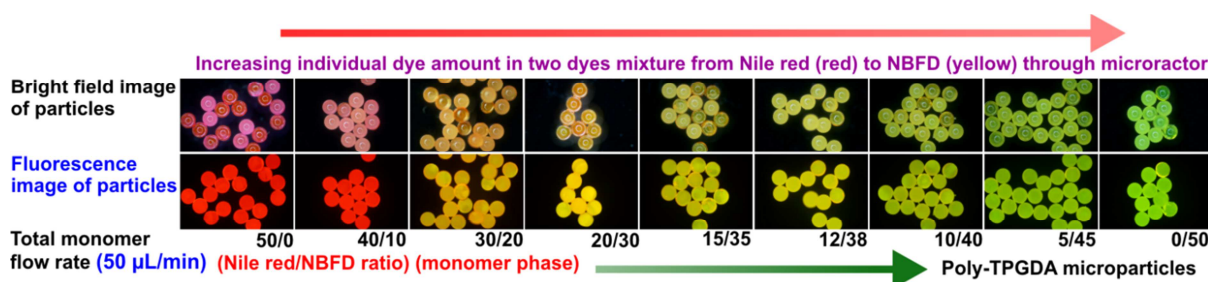


**Figure 4.3** Fluorescence microscope images of polyTPGDA microparticles generated by in-situ composition of two different colored dyes (Nile red /NBFD) during the continuous synthesis of particles. Total flow rate of monomer phase is 50  $\mu\text{L}/\text{min}$ .

For controlled fluorescence tuning, the microparticles were prepared by embedding different concentrations of fluorophores during the flow synthesis. Red colored particles with lower fluorescence intensity were obtained when 0.05 mg Nile red dye was used in the monomer phase. Fluorescence intensity continuously increases step by step with increasing dye concentration from 0.1 mg up to 1 mg in 1 mL solution. Similarly, the tuning in the fluorescence intensity was obtained at about 535 nm when different concentration of the NBFD dye has been used in the microparticles (**Figure 4.4**). In next experiment, the *in-situ* variation of flow rates was tuned for realization of a mixed fluorescence signal by mixing the two different dyes in the identical particles. In binary colored system, when a monomer flow rate of 25  $\mu\text{L}/\text{min}$  (50 %) from each of the two monomer solution was applied (total monomer flow rate is 50  $\mu\text{L}/\text{min}$ ), the obtained microparticles showing two different peaks at

different wavelength in a single fluorescence spectrum. Peak intensity of the individual dye depends on the related concentration of respective dye in the composed binary colored particles. For instance, an equivalent amount of the Nile red dye and Nbfd dye (50 % each) in the identical microparticles shows the fluorescence spectrum with two different peaks at 530 nm and 620 nm with similar intensity. In a similar way, the individual peak intensities can be systematically tune by varying the appropriate concentration ratio of the mixed fluorophores in microparticles.

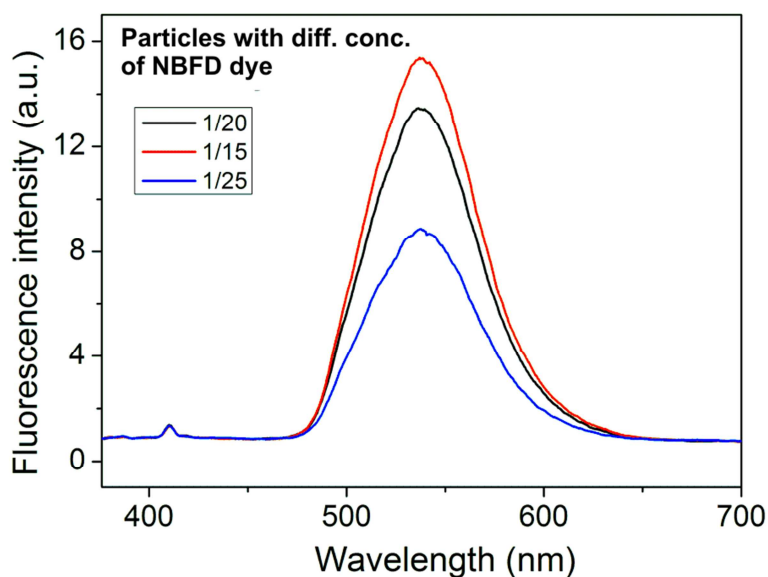


**Figure 4.4** Fluorescence spectra of the Nbfd (with different concentration) embedded polyTPGDA microparticles.

The mixing of hundreds of different sized particles with tens of different typed mix-colored particles can produce thousands of different patterns for mixed and tuned fluorescence at same time. Particularly, as shown in **Figure 4.5 a** that the similar sized two different colored particles integrated at single spot and creates a fluorescence pattern where red colored particles are excited at higher wavelength (510-560 nm) and yellow colored particles at lower one (450-490 nm). The particles which are generated after controlled in-situ composition of two different fluorophores retain mixed fluorescence property. Therefore, the mixture of two differently mix-colored particles creates a fluorescence pattern where red-color dominated particles are excited at higher wavelength (510-560 nm). In these experiments, fluorescence strength of the particles depends on the concentration of used fluorophores, size and in-situ composition of different colors. Hence, the composed trinary colored particles were mixed together which produce the colourful pattern of fluorescent polyTPGDA particles and they can be easily distinguished on the basis of colors as shown in **Figure 4.5 b**.



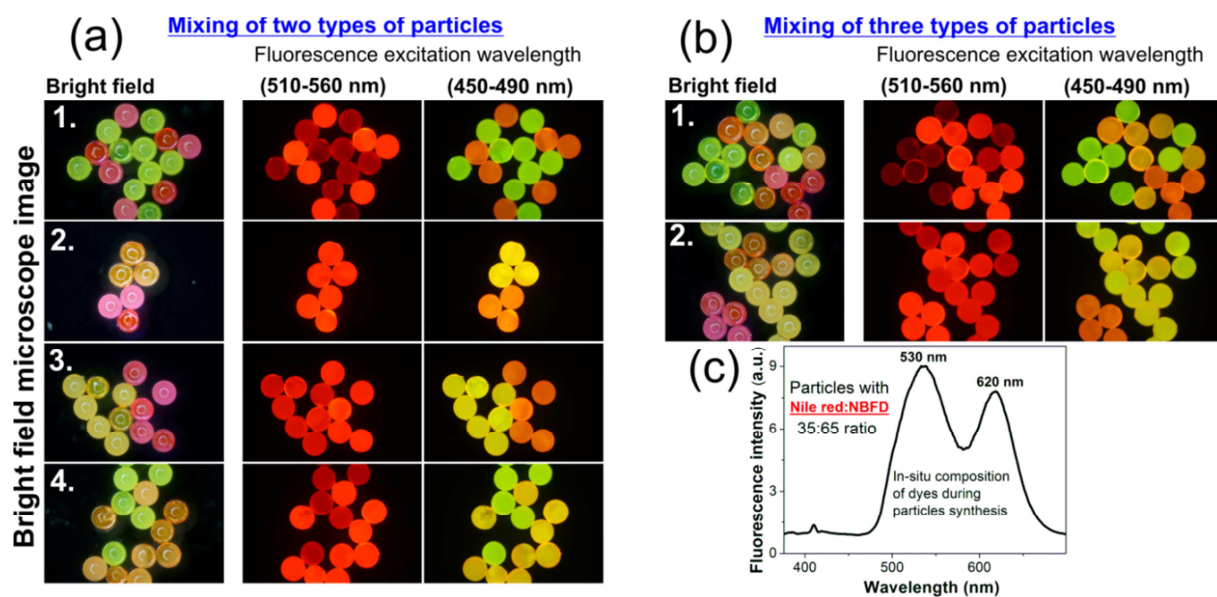


**Figure 4.5** Fluorescence microscope images of (a) two different types of poly-TPGDA microparticles (different conc. of Nile red and NBFd): (1) 50  $\mu\text{L}/\text{min}$ :0  $\mu\text{L}/\text{min}$  (Nile red:NBFd) and 0:50 (Nile red:NBFd), (2) 30:20 and 50:0, (3) 15:35 and 50:0, and (4) 35:15 and 5:45; (b) and (c) three and four types of poly-TPGDA particles with in-situ composition of two dyes, respectively: (1) 50:0, 35:15 and 0:50, and (2) 50:0, 30:20, 10:40 and 5:45, same spots (dark field images) excited at two different wavelength (510-560 nm and 450-490 nm); and (c) fluorescence spectrum of the particles embedded with 35 % (Nile red) and 65 % (NBFd).

Large number of chemical, genetic or pharmaceutical tests can be performed at a same time in the microfluidic platform via high-throughput screening process. It is because of a specific microreactor which provides a highly homogeneous streaming condition and produces a broad library of desired product via in-situ composition of many reactants. Particularly here, a library of fluorescent polyTPGDA microparticles with controlled composition of quaternary colored fluorophores are obtained by modifying the general microfluidic arrangement as shown in **Figure 2.3 c**. The continuous composition via online monitored flow variation program takes place in the manifold device which arranged in the monomer nozzle prior to the central orifice of microreactor. Twenty distinct compositions of four different monomer solutions such as, 25:10:10:5 ( $\mu\text{L}/\text{min}$ ), 20:15:5:10, 10:10:10:20 and so forth were supplied at the changing frequency of 30 second (total monomer flow rate 50  $\mu\text{L}/\text{min}$ ). Resultantly, the microparticles of mix-colors are produced accordingly which emit the fluorescence light at different wavelengths. Nile red and NBFd dye-doped microparticles are excited at 510-560 nm and 450-490 nm ranges, respectively. Two more dyes Sudan Black B and Reichardt's dye were used here. The quantum yield is not so high for these latter two dyes, but they give the composed color patterns for color tuning. The microparticles embedded with Sudan Black

B visualized as violet colored at the excitation wavelength of 395-440 nm range, and Reichardt's dye embedded blue colored microparticles are excited at 300-390 nm. **Figure 4.6** shows the obtained microparticles which are excited at different wavelength.

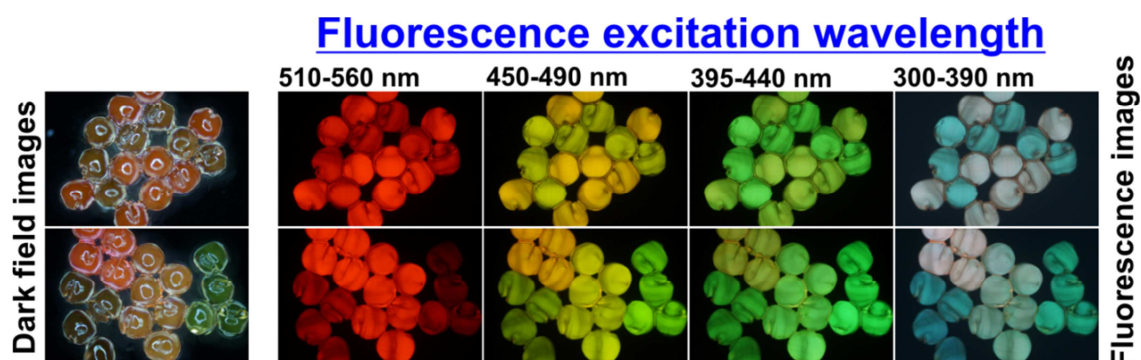


**Figure 4.6** Fluorescence microscope images of trinary (top row) and quaternary (bottom row) different kinds of microparticles produced by in-situ combination of variable concentration of four different dyes, Nile red, NBFD, Sudan Black B and Reichardt's dye.

In all above cases of monochromatic and mix-colored microparticles where different hydrophobic fluorophores were embedded in the particles interior and the entire polymer network realizing a fluorescence-active. To extend the strategy, different hydrophilic fluorescent microgel particles were also prepared by tuned composition of different aqueous fluorophores. A detailed procedure for the synthesis and different properties of the hydrogel microparticles is given in section 4.2. In below section, a brief description of fluorescent hydrogel particles is given with obtained results.

### 4.1.5 Fluorescent hydrogel particles

Fluorescent polyacrylamide microgel particles are prepared by *in-situ* embedding the single and mixed fluorescence dyes during the droplet-based microfluidic synthesis in the cross-flow setup as shown in **Figure 2.4**.

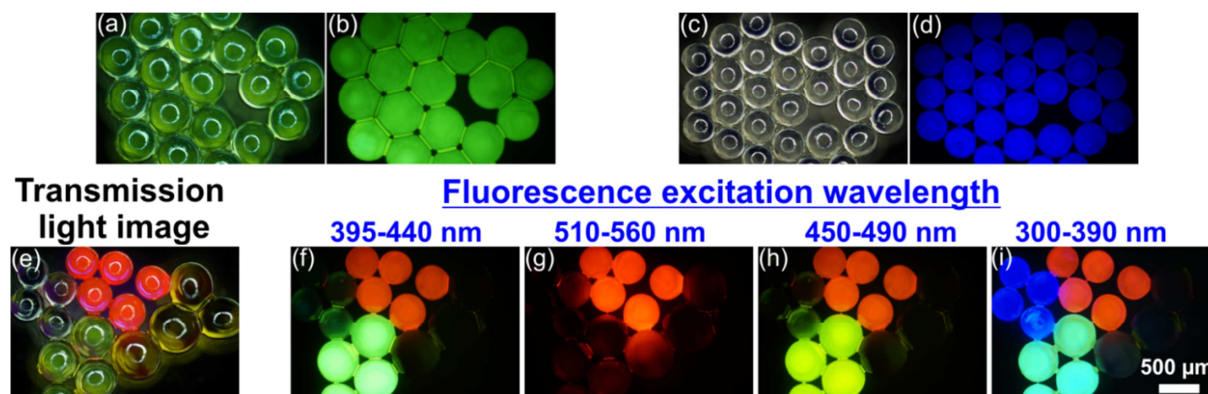


**Figure 4.7** Optical microscope images of fluorescent polyacrylamide hydrogel particles: (a), (c) and (e) are the transmission light images of fluorescein, titan yellow and four different dye-embedded particles, respectively. (b), (c) and (f-i) are the fluorescence images at different excitation wavelength (b and d are excited at 450-490 nm and 300-390 nm wavelength range). Scale bar for all images is same (500 μm).

The monochromatic particles where fluorescein and titan yellow dyes were embedded in the particles interior individually. The fluorescein embedded particles excited at the light range 450-490 nm and titan yellow embedded particles are visualized as blue colored by excitation at 300-390 nm light wavelength. Moreover, four different dyes (fluorescein, titan yellow, orange G and sulforhodamine B) were mixed controllably to obtain the size and color-tuned hydrogel particles as shown **Figure 4.7**.

Overall in section 4.1, the size and color-tuned hydrophobic and hydrophilic microparticles were prepared and characterized them by fluorescence microscopy and spectroscopy.

## 4.2 Microfluidic synthesis of sensor particles for SERS sensing

Here, size and composition tuned polyacrylamide hydrogel particles are synthesized in the cross-flow microfluidic arrangement. Size parameter study, tuning of the surface properties such as metal enhancement, simultaneous mechanism of photopolymerization-photoreduction, and tuned surface-enhanced Raman scattering (SERS) sensing effect of different biochemical and organic compounds are described in detail.

### 4.2.1 Size-tuned composite hydrogel microparticles

The generation of the polymer/silver composite particles is resulted from the co-initiation of photopolymerization and photoreduction during the light exposition in droplet-based micro flow arrangement. The monodispersed droplets formation [206] is crucial for homogeneous polymer particles production [11, 207] because size of the particles is comparable to the droplets diameter. Stable spherical droplets of aqueous solution are generated in the flowing continuous phase in the Si chip (with 40  $\mu\text{m}$  hole diameter) embedded microreactor as shown in **Figure 2.4**. The carrying nozzle diameter is of 500  $\mu\text{m}$  and the diameter of formed droplets is about 60  $\mu\text{m}$  which explains for the fact that the droplets are embedded inside the carrier solution. The droplets are solidified at irradiation zone within shorter residence time of about 0.5 sec. Here, *in-situ* formation of silver (Ag) nanoparticles inside the polymer matrix is takes place during the photosynthesis as color of the obtained microparticles corresponds well with typical plasmonic absorption of spherical Ag nanoparticles [208, 209]. When 10 mM  $\text{AgNO}_3$  solution of 30 % acrylamide monomer was used, the bright yellow colored composite polymer particles were obtained. Yellow, brown and black colored polyacrylamide particles sequentially generated when  $\text{AgNO}_3$  concentration was gradually increased from 15 mM up to 100 mM. Here, the homogeneous distribution of Ag nanoparticles in the polymer interior is achieved during the synchronized photopolymerization-photoreduction process.

The whole process is robust against a variation of surfactant concentration and flow rate ratio of both immiscible phases. Particles of about 55  $\mu\text{m}$  and 220  $\mu\text{m}$  diameter were obtained when 0.125 % and 0.062 % picosurf (in Novec 7500) has been used in the continuous phase at a flow rate ratio of 35 (350  $\mu\text{L}/\text{min}/10 \mu\text{L}/\text{min}$ , carrier/monomer), respectively (**Figure 4.8**). A late release of droplets resulted when surfactant concentration was not high enough. Therefore, the particles are obtained of larger size. Polymer rods of about 500  $\mu\text{m}$  diameter are obtained (**Figure 4.8 d**) with further increase in the monomer flow at decreased carrier flow rate (200/80, carrier/monomer). When surfactant was not present, smaller-sized

particles of about 230  $\mu\text{m}$  were also formed at very high carrier flow rate (1000  $\mu\text{L}/\text{min}$ ). Here in such case, the residence time for the generated droplets at irradiation zone is very short and hence the obtained particles are semi-polymerized which finally fused with each other in the collection tube. At 0.062 % picosurf concentration, the obtained particles are of 220  $\mu\text{m}$  when flow rate ratio was 35 (350/10  $\mu\text{L}/\text{min}$ , carrier/monomer). Similar sized (about 220  $\mu\text{m}$ ) particles were obtained at the flow rate ratio of only 5 (200/40  $\mu\text{L}/\text{min}$ , carrier/monomer) if a higher concentration of picosurf (0.125 %) was used. **Figure 4.8 e and 4.8 f** summarizes the result of obtained polymer particles sizes with respect to the variation in surfactant concentration and flow rate ratio of both immiscible phases.

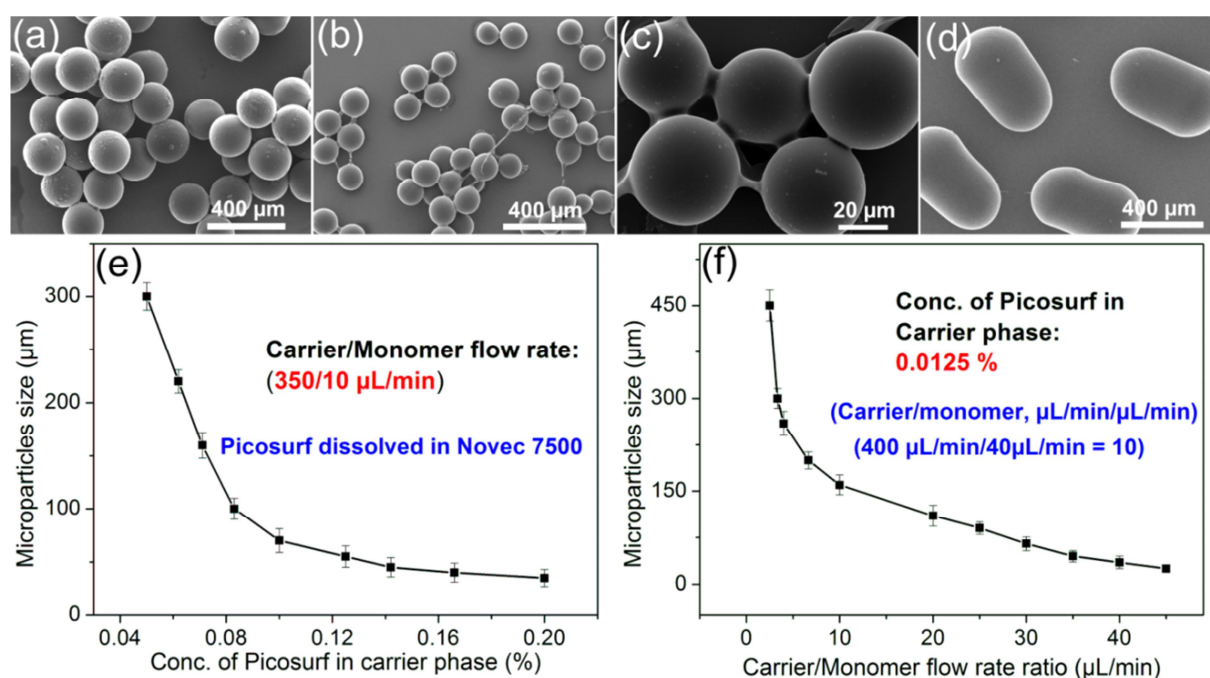


**Figure 4.8** SEM images of the size-tuned polyacrylamide microparticles obtained in the microfluidic platform at different flow rate ratios of carrier (0.125 % Picosurf in Novec 7500) and monomer phase: (a) 300/50 (carrier/monomer,  $\mu\text{L}/\text{min}$ ), (b) 300/20, (c) 400/12 (smaller particles), and (d) 200/80 (without Picosurf in carrier phase). (e) and (f) are the graphical results of obtained particles from the effect of flow rate ratio and surfactant concentration, respectively.

### 4.2.2 Surface porosity of the sensor particles

For enhanced sensing effect, particularly SERS, the sensor particles have to satisfy two basic requirements: (a) high porosity for the larger available surface area to interact with analytes and (b) high density of metallic materials at the surface. The water content in the microfluidically formed droplets is responsible for the formation of a gel-like state [24] of the obtained particles and is dependent on their swellability. The porous structure of polymer beads becomes clearly visible at the surface after drying process. The nano-pores with a diameter in the order of magnitude of about 200 nm and below were obtained as shown in **Figure 4.9 a**. It is supposed that the additional much smaller pores are also present in the polymer matrix. As the amount of cross-linking agent (bisacrylamide) increases in the monomer mixture, the matrix becomes harder and the porosity decreases gradually (**Figure 4.9 b**).

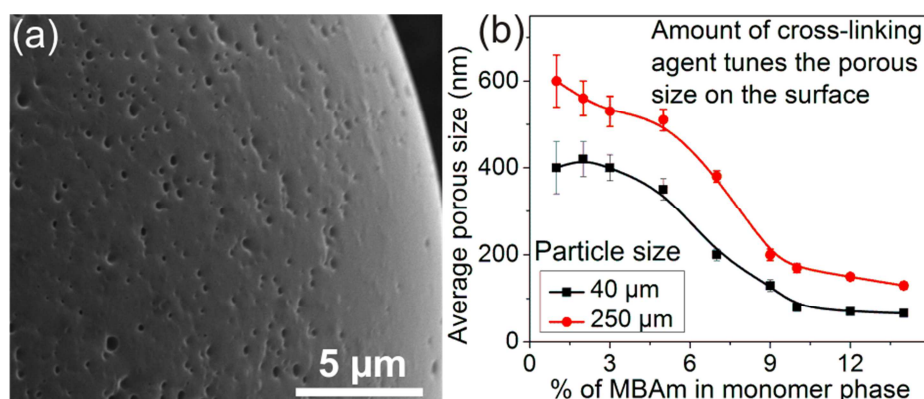


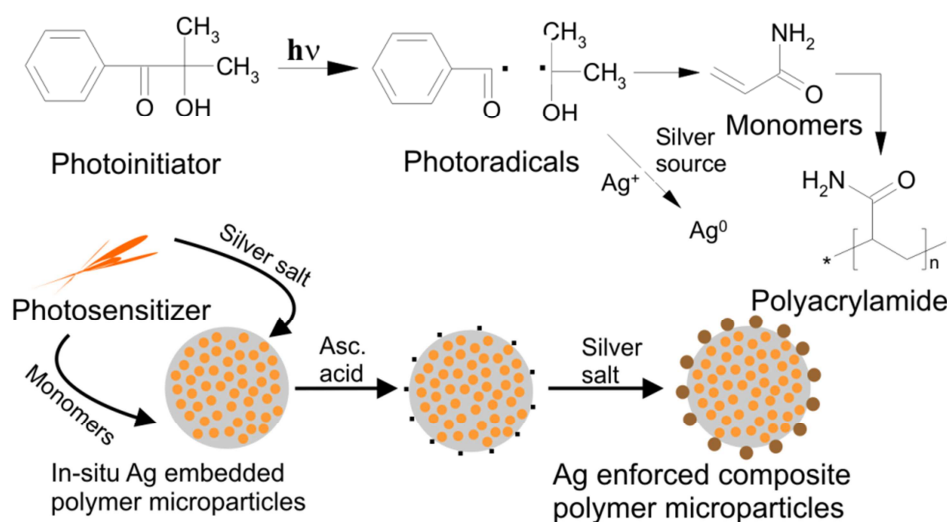
**Figure 4.9** (a) SEM image of polyacrylamide particle possess porosity on the surface, (b) graphical representation for the relation between obtained porous size on polymer particles surface and cross-linking agent amount in a monomer phase.

### 4.2.3 Silver tuning in sensor particles for SERS sensing

The UV source induces the photochemical activation for in-situ formation of Ag nanoparticles in the polymer matrix during microfluidic synthesis. In a triplet state, photoinitiator is known to undergo  $\alpha$ -cleavage and generates a pair of radicals [210] as shown in **Scheme 4.1**. The radicals quickly provide electrons and reducing  $\text{Ag}^+$  ions to form the Ag nanoparticles together with photopolymerization of monomer droplet. The homogeneous distribution of the formed Ag nanoparticles in polymer interior is achieved because of well dissolution of Ag salt in monomer solution. The effect of different concentrations of embedded Ag in the polymer matrix has been investigated here; higher the salt concentration,



more the numbers and larger Ag nanoparticles were obtained which can be concluded from the obtained colors of sensor particles. Optical microscope images of the Ag embedded particles are shown in **Figure 4.10 a-c**. Obtained polymer particles with high embedded Ag nanoparticles amount (80 mM) are dark brown in color (**Figure 4.10 b**) compared to the light brown colored particles of lower Ag loading (40 mM, **Figure 4.10 a**). The particles without Ag content are visualized colorless.



**Scheme 4.1** Scheme for the simultaneous photopolymerization-photoreduction of polymer composites microparticles.

The embedded Ag nanoparticles act as nuclei for further enforcement of Ag on the surface, because SERS sensing activity of the primarily formed particles can only be enhanced by higher density of Ag at bead surface. Thus, in order to further Ag enhancement, 50  $\mu$ L aqueous solution of ascorbic acid (5 mM) was added to the particles suspension which contains about 20 particles of 80  $\mu$ m diameter. 50  $\mu$ L  $\text{AgNO}_3$  (in the range between 2.5 mM and 10 mM depending on the intended degree of Ag enforcement) have been added in small portion of about 50  $\mu$ L under vigorous stirring condition to this mixture. The rapid formation of enhanced metallic Ag is observed on the polymer surface as color of the polymer particles converted to black immediately. The color change is realized due to the growth of Ag nanoparticles inside the polymer matrix through pores and at the surface. The formation and tuned deposition of Ag at different concentration can easily be identified by light microscopy characterization (**Figure 4.10 d-f**). Additionally, further variation of Ag nanoparticles (size up to 250 nm diameters) on surface can be systematically tuned by altering the concentration ratios of  $\text{AgNO}_3$  and ascorbic acid. When 2.5 mM ascorbic acid concentration was used, the

formed Ag nanoparticles are of about 40 nm and 65 nm size at 2 mM and 5 mM  $\text{AgNO}_3$  concentration, respectively. With further increase in ascorbic acid concentration, the Ag nanoparticles size increases at constant  $\text{AgNO}_3$  concentration because of spontaneous aggregation during growth. On other side, the formation of bigger Ag nanoparticles is resulted at higher  $\text{AgNO}_3$  concentration. Therefore, about 110 nm sized Ag nanoparticles on the bead surface are formed at 5 mM ascorbic acid and 7 mM  $\text{AgNO}_3$  solution. **Figure 4.10 g-i** and **Figure 4.11 a-c** shows the obtained results for size-tuned Ag nanoparticles and their densities on the surface of polymer microparticles.

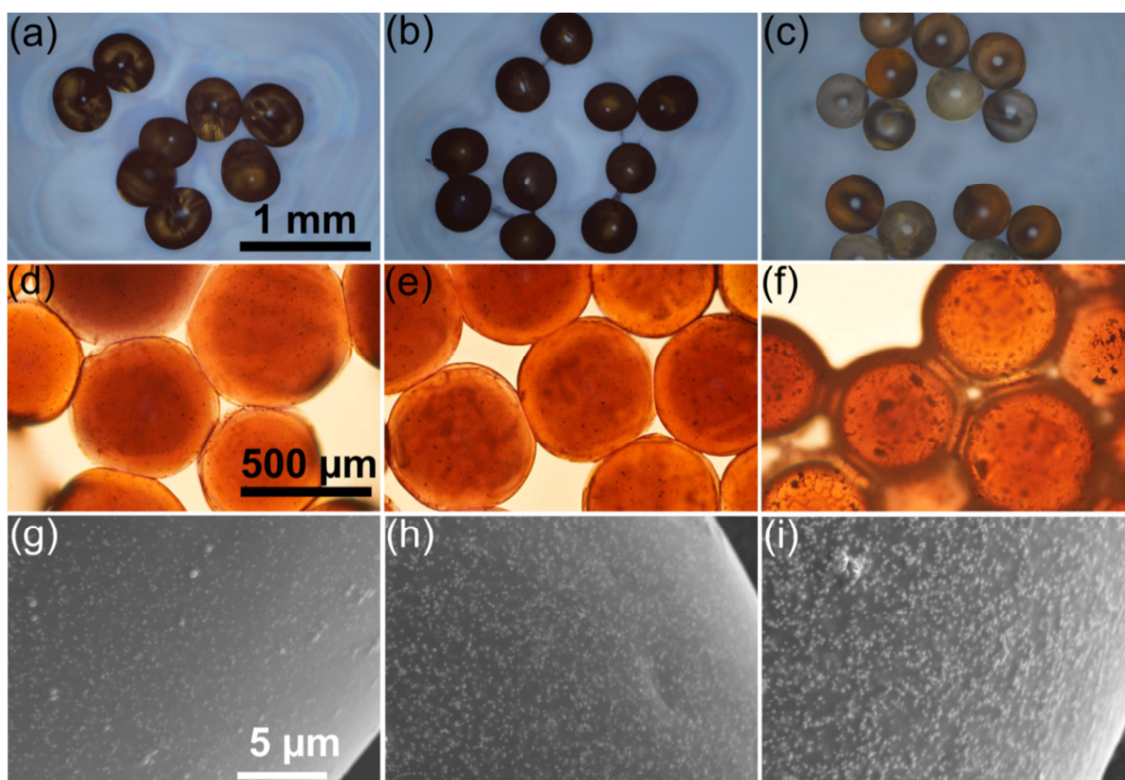


**Figure 4.10** (a-c) Light microscope images of the polyacrylamide microparticles with different amount of embedded Ag: (a) 40 mM, (b) 80 mM, and (c) microparticles mixture with different amount of embedded silver (0 mM, 10 mM, 20 mM and 30 mM), (d-f) optical images by transmission light of 60 mM Ag embedded particles with different concentration of enforced Ag: (d) 2.5 mM, (e) 5 mM, and (f) 10 mM. (g-i) SEM images of composite particles with different amount of enforced Ag: (g) 2.5 mM ascorbic acid and 2 mM  $\text{AgNO}_3$ , (h) 5 mM ascorbic acid and 2 mM  $\text{AgNO}_3$ , and (i) 5 mM ascorbic acid and 5 mM  $\text{AgNO}_3$ . Scale bar for image a-c is 1 mM, for d-f is 500  $\mu\text{m}$  and g-i is 5  $\mu\text{m}$ .

Plasmonic character of the sensor particles is well complemented by the optical spectra of particles suspension (**Figure 4.11 d**). The collective oscillation of the conduction electron takes place at the surface of Ag nanoparticles upon irradiation of light [211]. In the colloidal



suspension of pure Ag nanoparticles, it is marked by the characteristic strong absorption near about 400 nm of Ag nanoparticles.

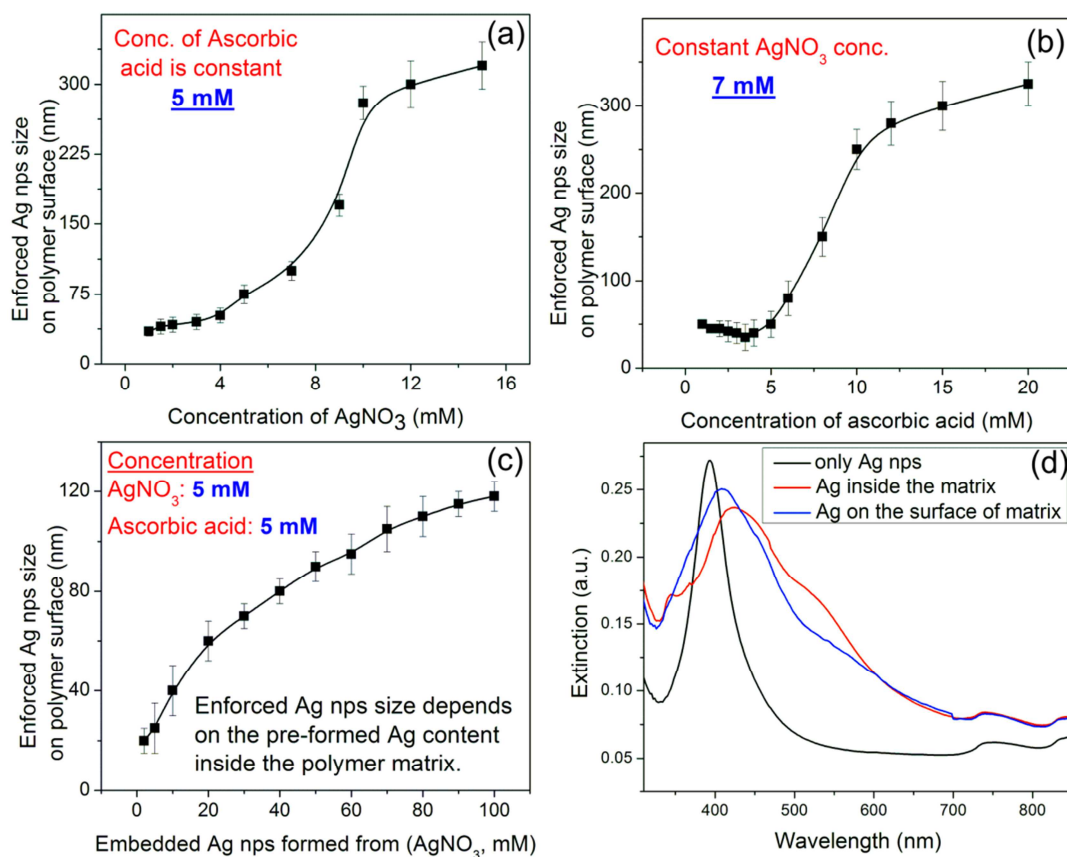


**Figure 4.11** Graphical results for the enforced Ag nanoparticles average size at the matrix surface with respect to different reaction conditions: (a) at different concentration of silver salt, (b) at different concentration reducing agent, and (c) at different AgNO<sub>3</sub> concentration in the matrix during in-situ synthesis. (d) UV/vis spectra of the polyacrylamide/silver composites microparticles of only colloidal Ag nanoparticles (black line), 40  $\mu$ m sized polymer matrix with 60 mM embedded Ag (in-situ formation of Ag nanoparticles when 60 mM AgNO<sub>3</sub> was used) (red line), and 40  $\mu$ m sized polymer matrix with 5 mM enforced Ag nanoparticles (blue line).

In contrast to the sharp plasmon absorption peak of smaller Ag nanoparticles [212], the peak become significantly broadened when Ag nanoparticles are embedded in a microgel interior. In addition, the absorption peak of composite microgel particles shifts to the higher wavelength. As shown in **Figure 4.11 d** the absorption peak moved to about 425 nm when Ag nanoparticles were distributed (during in-situ synthesis) inside the polymer matrix. Broadening and bathochromic shift of a fundamental plasmon peak is also enhanced with increasing silver deposition amount (aggregation size) on the surface of Ag-embedded polymer particles. It is proven that the plasmon peak becomes red-shifted and broadened with

enhancement in the Ag nanoparticles size [213]. Usually in anisotropic Ag nanoparticles, the SPR band is often divided into two different modes, a transverse mode and a longitudinal mode [211]. Here, the formation of larger Ag nanoparticles takes place in the case of higher AgNO<sub>3</sub> precursor solution which also gives two different peaks similar to the anisotropic nanoparticles. A detail study for the different shape-forming mechanisms of Ag nanoparticles is beyond the scope of this thesis. But, the detailed SERS study of differently composed sensor particles with various biochemical molecules are described in below section.

### **4.2.4 SERS sensing application**

Raman spectroscopy is an influential technique for detecting and identifying the analyte molecules in corresponds to their unique energy level of vibrations [214]. The local electromagnetic field around the roughened surface of metallic nanostructure enhance the Raman scattering outcome [95]. An intense local electric field within a few nanometers at nanostructure surface can be generated by LSPR. Such near-field effect can optimize the Raman scattering cross-section of molecules adsorbed onto the surface of metal nanoparticles. This phenomenon of enhancing the Raman scattering cross-section is called surface-enhanced Raman scattering (SERS) [215]. The LSPR is a heart in the SERS effect, because the SERS intensity depends crucially on the wavelength and strength of the plasmon propagating at the surface of nanostructure [216]. The SERS enhancement factor (ratio of Raman signals from the applied number of molecules in the presence and in the absence of the nanostructure) strongly depends on the size, shape and composition of the SERS substrate that give rise to the effect [217]. Rapid and sensitive fingerprint information of various analyte molecules with high reproducibility can only be obtained by using reliable, stable, well-defined and uniform SERS substrate [216-220]. In this thesis work, the polyacrylamide/silver composite particles were used as a powerful SERS substrate due to their enhanced Ag surface provides plenty of 'hot spots' for the uniform SERS outcome and also provide long term stability.

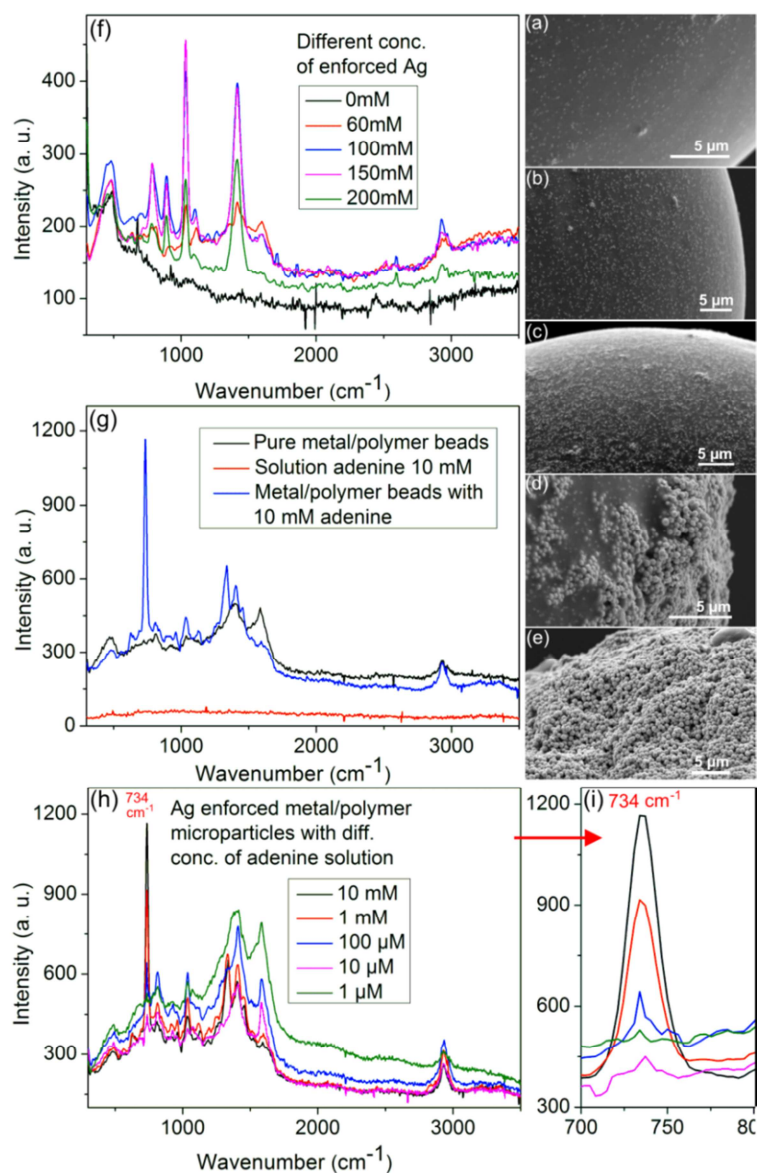


**Figure 4.12** SEM images of the silver/polymer composite microparticles with different Ag amount on surface: (a) 2 mM, (b) 5 mM, (c) 20 mM, (d) 80 mM, and (e) 160 mM. (f) Tuned SERS spectra at different Ag concentration. (g) Test SERS measurement of sensor particles at 10 mM adenine concentration (analyte). (h) and (i) normal and magnified SERS spectra at different concentrations of adenine.

SERS primary measurement is performed by using different size and composition tuned sensor particles. No any Raman signals were obtained when the particles without Ag enforcement are applied to the focus of Raman laser beam (green laser with 532 nm excitation laser source). On other hand, high SERS signals intensity realized if Ag nanoparticles were deposited on the surface of polymer matrix significantly (**Figure 4.12 a-f**). The obtained Raman peaks correspond to the vibration resonances of polymer matrix. The signal intensities consistently increase with increasing amount of Ag enhancement up to an applied concentration of 150 mM AgNO<sub>3</sub> in the enforcement procedure. Further AgNO<sub>3</sub>

concentrations (200 mM) causes the deposition of very dense Ag aggregates (**Figure 4.12 e**) on the surface and hence the SERS signal intensity decreased down drastically. In such case, the random and intense aggregation of Ag nanoparticles covers the entire matrix surface and fills the nanogaps between adjacent Ag nanoparticles from where huge enhanced effect might begin (hot spots) [217, 220].

For sensing the biochemical species through SERS platform, adenine analyte has been applied to the surface of sensor particles. The SERS effect is well reflected by the comparison of three spectra (**Figure 4.12 g**). Pure adenine solution as well as only sensor particles (without analyte interaction) is not showing any significant fingerprint information. The feature of the fingerprint information detected when adenine solution interact with sensor particles by enhancing Raman scattering cross-section of molecules adsorbed onto the surface of Ag nanoparticles. The broad band peaks arises between about  $1450\text{ cm}^{-1}$  and  $1650\text{ cm}^{-1}$  could be due to the interaction of Ag nanoparticles with polyacrylamide matrix. An intense and sharp SERS signal arise at  $738\text{ cm}^{-1}$  when adenine solution applied to the Ag enforced porous sensor particles. A strong Raman peak at  $738\text{ cm}^{-1}$  features due to the ring breathing effect, and another strong peak at  $1330\text{ cm}^{-1}$  can realized due to the ring stretching effect. The enhancement of SERS signals (intensity) is strongly depends on adenine concentrations. SERS signal at  $738\text{ cm}^{-1}$  observed with low intensity at lower adenine concentration ( $1\text{ }\mu\text{M}$ ) and increases regularly with increasing adenine concentration up to  $1\text{ mM}$  and  $10\text{ mM}$  (**Figure 4.12 h**).

SERS biosensing is a highly selective technique for application in the detection of wide range of biological samples and disease [221]. Molecules should possess polarizability to show the Raman scattering effect [222] where deformation of the electron configuration takes place upon light irradiation. L-lactic acid (analyte) with sensor particles, for instance, is showing Raman fingerprint information by giving intense spectral peaks at about  $860\text{ cm}^{-1}$  and  $1410\text{ cm}^{-1}$  (**Figure 4.13 a-c**). These characteristic Raman bands can be obtained due to the Ag–OH and Ag–O bond of carboxylic acid group of L-lactic acid and also could be due to the substrate (sensor particles with  $40\text{ mM}$  embedded Ag). It is also assumed that  $860\text{ cm}^{-1}$  band can be obtained from the C–CO stretching of L-lactic acid [223]. In case of free L-lactic acid solution ( $10\text{ mM}$ ) and L-lactic acid on sensor particles (without Ag deposition), no any Raman signals were obtained (**Figure 4.13 c**, blue line). The tuned SERS signals were observed when L-lactic acid (down to the lowest concentration of  $10\text{ }\mu\text{M}$ ) interact with Ag-enforced polymer beads (sensor particles). Therefore, it is supported by the fact that the used

sensor particles can be used as a versatile SERS substrate for the particles-based sensing application of various biomolecules. L-lactic acid is a significant metabolite in blood and an effective indicator for estimating physiological function [223-225]. The severe enhancement in the L-lactic acid concentration cause several clinical symptoms such as congestive heart failure [225]. Thus, the SERS platform provides an easy identification of L-lactic acid information upon utilization of a reliable SERS substrate.

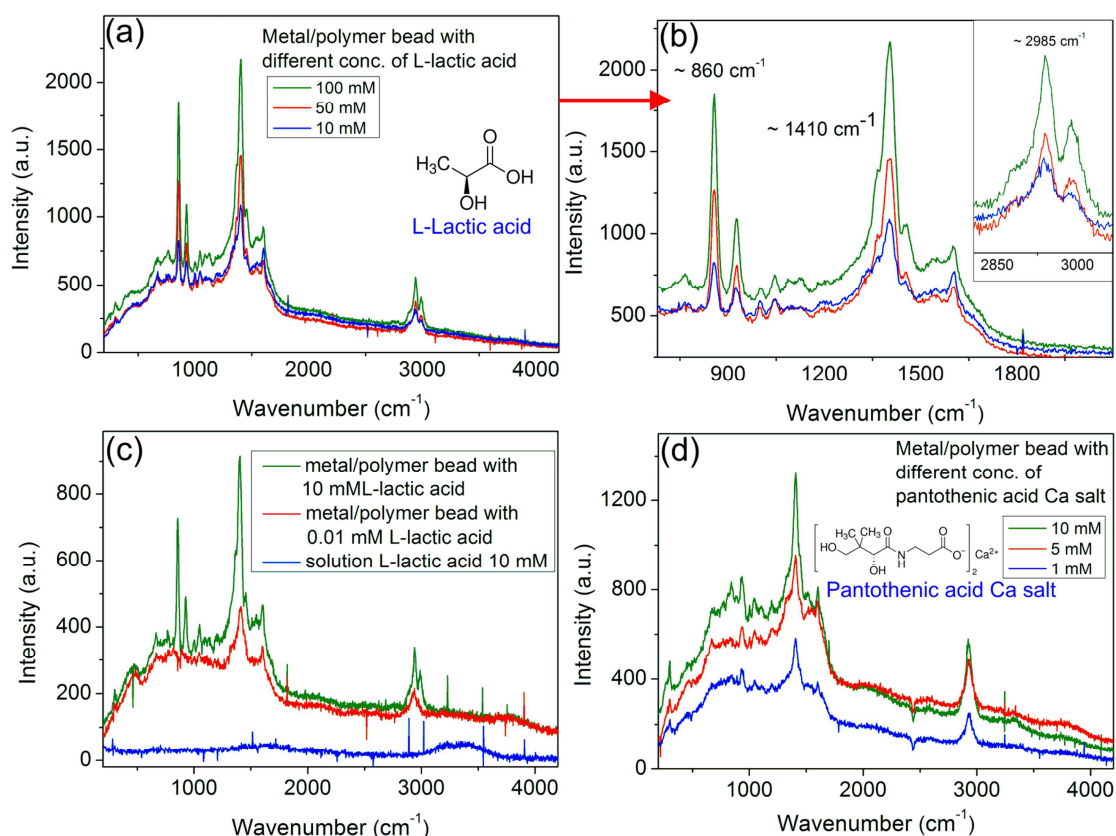


**Figure 4.13** SERS spectra of the sensor particles upon interaction with different concentrations of different analytes: (a) and (b) Normal and magnified SERS spectra at different concentrations of L-lactic acid (analyte). (c) Controlled measurement and comparison of SERS signal position with average and very low concentration of L-lactic acid analyte on microparticles. (d) Tuned SERS spectra of sensor particles at different concentrations of pantothenic acid analyte. The sensor particles with 60 mM embedded Ag and 40 mM enforced Ag was used for all measurements in this image.

Many other analytes such as vitamins and amino acids can also be detected through SERS platform by using microfluidically prepared sensor particles as a SERS substrate. Pantothenic acid is a water soluble vitamin and also an essential nutrient for many animals. The SERS band between 1300 cm<sup>-1</sup> and 1650 cm<sup>-1</sup> can be obtained after the interaction of Ag with polyacrylamide surface in presence of pantothenic acid (1 mM). The moderate peaks between

700  $\text{cm}^{-1}$  and 900  $\text{cm}^{-1}$  might be appeared due to the Ag–O bond vibrations (**Figure 4.13 d**). The SERS signal intensities consistently increases by applying enhanced concentrations of pantothenic acid. Particularly here, the SERS measurement with obtained results is compared with different concentration and type of analytes by using 532 nm laser powers. Overall, the composition tuned Ag/polyacrylamide sensor particles can be used as a powerful particle-based SERS substrate for identification of biomolecules in a batch condition. Moreover, the flow SERS measurement can be a promising strategy for identification and sequential analysis of multiple analytes at a time. This strategy is described in below section with detail.

### **4.3 Flow and sequential SERS measurement**

Integration of microfluidic techniques with SERS microscopy offer the platform where analysis, detection and accurate monitoring of a wide range of analytes can be performed. Microfluidic processes works at highly reduced volume of the reaction solution and provides efficient mixing atmosphere at continuous streaming condition [203]. It is therefore a powerful platform because many chemical and biological tests can be performed in a single experiment of high-throughput screening in flow. In current time, the sequential measurements of multiple analytes through a single SERS substrate have captured broad attention [225]. Hence, here in the compact Raman detection arrangement, the sequential SERS analysis in the continuous flow condition is performed by the application of alternative ringing procedure.

#### **4.3.1 Flow measurement concept and device arrangement**

For the arrangement of device, three syringe pumps actuating different active solutions alternatively to the sensor particles (about 100  $\mu\text{m}$  sized Ag/polyacrylamide microparticles with Ag enforcement) which are placed in the glass capillary as shown in **Figure 2.5**. The dark and reference spectra were captured prior to the SERS spectra of different analytes in flow at 1 second integration time. High reproducibility of SERS signals was observed with the two test analytes adenine (2 mM) and histidine (10 mM) by use of a compact Raman spectrometer (Raman System, R-3000). Typical measurement cycles were set at 1 minute range with flow rates of 40  $\mu\text{L}/\text{min}$  of individual analyte solution. The Raman laser (50 mW power with 532 nm excitation range) spot size is about 3 mM in diameter in compact glass capillary. In arrangement, the applied particles for the SERS sensing of another analyte can be regenerated by the application of a flow rinsing procedure by diluted sulphuric acid. Thus, this process is well suitable for the sequential measurements in continuous flow condition.

### 4.3.2 Sequential SERS measurements under flow conditions

Here in a flow arrangement, the switching of the analyte and rinsing solution (which make desorption of the adsorbed analyte from particles surface) produces the Raman fingerprints signature. Before the analyte actuate to sensor particles, only small Raman signal were observed from the particle matrix itself (**Figure 4.14**: basic line 1). In this case, a SERS signal at about  $1180\text{ cm}^{-1}$  can be interpreted by a polymer skeletal vibration [226]. The small band at about  $2935\text{ cm}^{-1}$  is probably related to the symmetric C-H<sub>2</sub>-stretching in the polymer matrix which was found at  $2931\text{ cm}^{-1}$  in polyacrylamide gel [226].

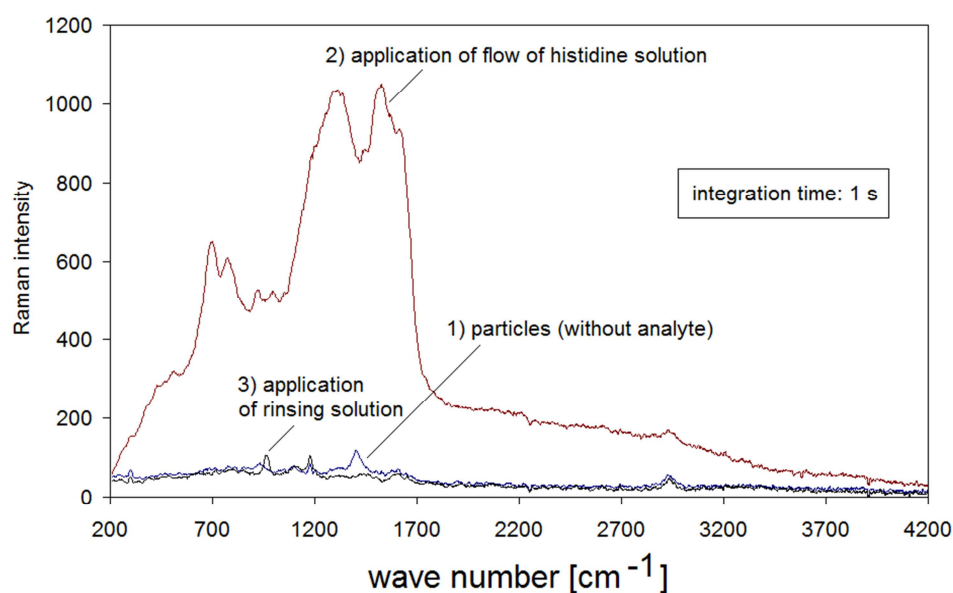


**Figure 4.14** Flow SERS measurements in the compact arrangement using sensor particles inside a glass capillary: (1) only sensor particles, (2) during the application of histidine solution and (3) after rinsing by diluted sulfuric acid.

The SERS signals with high intensity arise during the application of 10 mM histidine solution to the sensor particles. Histidine (amino acid) has a high affinity to Ag surface of sensor particles, and therefore the strong signals are probably realized which corresponds to the well-known SERS effect of histidine [227, 228]. Here in SERS spectra, very broad and strong double was found between about  $1200\text{ cm}^{-1}$  and  $1600\text{ cm}^{-1}$ . Very strong absorption at around  $1300\text{ cm}^{-1}$  corresponds to the strong resonances of breathing and deformation vibration of the imidazole ring in aqueous solution [229]. The smaller bands around  $700\text{ cm}^{-1}$  and  $780\text{ cm}^{-1}$  could be related to the ring breathing and out of plane bending [229]. The actual confirmation of histidine chemisorption at the surface of sensor particles is supported by the effect that the histidine spectrum was also observed after rinsing with aqueous solution. But, it was found



that a simple rinsing of sensor particles by sulfuric acid (regenerating solution) leads to a complete removal of histidine and the subsequent disappearing of the SERS spectrum (**Figure 4.14**, base line 3). This effect is probably due to the protonation of nitrogen atoms in the amino group and imidazole-group leading to a strong reduction of the interaction forces between histidine molecule and Ag surface of sensor particles.

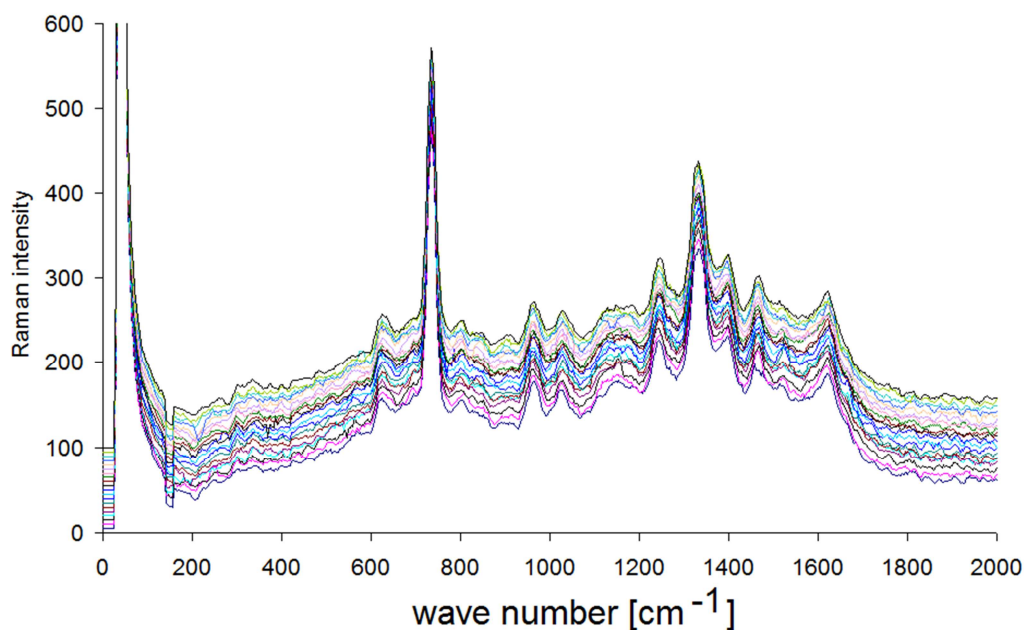


**Figure 4.15** Reproducibility of SERS-flow sensing: Individual SERS spectra of sensor particles during the flow of an adenine solution ( $40 \mu\text{L}/\text{min}$ ) at frequency of 1 Hz (the base line of the single spectra was shifted by 5 units between the individual measurements for better visibility).

A high signal-to-noise ratio was also observed by the application of other analytes. Molecules containing N-heterocycles or amino groups are well suitable for sequential sensing because of their high affinity to Ag surface. The continuous flow SERS spectra of the adenine, for instance, have been measured as shown in **Figure 4.15**.



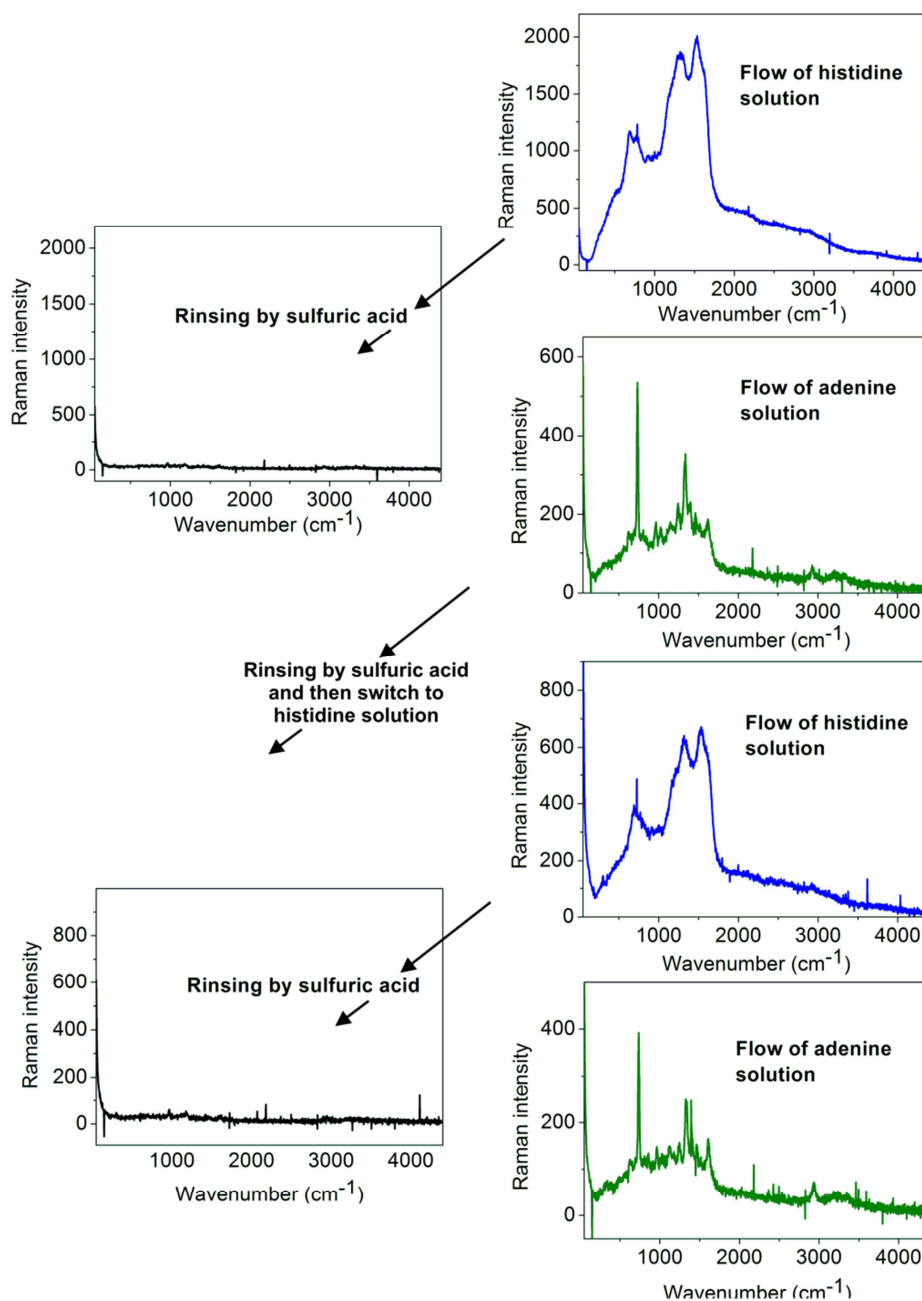


**Figure 4.16** Application and measurement of different analytes by repeated switching of flows of analytes solution and rinsing solution (flow rate: 40  $\mu\text{L}/\text{min}$ ; applied concentrations: histidine: 10 mM, adenine: 2 mM, sulfuric acid 3 %).

An intense peak at  $734\text{ cm}^{-1}$  can be assigned to the ring breathing effect [230]. Another prominent resonance at  $1336\text{ cm}^{-1}$  corresponds to the ring stretching, and it is usually a very strong resonance and was found in the single particle measurement, too. The reproducibility of SERS spectra is high as repeated measurements with an integration time of only 1 second was demonstrated (**Figure 4.15**). Moreover, no any thermally induced degradation processes have been observed in the continuous flow experiments using the fiber-coupled compact

Raman arrangement. The response of the sensor particles on the application of different analyte solutions was investigated by a repeated switching between a histidine solution, the rinsing solution and an adenine solution. This sequential measurement was realized by on- and off-switching of the different syringe pumps in flow arrangement without any change in the applied sensing particles. In all cases, the typical SERS spectra of the analytes disappeared after rinsing the sensor particles by the regenerating solution (diluted sulfuric acid) as shown in **Figure 4.16**. The spectra of the alternative analytes (histidine and adenine) in sequence were always found without any disturbance in SERS peak positions. The investigation reveals that the concept of a micro flow-Raman sensing by sensor particles can be realized in the compact SERS arrangement for sequential measurements of different types of analytes. The change between analyte application and rinsing for regeneration can be realized by a microfluidic setup which allows an automated switching between fluid input channels for analytes and for regeneration solutions in sequential continuous flow. An approach is well applicable for the mobile systems and for the site-of-care applications because of the application of compact Raman components and fiber coupling. It is clear in this finding that the realized accumulation time of one second and complete measurements cycles of about one minute show that the sequential sample application in series of measurements and miniaturized screenings can be performed in wide range.

## 5 Conclusion

In this work, various types of complex polymer nanoparticles and microparticles with their assembling and composition characters for labeling and sensoric applications are prepared in the microfluidic platform. The primary focus of this thesis was the optimization of microfluidic platform for producing the size, shape, morphology and composition tuned multi-scale polymer particles via emulsion and suspension polymerization process. The performed work leads to the following major conclusions:

- Here, the investigation reveals that the Si holeplate based cross-flow microfluidic arrangement is perfectly suitable for the production of well-defined hydrophilic and hydrophobic polymer nano and microparticles of different size, shape and composition.
- Spherical poly(methyl methacrylate) (PMMA) nanoparticles of the size range between 60 nm and 500 nm can be produced by varying the flow rates, flow rate ratios, concentration of anionic (SDS) as well as cationic (CTAB) surfactants and reactants composition in the microfluidic setup. The characterization by SEM and zeta potential measurement supported the dominating effect of surfactant concentration for uniform tuning in the nanoparticles size.
- It was observed through experiments that the regular streaming condition and efficient mixing of the reactants in the microreactor able to produce highly controlled compact non-spherical polymer nanoparticles in a single-step process. The analysis shows that the ellipsoidal-like PMMA nanoparticles can be realized at higher aqueous to monomer flow rate ratio whereas the dumbbell-like nanoparticles were obtained at lower flow rate ratio. The PSS-co-PM (polyelectrolyte) in aqueous phase play a key role for the formation of compact nanoparticles and it can be hypothetically explained by *in-situ* nanoassembling of growing particles on the basis of partial repulsion, limited polarization and controlled electrostatic interaction. By varying the PSS-co-PM concentrations and flow rate ratios, the ellipsoidal and dumbbell-like nanoparticles of aspect ratio between 1.1 and 2.3 (length between 150 nm and 510 nm whereas width between 120 nm and 260 nm) were produced. Moreover, it was found that the high monomer flow rates allow the formation of elongated linear (aspect ratio up to about 8) and branched polymer nanoparticles. On other side, by using non-ionic

polymer polyvinyl pyrrolidone (PVP) in the aqueous phase, the controlled flower-shaped PMMA nanoparticles of the size range between 200 nm and 1  $\mu$ m were produced. It can be assumed that the formation of fractured structure is a result of aggregation of multiple aggregate phases on the basis of solvation power and mobility factors.

- Polymer nanoparticles with shell-like surface layer by controlled copolymerization approach of PMMA (hydrophobic) and polyDADMAC (hydrophilic) domains were performed. It was observed that the mean particles size is consistently decreases with increasing concentration of hydrophilic monomers which supports the standard effect of interfacial stabilizing agent for size control of nanoparticles. But, interestingly, it is found that with further increase in the hydrophilic monomers concentration, the particles size is gradually increases which reveal the result of surface thickness of the hydrophilic polymeric (polyDADMAC) layer at constant PMMA core size. Here, it can also be summarize that the integration of fluorescent and plasmonic nanomaterials with such polymeric nanoparticles forms the controlled nanoassembly for LSPR, SERS and fluorescence activities.
- Four different strategies have been developed and successfully implemented here for the formation of fluorescent PMMA nanoparticles of the size range between 60 nm and 350 nm. In first strategy, the microfluidic assisted production of non-covalent linking of fluorophores in the nanoparticles interior is recognized. It was found that the high loading of fluorophore is realized in the nanoparticles interior by this technique. To avoid the leaking problem, the second strategy is developed where fluorophore can be covalently-linked to the network of polymer nanoparticles. In third strategy, hydrophilic charged fluorophore can act as a surface stabilizing agent too which control the size, surface charge and fluorescence intensity of the polymer nanoparticles simultaneously in a single-step process. The multi-layer approach is well-known for the planar surface, but here we learned that this strategy can be well applicable to the colloidal polymer particles, too. Three major functionalization steps were performed by covalent, electrostatic and secondary interactions on the spherical nanoparticles as a model system. The investigation shows that the interaction of dye-labelled streptavidin on the outer surface makes the entire network a fluorescence-active.

- The investigation and experimental results reveals that the Si holeplate-based microreactor able to produce the simultaneous size and color-tuned polyTPGDA microparticles of size ranges between 50  $\mu\text{m}$  and 350  $\mu\text{m}$ . Moreover, the modification in microreactor was applied for the production of multi-coloured microparticles which can be used for the fluorescence labeling applications.
- Highly controlled PMMA/Ag heterogeneous nanoassemblies were prepared by precisely adjusting the surface charges on both individual components in batch synthesis. It was found that the controlled surface charge and appropriate thermal conditions are key issues for producing the distance-controlled nanoassembly particles. Moreover, for providing the highly homogeneous reaction environment, a flow assembling process of the size and shape controlled polymer nanoparticles were performed for producing different types of assembly particles after discrete layers of the surface modifications. It was found that because of the flow parameters such as efficient mixing and reaction at high interface area, the assembly particles were obtained with extraordinary high homogeneity.
- An investigation shows that polymer/silver composite sensor particles of cross-linked polyacrylamide with controlled diameters between about 30  $\mu\text{m}$  and 600  $\mu\text{m}$  can be reproducibly prepared by the application of a micro cross-flow arrangement via droplet generation for a suspension polymerization. The required high content of distributed metallic silver inside the polymer matrix is achieved by a combination of *in-situ* formation of smaller metal nanoparticles during the flow process and a silver-catalyzed silver deposition in a subsequent batch process for SERS-active sensor particles. From the obtained experimental results, it can be concluded that these polyacrylamide/silver sensor particles could be used as versatile SERS substrate for sensing applications.
- It is found that the concept of a microflow SERS sensing by sensor particles could be realized using silver nanoparticle-doped polymer composite microparticles. Despite the fact that a direct exchange of analytes is not possible, the investigated examples of adenine and histidine demonstrate that an easy regeneration of the surface of the sensing-active gel-embedded silver nanoparticle is possible by a fast rinsing with acid solution in microflow condition.



## 6 References

- [1] Xu X, Asher SA; Synthesis and Utilization of Monodisperse Hollow Polymeric Particles in Photonic Crystals. *Journal of the American Chemical Society*, **2004**, *126*, 7940-7945.
- [2] Uhrich KE, Cannizzaro SM, Langer RS, Shakesheff KM; Polymeric Systems for Controlled Drug Release. *Chemical Reviews*, **1999**, *99*, 3181-3198.
- [3] Khan IU, Serra CA, Anton N, Vandamme T; Microfluidics: A focus on improved cancer targeted drug delivery systems. *Journal of Controlled Release*, **2013**, *172*, 1065-1074.
- [4] Whitesides GM; The origins and the future of microfluidics. *Nature*, **2006**, *442*, 368-373.
- [5] DeMello J, DeMello A; Microscale reactors: nanoscale products. *Lab on a Chip*, **2004**, *4*, 11N-15N.
- [6] Köhler JM, Li S, Knauer A; Why is Micro Segmented Flow Particularly Promising for the Synthesis of Nanomaterials? *Chemical Engineering & Technology*, **2013**, *36*, 887-899.
- [7] Xu Q, Hashimoto M, Dang TT, Hoare T, Kohane DS, Whitesides GM, Langer R, Anderson DG; Preparation of Monodisperse Biodegradable Polymer Microparticles Using a Microfluidic Flow-Focusing Device for Controlled Drug Delivery. *Small*, **2009**, *5*, 1575-1581.
- [8] Souilem I, Muller R, Holl Y, Bouquey M, Serra CA, Vandamme T, Anton N; A Novel Low-Pressure Device for Production of Nanoemulsions. *Chemical Engineering & Technology*, **2012**, *35*, 1692-1698.
- [9] Kim JH, Jeon TY, Choi TM, Shim TS, Kim S-H, Yang S-M; Droplet Microfluidics for Producing Functional Microparticles. *Langmuir*, **2014**, *30*, 1473-1488.
- [10] Serra CA, Cortese B, Khan IU, Anton N, de Croon MHJM, Hessel V, Ono T, Vandamme T; Coupling Microreaction Technologies, Polymer Chemistry, and Processing to Produce Polymeric Micro and Nanoparticles with Controlled Size, Morphology, and Composition. *Macromolecular Reaction Engineering*, **2013**, *7*, 414-439.
- [11] Kraus I, Li S, Knauer A, Schmutz M, Faerber J, Serra CA, Kohler M; Continuous-Microflow Synthesis and Morphological Characterization of Multiscale Composite Materials Based on Polymer Microparticles and Inorganic Nanoparticles. *Journal of Flow Chemistry*, **2014**, *4*, 72-78.
- [12] Abulateefeh SR, Spain SG, Aylott JW, Chan WC, Garnett MC, Alexander C; Thermoresponsive Polymer Colloids for Drug Delivery and Cancer Therapy. *Macromolecular Bioscience*, **2011**, *11*, 1722-1734.
- [13] Raghupathi K, Li L, Ventura J, Jennings M, Thayumanavan S; pH responsive soft nanoclusters with size and charge variation features. *Polymer Chemistry*, **2014**, *5*, 1737-1742.
- [14] Zhuang J, Gordon MR, Ventura J, Li L, Thayumanavan S; Multi-stimuli responsive macromolecules and their assemblies. *Chemical Society Reviews*, **2013**, *42*, 7421-7435.
- [15] Ali SI, Heuts JPA, van Herk AM; Vesicle-templated pH-responsive polymeric nanocapsules. *Soft Matter*, **2011**, *7*, 5382-5390.

- [16] Wang W, Liang H, Cheikh Al Ghanami R, Hamilton L, Fraylich M, Shakesheff KM, Saunders B, Alexander C; Biodegradable Thermoresponsive Microparticle Dispersions for Injectable Cell Delivery Prepared Using a Single-Step Process. *Advanced Materials*, **2009**, *21*, 1809-1813.
- [17] Musyanovych A, Landfester K; Polymer Micro- and Nanocapsules as Biological Carriers with Multifunctional Properties. *Macromolecular Bioscience*, **2014**, *14*, 458-477.
- [18] Sukhorukov G, Fery A, Möhwald H; Intelligent micro- and nanocapsules. *Progress in Polymer Science*, **2005**, *30*, 885-897.
- [19] Esser-Kahn AP, Odom SA, Sottos NR, White SR, Moore JS; Triggered Release from Polymer Capsules. *Macromolecules*, **2011**, *44*, 5539-5553.
- [20] Motornov M, Roiter Y, Tokarev I, Minko S; Stimuli-responsive nanoparticles, nanogels and capsules for integrated multifunctional intelligent systems. *Progress in Polymer Science*, **2010**, *35*, 174-211.
- [21] Hou J, Li Q, Han X, Lu C; Swelling/Deswelling-Induced Reversible Surface Wrinkling on Layer-by-Layer Multilayers. *The Journal of Physical Chemistry B*, **2014**, *118*, 14502-14509.
- [22] Yin J, Han X, Cao Y, Lu C; Surface Wrinkling on Polydimethylsiloxane Microspheres via Wet Surface Chemical Oxidation. *Sci. Rep.*, **2014**, *4*, 5710.
- [23] Liu S, Deng R, Li W, Zhu J; Polymer Microparticles with Controllable Surface Textures Generated through Interfacial Instabilities of Emulsion Droplets. *Advanced Functional Materials*, **2012**, *22*, 1692-1697.
- [24] Peppas NA, Hilt JZ, Khademhosseini A, Langer R; Hydrogels in biology and medicine: From molecular principles to bionanotechnology. *Advanced Materials*, **2006**, *18*, 1345-1360.
- [25] Resch-Genger U, Grabolle M, Cavaliere-Jaricot S, Nitschke R, Nann T; Quantum dots versus organic dyes as fluorescent labels. *Nature Methods*, **2008**, *5*, 763-775.
- [26] Campbell AI, Bartlett P; Fluorescent hard-sphere polymer colloids for confocal microscopy. *Journal of Colloid and Interface Science*, **2002**, *256*, 325-330.
- [27] Khan IU, Stolch L, Serra CA, Anton N, Akasov R, Vandamme TF; Microfluidic conceived pH sensitive core-shell particles for dual drug delivery. *International Journal of Pharmaceutics*, **2015**, *478*, 78-87.
- [28] Chang Z, Serra CA, Bouquey M, Prat L, Hadziioannou G; Co-axial capillaries microfluidic device for synthesizing size- and morphology-controlled polymer core-polymer shell particles. *Lab on a Chip*, **2009**, *9*, 3007-3011.
- [29] Li X, Yang Y-T, Wu L-J, Li Y-C, Ye M-Y, Chang Z-Q, Meng D-Q, Serra CA; Fabrication of electro- and color-responsive CB/PTFE Janus beads in a simple microfluidic device. *Materials Letters*, **2015**, *142*, 258-261.
- [30] Khan IU, Serra CA, Anton N, Li X, Akasov R, Messaddeq N, Kraus I, Vandamme TF; Microfluidic conceived drug loaded Janus particles in side-by-side capillaries device. *International Journal of Pharmaceutics*, **2014**, *473*, 239-249.



- 
- [31] Urban M, Freisinger B, Ghazy O, Staff R, Landfester K, Crespy D, Musyanovych A; Polymer Janus Nanoparticles with Two Spatially Segregated Functionalizations. *Macromolecules*, **2014**, *47*, 7194-7199.
- [32] Tian Z, Yu J, Wu C, Szymanski C, McNeill J; Amplified energy transfer in conjugated polymer nanoparticle tags and sensors. *Nanoscale*, **2010**, *2*, 1999-2011.
- [33] Wu C, Bull B, Christensen K, McNeill J; Ratiometric Single-Nanoparticle Oxygen Sensors for Biological Imaging. *Angewandte Chemie International Edition*, **2009**, *48*, 2741-2745.
- [34] Willner I, Zayats M; Electronic aptamer-based sensors. *Angewandte Chemie-International Edition*, **2007**, *46*, 6408-6418.
- [35] Cao JL, Nagl S, Kothe E, Kohler JM; Oxygen sensor nanoparticles for monitoring bacterial growth and characterization of dose-response functions in microfluidic screenings. *Microchimica Acta*, **2015**, *182*, 385-394.
- [36] Kursten D, Kothe E, Wetzel K, Bergmann K, Köhler JM; Micro-segmented flow and multisensor-technology for microbial activity profiling. *Environmental Science-Processes & Impacts*, **2014**, *16*, 2362-2370.
- [37] Champion JA, Katare YK, Mitragotri S; Making polymeric micro- and nanoparticles of complex shapes. *Proceedings of the National Academy of Sciences of the United States of America*, **2007**, *104*, 11901-11904.
- [38] Champion JA, Mitragotri S; Role of target geometry in phagocytosis. *Proceedings of the National Academy of Sciences of the United States of America*, **2006**, *103*, 4930-4934.
- [39] Farokhzad OC, Langer R; Impact of Nanotechnology on Drug Delivery. *ACS Nano*, **2009**, *3*, 16-20.
- [40] Simo A, Polte J, Pfander N, Vainio U, Emmerling F, Rademann K; Formation Mechanism of Silver Nanoparticles Stabilized in Glassy Matrices. *Journal of the American Chemical Society*, **2012**, *134*, 18824-18833.
- [41] Halder A, Kundu P, Viswanath B, Ravishankar N; Symmetry and shape issues in nanostructure growth. *Journal of Materials Chemistry*, **2010**, *20*, 4763-4772.
- [42] Viswanath B, Kundu P, Halder A, Ravishankar N; Mechanistic Aspects of Shape Selection and Symmetry Breaking during Nanostructure Growth by Wet Chemical Methods. *Journal of Physical Chemistry C*, **2009**, *113*, 16866-16883.
- [43] Visaveliya N, Köhler JM; A self-seeding synthesis of Ag microrods of tuned aspect ratio: ascorbic acid plays a key role. *Nanotechnology*, **2013**, *24*,
- [44] Xia Y, Xiong Y, Lim B, Skrabalak SE; Shape-Controlled Synthesis of Metal Nanocrystals: Simple Chemistry Meets Complex Physics? *Angewandte Chemie International Edition*, **2009**, *48*, 60-103.
- [45] Grzelczak M, Vermant J, Furst EM, Liz-Marzan LM; Directed Self-Assembly of Nanoparticles. *Acs Nano*, **2010**, *4*, 3591-3605.
- [46] Mock EB, De Bruyn H, Hawkett BS, Gilbert RG, Zukoski CF; Synthesis of anisotropic nanoparticles by seeded emulsion polymerization. *Langmuir*, **2006**, *22*, 4037-4043.
-

- [47] Peng B, Smalenburg F, Imhof A, Dijkstra M, van Blaaderen A; Colloidal Clusters by Using Emulsions and Dumbbell-Shaped Particles: Experiments and Simulations. *Angewandte Chemie-International Edition*, **2013**, *52*, 6709-6712.
- [48] Sheu HR, Elaasser MS, Vanderhoff JW; Phase-Separation in Polystyrene Latex Interpenetrating Polymer Networks. *Journal of Polymer Science Part a-Polymer Chemistry*, **1990**, *28*, 629-651.
- [49] Hwang DK, Dendukuri D, Doyle PS; Microfluidic-based synthesis of non-spherical magnetic hydrogel microparticles. *Lab on a Chip*, **2008**, *8*, 1640-1647.
- [50] Baghbanzadeh M, Carbone L, Cozzoli PD, Kappe CO; Microwave-Assisted Synthesis of Colloidal Inorganic Nanocrystals. *Angewandte Chemie-International Edition*, **2011**, *50*, 11312-11359.
- [51] Carbone L, Cozzoli PD; Colloidal heterostructured nanocrystals: Synthesis and growth mechanisms. *Nano Today*, **2010**, *5*, 449-493.
- [52] Vutukuri HR, Stiefelhagen J, Vissers T, Imhof A, van Blaaderen A; Bonding Assembled Colloids without Loss of Colloidal Stability. *Advanced Materials*, **2012**, *24*, 412-416.
- [53] Han Y, Zhang ZH, Liu YY, Niu YY, Ding DG, Wu BL, Hou HW, Fan YT; External Template-Assisted Self-Assembly: Design and Synthesis of 4,4'-bipy-Based Mo(W)/Cu/S Heteroatom-metallic Polymeric Clusters Directed by 1,1'-Bis(pyridinium)methylene Cation. *Crystal Growth & Design*, **2011**, *11*, 3448-3455.
- [54] Dendukuri D, Tsoi K, Hatton TA, Doyle PS; Controlled synthesis of nonspherical microparticles using microfluidics. *Langmuir*, **2005**, *21*, 2113-2116.
- [55] Jeon SJ, Yi GR, Yang SM; Cooperative Assembly of Block Copolymers with Deformable Interfaces: Toward Nanostructured Particles. *Advanced Materials*, **2008**, *20*, 4103-4108.
- [56] Polenz I, Datta SS, Weitz DA; Controlling the Morphology of Polyurea Microcapsules Using Microfluidics. *Langmuir*, **2014**, *30*, 13405-13410.
- [57] Park J-G, Forster JD, Dufresne ER; High-Yield Synthesis of Monodisperse Dumbbell-Shaped Polymer Nanoparticles. *Journal of the American Chemical Society*, **2010**, *132*, 5960-5961.
- [58] Deng R, Liu S, Liang F, Wang K, Zhu J, Yang Z; Polymeric Janus Particles with Hierarchical Structures. *Macromolecules*, **2014**, *47*, 3701-3707.
- [59] Knauer A, Koehler JM. 2014. Screening of nanoparticle properties in microfluidic syntheses. *Nanotechnology Reviews*, **2013**, *3*, 5-26.
- [60] Tao AR, Habas S, Yang P; Shape Control of Colloidal Metal Nanocrystals. *Small*, **2008**, *4*, 310-325.
- [61] Koehler JM, Moeller F, Schneider S, Guenther PM, Albrecht A, Gross GA; Size-tuning of monodisperse PMMA nanoparticles by micro-continuous-flow polymerization using a silicon micro-nozzle array. *Chemical Engineering Journal*, **2011**, *167*, 688-693.
- [62] Tsierkezos N, Haj Othman S, Ritter U, Hafermann L, Knauer A, Köhler JM; Nitrogen-doped multi-walled carbon nanotubes modified with platinum, palladium, rhodium and silver nanoparticles in electrochemical sensing. *Journal of Nanoparticle Research*, **2014**, *16*, 1-13.

- 
- [63] Panchuk RR, Prylutska SV, Chumak VV, Skorokhyd NR, Lehka LV, Evstigneev MP, Prylutskyi YI, Berger W, Heffeter P, Scharff P, Ritter U, Stoika RS; Application of C60 Fullerene-Doxorubicin Complex for Tumor Cell Treatment *In Vitro* and *In vivo*. *Journal of Biomedical Nanotechnology*, **2015**, *11*, 1139-1152.
- [64] Tsierkezos NG, Knauer A, Ritter U; Multi-Walled Carbon Nanotubes Modified with Gold Nanoparticles with Various Diameters for the Simultaneous Analysis of Dopamine and Uric Acid in a Single Experiment. *Sensor Letters*, **2014**, *12*, 153-159.
- [65] Prylutskyi YI, Evstigneev MP, Pashkova IS, Wyrzykowski D, Woziwodzka A, Golunski G, Piosik J, Cherepanov VV, Ritter U; Characterization of C60 fullerene complexation with antibiotic doxorubicin. *Physical Chemistry Chemical Physics*, **2014**, *16*, 23164-23172.
- [66] Balazs AC, Emrick T, Russell TP; Nanoparticle Polymer Composites: Where Two Small Worlds Meet. *Science*, **2006**, *314*, 1107-1110.
- [67] Lee S-K, Baek J, Jensen KF; High Throughput Synthesis of Uniform Biocompatible Polymer Beads with High Quantum Dot Loading Using Microfluidic Jet-Mode Breakup. *Langmuir*, **2014**, *30*, 2216-2222.
- [68] Duguet E, Desert A, Perro A, Ravaine S; Design and elaboration of colloidal molecules: an overview. *Chemical Society Reviews*, **2011**, *40*, 941-960.
- [69] Li F, Josephson DP, Stein A; Colloidal Assembly: The Road from Particles to Colloidal Molecules and Crystals. *Angewandte Chemie-International Edition*, **2011**, *50*, 360-388.
- [70] Peer D, Karp JM, Hong S, Farokhzad OC, Margalit R, Langer R; Nanocarriers as an emerging platform for cancer therapy. *Nature Nanotechnology*, **2007**, *2*, 751-760.
- [71] Farokhzad OC, Cheng JJ, Teply BA, Sherifi I, Jon S, Kantoff PW, Richie JP, Langer R; Targeted nanoparticle-aptamer bioconjugates for cancer chemotherapy in vivo. *Proceedings of the National Academy of Sciences of the United States of America*, **2006**, *103*, 6315-6320.
- [72] Zhang L, Gu FX, Chan JM, Wang AZ, Langer RS, Farokhzad OC; Nanoparticles in medicine: Therapeutic applications and developments. *Clinical Pharmacology & Therapeutics*, **2008**, *83*, 761-769.
- [73] Zhao Y, Zhao X, Sun C, Li J, Zhu R, Gu Z; Encoded silica colloidal crystal beads as supports for potential multiplex immunoassay. *Analytical Chemistry*, **2008**, *80*, 1598-1605.
- [74] Pregibon DC, Toner M, Doyle PS; Multifunctional encoded particles for high-throughput biomolecule analysis. *Science*, **2007**, *315*, 1393-1396.
- [75] Kursten D, Cao JL, Funfak A, Muller P, Kohler JM; Cultivation of *Chlorella vulgaris* in microfluid segments and microtoxicological determination of their sensitivity against CuCl<sub>2</sub> in the nanoliter range. *Engineering in Life Sciences*, **2011**, *11*, 580-587.
- [76] Laux EM, Behnke T, Hoffmann K, Resch-Genger U; Keeping particles brilliant - simple methods for the determination of the dye content of fluorophore-loaded polymeric particles. *Analytical Methods*, **2012**, *4*, 1759-1768.
- [77] Gao YL, Stanford WL, Chan WCW; Quantum-Dot-Encoded Microbeads for Multiplexed Genetic Detection of Non-amplified DNA Samples. *Small*, **2011**, *7*, 137-146.
-

- [78] Zhang Y, Wang TH; Quantum Dot Enabled Molecular Sensing and Diagnostics. *Theranostics*, **2012**, 2, 631-654.
- [79] Dey P, Olds W, Blakey I, Thurecht KJ, Izake EL, Fredericks PM; SERS-based detection of barcoded gold nanoparticle assemblies from within animal tissue. *Journal of Raman Spectroscopy*, **2013**, 44, 1659-1665.
- [80] Michalet X, Pinaud FF, Bentolila LA, Tsay JM, Doose S, Li JJ, Sundaresan G, Wu AM, Gambhir SS, Weiss S; Quantum dots for live cells, in vivo imaging, and diagnostics. *Science*, **2005**, 307, 538-544.
- [81] Yao J, Larson DR, Vishwasrao HD, Zipfel WR, Webb WW; Blinking and nonradiant dark fraction of water-soluble quantum dots in aqueous solution. *Proceedings of the National Academy of Sciences of the United States of America*, **2005**, 102, 14284-14289.
- [82] Marchuk K, Guo YJ, Sun W, Vela J, Fang N; High-Precision Tracking with Non-blinking Quantum Dots Resolves Nanoscale Vertical Displacement. *Journal of the American Chemical Society*, **2012**, 134, 6108-6111.
- [83] Spinicelli P, Mahler B, Buil S, Quelin X, Dubertret B, Hermier JP; Non-Blinking Semiconductor Colloidal Quantum Dots for Biology, Optoelectronics and Quantum Optics. *Chemphyschem*, **2009**, 10, 879-882.
- [84] Wang XY, Ren XF, Kahen K, Hahn MA, Rajeswaran M, Maccagnano-Zacher S, Silcox J, Cragg GE, Efros AL, Krauss TD; Non-blinking semiconductor nanocrystals. *Nature*, **2009**, 459, 686-689.
- [85] Wu CF, Szymanski C, Cain Z, McNeill J; Conjugated polymer dots for multiphoton fluorescence imaging. *Journal of the American Chemical Society*, **2007**, 129, 12904-12905.
- [86] Wu C, Bull B, Szymanski C, Christensen K, McNeill J; Multicolor Conjugated Polymer Dots for Biological Fluorescence Imaging. *Acs Nano*, **2008**, 2, 2415-2423.
- [87] Fernandez-Suarez M, Ting AY; Fluorescent probes for super-resolution imaging in living cells. *Nature Reviews Molecular Cell Biology*, **2008**, 9, 929-943.
- [88] Mitchell P; Turning the spotlight on cellular imaging - Advances in imaging are enabling researchers to track more accurately the localization of macromolecules in cells. *Nature Biotechnology*, **2001**, 19, 1013-1017.
- [89] Wang XM, Xu SP, Liang CY, Li HR, Sun F, Xu WQ; Enriching PMMA nanospheres with adjustable charges as novel templates for multicolored dye@PMMA nanocomposites. *Nanotechnology*, **2011**, 22, 275608.
- [90] Wang XM, Xu SP, Xu WQ; Synthesis of highly stable fluorescent Ag nanocluster@ polymer nanoparticles in aqueous solution. *Nanoscale*, **2011**, 3, 4670-4675.
- [91] Muller M, Zentel R, Maka T, Romanov SG, Torres CMS; Dye-containing polymer beads as photonic crystals. *Chemistry of Materials*, **2000**, 12, 2508-2512.
- [92] Han MY, Gao XH, Su JZ, Nie S; Quantum-dot-tagged microbeads for multiplexed optical coding of biomolecules. *Nature Biotechnology*, **2001**, 19, 631-635.
- [93] Grøndahl L, Battersby BJ, Bryant D, Trau M; Encoding Combinatorial Libraries: A Novel Application of Fluorescent Silica Colloids. *Langmuir*, **2000**, 16, 9709-9715.

- 
- [94] Shah NC, Lyandres O, Walsh JT, Glucksberg MR, Van Duyne RP; Lactate and sequential lactate-glucose sensing using surface-enhanced Raman spectroscopy. *Analytical Chemistry*, **2007**, *79*, 6927-6932.
- [95] Dieringer JA, McFarland AD, Shah NC, Stuart DA, Whitney AV, Yonzon CR, Young MA, Zhang XY, Van Duyne RP; Surface enhanced Raman spectroscopy: new materials, concepts, characterization tools, and applications. *Faraday Discussions*, **2006**, *132*, 9-26.
- [96] Lin X-M, Cui Y, Xu Y-H, Ren B, Tian Z-Q; Surface-enhanced Raman spectroscopy: substrate-related issues. *Analytical and Bioanalytical Chemistry*, **2009**, *394*, 1729-1745.
- [97] Park JI, Saffari A, Kumar S, Gunther A, Kumacheva E; Microfluidic Synthesis of Polymer and Inorganic Particulate Materials. *Annual Review of Materials Research*, **2010**, *40*, 415-443.
- [98] Günther A, Jensen KF; Multiphase microfluidics: from flow characteristics to chemical and materials synthesis. *Lab on a Chip*, **2006**, *6*, 1487-1503.
- [99] Cao J, Schneider S, Schultheiß R, Schober A, Köhler JM, Groß GA; "From microtiter plates to droplets" tools for micro-fluidic droplet processing. *Microsystem Technologies*, **2015**, *21*, 539-548.
- [100] Budden M, Schneider S, Groß GA, Kielpinski M, Henkel T, Cahill B, Köhler JM; Microfluidic encoding: Generation of arbitrary droplet sequences by electrical switching in microchannels. *Sensors and Actuators A: Physical*, **2013**, *189*, 288-297.
- [101] Song H, Chen DL, Ismagilov RF; Reactions in Droplets in Microfluidic Channels. *Angewandte Chemie International Edition*, **2006**, *45*, 7336-7356.
- [102] Valencia PM, Pridgen EM, Rhee M, Langer R, Farokhzad OC, Karnik R; Microfluidic Platform for Combinatorial Synthesis and Optimization of Targeted Nanoparticles for Cancer Therapy. *ACS Nano*, **2013**, *7*, 10671-10680.
- [103] El-Ali J, Sorger PK, Jensen KF; Cells on chips. *Nature*, **2006**, *442*, 403-411.
- [104] Jensen KF; Microreaction engineering—is small better? *Chemical Engineering Science*, **2001**, *56*, 293-303.
- [105] Steinbacher JL, McQuade DT; Polymer chemistry in flow: New polymers, beads, capsules, and fibers. *Journal of Polymer Science Part A: Polymer Chemistry*, **2006**, *44*, 6505-6533.
- [106] Zang E, Brandes S, Tovar M, Martin K, Mech F, Horbert P, Henkel T, Figge MT, Roth M; Real-time image processing for label-free enrichment of Actinobacteria cultivated in picolitre droplets. *Lab on a Chip*, **2013**, *13*, 3707-3713.
- [107] Teh SY, Lin R, Hung LH, Lee AP; Droplet microfluidics. *Lab on a Chip*, **2008**, *8*, 198-220.
- [108] Theberge AB, Courtois F, Schaerli Y, Fischlechner M, Abell C, Hollfelder F, Huck WTS; Microdroplets in Microfluidics: An Evolving Platform for Discoveries in Chemistry and Biology. *Angewandte Chemie-International Edition*, **2010**, *49*, 5846-5868.
- [109] Anton N, Bally F, Serra CA, Ali A, Arntz Y, Mely Y, Zhao M, Marchioni E, Jakhmola A, Vandamme TF; A new microfluidic setup for precise control of the polymer nanoprecipitation process and lipophilic drug encapsulation. *Soft Matter*, **2012**, *8*, 10628-10635.
-

- [110] Khan IU, Serra CA, Anton N, Vandamme T; Continuous-flow encapsulation of ketoprofen in copolymer microbeads via co-axial microfluidic device: Influence of operating and material parameters on drug carrier properties. *International Journal of Pharmaceutics*, **2013**, *441*, 809-817.
- [111] Glawdel T, Elbuken C, Ren CL; Droplet formation in microfluidic T-junction generators operating in the transitional regime. I. Experimental observations. *Physical Review E*, **2012**, *85*, 016322.
- [112] Pompano RR, Platt CE, Karymov MA, Ismagilov RF; Control of Initiation, Rate, and Routing of Spontaneous Capillary-Driven Flow of Liquid Droplets through Microfluidic Channels on SlipChip. *Langmuir*, **2012**, *28*, 1931-1941.
- [113] Pang Y, Kim H, Liu Z, Stone HA; A soft microchannel decreases polydispersity of droplet generation. *Lab on a Chip*, **2014**, *14*, 4029-4034.
- [114] Cartas-Ayala M, Karnik R; Time limitations and geometrical parameters in the design of microfluidic comparators. *Microfluidics and Nanofluidics*, **2014**, *17*, 359-373.
- [115] Parida D, Serra CA, Garg DK, Hoarau Y, Bally F, Muller R, Bouquey M; Coil Flow Inversion as a Route To Control Polymerization in Microreactors. *Macromolecules*, **2014**, *47*, 3282-3287.
- [116] Serra CA, Chang Z; Microfluidic-Assisted Synthesis of Polymer Particles. *Chemical Engineering & Technology*, **2008**, *31*, 1099-1115.
- [117] Baroud CN, Gallaire F, Dangla R; Dynamics of microfluidic droplets. *Lab on a Chip*, **2010**, *10*, 2032-2045.
- [118] Li Y, Yamane DG, Li S, Biswas S, Reddy RK, Goettert JS, Nandakumar K, Kumar CSSR; Geometric optimization of liquid-liquid slug flow in a flow-focusing millifluidic device for synthesis of nanomaterials. *Chemical Engineering Journal*, **2013**, *217*, 447-459.
- [119] Lim J-M, Bertrand N, Valencia PM, Rhee M, Langer R, Jon S, Farokhzad OC, Karnik R; Parallel microfluidic synthesis of size-tunable polymeric nanoparticles using 3D flow focusing towards in vivo study. *Nanomedicine: Nanotechnology, Biology and Medicine*, **2014**, *10*, 401-409.
- [120] Nunes JK, Tsai SSH, Wan J, Stone HA; Dripping and jetting in microfluidic multiphase flows applied to particle and fibre synthesis. *Journal of Physics D-Applied Physics*, **2013**, *46*,
- [121] Boskovic D, Loebbecke S. 2014. Synthesis of polymer particles and capsules employing microfluidic techniques. *Nanotechnology Reviews*, **2010**, *3*, 27-38.
- [122] Malsch D, Kielpinski M, Merthan R, Albert J, Mayer G, Köhler JM, Süße H, Stahl M, Henkel T;  $\mu$ PIV-Analysis of Taylor flow in micro channels. *Chemical Engineering Journal*, **2008**, *135*, Supplement 1, S166-S172.
- [123] Günther A, Jhunjhunwala M, Thalmann M, Schmidt MA, Jensen KF; Micromixing of miscible liquids in segmented gas-liquid flow. *Langmuir*, **2005**, *21*, 1547-1555.
- [124] Woitalka A, Kuhn S, Jensen KF; Scalability of mass transfer in liquid-liquid flow. *Chemical Engineering Science*, **2014**, *116*, 1-8.

- 
- [125] Li S, Roy A, Lichtenberg H, Merchan G, Kumar CSSR, Köhler JM; Local Structure of ZnO Micro Flowers and Nanoparticles Obtained by Micro-Segmented Flow Synthesis. *ChemPhysChem*, **2012**, *13*, 1557-1561.
- [126] Bošković D, Loebbecke S; Modelling of the residence time distribution in micromixers. *Chemical Engineering Journal*, **2008**, *135*, Supplement 1, S138-S146.
- [127] Bošković D, Loebbecke S, Gross GA, Koehler JM; Residence Time Distribution Studies in Microfluidic Mixing Structures. *Chemical Engineering & Technology*, **2011**, *34*, 361-370.
- [128] Duraiswamy S, Khan SA; Plasmonic Nanoshell Synthesis in Microfluidic Composite Foams. *Nano Letters*, **2010**, *10*, 3757-3763.
- [129] Duraiswamy S, Khan SA; Droplet-Based Microfluidic Synthesis of Anisotropic Metal Nanocrystals. *Small*, **2009**, *5*, 2828-2834.
- [130] Song H, Tice JD, Ismagilov RF; A Microfluidic System for Controlling Reaction Networks in Time. *Angewandte Chemie International Edition*, **2003**, *42*, 768-772.
- [131] Knauer A, Csaki A, Fritzsche W, Serra CA, Leclerc N, Kohler JM; Micro continuous flow-through synthesis of triangular silver nanoprisms and their incorporation in complexly composed polymer microparticles. *Chemical Engineering Journal*, **2013**, *227*, 191-197.
- [132] Knauer A, Csaki A, Moller F, Huhn C, Fritzsche W, Kohler JM; Microsegmented Flow-Through Synthesis of Silver Nanoprisms with Exact Tunable Optical Properties. *Journal of Physical Chemistry C*, **2012**, *116*, 9251-9258.
- [133] Wagner J, Köhler JM; Continuous Synthesis of Gold Nanoparticles in a Microreactor. *Nano Letters*, **2005**, *5*, 685-691.
- [134] Krishna KS, Li Y, Li S, Kumar CSSR; Lab-on-a-chip synthesis of inorganic nanomaterials and quantum dots for biomedical applications. *Advanced Drug Delivery Reviews*, **2013**, *65*, 1470-1495.
- [135] Sebastian Cabeza V, Kuhn S, Kulkarni AA, Jensen KF; Size-Controlled Flow Synthesis of Gold Nanoparticles Using a Segmented Flow Microfluidic Platform. *Langmuir*, **2012**, *28*, 7007-7013.
- [136] Khan SA, Günther A, Schmidt MA, Jensen KF; Microfluidic Synthesis of Colloidal Silica. *Langmuir*, **2004**, *20*, 8604-8611.
- [137] Li S, Gross GA, Günther PM, Köhler JM; Hydrothermal micro continuous-flow synthesis of spherical, cylinder-, star- and flower-like ZnO microparticles. *Chemical Engineering Journal*, **2011**, *167*, 681-687.
- [138] Li S, Guenther PM, Koehler JM; Micro Segmented-Flow Technique for Continuous Synthesis of Different Kinds of ZnO Nanoparticles in Aqueous and in DMSO Solution. *Journal of Chemical Engineering of Japan*, **2009**, *42*, 338-345.
- [139] Karnik R, Gu F, Basto P, Cannizzaro C, Dean L, Kyei-Manu W, Langer R, Farokhzad OC; Microfluidic platform for controlled synthesis of polymeric nanoparticles. *Nano Letters*, **2008**, *8*, 2906-2912.
-

- [140] Bally F, Garg DK, Serra CA, Hoarau Y, Anton N, Brochon C, Parida D, Vandamme T, Hadziioannou G; Improved size-tunable preparation of polymeric nanoparticles by microfluidic nanoprecipitation. *Polymer*, **2012**, *53*, 5045-5051.
- [141] Seo M, Nie Z, Xu S, Mok M, Lewis PC, Graham R, Kumacheva E; Continuous Microfluidic Reactors for Polymer Particles. *Langmuir*, **2005**, *21*, 11614-11622.
- [142] Nie Z, Xu S, Seo M, Lewis PC, Kumacheva E; Polymer Particles with Various Shapes and Morphologies Produced in Continuous Microfluidic Reactors. *Journal of the American Chemical Society*, **2005**, *127*, 8058-8063.
- [143] Lewis PC, Graham RR, Nie Z, Xu S, Seo M, Kumacheva E; Continuous Synthesis of Copolymer Particles in Microfluidic Reactors. *Macromolecules*, **2005**, *38*, 4536-4538.
- [144] Serra CA, Khan IU, Chang Z, Bouquey M, Muller R, Kraus I, Schmutz M, Vandamme T, Anton N, Ohm C, Zentel R, Knauer A, Koehler M; Engineering Polymer Microparticles by Droplet Microfluidics. *Journal of Flow Chemistry*, **2013**, *3*, 66-75.
- [145] Marre S, Jensen KF; Synthesis of micro and nanostructures in microfluidic systems. *Chemical Society Reviews*, **2010**, *39*, 1183-1202.
- [146] <https://en.wikipedia.org/wiki/SEM>.
- [147] © Malvern Instruments Ltd. (Dynamic light scattering) 2003 to 2008, 2009.
- [148] © Malvern Instruments Ltd. (Zeta Potential) 2003 to 2008, 2009.
- [149] [https://en.wikipedia.org/wiki/Fluorescence\\_spectroscopy](https://en.wikipedia.org/wiki/Fluorescence_spectroscopy).
- [150] [https://en.wikipedia.org/wiki/Fluorescence\\_microscope](https://en.wikipedia.org/wiki/Fluorescence_microscope).
- [151] Lu X, Rycenga M, Skrabalak SE, Wiley B, Xia Y. 2009. Chemical Synthesis of Novel Plasmonic Nanoparticles. In *Annual Review of Physical Chemistry*, pp. 167-192
- [152] [https://en.wikipedia.org/wiki/Beer-Lambert\\_law](https://en.wikipedia.org/wiki/Beer-Lambert_law).
- [153] Cialla D, Maerz A, Boehme R, Theil F, Weber K, Schmitt M, Popp J; Surface-enhanced Raman spectroscopy (SERS): progress and trends. *Analytical and Bioanalytical Chemistry*, **2012**, *403*, 27-54.
- [154] Stiles PL, Dieringer JA, Shah NC, Van Duyne RR. Surface-Enhanced Raman Spectroscopy. *Annual Review of Analytical Chemistry*, **2008**, *1*, 601-626.
- [155] Xu S, Nie Z, Seo M, Lewis P, Kumacheva E, Stone HA, Garstecki P, Weibel DB, Gitlin I, Whitesides GM; Generation of monodisperse particles by using microfluidics: Control over size, shape, and composition (vol 44, pg 724, 2005). *Angewandte Chemie-International Edition*, **2005**, *44*, 3799-3799.
- [156] Rhee M, Valencia PM, Rodriguez MI, Langer R, Farokhzad OC, Karnik R; Synthesis of Size-Tunable Polymeric Nanoparticles Enabled by 3D Hydrodynamic Flow Focusing in Single-Layer Microchannels. *Advanced Materials*, **2011**, *23*, H79-H83.
- [157] Visaveliya N, Kohler JM; Simultaneous size and color tuning of polymer microparticles in a single-step microfluidic synthesis: particles for fluorescence labeling. *Journal of Materials Chemistry C*, **2015**, *3*, 844-853.



- 
- [158] Nie ZH, Xu SQ, Seo M, Lewis PC, Kumacheva E; Polymer particles with various shapes and morphologies produced in continuous microfluidic reactors. *Journal of the American Chemical Society*, **2005**, *127*, 8058-8063.
- [159] Seo M, Nie ZH, Xu SQ, Mok M, Lewis PC, Graham R, Kumacheva E; Continuous microfluidic reactors for polymer particles. *Langmuir*, **2005**, *21*, 11614-11622.
- [160] Kim JH, Jeon TY, Choi TM, Shim TS, Kim SH, Yang SM; Droplet Microfluidics for Producing Functional Microparticles. *Langmuir*, **2014**, *30*, 1473-1488.
- [161] Wang W, Zhang MJ, Chu LY; Functional Polymeric Microparticles Engineered from Controllable Microfluidic Emulsions. *Accounts of Chemical Research*, **2014**, *47*, 373-384.
- [162] Waters SL, Grotberg JB; The propagation of a surfactant laden liquid plug in a capillary tube. *Physics of Fluids*, **2002**, *14*, 471-480.
- [163] Chern CS; Emulsion polymerization mechanisms and kinetics. *Progress in Polymer Science*, **2006**, *31*, 443-486.
- [164] Koehler JM, Visaveliya N, Knauer A; Controlling formation and assembling of nanoparticles by control of electrical charging, polarization, and electrochemical potential. *Nanotechnology Reviews*, **2014**, *3*, 553-568.
- [165] Alivisatos AP, Johnsson KP, Peng XG, Wilson TE, Loweth CJ, Bruchez MP, Schultz PG; Organization of 'nanocrystal molecules' using DNA. *Nature*, **1996**, *382*, 609-611.
- [166] Hu J, Zhou SX, Sun YY, Fang XS, Wu LM; Fabrication, properties and applications of Janus particles. *Chemical Society Reviews*, **2012**, *41*, 4356-4378.
- [167] Min YJ, Akbulut M, Kristiansen K, Golan Y, Israelachvili J; The role of interparticle and external forces in nanoparticle assembly. *Nature Materials*, **2008**, *7*, 527-538.
- [168] Haeberle S, Zengerle R; Microfluidic platforms for lab-on-a-chip applications. *Lab on a Chip*, **2007**, *7*, 1094-1110.
- [169] Cheng L, Ma C, Yang G, You H, Fang J; Hierarchical silver mesoparticles with tunable surface topographies for highly sensitive surface-enhanced Raman spectroscopy. *Journal of Materials Chemistry A*, **2014**, *2*, 4534-4542.
- [170] Polte J, Herder M, Erler R, Rolf S, Fischer A, Wurth C, Thunemann AF, Kraehnert R, Emmerling F; Mechanistic insights into seeded growth processes of gold nanoparticles. *Nanoscale*, **2010**, *2*, 2463-2469.
- [171] Polte J, Tuaeov X, Wuithschick M, Fischer A, Thunemann AF, Rademann K, Kraehnert R, Emmerling F; Formation Mechanism of Colloidal Silver Nanoparticles: Analogies and Differences to the Growth of Gold Nanoparticles. *Acs Nano*, **2012**, *6*, 5791-5802.
- [172] Köhler JM, Li SN, Knauer A; Why is Micro Segmented Flow Particularly Promising for the Synthesis of Nanomaterials? *Chemical Engineering & Technology*, **2013**, *36*, 887-899.
- [173] Zhang L, Chan JM, Gu FX, Rhee J-W, Wang AZ, Radovic-Moreno AF, Alexis F, Langer R, Farokhzad OC; Self-assembled lipid-polymer hybrid nanoparticles: A robust drug delivery platform. *Acs Nano*, **2008**, *2*, 1696-1702.
-

- [174] Valencia PM, Basto PA, Zhang L, Rhee M, Langer R, Farokhzad OC, Karnik R; Single-Step Assembly of Homogenous Lipid - Polymeric and Lipid - Quantum Dot Nanoparticles Enabled by Microfluidic Rapid Mixing. *Acs Nano*, **2010**, *4*, 1671-1679.
- [175] Knauer A, Eisenhardt A, Krischok S, Koehler JM; Nanometer precise adjustment of the silver shell thickness during automated Au-Ag core-shell nanoparticle synthesis in micro fluid segment sequences. *Nanoscale*, **2014**, *6*, 5230-5238.
- [176] Reiss P, Protière M, Li L; Core/Shell Semiconductor Nanocrystals. *Small*, **2009**, *5*, 154-168.
- [177] Samal AK, Polavarapu L, Rodal-Cedeira S, Liz-Marzán LM, Pérez-Juste J, Pastoriza-Santos I; Size Tunable Au@Ag Core-Shell Nanoparticles: Synthesis and Surface-Enhanced Raman Scattering Properties. *Langmuir*, **2013**, *29*, 15076-15082.
- [178] Swierczewska M, Lee S, Chen XY; The design and application of fluorophore-gold nanoparticle activatable probes. *Physical Chemistry Chemical Physics*, **2011**, *13*, 9929-9941.
- [179] Grondahl L, Battersby BJ, Bryant D, Trau M; Encoding combinatorial libraries: A novel application of fluorescent silica colloids. *Langmuir*, **2000**, *16*, 9709-9715.
- [180] Täuscher E, Weiss D, Beckert R, Fabian J, Assumpcao A, Gorls H; Classical heterocycles with surprising properties: the 4-hydroxy-1,3-thiazoles. *Tetrahedron Letters*, **2011**, *52*, 2292-2294.
- [181] Stone JD, Artyomov MN, Chervin AS, Chakraborty AK, Eisen HN, Kranz DM; Interaction of Streptavidin-Based Peptide-MHC Oligomers (Tetramers) with Cell-Surface TCRs. *Journal of Immunology*, **2011**, *187*, 6281-6290.
- [182] Park K, Lee S, Kang E, Kim K, Choi K, Kwon IC; New Generation of Multifunctional Nanoparticles for Cancer Imaging and Therapy. *Advanced Functional Materials*, **2009**, *19*, 1553-1566.
- [183] Volodkin DV, Schaaf P, Mohwald H, Voegel JC, Ball V; Effective embedding of liposomes into polyelectrolyte multilayered films: the relative importance of lipid-polyelectrolyte and interpolyelectrolyte interactions. *Soft Matter*, **2009**, *5*, 1394-1405.
- [184] Schonhoff M, Ball V, Bausch AR, Dejugnat C, Delorme N, Glinel K, Klitzing RV, Steitz R; Hydration and internal properties of polyelectrolyte multilayers. *Colloids and Surfaces a-Physicochemical and Engineering Aspects*, **2007**, *303*, 14-29.
- [185] Zhou J, Wang B, Tong WJ, Maltseva E, Zhang G, Krastev R, Gao C, Mohwald H, Shen JC; Influence of assembling pH on the stability of poly(L-glutamic acid) and poly(L-lysine) multilayers against urea treatment. *Colloids and Surfaces B-Biointerfaces*, **2008**, *62*, 250-257.
- [186] Vinzenz X, Huger E, Himmerlich M, Krischok S, Busch S, Wollenstein J, Hoffmann C; Preparation and characterization of poly(L-histidine)/poly(L-glutamic acid) multilayer on silicon with nanometer-sized surface structures. *Journal of Colloid and Interface Science*, **2012**, *386*, 252-259.
- [187] Schmitt K, Schirmer B, Hoffmann C, Brandenburg A, Meyrueis P; Interferometric biosensor based on planar optical waveguide sensor chips for label-free detection of surface bound bioreactions. *Biosensors and Bioelectronics*, **2007**, *22*, 2591-2597.

- 
- [188] Grohmann S, Rothe H, Eisenhuth S, Hoffmann C, Liefelth K; Biomimetic assembly of polyelectrolyte multilayers containing phosphitin monitored with reflectometric interference spectroscopy. *Biointerphases*, **2011**, *6*, 54-62.
- [189] Büchner K, Ehrhardt N, Cahill BP, Hoffmann C; Internal reflection ellipsometry for real-time monitoring of polyelectrolyte multilayer growth onto tantalum pentoxide. *Thin Solid Films*, **2011**, *519*, 6480-6485.
- [190] Schmitt K, Oehse K, Sulz G, Hoffmann C; Evanescent field Sensors Based on Tantalum Pentoxide Waveguides – A Review. *Sensors*, **2008**, *8*, 711.
- [191] Vinzenz X, Hüger E, Himmerlich M, Krischok S, Busch S, Wöllenstein J, Hoffmann C; Preparation and characterization of poly(L-histidine)/poly(L-glutamic acid) multilayer on silicon with nanometer-sized surface structures. *Journal of Colloid and Interface Science*, **2012**, *386*, 252-259.
- [192] Elia G, Fugmann T, Neri D; From target discovery to clinical trials with armed antibody products. *Journal of Proteomics*, **2014**, *107*, 50-55.
- [193] Lagunas A, Comelles J, Martinez E, Samitier J; Universal Chemical Gradient Platforms Using Poly(methyl methacrylate) Based on the Biotin Streptavidin Interaction for Biological Applications. *Langmuir*, **2010**, *26*, 14154-14161.
- [194] Schmitt K, Rist J, Hoffmann C; Optical waveguides for the evanescent wave-induced cleavage of photolabile linker compounds. *Analytical and Bioanalytical Chemistry*, **2011**, *401*, 777-782.
- [195] Deng L, Kitova EN, Klassen JS; Dissociation Kinetics of the Streptavidin-Biotin Interaction Measured Using Direct Electrospray Ionization Mass Spectrometry Analysis. *Journal of the American Society for Mass Spectrometry*, **2013**, *24*, 49-56.
- [196] Ajayan PM, Marks LD; Quasimelting and phases of small particles. *Physical Review Letters*, **1988**, *60*, 585-587.
- [197] Smith DJ, Petfordlong AK, Wallenberg LR, Bovin JO; Dynamic Atomic-Level Rearrangements in Small Gold Particles. *Science*, **1986**, *233*, 872-875.
- [198] Johnson CJ, Dujardin E, Davis SA, Murphy CJ, Mann S; Growth and form of gold nanorods prepared by seed-mediated, surfactant-directed synthesis. *Journal of Materials Chemistry*, **2002**, *12*, 1765-1770.
- [199] Sun YG, Mayers B, Herricks T, Xia YN; Polyol synthesis of uniform silver nanowires: A plausible growth mechanism and the supporting evidence. *Nano Letters*, **2003**, *3*, 955-960.
- [200] Wang ZL; Transmission electron microscopy of shape-controlled nanocrystals and their assemblies. *Journal of Physical Chemistry B*, **2000**, *104*, 1153-1175.
- [201] Gao Y, Jiang P, Liu DF, Yuan HJ, Yan XQ, Zhou ZP, Wang JX, Song L, Liu LF, Zhou WY, Wang G, Wang CY, Xie SS, Zhang JM, Shen AY; Evidence for the monolayer assembly of poly(vinylpyrrolidone) on the surfaces of silver nanowires. *Journal of Physical Chemistry B*, **2004**, *108*, 12877-12881.
- [202] Decher G; Fuzzy nanoassemblies: Toward layered polymeric multicomposites. *Science*, **1997**, *277*, 1232-1237.
-

- [203] Atencia J, Beebe DJ; Controlled microfluidic interfaces. *Nature*, **2005**, *437*, 648-655.
- [204] Fujioka H, Grotberg JB; The steady propagation of a surfactant-laden liquid plug in a two-dimensional channel. *Physics of Fluids*, **2005**, *17*,
- [205] Dendukuri D, Doyle PS; The Synthesis and Assembly of Polymeric Microparticles Using Microfluidics. *Advanced Materials*, **2009**, *21*, 4071-4086.
- [206] Serra CA, Khan IU, Chang ZQ, Bouquey M, Muller R, Kraus I, Schmutz M, Vandamme T, Anton N, Ohm C, Zentel R, Knauer A, Kohler M; Engineering Polymer Microparticles by Droplet Microfluidics. *Journal of Flow Chemistry*, **2013**, *3*, 66-75.
- [207] Xu SQ, Nie ZH, Seo M, Lewis P, Kumacheva E, Stone HA, Garstecki P, Weibel DB, Gitlin I, Whitesides GM; Generation of monodisperse particles by using microfluidics: Control over size, shape, and composition. *Angewandte Chemie-International Edition*, **2005**, *44*, 724-728.
- [208] Kelly KL, Coronado E, Zhao LL, Schatz GC; The optical properties of metal nanoparticles: The influence of size, shape, and dielectric environment. *Journal of Physical Chemistry B*, **2003**, *107*, 668-677.
- [209] Li M, Schnablegger H, Mann S; Coupled synthesis and self-assembly of nanoparticles to give structures with controlled organization. *Nature*, **1999**, *402*, 393-395.
- [210] McGilvray KL, Decan MR, Wang DS, Scaiano JC; Facile photochemical synthesis of unprotected aqueous gold nanoparticles. *Journal of the American Chemical Society*, **2006**, *128*, 15980-15981.
- [211] Lu XM, Rycenga M, Skrabalak SE, Wiley B, Xia YN; Chemical Synthesis of Novel Plasmonic Nanoparticles. *Annual Review of Physical Chemistry*, **2009**, *60*, 167-192.
- [212] Lee KS, El-Sayed MA; Gold and silver nanoparticles in sensing and imaging: Sensitivity of plasmon response to size, shape, and metal composition. *Journal of Physical Chemistry B*, **2006**, *110*, 19220-19225.
- [213] Bastus NG, Merkoci F, Piella J, Puntès V; Synthesis of Highly Monodisperse Citrate-Stabilized Silver Nanoparticles of up to 200 nm: Kinetic Control and Catalytic Properties. *Chemistry of Materials*, **2014**, *26*, 2836-2846.
- [214] Anker JN, Hall WP, Lyandres O, Shah NC, Zhao J, Van Duyne RP; Biosensing with plasmonic nanosensors. *Nature Materials*, **2008**, *7*, 442-453.
- [215] McFarland AD, Young MA, Dieringer JA, Van Duyne RP; Wavelength-scanned surface-enhanced Raman excitation spectroscopy. *Journal of Physical Chemistry B*, **2005**, *109*, 11279-11285.
- [216] Cialla D, Marz A, Bohme R, Theil F, Weber K, Schmitt M, Popp J; Surface-enhanced Raman spectroscopy (SERS): progress and trends. *Analytical and Bioanalytical Chemistry*, **2012**, *403*, 27-54.
- [217] Fan MK, Andrade GFS, Brolo AG; A review on the fabrication of substrates for surface enhanced Raman spectroscopy and their applications in analytical chemistry. *Analytica Chimica Acta*, **2011**, *693*, 7-25.
- [218] Lin XM, Cui Y, Xu YH, Ren B, Tian ZQ; Surface-enhanced Raman spectroscopy: substrate-related issues. *Analytical and Bioanalytical Chemistry*, **2009**, *394*, 1729-1745.

- 
- [219] Zhang L, Jiang C, Zhang Z; Graphene oxide embedded sandwich nanostructures for enhanced Raman readout and their applications in pesticide monitoring. *Nanoscale*, **2013**, *5*, 3773-3779.
- [220] Han Y, Liu S, Liu B, Jiang C, Zhang Z; In situ loading of Ag nanocontacts onto silica nanospheres: a SERS platform for ultrasensitive detection. *Rsc Advances*, **2014**, *4*, 2776-2782.
- [221] Shafer-Peltier KE, Haynes CL, Glucksberg MR, Van Duyne RP; Toward a glucose biosensor based on surface-enhanced Raman scattering. *Journal of the American Chemical Society*, **2003**, *125*, 588-593.
- [222] Chrimes AF, Khoshmanesh K, Stoddart PR, Mitchell A, Kalantar-zadeh K; Microfluidics and Raman microscopy: current applications and future challenges. *Chemical Society Reviews*, **2013**, *42*, 5880-5906.
- [223] Cassanas G, Morssli M, Fabrègue E, Bardet L; Vibrational spectra of lactic acid and lactates. *Journal of Raman Spectroscopy*, **1991**, *22*, 409-413.
- [224] Hsu P-H, Chiang HK; Surface-enhanced Raman spectroscopy for quantitative measurement of lactic acid at physiological concentration in human serum. *Journal of Raman Spectroscopy*, **2010**, *41*, 1610-1614.
- [225] Shah NC, Lyandres O, Walsh JT, Glucksberg MR, Van Duyne RP; Lactate and Sequential Lactate-Glucose Sensing Using Surface-Enhanced Raman Spectroscopy. *Analytical Chemistry*, **2007**, *79*, 6927-6932.
- [226] Gupta MK, Bansil R; Laser Raman-Spectroscopy of Polyacrylamide. *Journal of Polymer Science Part B-Polymer Physics*, **1981**, *19*, 353-360.
- [227] Stewart S, Fredericks PM; Surface-enhanced Raman spectroscopy of peptides and proteins adsorbed on an electrochemically prepared silver surface. *Spectrochimica Acta Part a-Molecular and Biomolecular Spectroscopy*, **1999**, *55*, 1615-1640.
- [228] Stewart S, Fredericks PM; Surface-enhanced Raman spectroscopy of amino acids adsorbed on an electrochemically prepared silver surface. *Spectrochimica Acta Part a-Molecular and Biomolecular Spectroscopy*, **1999**, *55*, 1641-1660.
- [229] Martusevicius S, Niaura G, Talaikyte Z, Razumas V; Adsorption of L-histidine on copper surface as evidenced by surface-enhanced Raman scattering spectroscopy. *Vibrational Spectroscopy*, **1996**, *10*, 271-280.
- [230] Bell SEJ, Sirimuthu NMS; Surface-enhanced Raman spectroscopy (SERS) for sub-micromolar detection of DNA/RNA mononucleotides. *Journal of the American Chemical Society*, **2006**, *128*, 15580-15581.



## 7 Appendix

### 7.1 Chemicals

All chemicals were used as received without further purification in the work and list them in **Table 2.3**. Deionized water (Aqua purificator G 7795, Miele, Germany) was used throughout the experiments.

**Table 2.3** Chemicals list used in the experiments.

Chemical name	Abbreviation/Chemical formula	Source
Silver nitrate	AgNO <sub>3</sub>	Merck, Germany
Ascorbic acid	C <sub>6</sub> H <sub>8</sub> O <sub>6</sub>	Roth, Germany
Polyvinyl pyrrolidone	PVP (25 kDa, 40 kDa, 55 kDa)	Sigma Aldrich
Ethylene glycol	EG	VWR, Belgium
Methyl methacrylate	MMA	Sigma-Aldrich
Ethylene glycodimethacrylate	EGDMA	Sigma-Aldrich
Azobisisobutyronitrile	AIBN	Sigma-Aldrich
Cetyl trimethylammonium bromide	CTAB	Sigma-Aldrich
Sodium dodecylsulfonate	SDS	Sigma-Aldrich
Sodium hydroxide	NaOH	Merck Germany
Poly(4-styrenesulfonic acid-co-maleic acid) sodium salt	PSS-co-PM (20 kDa)	Sigma-Aldrich
Poly(sodium-p-styrenesulfonate)	PSSS (70 kDa, 500 kDa, 1000 kDa)	Sigma-Aldrich
Polyanetholesulfonic acid sodium salt	PAES (10 kDa)	Sigma-Aldrich
Acrylamide:Bisacrylamide 19:1	C <sub>3</sub> H <sub>5</sub> NO: C <sub>7</sub> H <sub>10</sub> N <sub>2</sub> O <sub>2</sub>	Fischer scientific
Novec 7500	Solvent	Product of 3M <sup>TM</sup>
Picosurf	5 % in Novec 7500	Sphere fluidic
2-Hydroxy-2-methylpropiophenone	C <sub>6</sub> H <sub>5</sub> COC(CH <sub>3</sub> ) <sub>2</sub> OH	Sigma-Aldrich
Tripropylene glycol diacrylate	TPGDA	ABCR GmbH, Germany

Nile red	$C_{20}H_{18}N_2O_2$	Sigma, Sigma-Aldrich
12-(7-Nitrobenzofuran-4-ylamino)dodecanoic acid	NBFD	Fluka, Sigma-Aldrich
Sudan black B	$C_{29}H_{24}N_6$	Merck, Germany
Reichardt's dye	$C_{41}H_{29}NO$	Sigma-Aldrich
Titan yellow	$C_{28}H_{19}N_5Na_2O_6S_4$	Merck, Germany
Poly-L-lysine	PLL	Sigma-Aldrich
Poly-L-Glutamic acid	PGA	Sigma-Aldrich
NHS-LC-LC-Biotin	$C_{26}H_{41}O_7N_5S$	Thermo Fisher Scientific
AlexaFluor 594 conjugate	Dye labelled-streptavidin	Life Technologies
Adenine	$C_5H_5N_5$	AppliChem GmbH, Germany
Histidine	$C_6H_9N_3O_2$	AppliChem GmbH, Germany
Sulfuric acid	$H_2SO_4$	Merck, Germany
Fluorescein	$C_{20}H_{12}O_5$	Sigma-Aldrich
Orange G	$C_{16}H_{10}N_2Na_2O_7S_2$	Merck, Germany
Sulphorhodamine B	$C_{27}H_{29}N_2NaO_7S_2$	Fluka
Tetrachloroauric acid trihydrate	$HAuCl_3 \cdot 3H_2O$	Roth, Germany
Sodium borohydride	$NaBH_4$	Merck, Germany
Trisodium citrate	$Na_3C_6H_5O_7$	Merck, Germany
Diallyldimethyl ammonim chloride	DADMAC	Sigma-Aldrich
Poly(diallyldimethyl ammonium chloride)	polyDADMAC	Sigma-Aldrich
6-propionyl-2-dimethyl aminonaphthalene (Prodan)	$C_{15}H_{17}NO$	Molecular probes
L-(+)-Lactic acid	$C_3H_6O_3$	Sigma-Aldrich
D-Pantothenic acid calcium salt	$C_{18}H_{32}CaN_2O_{10}$	AppliChem GmbH, Germany



## 7.2 Abbreviations

ID	Internal diameter
LCST	Lower critical solution temperature
LBL	Laye-by-layer
PDMS	Polydimethylsiloxane
RTD	Residence time distribution
FEP	Fluorinated ethylene propylene
SDS	Sodium dodecyl sulfonate
CTAB	Cetyl trimethylammonium bromide
MMA	Methyl methacrylate
PMMA	Poly(methyl methacrylate)
EGDMA	Ethylene glycol dimethacrylate
AIBN	Azobisisobutyronitrile
PS-co-PM	Poly(4-styrenesulfonic acid-co-maleic acid) sodium salt
PSSS	Poly(sodium-p-styrenesulfonate)
PVP	Polyvinylpyrrolidone
DADMAC	Diallyldimethyl ammonium chloride
PLG	Poly-L-glutamic acid
PLL	Poly-L-lysine
TPGDA	Tripropylene glycol diacrylate
HMPP	2-Hydroxy-2-methylpropiophenone
PolyTPGDA	Poly(tripropylene glycol diacrylate)
SERS	Surface-enhanced Raman Spectroscopy
SEM	Scanning electron microscopy
UV/Vis	Ultraviolet/visible spectroscopy
DLS	Dynamic light scattering
EG	Ethylene glycol
NBFD	12-(7-Nitrobenzofuran-4-ylamino)dodecanoic acid
CMC	Critical micelle concentration
Qdots	Quantum dots
PTFE	Polytetrafluoroethylene

### 7.3 Scientific publications

#### Journal publications

1. **N. Visaveliya**, C. Hoffmann, A. Groß, E. Täuscher, U. Ritter, and J. M. Köhler. “Micro-flow assisted synthesis of fluorescent polymer nanoparticles with tuned size and surface properties” *Nanotechnology Reviews*, **2015** (Accepted).
2. **N. Visaveliya** and J. M. Köhler. “Microfluidic Assisted Synthesis of Multipurpose Polymer Nanoassembly Particles for Fluorescence, LSPR, and SERS Activities” *Small*, **2015**, DOI: 10.1002/sml.201502364 (In press).
3. **N. Visaveliya**, S. Lenke and J. M. Köhler, “Composite Sensor Particles for Tuned SERS Sensing: Microfluidic Synthesis, Properties and Applications”, *ACS Appl. Mater. Interfaces*, **2015**, 7 (20), 10742–10754.
4. **N. Visaveliya**, S. Lenke, and J. M. Köhler, “Microflow SERS Measurements Using Sensing Particles of Polyacrylamide/Silver Composite Materials”, *Chem. Eng. Technol.*, **2015**, 38 (7), 1144-1149.
5. **N. Visaveliya** and J. M. Köhler, “Role of Self-Polarization in a Single-Step Controlled Synthesis of Linear and Branched Polymer Nanoparticles”, *Macromol. Chem. Phys.*, **2015**, 216 (11), 1212-1219.
6. **N. Visaveliya** and J. M. Köhler, “Simultaneous Size and Color Tuning of Polymer Microparticles in a Single-Step Microfluidic Synthesis: Particles for Fluorescence Labeling”, *J. Mater. Chem. C*, **2015**, 3, 844–853.
7. D. Kürsten, F. Möller, A. Gross, C. Lenk, **N. Visaveliya**, T. Schüler, J. M. Köhler, , “Identification of Response Classes from Heavy Metal-Tolerant Soil Microorganism Communities by Highly Resolved Concentration-Dependent Screenings in a Microfluidic System” *Methods in Ecology and Evolution*, **2015**, 6 (5), 600-609.
8. **N. Visaveliya** and J. M. Köhler, “Control of Shape and Size of Polymer Nanoparticles Aggregates in a Single-Step Micro Continuous Flow Process: A Case of Flower and Spherical Shapes”, *Langmuir*, **2014**, 30, 12180–12189.
9. **N. Visaveliya** and J. M. Köhler, “Single-Step Microfluidic Synthesis of Various Non-Spherical Polymer Nanoparticles via in-Situ Assembling: Dominating Role of Polyelectrolytes Molecules”, *ACS Appl. Mater. Interfaces*, **2014**, 6 (14), 11254–11264.
10. J. M. Köhler, **N. Visaveliya** and A. Knauer “Controlling Formation and Assembling of Nanoparticles by Control of Electrical Charging, Polarization, and Electrochemical Potential”, *Nanotechnology Reviews*, **2014**, 3(6), 553-568.

11. P. Dhasaiyan, P R Pandey, **N. Visaveliya**, S. Roy and BLV. Prasad “Vesicle Structures from Bolaamphiphilic Biosurfactants: Experimental and Molecular Dynamics Simulation Studies on the Effect of Unsaturation on Sophorolipid Self-Assemblies”, *Chem. Eur. J.*, **2014**, 20 (21), 6246-6250.
12. **N. Visaveliya**, S. Li and J. M. Köhler, “Heterogeneous Nanoassembling: Microfluidically Prepared Poly(methyl methacrylate) Nanoparticles on Ag Microrods and ZnO Microflowers”, *Part. Part. Syst. Charact.* **2013**, 30, 614–623.
13. **N. Visaveliya** and J. M. Köhler, “A Self-Seeding Synthesis of Ag Microrods of Tuned Aspect Ratio: Ascorbic Acid Plays a Key Role”, *Nanotechnology*, **2013**, 24(34), 345604.
14. A. Knauer, **N. Visaveliya** and J. M. Köhler “Spontaneous Transformation of Polyelectrolyte-Stabilized Silver Nanoprisms by Interaction with Thiocyanate”, *J. Colloid and Interface Science*, **2013**, 394, 78–84.
15. P. Dhasaiyan, A. Banerjee, **N. Visaveliya** and BLV Prasad “Influence of the Sophorolipid Molecular Geometry on their Self-Assembled Structures”, *Chem. Asian J.*, **2013**, 8, 369 – 372.

#### Posters and Talks (Conferences)

1. 1st International Conference & 3rd International MacroNano Colloquium on the Challenges and Perspectives of Functional Nanostructures, July 29-31, 2014, Organized by Technical university of Ilmenau, Ilmenau, Germany.  
**Talk:** “Microfluidic Synthesis of Non-Spherical Polymer Nanoparticles”.  
**Poster:** “Microfluidically Prepared Size-Tuned polymer/Silver Composite Particles for SERS Sensing”.
2. 7th Workshop of Chemical and Biological Micro Laboratory Technology, February 25-27, 2014, Elgersburg, Germany.  
**Poster:** “Microfluidic Synthesis of Polymer Composite Microparticles for SERS Sensing Application”
3. 11th Workshop on Polymer Reaction Engineering" May 21-24, 2013 University of Hamburg, Hamburg, Germany.  
**Poster:** “Microfluidic Synthesis of Elliptical, Dumbbell and Chain-Like Polymer Nanoparticles”.

4. 6th Workshop of “Chemical and Biological Micro Laboratory Technology”, March 20.-22, 2012, Elgersburg, Germany.

**Poster:** “Microfluidic Synthesis of Shape-Controlled Anisotropic PMMA Nanoparticles”.

5. 4th European Conference on Microfluidics, December 10-12, 2014, Limerick, Ireland.

**Paper:** “Production of Size-Tunable Nanoemulsion in an Elongational Flow Microdevice and its Application to the Synthesis of Multi/Scale Composite polymeric Microparticles”. By W. Yu, N. Visaveliya, I. U. Khan, C. A. Serra, J. M. Köhler, R. Muller, Y. Holl, and M. Bouquey.

---

## 7.4 Curriculum vitae

### Personal Information

**Name:** Nikunj Kumar Visaveliya

**Birth date:** 12.04.1986

**Nationality:** Indian

**Email:** [nikunj.kumar.visaveliya@tu-ilmenau.de](mailto:nikunj.kumar.visaveliya@tu-ilmenau.de)

### Education Background and Work Experience

**September 2010 – November 2015**      **PhD** in Microreaction Technology  
Technical University of Ilmenau, Germany  
**Topic:** “Microfluidic Synthesis and Assembly of Multi-Scale Composite Particles Towards Sensoric and Labeling applications”.

**July 2011 – August 2011**      **Research Visit**  
Institute of Bioprocess and Analytical Measurements (iba),  
Heiligenstadt, Germany.  
**Topic:** “Bio-functionalization of polymer and metal nanoparticles”

**January 2009 - May 2010**      **Research Project Assistant**  
National Chemical Laboratory, Pune, India  
**Topic:** “Biosynthesis of Sophorolipids Biosurfactants”.

**July 2006 - May 2008**      **Master of Science** (Organic Chemistry)  
Sardar Patel University, India

**June 2003 - May 2006**      **Bachelor of Science** (Chemistry)  
Sardar Patel University, India

## 7.5 Acknowledgement

During the course of my Ph.D., there are many people who have been so cooperative, and I am deeply thankful to all of them.

Firstly, I would like to express my sincere and very respectful thanks to my Ph.D. supervisor Prof. J. Michael Köhler for his valuable guidance and academic as well as financial support throughout the course of my doctoral work. Along with the scientific advice, his well human being nature has influenced significantly. It was great to see his scientifically rich mind with lot of working idea at a time to explore the science in the lab.

I am thankful to Prof. Christophe A. Serra and Prof. Uwe Ritter for their willingness to prepare the report of my dissertation work.

I am very grateful to all my colleagues of our MRT group in Ilmenau. Especially, Steffen Schneider whose valuable cooperation in the administrative assistance, language, academic and research perspective is gratefully acknowledged. He is the person who helped me in every situation from first day of my arrival to Germany until last day of my Ph.D. On other side, I am thankful to Dr. Alexander Gross for his very effective discussions and research cooperation in the lab to explore the lot of new ideas. My thanks are also extended to Dr. Mike Günther for his instrumental and laboratory instructions with lot of care right from the beginning to an end of the course. I gratefully acknowledged Dr. Andrea Knauer for sharing the materials, for her effective cooperation during the all scientific presentations, examinations and thesis work. Her support and advice was very helpful to progress in the research outcome. I would also like to thank Ms. Frances Möller for ordering the chemicals and materials whenever needed on immediate basis, and also Mr. Tilo Nicolai for his administrative support. I acknowledge Mr. Steffen Lenke to cooperate with my work during his master thesis in our group. Many thanks are also extended to my other colleagues Dr. Shuning Li, Dr. Jialan Cao, Dana Kürsten, Claudia Lenk, Jessika Teuber, Lars Hafermann, Katharina Wetzl and Katja Bergmann for their valuable cooperation during the working hours in the University. I extend my thanks to Sukhdeepbhai and his family for his accompany in research, cooking and sports perspective, and also to all my friends in Ilmenau for their kind cooperation during exploring the beautiful places of Ilmenau, Germany and Europe.

I acknowledge Dr. Arne Albrecht for SEM and clean room instructions in ZMN. In addition, I like to thank Ms. Magali Camargo for Zetasizer instruction/assistance, and also Dr. Eric Täuscher and Prof. Uwe Ritter for allowing me to work in their lab for fluorescence measurements. I owe sincere thanks to Mr. Wei Yu and Prof. Christophe A. Serra for the research collaboration during the research visit of Mr. Yu at TU Ilmenau in spring 2014. Regarding my research visit to iba Heiligenstadt in summer 2012, I express thanks to Dr. Christian Hoffmann for his keen interest, strong motivation and consistent encouragement during the course of my work. I also like to thank Ms. Olga Artes for her experimental assistance during the iba visit. My sincere thanks and respect to my previous project supervisor Dr. B. L. V. Prasad (NCL, India) for his valuable research advice and guidance during his 3 months visit to TU Ilmenau in autumn 2012. I am very grateful to all the unknown reviewers of my research papers who have spent their precious time and energy; their comments were really helpful for deepening the understanding in scientific knowledge.

For partial financial support, I would like to thank BMBF (Project: SOD), DFG (Project: composite particles) and State of Thuringia (Landesgraduiertenstipendium).

In addition, I am also very thankful to all the people in my life who have taken care with lot of love during my every efforts. I feel very blessed after getting the unconditional love from the incredible people connected to me. And at the last, I am tangibly seeing a wonderful life to walk together with my wife Lopa forever. Her spiritual support during the final phase of my Ph.D. is gratefully acknowledged.

Sincerely

M. Sc. Nikunj Kumar Visaveliya





## 7.6 Selbstständigkeitserklärung

Promotionsordnung – Allgemeine Bestimmungen -

Ich versichere, dass ich die vorliegende Arbeit ohne unzulässige Hilfe Dritter und ohne Benutzung anderer als der angegebenen Hilfsmittel angefertigt habe. Die aus anderen Quellen direkt oder indirekt übernommenen Daten und Konzepte sind unter Angabe der Quelle gekennzeichnet.

Bei der Auswahl und Auswertung folgenden Materials haben mir die nachstehend aufgeführten Personen in der jeweils beschriebenen Weise unentgeltlich geholfen:

1. Die in Abschnitt 3.4.1 angegebene chemische Verbindung (5-Methyl-2-(pyridin-2-yl)-thiazol-4-yl methacrylate) wurde von Dr. Eric Täuscher (TU Ilmenau, FG Chemie) hergestellt.
2. Die Arbeiten in Abschnitt 3.4.3 wurden von Dr. Christian Hoffmann und Olga Artes (IBA Heiligenstadt) unterstützt.

Weitere Personen waren an der inhaltlich-materiellen Erstellung der vorliegenden Arbeit nicht beteiligt. Insbesondere habe ich hierfür nicht die entgeltliche Hilfe von Vermittlungs- bzw. Beratungsdiensten (Promotionsberater oder anderer Personen) in Anspruch genommen. Niemand hat von mir unmittelbar oder mittelbar geldwerte Leistungen für Arbeiten erhalten, die im Zusammenhang mit dem Inhalt der vorgelegten Dissertation stehen.

Die Arbeit wurde bisher weder im In- noch im Ausland in gleicher oder ähnlicher Form einer Prüfungsbehörde vorgelegt.

Ich bin darauf hingewiesen worden, dass die Unrichtigkeit der vorstehenden Erklärung als Täuschungsversuch angesehen wird und gemäß § 7 Abs. 10 der Promotionsordnung den Abbruch des Promotionsverfahrens zu Folge hat.

(Ort, Datum)

(Unterschrift)